Subcellular localization of the mitotic checkpoint kinase MPS1: Mechanisms and regulation

Wilco Nijenhuis

ISBN: 978-94-6108-583-2

Cover: an assembled immunofluorescence image of HeLa cells in the process of chromosomal alignment. Chromosomes are depicted in cyan and microtubules in red.

Printed by: Gildeprint Drukkerijen - The Netherlands

Subcellular localization of the mitotic checkpoint kinase MPS1: Mechanisms and regulation

Subcellulaire lokalisatie van de mitotische checkpoint kinase MPS1: Mechanismen en regulatie

(met een samenvatting in het Nederlands)

Proefschrift

ter verkrijging van de graad van doctor aan de Universiteit Utrecht
op gezag van de rector magnificus, prof. dr. G.J. van der Zwaan,
ingevolge het besluit van het college voor promoties
in het openbaar te verdedigen op
dinsdag 28 januari 2014 des middags te 2.30 uur

door

Wilco Nijenhuis

geboren op 9 juli 1984
te Harmelen

Promotor: Prof. dr. G.J.P.L. Kops

The most exciting phrase to hear in science,

the one that heralds the most discoveries,

is not “Eureka!”

but “That’s funny...”

- Isaac Asimov -

Table of contents

Abbreviations

APC/C:	anaphase promoting complex/cyclosome
BUB:	budding-uninhibited by benomyl
CCAN:	constitutive centromere-associated network
CDK:	cyclin-dependent kinase
CENP:	centromere protein
CH:	calponin-homology domain
CPC:	chromosomal passenger complex
DUB:	deubiquitinating enzyme
FRT:	Flp recognition target
HeLaK:	HeLa Kyoto
K-fiber:	kinetochore fiber
KARD:	kinetochore attachment and regulatory domain
KD:	kinase dead
KMN:	KNL1-MIS12-NDC80 network
lacO:	*lac* operator
LAP:	localization and affinity purification tag
MAD:	mitotic-arrest-deficient
MCC:	mitotic checkpoint complex
MM:	molecular mass
MPS1:	monopolar spindle 1
NEB:	nuclear envelope breakdown
NTE:	N-terminal extension
RZZ:	ROD1-Zwilch-ZW10 complex
SAC:	spindle assembly checkpoint
STLC:	S-Trityl-L-cysteine
TetR:	tetracycline repressor
TFR:	Transferrin receptor protein 1
TPR:	tetratricopeptide repeat domain
WT:	wild-type

Chapter 1

General introduction

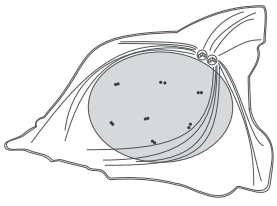

Mitosis is the process in which an eukaryotic cell divides to form two daughter cells. The division may be symmetric or asymmetric, but the goal of mitosis is to ensure that both daughter cells are endowed with identical genomic information, which is transmitted in the form of duplicated chromosomes. Mitosis allows the expansion of a single fertilized oocyte into the trillions of cells that make up a human body. Moreover, mitosis allows the maintenance of tissues and organs by the continuous replenishment of damaged cells.

As a cell progresses from one division to the next, it cycles through several stages. A newly formed cell starts a cell cycle with a gap (G) phase, known as G_1. During G_1, a cell is either committed to further cycling, or under influence of inhibitory signals or unfavorable conditions it enters a prolonged nondividing state known as G_0. Most of the nondividing, terminally differentiated cells in tissues are in G_0. If the cell cycle does progress, it enters a synthetic (S) phase during which the genome is replicated. This gives rise to duplicated chromosomes. The centrosomes are also duplicated at this time. S-phase is followed by a second gap phase (G_2). During the Gap phases and S-phase, cellular morphology remains relatively similar when compared to the profound changes to cellular organization during mitosis. Therefore, these phases are collectively known as interphase.

Morphological changes and the phases of mitosis

Following replication, the duplicated chromosomes are connected by ring-like protein complexes called cohesin (reviewed in *1*). In mitosis, segregation of the duplicated chromosomes to the daughter cells is mediated by the mitotic spindle. This dynamic structure of microtubule bundles attaches to individual chromosomes and creates the pulling forces that separate chromosomes during anaphase. The spindle is formed by two centrosomes, which are microtubule-nucleating centers that localize to opposite poles of the spindle. The orientation of the mitotic spindle defines the plane of division. The two centrosomes were connected since their duplication in S-phase, but are separated in prophase. Subsequently, the centrosomes traverse around the nucleus and this allows rapid assembly of the spindle after breakdown of the nuclear envelope (Figure 1). Other cytoskeletal rearrangements cause cells to detach from their environment and round up. This spatial organization promotes efficient chromosome capture by spindle microtubules in prometaphase (*2*). Additionally, for efficient distribution of the duplicated chromosomes, chromosomes are condensed during prophase to form stiff rodlike structures. Prometaphase begins with breakdown of the nuclear envelope, which frees the condensed chromosomes into the cytosol and allows the spindle microtubules to attach to the chromosomes. Pulling forces from the spindle microtubules, as well as the activities of chromosome-based motor proteins, drive chromosome congression towards the center of the mitotic spindle. When all chromosomes have been attached by spindle microtubules and aligned into a central plane, metaphase has been achieved. From the metaphase plate, the duplicated sister chromatids are then pulled towards the opposite poles of the spindle in anaphase. In telophase, mitosis is completed by reformation of the nuclear envelope around the segregated chromosomes and disassembly of the mitotic spindle. Simultaneously, ingression of the plasma membrane initiates the process of abscission of the two daughter cells that is completed during cytokinesis.

Assembling the microtubule attachment site: centromeres and kinetochores

Spindle microtubules attach to chromosomes by interacting with kinetochores, a specialized organelle that is assembled on the centromere region of each chromatid. EM ultrastructure analyses have shown that kinetochores consist of an inner centromere and a dense circular plate-like outer kinetochore. These are separated by a more open middle layer. The outer kinetochore, which

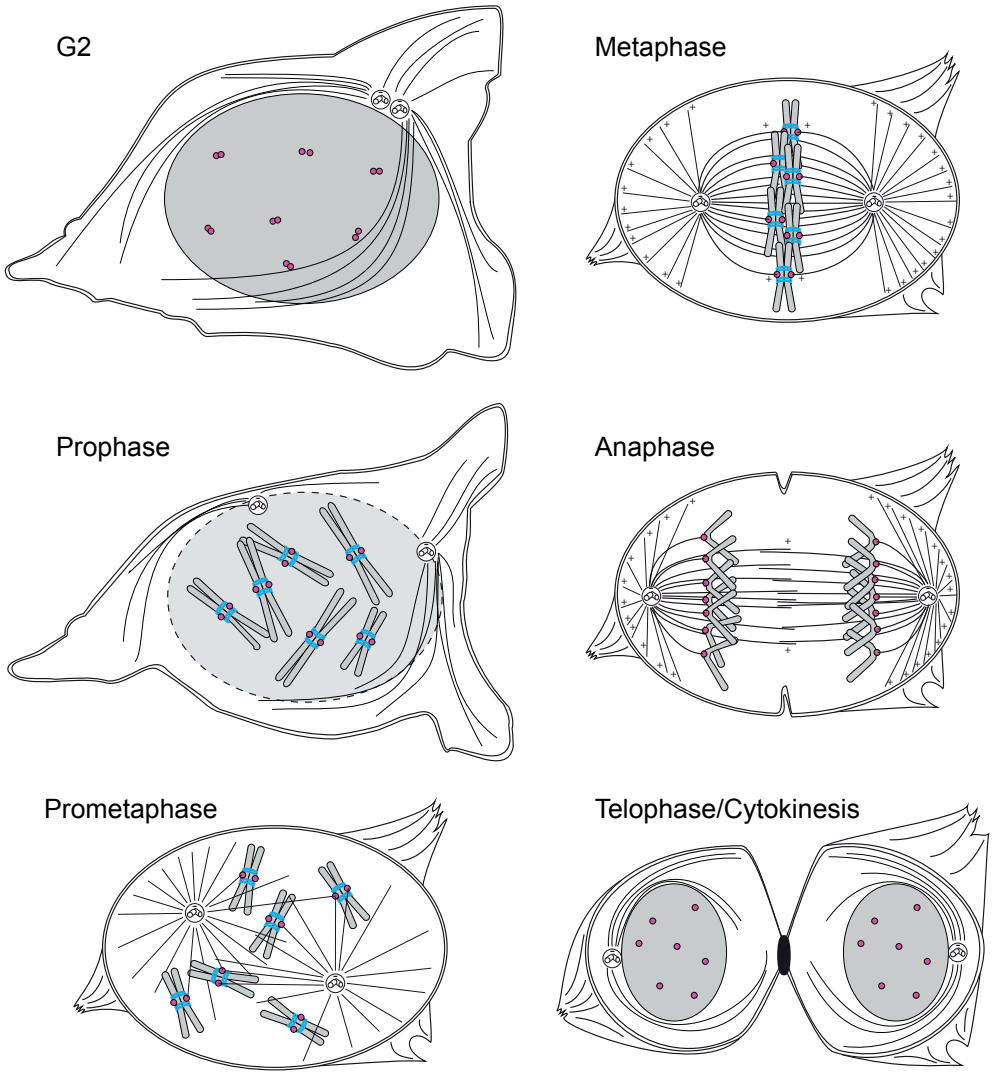

Figure 1: **The phases of mitosis**. Schematic model of the changes in cellular morphology during mitotic progression. Nucleus depicted in grey, kinetochores in magenta, cohesin rings in blue. Plus and minus signs indicate microtubule polarity.

forms the microtubule-interaction surface, is decorated by a so-called fibrous corona. It is not well understood which proteins make up this corona, but it likely composes the microtubule-binding interface of the kinetochore (*3-6*).

There is large variation in centromere size among eukaryotes, from holocentromeres that stretch the length of entire chromosomes in *C. elegans* to genetically defined point centromeres in budding yeast that stretch 120 bp of DNA (reviewed in *7*). In human cells, centromeres are enriched in α-satellite DNA repeats (8), which contain 17 bp CENP-B boxes (9) that bind centromere protein B (CENP-B; 10, 11). These repeats are, however, neither sufficient nor essential for centromere identity (reviewed in

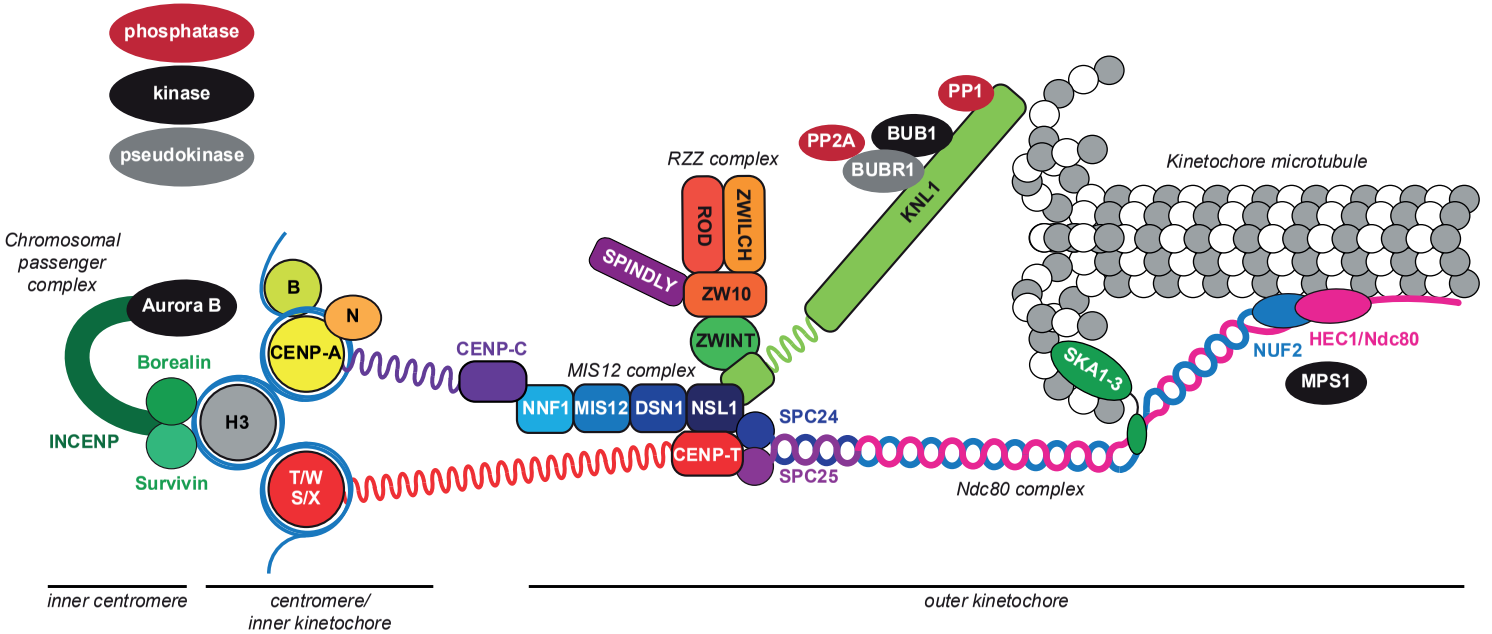

Figure 2: **Molecular organization of the centromere, the KMN network and associated proteins**. Schematic model of the kinetochore. The KMN network is formed by KNL1, the MIS12 complex and the Ndc80 complex. The SKA complex is recruited to the Ndc80 complex upon microtubule attachment. CCAN not depicted for simplicity. DNA depicted as blue line.

7). Instead, centromeres are specified epigenically by nucleosomes that contain a specialized histone H3 variant, CENP-A (12-15), and by nucleosomes that are composed of CENP-T/W/S/X (*16, 17*; Figure 2). These CENP-A and CENP-T containing nucleosomes are interspersed with canonical histone H3 nucleosomes that carry H3K4me2 (*18*) or H3K9me3 modifications (*19*). Together, CENP-A and CENP-T nucleosomes allow the assembly of a constitutive centromere-associated network (CCAN) that is composed of at least 12 other CENPs (CENP-C, CENP-H, CENP-I, CENP-K, CENP-L, CENP-M, CENP-N, CENP-O, CENP-P, CENP-Q, CENP-R, CENP-U; reviewed in *20*). The details of CCAN assembly, and the extent to which CCAN proteins contribute to kinetochore assembly and the regulation of kinetochore-microtubule interactions remain largely unclear (reviewed in *20*). However, current models pose that at least two kinetochore assembly pathways connect the inner and the outer kinetochore.

One such pathway originates at CENP-A nucleosomes, which recruit both CENP-N and CENP-C (*21-24*). CENP-C in turn interacts with the NNF1 (also known as PMF1) subunit of the outer kinetochore MIS12 complex (*25-27*). Another assembly pathway is dependent on CENP-T nucleosomes. The elongated N-terminal tail of CENP-T reaches out from the inner kinetochore, where it binds directly to the outer kinetochore Ndc80 complex and (weakly) to the MIS12 complex (*26, 28*). When co-localized to ectopic chromosomal sites, N-terminal fragments are sufficient for the assembly of the core outer kinetochore (*26*). The N-terminal tail of CENP-T forms a flexible linker between the inner and the outer kinetochore, that is stretched upon kinetochore biorientation (*3*). This is likely also true for CENP-C.

Spindle microtubules attach directly to the outer kinetochore (*5, 6*). The kinetochore-microtubule binding interface is formed by the KNL1, MIS12 and Ndc80 complexes, which together form the 10-protein KMN network (*29-31*). The KMN network contains two distinct microtubule-binding sites. One of these is located in KNL1 (also known as Blinkin, AF15q14, CASC5, Spc7 and Spc105) which binds directly to microtubules by an N-terminal basic patch (*29, 32, 33*). KNL1 is a large, mostly unstructured, protein that functions as a scaffold for the recruitment of the spindle assembly checkpoint (SAC) proteins BUB1, BUBR1 and BUB3, the RZZ complex and the phosphatase PP1γ (*34-36*). BUB1 and BUBR1 interact directly with KNL1 via two so-called KI motifs in the N-terminal region of KNL1 (*34, 37, 38*). The KNL1-BUB1 interaction is additionally mediated by BUB3-dependent binding to a series of MELT motifs in KNL1 (*39-42*).

The main microtubule-binding interface in the KMN network resides in the Ndc80 complex (*29, 43*), that is composed of HEC1 (also known as Ndc80), NUF2, SPC24 and SPC25 (*44*). Depletion of Ndc80 network components precludes the formation of stable kinetochore-microtubule attachments (*44-47*). The microtubule-binding interface itself is composed of two calponin-homology (CH) domains that reside in the N-terminal regions of HEC1 and NUF2 and the basic N-terminal tail of HEC1 (*48-53*). The Ndc80 complex has an elongated structure, which enables the microtubule-binding domains of HEC1 and NUF2 to reach outwards from the KMN network into the cytosol (*49*). The MIS12 complex, which is formed by DSN1, NNF1, NSL1 and MIS12 (*54*) is important for kinetochore assembly by binding directly to KNL1 and the Ndc80 complex (*55*). The MIS12 complex does not interact with microtubules directly, but does increase the microtubule-binding affinity of the KMN network *in vitro* (*29*). An additional microtubule-binding capacity is provided in budding yeast by the Dam1 complex (*56, 57*), which allows kinetochore plus-end tracking by oligomerizing as ring structure around microtubule bundles. Presumably, this ring-like organization of Dam1 allows kinetochore sliding on a depolymerizing microtubule, and docking to the Ndc80 complex (*58-64*). In mammalian

cells, a similar function is fulfilled by the SKA complex, although it bears no sequence homology to the Dam1 complex, and does not appear to form ring-like structures. (*65-69*). The SKA complex also binds the Ndc80 complex and allows kinetochores to track depolymerizing microtubules by binding to curving protofilaments (*70, 71*).

An important auxiliary kinetochore complex is the RZZ complex, which consists of ROD1, Zwilch and ZW10 (reviewed in *72*). The RZZ complex docks to the C-terminal region of KNL1, via the intermediate Zwint-1 (*34*). The RZZ module does not appear to be involved in kinetochore structure or kinetochore-microtubule attachment, but functions predominantly by mediating the kinetochore binding of dynein. Dynein, a minus-end directed motor complex, is recruited to RZZ via a direct interaction between ZW10 and the dynein subunit p50/dynamitin (*73, 74*). Dynein drives the poleward movement of misaligned chromosomes in prometaphase, but this is independent of the kinetochore localization of dynein (*75-77*). Kinetochore dynein appears to contribute to mitotic progression mainly by stripping the SAC proteins MAD1 and MAD2 from kinetochores upon microtubule attachment (*69, 76, 78-80*), an important mechanism for SAC silencing (discussed later), and by facilitating poleward chromosome movements during anaphase (*81, 82*). The RZZ subunit ZW10 is also required for SAC activation, likely by mediating the kinetochore recruitment of MAD1 and MAD2 (*83-85*).

Moving chromosomes around: microtubules, motors and force generation

Directly after nuclear envelope breakdown, the duplicated chromosomes are spread out in the center of the cell, near the future spindle equator (*2*). At this time, kinetochore-microtubule attachments are initiated. Microtubule bundles form long polarized protofilaments that associate into a microtubule lattice. These bundles are nucleated from their minus end at centrosomes. The plus end of the microtubule bundle grows dynamically to form an array that stretches into the cytosol. Individual tubulin dimers exist in solution in a GTP-bound state. Upon polymerization into a bundle, one of the GTP moieties in a tubulin dimer is hydrolyzed to GDP. This weakens the intermolecular bonds and destabilizes the microtubule bundle. However, microtubule bundles grow and shrink from their ends. Therefore, the conversion of GTP to GDP does not cause the microtubule bundle to depolymerize as long as the microtubule plus-end is capped by stable GTP-containing tubulin. As long as the rate of microtubule growth exceeds the speed of GTP to GDP hydrolysis, the microtubule bundle is allowed to grow. However, loss of the GTP cap results in rapid depolymerization of the microtubule bundle. This is known as microtubule catastrophe. Therefore, microtubules grow by slow polymerization and shrink by rapid depolymerization. This creates a state of dynamic instability (reviewed in *86*). The dynamic growth of numerous tubulin bundles from the centrosomes into the cytosol allows the spindle to stochastically attach to chromosomes, in a manner termed “search and capture”, first proposed by Kirschner and Mitchison (*86*). However, additional mechanisms exist to bias the search. These include microtubule nucleation by kinetochores, and a RanGTP gradient that enhances MT growth near the chromosomes (*87-90*).

Importantly, microtubule bundles are stabilized by end-on attachments to kinetochores that are under force (*91*). This prevents microtubule catastrophe and allows for the formation of stable kinetochore-microtubule interactions. Individual kinetochores are attached by 20-40 microtubules (*92*), that are collectively referred to as kinetochore fibers (K-fibers). Depolymerization of an individual microtubule does therefore not cause the detachment of an entire kinetochore. Thus, the microtubule bundles can grow and shrink while remaining attached to kinetochores. This essentially tethers chromosomes to a dynamically growing and shrinking cable which provides a pulling and

pushing force. And as chromosomes in mitosis exist in duplicated pairs, this means that attachment of sister kinetochores by microtubules of opposing spindle poles subjects the kinetochores to tension. This tug of war between the opposing spindle poles results in alignment of bioriented chromosomes at the spindle equator.

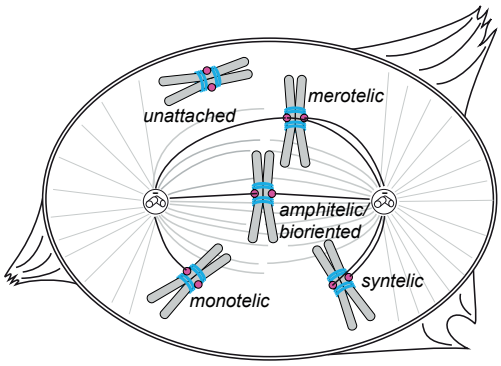

Figure 3: **The modes of kinetochore attachment.** Schematic model of possible kinetochore-microtubule attachments in human cells. Kinetochores depicted in gray, cohesion rings in blue, microtubules in black and gray.

In addition, chromosome alignment is aided by the activities of several kinetochore-based motor proteins. Laterally-attached chromosomes are transported towards the spindle poles by the minus-end directed motor dynein (*75, 82*). From here, mono-oriented chromosomes can slide towards the spindle equator along established K-fibers. This is mediated by the activity of the processive plus-end directed motor CENP-E (*93*). Upon biorientation, the forces that are exerted on the sister kinetochores by K-fibers are balanced by the kinetochore in order to prevent overstretching. This causes kinetochore pairs to oscillate along the metaphase plate, meaning that while one of the kinetochores is moving poleward, the sister kinetochore is moving antipoleward (*94*). Kinetochore oscillation is a complex process that requires opposite activities of several motors at the two kinetochores. Poleward motion is mediated by the microtubule depolymerizing motor MCAK. Antipoleward movement is mediated by polar ejection forces (pushing forces that are exerted on the chromosome arms) that are controlled by the chromokinesins Kid and KIF4A. The amplitude of the oscillation is controlled by KIF18A, which accumulates at microtubule plus ends. There, KIF18A suppresses microtubule growth in a length-dependent manner (*95-97*). Together, these activities moderate chromosome movement upon alignment to ensure that chromosomes remain clustered together on the metaphase plate.

Error correction and Aurora B

In order to faithfully divide the duplicated chromosomes in such a way that both daughter cells inherit a single copy of each chromosome, it is essential that the sister chromatids are attached by K-fibers from opposite poles of the mitotic spindle (bioriented). However, the formation of kinetochore-microtubule attachments is a stochastic process. Many erroneous attachments are formed during prometaphase and these need to be corrected. Different types of erroneous attachments can occur (Figure 3): on mono-oriented chromatids, only a single kinetochore on a duplicated set of chromatids is attached. The sister kinetochores may also be attached by two K-fibers from the same spindle pole, which is referred to as a syntelic attachment. It is also possible that one of the sister kinetochores is attached by a K-fiber from one pole, while the other kinetochore is bound by microtubules that emanate from both spindle poles. This is known as merotely. Syntelic or merotelic attachments do not activate the SAC (discussed in detail later), but will cause chromosomal segregation errors if left uncorrected.

The resolution of erroneous kinetochore-microtubule attachments (error-correction) is mediated

by phospho-regulation of the KMN network at the kinetochore-microtubule binding interface, by the kinase Aurora B. Together with the regulatory subunits INCENP, Survivin and Borealin, Aurora B forms the chromosomal passenger complex (CPC; reviewed in *98*). The role of phosphoregulation in error correction was discovered in budding yeast by perturbations of the PP1 homolog Glc7 or the Aurora B kinase homolog Ipl1. Deletions of Glc7 or Ipl1 cause a SAC-dependent metaphase arrest as a result of disrupted kinetochore-microtubule attachments (*99, 100*). In human cells, Aurora B inhibition causes chromosome alignment defects and a high incidence of syntelic attachments, that are not corrected (*101, 102*).

Whereas the microtubule-binding sites of the KMN network are localized at the outer kinetochore, the CPC resides at the inner centromere. The CPC is activated by its accumulation at the inner centromere via Haspin-dependent phosphorylation of histone H3 and BUB1-dependent phosphorylation of H2A (*103-107*). These epigenetic marks create a high concentration of Aurora B at the inner centromere, which stimulates transactivation of the kinase. From there, a diffusion gradient of active kinase allows Aurora B activity to extend out to the outer kinetochore when kinetochores are unattached (*108*). This is supported by the observation that a population of active Aurora B kinase is enriched at the outer kinetochore in early prometaphase (*109*).

The difference in location between kinase and substrates has led to the model that error-correction is directly regulated by kinetochore stretching (*110*). As stably attached K-fibers still undergo microtubule flux, bioriented kinetochores are put under tension by pulling forces that are exerted on both sister kinetochores. These forces cause kinetochore stretching and thereby increase the distance between the inner centromere and the outer kinetochore (*3, 111, 112*). As a result, Aurora B is spatially separated from its substrates in the outer kinetochore. Thereby, biorientation would enable dephosphorylation of the KMN network. This model is supported by several lines of evidence: phosphorylation of Aurora B substrates is high on misaligned chromosomes and suppressed upon alignment (*33, 110*). Unreplicated minichromosomes, which can attach to only a single K-fiber in budding yeast and therefore do not form stable attachments, remain attached to the spindle pole body in the absence of Ipl1/Aurora B activity (*113*). Furthermore, kinetochore-microtubule attachments are stabilized by tension in cells (*114*) and *in vitro* (*91*). Finally and most importantly, the phosphorylation of Aurora B substrates is dependent on the distance between kinase and substrate (*110*). However, in budding yeast, chromosomal biorientation is not dependent on the localization of the CPC to centromeres. Instead, CPC clustering on microtubules or chromatin may be sufficient for Aurora B activation and error correction (*115*). Since budding yeast kinetochores cannot form merotelic attachments, error correction is likely to be less complicated in budding yeast than in mammalian cells. Therefore, error correction in *S. cerevisiae* may not require finely tuned regulation. The resolution of erroneous attachments is mediated mainly via phosphorylation of the KMN network. Aurora B directly phosphorylates the KMN network proteins DSN1, KNL1 and HEC1 and thereby directly regulates the affinity of the main microtubule-binding interfaces for K-fibers (*29, 33, 43*). Preventing HEC1 phosphorylation, by mutation of the Aurora B-dependent phosphorylation sites, enhances kinetochore stretching and causes premature anaphase with unaligned chromosomes (*43, 50*). Aurora B phosphorylates DSN1, KNL1 and HEC1 in a graded, tension-dependent manner. As the KMN substrates are not equidistant from the inner centromere, this allows the kinetochore affinity for microtubules to be finely tuned in response to kinetochore tension (*33*). Aurora B additionally phosphorylates the Dam1 complex in *S. cerevisiae* (*116*) and the SKA complex in metazoans (*117, 118*). Aurora B-dependent phosphorylation of the SKA complex regulates its microtubule-binding

affinity as well as its recruitment to kinetochores (*117, 118*).

Aurora B activity at kinetochores is antagonized by PP1 and PP2A phosphatases (*36, 119, 120*). PP2A is recruited to prometaphase kinetochores in complex regulatory subunits of the B56 family via a direct interaction with BUBR1. This ensures the formation of stable kinetochore-microtubules, presumably by allowing dynamic phosphorylation of the KMN network in prometaphase (*120-123*). In contrast, PP1 is maximally recruited to kinetochores in metaphase. PP1 is localized by kinetochores by docking to two N-terminal PP1-binding motifs in KNL1 and this is opposed by Aurora B-dependent phosphorylation of these motifs (*36* and chapter 3 of this thesis). PP1 suppresses the phosphorylation of Aurora B substrates in the KMN network (*36*). Therefore, the inactivation of Aurora B by its spatial dislocation is coupled with the activation of an antagonizing phosphatase and this allows a rapid dephosphorylation of the KMN network and stabilization of kinetochore-microtubule attachments before anaphase onset.

Inhibiting anaphase onset: the anaphase promoting complex and the SAC

Cyclin B/CDK1 and the anaphase promoting complex

Progression through the cell cycle is mediated by the phased expression and degradation of cyclin proteins. Cyclins are regulatory subunits that determine the activity and substrate specificity of the cyclin-dependent kinases (CDK; reviewed in *124*). In mitosis, CDK1 forms a complex with Cyclin B. Cyclin B-CDK1 establishes a vast number of mitosis-specific phosphorylations. These phosphorylations drive the extensive rearrangements of cellular organization in prophase and, in general, maintain a mitotic state. (*125, 126*). Thus, mitotic entry is triggered by increasing levels of Cyclin B-CDK1 activity and this defines the start of prophase (*127*). Conversely, CDK1 inactivation, by proteasomal degradation of Cyclin B, initiates the metaphase to anaphase transition and mitotic exit. Cyclin B is targeted for proteasomal destruction by the anaphase promoting complex or cyclosome (APC/C; Fig. 4A; *128, 129*). The APC/C is a large multi-subunit ubiquitin E3 ligase that controls mitotic progression by targeting many substrates for proteasomal degradation. In addition to Cyclin B, a key APC/C substrate is Securin (*130-133*). Securin is an inhibitor of the protease Separase, that cleaves the Scc1 subunit of the cohesion complex. This resolves sister chromatid cohesion and allows the initiation of anaphase (*134-136*).

The APC/C is composed of 16 subunits (reviewed in *137*) that structurally assemble to form three domains: a catalytic core, a platform and an “arc lamp” fold (*138-140*). These domains surround a cavity that forms an interaction interface for substrates and regulatory cofactors. APC/C substrate specificity is defined by the coactivators CDH1 or CDC20. These are recruited sequentially: the APC/C is activated by CDC20 from prophase until early anaphase, when CDC20 is degraded. Subsequently, the APC/C switches to CDH1, which maintains APC/C activity through mitotic exit and G1 (reviewed in *141*). CDC20 and CDH1 bind to the APC/C by docking to CDC27, in the bottom of the arc lamp overhang (*138, 142, 143*). APC/C^{CDC20} forms two separate substrate recognition motifs: a cleft between CDC20 and APC10 allows the docking of D-box degrons (*144, 145*), whereas a depression on the surface of CDC20 allows the binding of KEN-box degrons (*146, 147*). APC/C substrate ubiquitination is initiated by the E2 enzyme UBCH10 (*148, 149*). Another E2, UBE2S, subsequently associates with the APC/C to allow ubiquitin chain elongation and as such promotes APC/C processivity (*150, 151*). APC/C activity is countered by the deubiquitinating enzyme (DUB) USP44 (*152*).

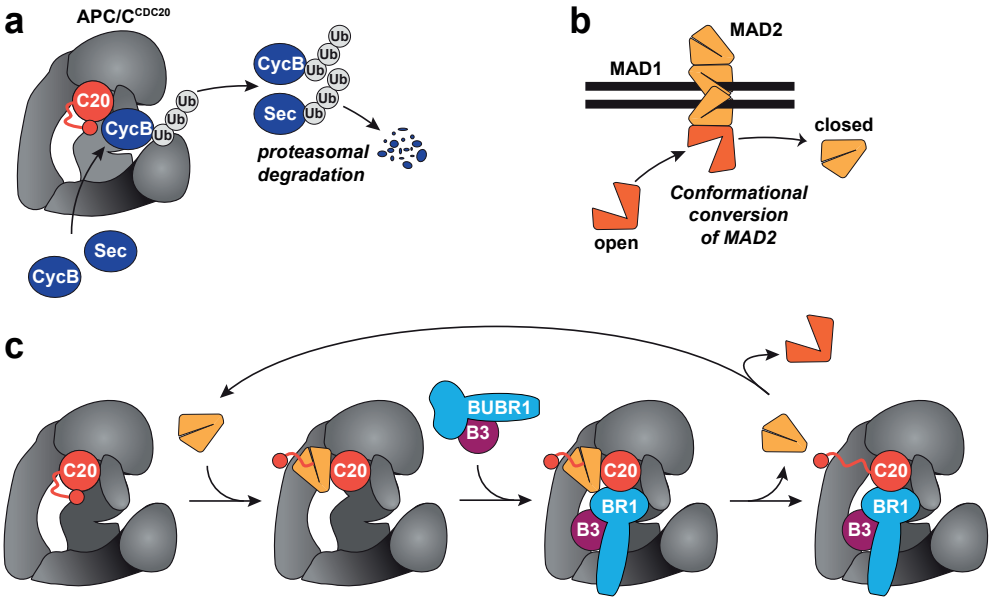

Figure 4: **Mechanism of APC/C inhibition by the MCC.** (**A**) Schematic model that depicts substrate ubiquitination by APC/C^{CDC20}. (**B**) Schematic model of MAD2 conformational conversion by dimerization to C-MAD2-MAD1 heterotetramers. (**C**) Speculative model of MCC loading onto APC/C^{CDC20}. C-MAD2 binding induces a conformational change in CDC20 and thereby enables loading of BUBR1-BUB3 onto APC^{CDC20}. However, C-MAD2-CDC20 or pre-assembled MCC may be loaded as a complex instead. C-MAD2 is subsequently released and either converted to O-MAD2 or recycled to bind another APC^{CDC20} molecule. APC/C is depicted in gray. C20: CDC20; CycB: Cyclin B; Sec: Securin; Ub: ubiquitin; B3: BUB3; BR1: BUBR1. See section "Inhibiting anaphase onset: the anaphase promoting complex and the SAC" for details.

The spindle assembly checkpoint

To ensure that both daughter cells inherit an uncompromised and complete set of chromosomes, it is essential that anaphase onset is prevented until the mitotic spindle has been formed and all chromosomes have been correctly attached by spindle microtubules. A mitotic feedback network, termed the spindle assembly checkpoint (SAC) or mitotic checkpoint, has evolved to ensure that cells arrest in mitosis when kinetochore-microtubule attachments are compromised. Anaphase onset is halted by the SAC until the last unattached kinetochore has been attached or destroyed (*153, 154*). The SAC was identified in a seminal set of genetic screens in budding yeast where viability in the presence of spindle poisons was found to be dependent on the MAD (mitotic-arrest-deficient) proteins MAD1, MAD2 and MAD3 (also known as BUBR1 in vertebrates and flies) and the BUB (budding-uninhibited by benomyl) proteins BUB1 and BUB3 (*155, 156*). The subsequent observation that MPS1 was required for a SAC response to nocodazole completed the identification of the core SAC proteins (*157*). However, many other proteins contribute to SAC signaling indirectly by controlling the kinetochore localization or activation of SAC proteins.

Inhibition of the APC/C is key to protect Cyclin B and Separase from proteasomal degradation and thereby maintain a mitotic state. It is therefore not surprising that the SAC functions by suppressing APC/C activity. The SAC is generated at unattached kinetochores, but suppresses APC/C activity by producing an inhibitory complex that can freely diffuse to bind cytosolic APC/C. This inhibitor,

termed the mitotic checkpoint complex (MCC), has been proposed to consist of BUBR1, BUB3 and MAD2, which have all been found interact with CDC20 and the APC/C during mitotic arrest (*158-165*). However, the reported stoichiometry of MCC components has been inconsistent between studies, and as such the identity of the APC/C inhibitor has thus been a matter of controversy (*146, 164, 166, 167*).

MCC production is critically dependent on the conformational conversion of MAD2 at kinetochores. Extensive structural work has demonstrated that MAD exists in an open and closed conformation (O-MAD2 and C-MAD2; *168-172*). Free cytosolic MAD2 is predominantly in the energetically favorable open conformation. The less abundant C-MAD2 is found in complex with MAD1 or CDC20 (*168, 171, 173, 174*). The structural conversion of MAD2 is facilitated by dimerization of the O-MAD2 to C-MAD2 (*175*). As a pool of C-MAD2 is stably associated with MAD1, kinetochore based MAD1-C-MAD2 dimers are thought to transiently recruit cytosolic O-MAD2. Upon dimerization with C-MAD2, O-MAD2 is converted to C-MAD2 and released (*175-177*; model in Fig. 4B). MAD2 mutants that are fixed in the open conformation or unable to dimerize cannot engage the SAC (*169, 175, 178*). At high levels, MAD2 can directly inhibit the APC/C by sequestering CDC20 (*158, 162, 164*). However, at physiological concentrations, *in vitro* APC/C inhibition requires both MAD2 and BUBR1-BUB3 (*164, 167, 179*), and BUBR1 appears a more potent inhibitor of the APC/C (*165, 180*). Indeed, Han and coworkers showed that C-MAD2 is required to load BUBR1-BUB3 onto APC/C^{CDC20}, after which MAD2 becomes dispensable for APC/C inhibition *in vitro*. Moreover, if MCC disassembly was prevented, MAD2 was also dispensable for the maintenance of the SAC after it had been established. In contrast, BUBR1 was essential in all conditions tested. Together these findings demonstrated that BUBR1-BUB3 is the predominant APC/C^{CDC20} inhibitor. In addition, MAD2 was shown to release an intramolecular association within CDC20, which allowed a previously masked docking site on CDC20 to bind BUBR1-BUB3. This suggests a model for APC/C inhibition (Fig. 4C) in which dimerization of MAD2 at kinetochores drives the production of C-MAD2. C-MAD2 then induces a structural rearrangement of APC/C-associated CDC20. Thereby, C-MAD2 allows loading BUBR1-BUB3 onto APC/C^{CDC20}. MAD2 is subsequently released, to facilitate the loading of additional BUBR1 molecules into inhibitory complexes. This would allow C-MAD2 to cytosolically amplify the inhibitory signal that is initially generated at kinetochores. This model could explain how a single unattached kinetochore can produce sufficient MCC to halt anaphase onset (*179*).

While the roles of MAD1, MAD2, BUBR1 and BUB3 in the SAC have been well characterized, this is less so for the roles of BUB1 and MPS1. The kinase BUB1 may contribute to SAC signaling via several mechanisms. BUB1 stimulates kinetochore recruitment of BUBR1, MAD1 and MAD2 (*181-184*). These activities require the kinetochore localization of BUB1 but not its kinase activity, and this is true in most model organisms (*183-188*). BUB1 may therefore function as a scaffold for SAC proteins at kinetochores. Nevertheless, BUB1 kinase activity has been proposed to contribute to SAC activity. *In vitro*, BUB1 can inhibit the APC/C directly via phosphorylation of CDC20 (*189, 190*). Perhaps more importantly, BUB1 kinase activity in cells also functions to activate Aurora B. BUB1-dependent phosphorylation of H2A promotes the binding of Shugoshin to centromeric H2A-containing nucleosomes (*105, 107, 191-193*). Shugoshin in turn recruits the CPC via Borealin (*106*) and this drives centromeric clustering of the CPC and subsequent activation of Aurora B (*108, 194*). As Aurora B impinges on the SAC by controlling the kinetochore localization of MPS1 (*195, 196* and discussed hereafter), this pathway constitutes an important mechanism of SAC activation.

MPS1

Monopolar spindle 1 (MPS1) is an essential SAC kinase in eukaryotes (*157, 197-202*), with the possible exception of *C. elegans*, in which no MPS1 homolog has been identified. The kinase activity of MPS1 is required to maintain a metaphase delay in an unperturbed mitosis and to maintain a mitotic arrest in response to nocodazole (*198, 203-205*). Inhibition or depletion of MPS1 causes early anaphase onset with lagging chromosomes (*204, 205*), which can culminate in chromosomal translocations (*206*).

The kinase domain of MPS1 is located C-terminally (Fig. 5A). The N-terminal region shares sequence homology with BUB1 and BUBR1 (reviewed in *207*) and is required for kinetochore localization of MPS1 (*208, 209*). The structural and functional characteristics of the kinetochore-binding module of MPS1 are addressed in chapter 2 of this thesis. The ~300 amino acids that stretch between the kinase and kinetochore localization domains have not been characterized functionally or structurally. MPS1 exists as a dimer in cells, but it remains to be determined if this is functionally important or regulated (*210-212*).

MPS1 function in the SAC

Several lines of evidence suggest that MPS1 is the dominant activator of the SAC. In budding yeast, Mps1 overexpression induces a mitotic arrest by causing persistent SAC activation in the absence of spindle abnormalities (*213, 214*). Similarly, artificially tethering MPS1 to kinetochores causes human cells to arrest in metaphase with high kinetochore levels of MAD1 and MAD2 (*215*). It however remains enigmatic how MPS1 performs its critical role in the SAC.

MPS1 has been suggested to activate the SAC via several mechanisms (Fig. 5B). Its activity is required for the kinetochore loading of BUB1 by phosphorylation of the KNL1 MELT motifs (*39, 41, 42*). In fungi, this is required for SAC maintenance. In addition, MPS1 activity ensures kinetochore binding of MAD1 and MAD2 (Fig. 5B; *198, 204, 205, 208, 210, 215-218*), but this could be indirect through its impact on BUB1. Importantly, artificially tethering MAD1 to kinetochores arrested cells in metaphase, but this arrest was still dependent on MPS1 activity (*219*). MPS1 thus has functions downstream of MAD1 kinetochore binding. In line with this, MPS1 is needed for the binding of O-MAD2 to C-MAD2-MAD1 at kinetochores in mammalian cells (Fig. 5B), although it is not required for MAD2 dimerization *in vitro* (*177*). Studies in fission yeast have indicated that the MPS1 homolog Mph1 can stimulate the SAC by phosphorylation of MAD2 (*220*). Therefore, both in fission yeast and human cells, MPS1 may impinge on the SAC by regulating the conformational conversion of Mad2.

In addition to BUB1, MAD1 and MAD2, MPS1 has been reported to localize CDC20, Spindly, PLK1, Zwilch and ZW10 to kinetochores (*210, 216-218*). The dependence of CENP-E and BUBR1 localization on MPS1 is more controversial. (*198, 204, 208, 210, 216, 218*). Indeed, the kinetochore localization of all these proteins may be directly mediated by BUB1. Finally, in budding yeast, Mps1 has been implicated in SAC activation by phosphorylation of the microtubule-binding domain of Ndc80/HEC1 (*221*). It is however unclear how this activity could activate the SAC.

Other functions of MPS1

Separately from its role in the SAC, MPS1 stimulates chromosome biorientation by promoting error correction (*205, 222*). Inactivation of MPS1 results in chromosome alignment defects (*205, 210, 216-218*). These defects result from the impaired centromere localization and activation of Aurora

B following MPS1 inactivation (*194, 205*). MPS1 activates Aurora B by phosphorylation of the CPC protein Borealin (Fig. 5B), which stimulates its dimerization (*205, 223*). MPS1 also stimulates Aurora B activation via the kinetochore recruitment of BUB1. BUB1 phosphorylates centromeric H2A, and this in turn recruits Borealin to centromeres via the intermediate Shugoshin (*107, 194*). Moreover, in budding yeast, MPS1 has been proposed to stimulate the formation of stable kinetochore-microtubule attachments by phosphorylating Dam1 (*224*). In addition to its role in error correction, MPS1 may also promote biorientation by driving CENP-E dependent chromosome congression. *Xenopus* Mps1 phosphorylates the C-terminal tail of CENP-E *in vitro* (*225*). This relieves autoinhibition of the CENP-E motor and thereby stimulates CENP-E motility. It however remains unknown if MPS1-dependent CENP-E phosphorylation is functionally relevant in cells.

Mps1 was originally identified in budding yeast, where it was demonstrated to be involved in spindle pole body duplication (*226*). MPS1 has been suggested to have a similar function in the control of centrosome duplication in mammalian cells. A reduction in MPS1 levels in S-phase by CDK2-dependent phosphorylation and subsequent destabilization of MPS1 is suggested to prevent MPS1-dependent phosphorylation of centrin-2 and centrosome reduplication (*200, 227-229*). However, this role of MPS1 in centrosome duplication remains controversial (*199, 208, 209*).

MPS1 has been proposed to drive tumorigenesis in oncogenic B-RAF-expressing melanoma cells. In these cells, oncogenic B-RAF has been reported to stabilize and activate MPS1 (*230*) and thereby drive

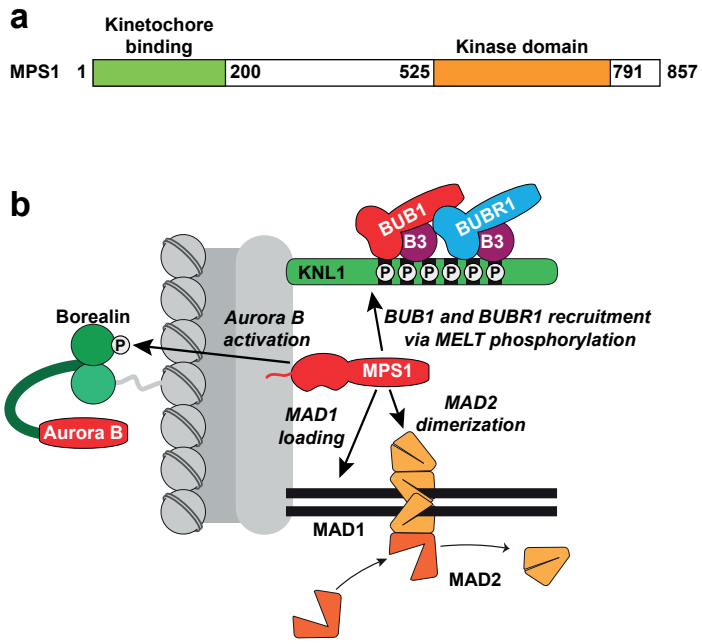

Figure 5: **Structure and functions of MPS1.** (**A**) Schematic model of the domain organization of human MPS1. (**B**) Model showing the functions of MPS1 in the SAC and error-correction. B3: BUB3; P: phosphorylation event. See section "MPS1" for details.

chromosomal instability (*231*). Moreover, MPS1 has been reported to inhibit B-RAF/ERK signaling by activation of PKB/AKT signaling. The mechanism of this, which has been proposed to be independent of MPS1 kinase activity, is however unclear (*232*). MPS1 has also been reported to be involved in DNA damage checkpoint signaling, by activation of CHK2. *In vitro*, MPS1 directly binds and phosphorylates CHK2 (*233*). In turn, CHK2 upregulates MPS1 expression in DNA-damaged cells, which creates a reciprocal activation cascade between MPS1 and CHK2 (*234*). Indeed, MPS1-depleted cells fail to arrest in response to DNA damage, possibly as a result of defective CHK2 activation (*233*). MPS1 may also stimulate DNA damage-repair by activating the RecQ-helicase BLM (*235*).

Regulation of MPS1 kinetochore localization

MPS1 is recruited to unattached kinetochores and this is required for activation of the SAC (*195, 198, 208*). The kinetochore receptor for MPS1 however remains elusive. In *S. cerevisiae*, Mps1 has been reported to bind directly to the microtubule-binding domain of Ndc80/HEC1 (*221*). Indeed, the kinetochore localization of MPS1 depends on the CH domain of HEC1 in human cells (chapter 2 of this thesis; *47, 199, 236*).

The accumulation of MPS1 at kinetochores promotes MPS1 autoactivation by creating a sufficiently high concentration of kinase in the vicinity of kinetochores. Such high concentrations cause MPS1 to self-activate by autophosphorylation of the kinase activation loop (*237-239*). As MPS1 activity additionally promotes its own release from kinetochores, MPS1 opposes its own activity by moderating the levels of active kinase at kinetochores (*215*). It is however unknown how MPS1 regulates its own turnover: MPS1 is extensively autophosphorylated, but none of these phosphorylations have been reported to perturb MPS1 localization (*125, 238-244*). On the contrary, autophosphorylation of MPS1 at Thr12 and Ser15 has been suggested to be required for MPS1 localization (*243*). However, other individual phosphorylations could negatively regulate MPS1 kinetochore localization.

Other kinases also impinge on MPS1 localization. MAPK phosphorylates MPS1 *in vitro* and this is required for Mps1 kinetochore localization in *Xenopus* egg extracts (*245*). In addition, kinetochore localization of MPS1 depends on Aurora B activity (*195, 196*). Aurora B activity stimulates the rapid and potent kinetochore recruitment of MPS1 in prophase. Thereby, Aurora B potentiates activation of the SAC (*195*). Regulation of MPS1 kinetochore localization by Aurora B is addressed in chapters 2 and 3 of this thesis.

Silencing the spindle assembly checkpoint

Upon the attachment of the last unattached kinetochore, the SAC is rapidly silenced and the inhibition of the APC/C is relieved (*153, 154, 246*). Efficient SAC silencing is dependent on several pathways: MCC formation is halted upon the attachment of individual kinetochores during prometaphase. This is mediated by selective removal of SAC components from attached chromosomes (Fig. 6A). Additionally, selective recruitment of PP1 phosphatase to bioriented chromosomes ensures dephosphorylation of the outer kinetochore (Fig. 6A). Thereby, PP1 likely counters phosphorylations that engage the SAC. In metaphase, APC/C inhibition is relieved by disassembly of APC/C^{MCC} (Fig. 6B). Moreover, cytosolic amplification of the SAC signal by C-MAD2 is likely blocked in metaphase. Together, these mechanisms ensure inhibition of the APC/C until attachment of the last kinetochore but also rapid activation of the APC/C once that last attachment has been made.

Removal of SAC components from attached kinetochores

Several SAC proteins, including MAD1 and MAD2 are depleted from attached kinetochores by dynein-dependent stripping along K-fibres (Fig. 6A; *76, 78-80*). Dynein is a multi-subunit minus-end directed microtubule motor complex, which can associated with numerous adaptor proteins that regulate localization and activation of the complex (*247*). Inhibition of the release of cargo from the dynein motor complex causes the accumulation of MAD1 and MAD2 proteins at spindle poles (*76, 248-250*). Although depletions of many dynein subunits cause a mitotic delay indirectly by disrupting spindle assembly and chromosome alignment defects (*77, 251, 252*), depletions of dynactin subunits specifically induce a SAC-dependent metaphase delay in the absence of chromosomal congression

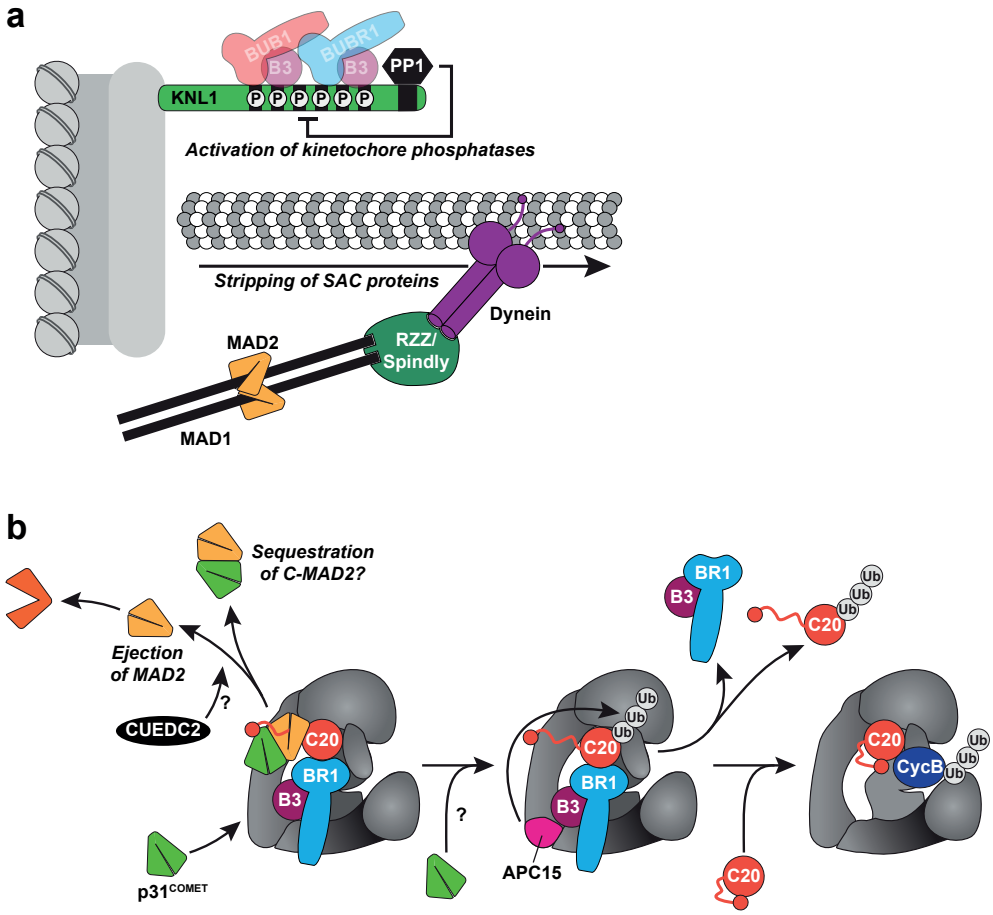

Figure 6: **Mechanisms of SAC silencing.** (**A**) Model of SAC silencing at kinetochores. Kinetochore-localized PP1 mediates the dephosphorylation of the KMN network, including the MELT motifs of KNL1. Minus-end directed motor activity of kinetochore dynein strips MAD1/MAD2 towards spindle poles. (**B**) Model of MCC disassembly. Ejection of C-MAD2 from APC/C^{MCC} is mediated by p31^{comet} and possibly by CUEDC2. Ejected C-MAD2 is converted to O-MAD2 or possibly sequestered by p31^{comet}. Dissociation of BUBR1-BUB3 from APC/C^{CDC20} is mediated by CDC20 ubiquitination. This is stimulated by APC15. BUBR1-BUB3 ejection may also be stimulated by p31^{comet}. See section "Silencing the spindle assembly checkpoint" for details.

defects (*77*). This is most likely due to the role of dynactin in localizing dynein specifically to kinetochores. Like dynactin, the protein Spindly is also required for kinetochore binding of dynein, even though no direct interaction between Spindly and dynein has been reported (*77, 248, 249, 253*). Spindly depletion causes a mitotic arrest with misaligned chromosomes (*77, 248, 249, 253*) but interestingly, mutation of the conserved Spindly motif that specifically prevents kinetochore localization of dynein results in an accumulation of MAD1 and MAD2 proteins on bioriented kinetochores and causes cells to delay in metaphase (*249, 253*).

Dynein-dependent stripping of SAC proteins may be regulated and stimulated upon chromosome biorientation. This is supported by the observation that the kinetochore localization of ZW10 is dependent on Zwint-1 phosphorylation by Aurora B and that a phosphomimicking mutant of Zwint-1 causes a metaphase delay (*254*). It is however equally possible that the stripping pathway is constitutively active and that dynein-dependent stripping is activated solely by the proximity of microtubules.

A dynein-independent pathway for removing SAC proteins from attached kinetochores has been suggested, based on the observation that Spindly depletion, while preventing kinetochore binding of dynein, does not prevent SAC protein removal from attached kinetochores (*249*). The existence of such a pathway, the identity of which is at present unknown, would be predicted also on the basis of the fact that kinetochore dynein is absent from most eukaryotic species that nevertheless need to silence MCC production from attached kinetochores.

Countering SAC kinase activity

In fungi and nematodes, SAC silencing requires the activity of PP1 phosphatases. In *S. pombe*, Dis2/PP1 is required to exit from a metaphase arrest and to silence the SAC following Ark1/Aurora B inhibition in the presence of unattached kinetochores (*255*). In *S. cerevisiae,* overexpression of the PP1 homolog Glc7 overrides the SAC in nocodazole-arrested cells (*256*). Opposition of Ipl1/Aurora B activity by Glc7 is important in the regulation of kinetochore-microtubule attachments. Ipl1 activity is however not required for the SAC in budding yeast. It is therefore likely that Glc7 promotes SAC signaling by antagonizing other kinases than Ipl1 (*256*). Indeed, Glc7 is required to exit from a metaphase arrest that results from MPS1 overexpression (*256*). Importantly, Glc7 opposes MPS1-dependent phosphorylation of the KNL1 MELT motifs (*39*). Dephosphorylation of these sites may be a prerequisite for SAC inactivation (Fig. 6A).

In mammalian cells, nematodes and fungi, PP1 associates with KNL1 in a tension-dependent manner (*32, 36, 41, 257*). In budding yeast, Glc7 binding to Spc105/KNL1 is essential for cellular viability. Decreased viability as a result of inability to recruit PP1 to KNL1 could be rescued by inactivation of the SAC. This suggests that the KNL1-associated PP1 is required to silence SAC silencing. In nematodes, preventing PP1-KNL1 binding prolongs the SAC response to monopolar spindles (*32*). In mammalian cells, such interruption of PP1-KNL1 is achieved by Aurora B-dependent phosphorylation of KNL1 (*36*). The role of phosphoregulated PP1 localization to KNL1 in the regulation of SAC maintenance and silencing in mammalian cells is adressed in chapters 3 and 4 of this thesis.

In fission yeast, efficient SAC silencing additionally requires PP1 docking to the heterodimeric Klp5-6 kinesin 8 motor (*258*). This function may be conserved in metazoans since PP1 also directly binds to the human kinesin-8 homolog KIF18A, which promotes efficient chromosome alignment and sister-

kinetochore oscillations (*259*).

Relieving APC/C inhibition

Dissociation of MCC from the APC/C is required for APC/C activation in metaphase. An important process in MCC disassembly is CDC20 ubiquitination. During a SAC arrest, CDC20 is continuously ubiquitinated by APC/C^{MCC} (*166, 260, 261*). This is dependent on the interaction of CDC20 with Mad2 and Mad3 (*260-262*). Ubiquitination of CDC20 destabilizes its interaction with MAD2 and thereby mediates MCC disassembly (*263*). This however does not depend on proteasomal degradation of CDC20 (*263*). Thus, the APC/C can relieve its own inhibition by destabilizing the MCC via ubiquitination of CDC20. CDC20 ubiquitination is stimulated by the E2 UbcH10 and countered by the DUB USP44 (*152, 263*). It is however unknown if and how these activities are regulated.

Several other factors impinge on CDC20 ubiquitination and MCC stability (Fig. 6B). CDC20 ubiquitination is dependent on the constitutive APC/C subunit APC15 (*262, 264, 265*). Depletion of APC15 causes a SAC dependent metaphase delay and accumulates CDC20, BUB3, BUBR1 and MAD2 on the APC/C (*262*). APC15 is not required for general APC/C activity, but specifically permits CDC20 autoubiquitination by APC/C^{MCC}. How APC15 mediates CDC20 ubiquitination is unclear. Possibly, APC15 repositions CDC20 to bring it in proximity with the catalytic subunit of the APC/C (*262, 264, 265*). Moreover, it is unknown if CDC20 ubiquitination is cause or consequence of MCC disassembly. The CUE domain containing protein CUEDC2 has also been suggested to promote MCC destabilization by ejecting MAD2 from APC/C^{MCC}. CUEDC2 is associated with the APC/C in mitosis and binds to CDC20 *in vitro*. Depletion of CUEDC2 causes a SAC-dependent metaphase arrest. The mechanism by which CUEDC2 could regulate MCC stability is however unclear (*266*).

Another important factor for MCC destabilization in mammals is $p31^{comet}$, a structural mimic of closed MAD2 (*267*). $p31^{comet}$ was first identified in a yeast-two-hybrid screen as a MAD2 binding protein (*268*). Depletion of $p31^{comet}$ causes cells to arrest at metaphase. Conversely, $p31^{comet}$ overexpression drives precocious mitotic exit in nocodazole-arrested cells (*268-272*). This function of $p31^{comet}$ is dependent on its dimerization with MAD2 (*267*). $p31^{comet}$ binds selectively to closed MAD2 (*269, 272*) and forms a ternary complex with MAD2 and CDC20 (*269*). The structural similarity between $p31^{comet}$ and C-MAD2 and their interaction suggest several possible roles of $p31^{comet}$ in SAC silencing. By capping C-MAD2, either at kinetochores or in the cytosol, $p31^{comet}$ could prevent MAD2 dimerization and thereby prevent the production of new O-MAD2. $p31^{comet}$ could also function by extracting MAD2 from the APC/C. Indeed, $p31^{comet}$ can interact with C-MAD2-MAD1 at kinetochores. However, while $p31^{comet}$ can remove O-MAD2 from C-MAD2-MAD1 scaffolds *in vitro* (*177*), it does not modulate the kinetochore localization of O-MAD2 in cells (*272*). It is therefore unlikely that $p31^{comet}$ prevents the production of a C-MAD2 MCC catalyst at kinetochores by capping the MAD1 scaffold (*272*).

Instead, $p31^{comet}$ is required for APC/C activation following SAC inactivation (*269, 273*). Although low levels of $p31^{comet}$ are associated with APC/C^{MCC} during a SAC arrest, $p31^{comet}$ transiently accumulates on the APC/C following MAD2 removal during SAC inactivation (*269*). Importantly, depletion of $p31^{comet}$ stabilizes the interaction between MAD2 and BUBR1 in cells and excess $p31^{comet}$ dissociates MAD2 from BUBR1 *in vitro*. Therefore, it is likely that $p31^{comet}$ antagonizes the SAC by extracting C-MAD2 from the MCC (*272*). This is supported by the observation that p31 binds preferentially to MAD2-bound APC^{CDC20} (*272*). Moreover, $p31^{comet}$ also prevents APC/C-MAD2 association *in vitro* and may thereby limit the cytosolic amplification of SAC signaling in cells (*272*). Such a mechanism would

be enforced if p31^{comet} stimulate the structural conversion of ejected C-MAD2 back to free O-MAD2. Intriguingly, p31^{comet} likely also impinges on APC/C activation by destabilizing the interaction between BUBR1-BUB3 and the APC/C in a MAD2-independent manner. In p31^{comet}-depleted cells, MAD2 is dispensable for APC/C inhibition after the BUBR1-BUB3 inhibitor has been loaded onto APC/C (*179*). This suggests that p31^{comet} functions by first ejecting MAD2 from the APC/C and subsequently by removing BUBR1-BUB3.

Scope of this thesis

The research described in this thesis focuses on MPS1 kinetochore localization because this is a critical mechanism in regulation of the spindle assembly checkpoint (SAC). As such, deeper understanding of the mechanisms that dictate MPS1 localization can explain how the SAC is activated and silenced in response to kinetochore-microtubule interactions and other stimuli. The studies presented in this thesis aimed to elucidate mechanisms of MPS1 regulation, by using RNAi-based protein knockdown and reconstitution in human cells. Reconstitution was done via doxycycline-inducible expression from a single genomic integration site, to permit functional characterization of exogenous proteins at near endogenous levels in an isogenic background. This system enabled structure-function analyses of panels of MPS1, HEC1 and KNL1 mutants, by quantitative immunofluorescence microscopy and time-lapse imaging.

Outline of this thesis

In **chapter 2**, we examine the molecular organization of the N-terminal kinetochore-binding module of MPS1. We find that MPS1 kinetochore binding is mediated predominantly via its N-terminal-most 60-amino acids, hereafter referred to as the N-terminal extension (NTE). In collaboration with the Perrakis lab at the Netherlands Cancer Institute, we show that the kinetochore-binding module of MPS1 additionally contains a TPR domain, of which we resolve the structure. Whereas this TPR domain confers weak kinetochore-binding capacity to the full length protein, it functions mainly by inhibiting NTE-dependent kinetochore localization. We moreover find that the kinetochore localization of MPS1 is essential for activation of the SAC. When we study the regulation of MPS1 by Aurora B, we find that Aurora B impinges on MPS1 localization by relieving TPR-dependent inhibition of the NTE. Moreover, we demonstrate that the kinetochore localization of MPS1 is dependent on the calponin homology domain of HEC1. As this domain is part of the main kinetochore-microtubule-binding interface, we propose that MPS1 localization may be directly inhibited by kinetochore-microtubule attachments. In **chapter 3**, we further investigate the regulation of MPS1 kinetochore localization by Aurora B. We find that Aurora B impinges predominantly on MPS1 in an indirect manner, by controlling the kinetochore localization of PP1 phosphatases. We show that Aurora B inhibits PP1 kinetochore localization by phosphorylation of the PP1-docking motifs in KNL1. Mutation of these motifs prevents PP1 kinetochore localization and thereby desensitizes MPS1 kinetochore localization and the SAC to Aurora B inhibition. Moreover, we show that preventing PP1 kinetochore localization is a prerequisite for robust SAC establishment. In **chapter 4**, we further examined the function and regulation of PP1 kinetochore binding. We show that PP1 and another phosphatase PP2A-B56 are involved in a negative feedback loop that serves to reduce their levels at kinetochores. We show that PP1 suppresses the kinetochore localization of PP2A-B56 by dephosphorylation of its docking site. In turn, PP2A-B56 dephosphorylates the PP1-binding motifs in KNL1, causing PP1 localization. We show that efficient SAC silencing requires the kinetochore localization of both phosphatases. Finally, we propose that localized negative feedback between PP1 and PP2A-B56 ensures finely-tuned low levels of SAC-silencing phosphatase activity at kinetochores in prometaphase. In **chapter 5**, our results described in this thesis are summarized and discussed. We review our findings in the light of recent literature and propose how further research can enlighten mechanisms that control MPS1 kinetochore localization and the SAC.

Chapter 2

A TPR domain-containing N-terminal module of MPS1 is required for its kinetochore localization by Aurora B

Wilco Nijenhuis[1,2], Eleonore von Castelmur[4], Eelco Tromer[1,2,5], Dene Littler[4], Mathijs Vleugel[1,2], Valeria De Marco[4,6], Maria H.J. van Osch[1], Berend Snel[5], Anastassis Perrakis[4,6] and Geert J.P.L Kops[1,2,3,6]

[1] Molecular Cancer Research and

[2] Department of Medical Oncology and

[3] Cancer Genomics Netherlands, University Medical Center Utrecht, 3584 CG, Utrecht, The Netherlands.

[4] Division of Biochemistry, The Netherlands Cancer Institute, 1066 CX, Amsterdam, The Netherlands.

[5] Theoretical Biology and Bioinformatics, Department of Biology, Science Faculty, Utrecht University, Padualaan 8, 3584 CH Utrecht, The Netherlands

[6] These authors have contributed equally

Adapted from The Journal of Cell Biology 201(2):217-31, April 2013

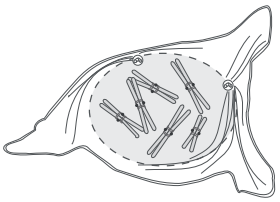

Abstract

The mitotic checkpoint ensures correct chromosome segregation by delaying cell cycle progression until all kinetochores have attached to the mitotic spindle. Here we show that the mitotic checkpoint kinase MPS1 contains an N-terminal localization module, organized in an N-Terminal-Extension (NTE) and a tetratricopeptide repeat (TPR) domain, for which we have determined the crystal structure. While the module was necessary for kinetochore localization of MPS1 and essential for the mitotic checkpoint, the predominant kinetochore binding activity resided within the NTE. MPS1 localization further required HEC1 and Aurora B activity. We show that MPS1 localization to kinetochores depended on the calponin homology domain of HEC1 but not on Aurora B-dependent phosphorylation of the HEC1 tail. Rather, the TPR domain was the critical mediator of Aurora B control over MPS1 localization, as its deletion rendered MPS1 localization insensitive to Aurora B inhibition. These data are consistent with a model in which Aurora B activity relieves a TPR-dependent inhibitory constraint on MPS1 localization.

Introduction

Faithful chromosome segregation is essential to maintain genomic stability. A mitotic checkpoint has evolved to prevent the onset of anaphase until all chromosomes have attached to spindle microtubules, a prerequisite for error-free chromosome segregation (*274*). Components of the mitotic checkpoint such as MAD1 and MAD2 are recruited specifically to kinetochores devoid of microtubules, while microtubule attachments to kinetochores cause removal of these components and local silencing of the checkpoint signal (*275*).

Unattached kinetochores elicit a checkpoint response by recruiting various checkpoint proteins including MAD1/MAD2 heterotetramers. This subsequently culminates in the production of an anaphase inhibitor consisting of BUBR1, BUB3 and MAD2 (*146, 159, 164*). This inhibitor, known as the mitotic checkpoint complex, prevents premature activation of the APC/C-CDC20 complex that triggers anaphase by licensing Cyclin B and Securin for proteasomal degradation (*276*). Unattached kinetochores also recruit and activate the mitotic kinase MPS1 that simultaneously promotes efficient activation of the error-correction and mitotic checkpoint machineries (*277*). MPS1 is required for kinetochore localization of at least MAD1, MAD2, CDC20 and BUB1 (*277*). Although not required *in vitro* (*177*), MPS1 is needed for MAD2 dimerization in cells (*210*). Once activated, MPS1 also promotes its own dissociation from kinetochores, a process that permits removal of the MAD1/MAD2 complexes and checkpoint silencing when kinetochores have properly bioriented (*215*). Consequently, loss of MPS1 activity results in failure to delay mitosis when unattached kinetochores persist, in a dramatic shortening of mitosis and in anaphases with severe chromosome missegregations that can culminate in chromosomal translocations (*204-206, 216, 218*).

Localization of MPS1 to unattached kinetochores at the onset of mitosis depends on the outer-kinetochore proteins HEC1 and NUF2 (*47, 199, 236*) and is regulated by the Aurora B kinase (*195, 196*). These proteins operate in one pathway, as the ability of centromere-tethered Aurora B to recruit MPS1 in G2-phase cells depends on HEC1 (*195*). The Aurora B-HEC1-MPS1 pathway is critical for rapid establishment of mitotic checkpoint activity at the onset of mitosis (*195*).

We sought to examine the molecular mechanism of MPS1 kinetochore binding and regulation thereof. We here present the crystal structure of a tetratricopeptide repeat (TPR) domain in the kinetochore-binding region of MPS1 and provide evidence that association of MPS1 with kinetochores is essential for mitotic checkpoint activity. This association depends on the microtubule-binding domain of HEC1 and is regulated by the TPR domain in an Aurora B-dependent manner.

Results

Crystal structure of a TPR-like fold in the kinetochore-targeting region of MPS1

The N-terminal 301 amino acids of MPS1 are sufficient for localization of the kinase to kinetochores during mitosis (*208, 209*), while the N-terminal 100 amino acids, although not sufficient, are essential for MPS1 kinetochore binding (*209, 218*). Sequence similarity searches using Psi-Blast suggest that the MPS1 N-terminal region has significant similarity with the TPR domains in BUB1 (*278*) and BUBR1 (*279-281*), as recently modeled (*211*). To understand the molecular mechanism by which the TPR-containing N-terminal region of MPS1 regulates binding to kinetochores, we determined its three-

dimensional structure. A number of MPS1 protein fragments were expressed, purified, and screened for crystallization. The best diffracting crystals were obtained from a construct consisting of residues 62-239, MPS1$^{62-239}$. The structure was determined to 2.2 Å resolution by single-wavelength anomalous dispersion using seleno-methionine substituted protein, and was refined to an R_{free} of 18.6 % without any Ramachandran plot outliers (for crystallographic details see Materials and Methods and Table 1). The asymmetric unit contained four molecules, which were all well-ordered with the exception of the 40 C-terminal residues that were not visible in the electron density and were not included in the model. The structure was formed by seven helices, the first six of which are arranged in three TPR repeats (TPR1-3) that fold together to produce a concave "C"-shaped cross-section (Figure 1A-C). The inner concave surface, the typical ligand-binding site for many TPR domains, is well-conserved, but surface patches with good sequence conservation are also clearly present in the outer convex surface (Figure 1C).

Evolutionary conservation of the MPS1 TPR domain and similarities with the BUB family of TPR domains

Structure similarity searches using DALI (*282*) show that the MPS1 TPR domain is most similar to the N-terminal TPR domains of BUBR1 (Protein Data Bank accession no. 2WVI) and BUB1 (Protein Data Bank accession no. 4A1G; Figure 1D). Although the structure-based sequence alignment of MPS1, BUBR1 and BUB1 shows limited sequence similarity (Figure 1E), the MPS1 TPR domain should also be considered a member of this family. Some differences between the three TPR domains are notable. Whereas in BUB1 the residues following the C-terminal helix point away from the inner concave surface of the domain, the first few residues after the C-terminal capping helix in the MPS1 structure turn towards the inner concave surface of the domain, extending it (Figure 1A,B). The 3_{10} helix connecting the first two TPR motifs in BUB1 and BUBR1 is substituted by a single-turn α-helix in MPS1 (α2' in Figure 1B). Similarly, both the GIG and G(N/D)D motifs connecting the last two TPR repeats in BUB1 and BUBR1, which have been shown to be important for structural integrity, are missing in MPS1, but the overall arrangement of the domain is retained. Both the BUB1 and the BUBR1 TPR domains bind KNL1 through a characteristic depression in their convex surface (*37, 38*). That exact mode of binding is unlikely to be conserved in the MPS1 TPR domain, as this surface depression is not present (Figure 1C, S1A). However, ligand binding on the convex surface of the MPS1 TPR domain remains a possibility, for instance through other conserved patches (Figure 1C). Finally, the BUB1 TPR domain dimerizes in solution and in the crystal structure, which is mediated by contacts made through a short loop between the N-terminal helix (absent in our MPS1 structure) and the first helix of TPR1 (*278*). Although MPS1 forms dimers in cells (*210, 211*), dimerization is unlikely to be mediated by the TPR domain or the N-terminal region of MPS1 that includes the TPR domain. First, *in vitro,* four different MPS1 constructs containing various regions of the N-terminus (MPS1$^{1-196}$, MPS1$^{9-255}$, MPS1$^{62-239}$, MPS1$^{1-239}$) were monomers in solution as shown by multi-angle laser light scattering (Figure S1B). Second, immunoprecipitation experiments using mitotic 293T cells showed that MPS1 dimerization in cells did not rely on the N-terminal 192 amino acids of MPS1 (Figure S1C).

Given the strong conservation of the BUB TPR domains (*283*) and their similarity to the TPR domain of human MPS1, we examined origin and evolution of the TPR-fold sequence in eukaryotic MPS1 homologs (*274*). A hidden Markov model profile constructed from the TPR domain sequences of human MPS1 homologs could identify additional TPR domain sequence homology only in vertebrates and in some distantly related eukaryotes such as green algae and choanoflagellates (Figure S2). These homologous sequences were all predicted to fold into helical arrays, consistent with the TPR-

Table 1.
X-ray data statistics and model refinement parameters

Parameters	Values
Diffraction data	
Spacegroup	$P2_12_12_1$
Unit cell: a, b, c (Å)	79.9, 80.1, 142.2
Molecules (a.u.)/solvent content	4 /61%
Resolution (Å)	44.28-2.2 (2.32-2.20)
Completeness (%)	98.8 (92.7)
Unique reflections	46558 (6239)
R_{merge}	0.07 (0.45)
<(I)/σ(I)>	14.1 (2.8)
Multiplicity	5.8 (3.7)
Wilson B-factor (Å^2)	41.5
Model statistics	
R-factor (%)	17.0
R_{free} (%)	18.6
Ramachandran plot favored (%)	99.1
Ramachandran plot outliers (%)	0.0
Protein atom number	4475
Ligand atom number	365
Water atom number	232
Protein B factor	50
Ligand B factor	68
Water B factor	46
RMSD Bond lengths (Å)	0.01
RMSD Bond angles (°)	0.97

The R-free set comprised 2362 reflections corresponding to 5% of the total data. Numbers in parentheses denote high resolution statistics. a.u., asymmetric unit; RMSD, root-mean-square deviation

like fold. Given the presence of a TPR domain in early branching species and loss in several later branching species, we infer the presence of a MPS1 with an N-terminal TPR domain in the common ancestor of all eukaryotes (last eukaryotic common ancestor) and subsequent parallel loss in distinct eukaryotic lineages. Although the TPR domain of MPS1 belongs to the same structural family as BUB1 and BUBR1 TPR domains, parallel gain of the MPS1 TPR domain from BUB-like sequences is highly unlikely, because both groups of TPR domains show monophyletic clustering in a tree of the TPR domains. Finally, the patchy phyletic distribution of the TPR domain is not the result of horizontal gene transfer of MPS1 proteins, because the kinase tree for MPS1 orthologs is consistent with the species tree. In summary, the MPS1 TPR domain is likely ancient but maintained in only few branches of the eukaryotic tree of life.

The N-terminal region of MPS1 harbors a localization module required for checkpoint function

To examine the functional significance of the MPS1 TPR domain, we designed various MPS1 mutants based on the structure and generated cell lines stably expressing them (Figure 2A, B, S3A) from a doxycycline-inducible promoter in a single integration site to ensure comparable genetic background and expression levels (*183*). The localization of LAP-tagged MPS1 proteins was assayed in cells depleted of endogenous MPS1 to prevent confounding effects of dimerization or competition for kinetochore ligands (see Figure S4A, B), and in the presence of the small molecule MPS1 inhibitor reversine (*217*) to prevent indirect effects on localization by changes in MPS1 activity (*210, 215*). These experiments showed that the N-terminal region of MPS1 that encompasses the TPR domain (MPS1$^{1\text{-}192}$) localized weakly but reproducibly to kinetochores during prophase (Figure 2C), which is when maximal kinetochore enrichment of MPS1 is normally observed (*195*). The inefficient prophase localization and the absent prometaphase localization of MPS1$^{1\text{-}192}$ compared to wild-type MPS1 (MPS1^{WT}) further suggested that additional, yet undefined residues in MPS1 contribute to efficient MPS1 kinetochore binding. Consistently, whereas MPS1^{WT} localized to kinetochores efficiently, a truncated MPS1 mutant lacking this N-terminal region (MPS1$^{\Delta 200}$) was undetectable at kinetochores (Figure 2D, E). Thus, the MPS1 N-terminal region that encompasses the TPR domain is necessary for kinetochore binding. Surprisingly, however, deletion of the TPR domain (aa 61-192; MPS1$^{\Delta TPR}$) did not potently disturb localization of MPS1 to kinetochores (Figure 2D, E). The difference in localization between MPS1$^{\Delta 200}$ and MPS1$^{\Delta TPR}$ suggested that the 60 amino acids preceding the TPR domain are crucial for localizing MPS1. In support of this, a mutant that lacks this N-terminal extension (NTE; MPS1$^{\Delta 60}$) showed strongly reduced kinetochore

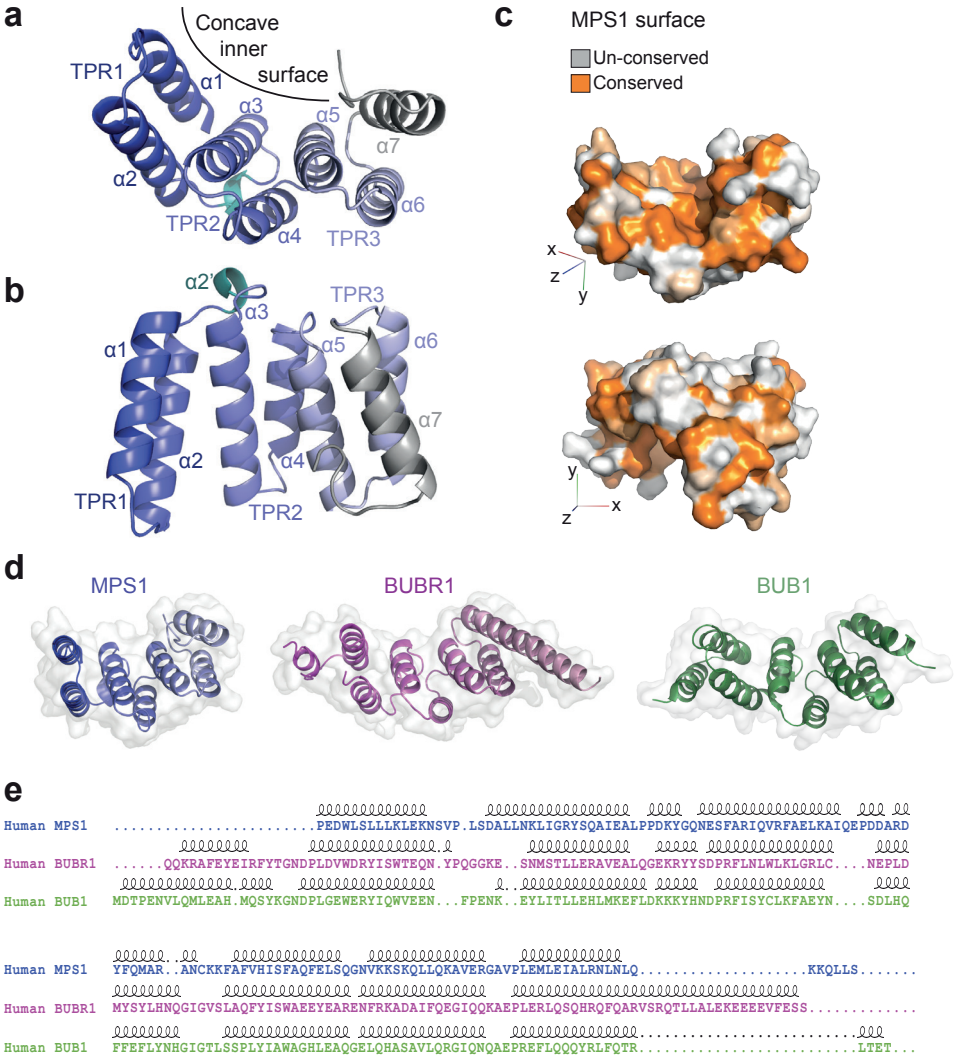

Figure 1. **Crystal structure of the MPS1 TPR domain.** (**A**) Crystal structure of the TPR domain. A cartoon diagram of the three TPR1-3 helical doublets forming the concave surface is shown in blue shades that fade towards grey form the N- towards the C- terminus; the C-terminal helix is in grey and the α2' short helix between TPR1 and TPR2 in cyan. (**B**) A side view of the TPR domain. (**C**) A surface representation of the TPR domain colored by sequence conservation among vertebrate MPS1 TPR domains; the top view emphasizes the conservation of the concave inner surface and the bottom view some conserved patches on the generally un-conserved outer surface. (**D**) The TPR domains of MPS1, BUBR1 and BUB1 shown in the same orientation following structural superposition, as cartoon diagrams within a transparent surface. (**E**) The sequence alignment resulting from the structural superposition of the three TPR domains above is shown together with secondary structure elements.

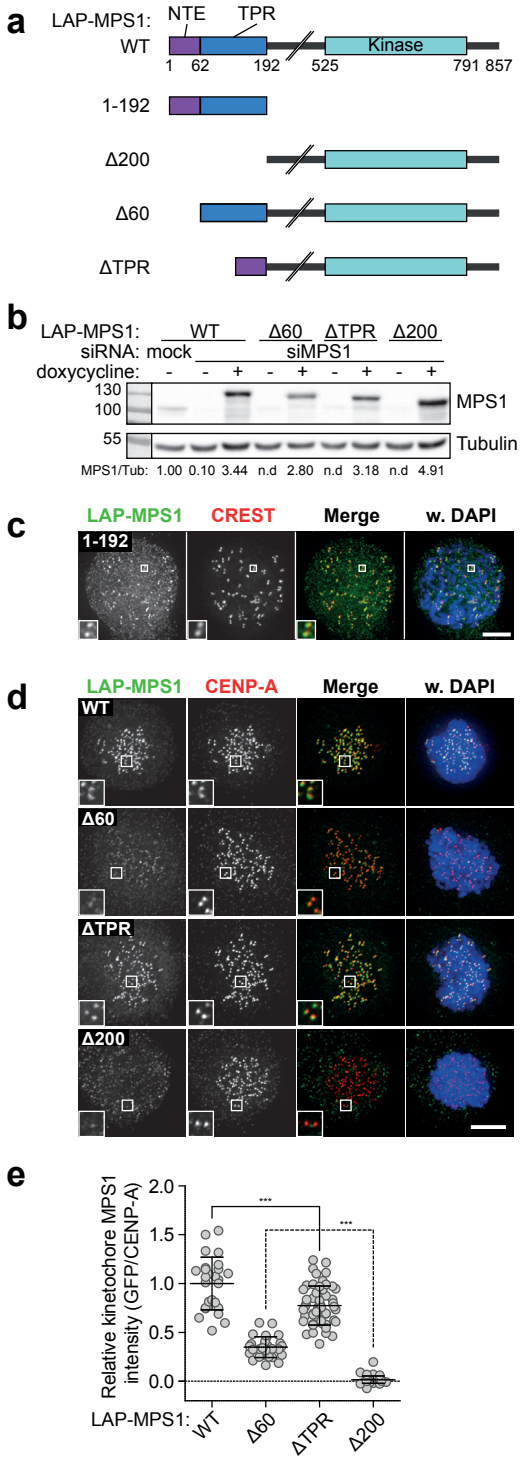

binding compared to both MPS1^{WT} and MPS1$^{\Delta TPR}$ (Figure 2D, E). Quantitation of the signal revealed that kinetochore levels of MPS1$^{\Delta 60}$ were significantly higher than those of MPS1$^{\Delta 200}$, which was undetectable at kinetochores. MPS1$^{\Delta 60}$ therefore retains residual low affinity for kinetochores that is provided by the TPR domain.

We next assessed whether the NTE and the TPR are needed for MPS1 function. Cells depleted of endogenous MPS1 and expressing the various RNAi-resistant mutants (*205*) were examined for mitotic checkpoint activity by measuring mitotic index upon treatment of cells with the spindle depolymerizing drug nocodazole and by real-time imaging of mitotic delay in nocodazole-treated cells. As expected, cells depleted of MPS1 failed to accumulate in mitosis in response to nocodazole (Figure 3A, B). This was largely rescued by expression of LAP-tagged RNAi-resistant MPS1^{WT} but not by kinase-deficient MPS1^{D664A} (*205*). In accordance with its

Figure 2. **MPS1 kinetochore localization is mediated by the NTE-TPR module.** (**A**) Schematic representation of the domain organization of various MPS1 proteins used throughout this study. (**B**) Immunoblot of whole cell lysates from mitotic HeLa Flp-in LAP-MPS1 cell lines that were transfected with mock or MPS1 siRNA and induced (+ doxycycline) to express the indicated LAP-MPS1 proteins; band intensity of MPS1/tubulin relative to 'mock' is indicated (n.d., not determined). (**C**) Immunolocalization of LAP-MPS1$^{1-192}$ and centromeres (CREST) in nocodazole-treated, MPS1-depleted HeLaK FRT TetR cells. Cells were imaged for prophase figures. DNA (DAPI) is in blue. Scale bar is 5 µm. Insets were magnified by 300%. (**D** and E) Representative images (D) and quantification (E) of immunolocalization of the various LAP-MPS1 proteins and centromeres (CENP-A) in nocodazole, reversine (500 nM) and MG132-treated, MPS1-depleted Flp-in HeLa cells. DNA (DAPI) is in blue. Scale bar is 5 µm. Insets were magnified by 240%. Graph in E displays total kinetochore intensities (± SD) of the indicated LAP-MPS1 proteins relative to centromeres (CENP-A) in cells treated as in D. Data are representative of 3 experiments. Ratios for LAP-MPS1^{WT} are set to 1. One dot represents one cell. Line indicates average +SD. ***: significant (student t-test, unpaired, p<0.0001).

observed inability to localize to kinetochores, MPS1$^{\Delta 200}$ could not restore mitotic checkpoint function in either assay (Figure 3A, B). In contrast, both MPS1$^{\Delta TPR}$ and MPS1$^{\Delta 60}$ displayed weakened checkpoint function. Mitotic index in nocodazole-treated cells expressing MPS1$^{\Delta TPR}$ or MPS1$^{\Delta 60}$ was reduced by approximately 30% relative to MPS1^{WT}. In addition, 28% and 22% of MPS1$^{\Delta TPR}$ and MPS1$^{\Delta 60}$-expressing cells, respectively, were unable to maintain a mitotic delay for five hours (Figure 3A, B). Fluorescence recovery after photobleaching showed that kinetochore-bound LAP-MPS1$^{\Delta TPR}$ in nocodazole-treated cells had similar rapid turnover as MPS1^{WT} (Figure S4C, D), and analysis of *in vitro* kinase activity of the various mutants immunoprecipitated from mitotic HEK 293T cells showed that none of the mutants suffered from compromised kinase activity (Figure S4E, F). Of note, MPS1$^{\Delta TPR}$ displayed elevated levels of auto-phosphorylation (~2 fold higher than MPS1^{WT}), indicating that the TPR domain may be involved in regulating kinase activity which could somehow contribute to compromised checkpoint function in MPS1$^{\Delta TPR}$-expressing cells. Finally, artificial tethering of localization-deficient MPS1 by fusion to the constitutive kinetochore protein MIS12 (*215*) was able to restore mitotic checkpoint activity (Figure 3D). Collectively, these data support the hypothesis that functional defects of MPS1 N-terminal truncation/deletion mutants are due primarily to their inability to efficiently bind kinetochores.

Interestingly, MPS1$^{\Delta 200}$ was readily detectable at kinetochores of cells containing normal levels of endogenous MPS1 (Figure S4A, B), in contrast to cells in which endogenous MPS1 was depleted (Figure 2D). Similar observations using mouse oocytes have been reported (*212*). Dimerization to kinetochore-localized forms of MPS1 may thus endow N-terminal truncation mutants with some kinetochore localization and function, possibly explaining why a recent study reported significant mitotic checkpoint signaling in cells expressing MPS1$^{\Delta 100}$ (*218*).

NTE-mediated kinetochore localization of MPS1 requires the microtubule-binding domain of HEC1

Having established that the primary localization signal in MPS1 resides in the N-terminal 192 amino acids with a dominant contribution from the NTE, we next wished to investigate the kinetochore requirements for MPS1 localization. As predicted by our structural analysis, KNL1 did not seem to contribute significantly to MPS1 kinetochore binding: depletion of KNL1 reduced MPS1 localization only slightly (Figure 4A, B), a reduction that is explained by a similar reduction in kinetochore HEC1 levels (Figure 4C, D and see below).

The localization of MPS1 to kinetochores depends on the NDC80 complex members HEC1 and its obligate binding partner NUF2 (*47, 236*). In agreement with this, localization of MPS1^{WT} to unattached kinetochores in our inducible stable cell lines was lost upon depletion of HEC1 or NUF2 (Figure 4E, F). Similar results were obtained when examining localization of MPS1$^{\Delta TPR}$ (Figure 4G, H), showing that the affinity of the NTE for kinetochores relies on presence of the NDC80 complex.

Full-length *S. cerevisiae* MPS1 interacts with amino acids 1-257 of ScNdc80 (the N-terminal tail and the calponin homology (CH) domain) when co-expressed in *E. coli* (*221*). In addition, PtK1 cells expressing a HEC1$^{\Delta 1\text{-}207}$ protein (that lacks both the tail and the CH domain) have reduced ability to delay mitosis in the absence of kinetochore-microtubule attachments (*50*). Incomplete HEC1 depletion does not prevent checkpoint activation in human cells (*236*), likely due to insufficient penetrance of MPS1 displacement (*195*). It does, however, sensitize the checkpoint to slight reductions in MPS1 activity or inhibition of Aurora B (*195, 196*). We wished to use this sensitization to ask whether the CH domain

and tail of HEC1 are involved in the mitotic checkpoint. To this end, we created a set of stable, isogenic cell lines that inducibly express GFP-HEC1^{WT}, GFP-HEC1$^{\Delta 207}$ or GFP (Figure S3B). While nocodazole-treated cells depleted of HEC1 or treated with the Aurora B inhibitor ZM447439 (*284*) maintained mitotic arrest for many hours, addition of ZM447439 to HEC1-depleted cells caused rapid mitotic exit (Figure 5A and *195*). This phenotype was rescued by expression of RNAi-insensitive wild-type GFP-HEC1^{WT}, but not by GFP-HEC1$^{\Delta 207}$ (Figure 5A). In agreement with this, HEC1 depletion delocalized MPS1 from kinetochores, which was recovered by expression of GFP-HEC1^{WT} (Figure 5B-D). The amount of MPS1 recruited to kinetochores correlated with the amount of kinetochore HEC1 (Figure 5D). Consistently, expression of GFP-HEC1$^{\Delta 207}$ that was unable to re-instate a robust checkpoint response (Figure 5A) could not recover MPS1 localization (Figure

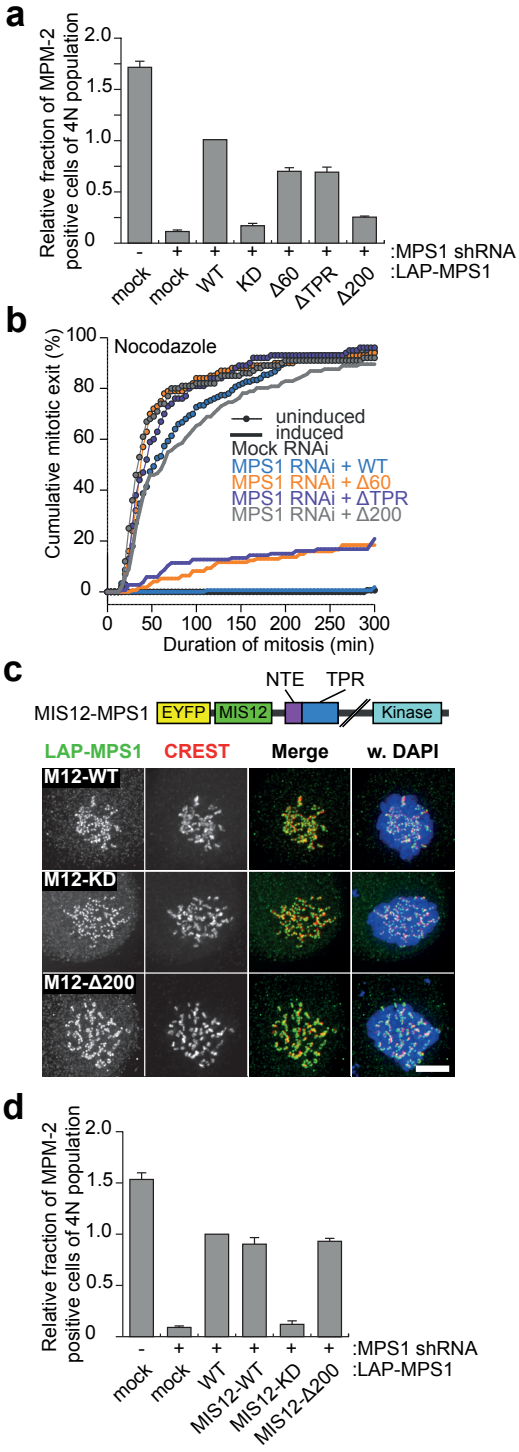

Figure 3. **The NTE-TPR module is essential for mitotic checkpoint activity.** (**A**) Mitotic index from flow cytometric analysis of MPM-2 positivity within a population of cells transfected with mock or MPS1 shRNA plasmids along with the indicated RNAi-resistant MPS1 alleles and treated with nocodazole for 16 hrs. Graph represents averages of ≥5 independent experiments (± SEM), average for LAP-MPS1^{WT} reconstitution is set to 1. (**B**) Time-lapse analysis of duration of mitotic arrest in nocodazole-treated Flp-in HeLa cells transfected with mock or MPS1 siRNA and expressing the indicated LAP-MPS1 proteins. Data indicate cumulative percentage of cells (from a total of ≥100 cells) that exit mitosis (scored as cell flattening) at the indicated times after nuclear envelop breakdown (NEB) and are representative of ≥2 independent experiments. Data for mock siRNA treated cells and MPS1 siRNA treated cells expressing LAP-MPS1^{WT} overlap. (**C**) Immunolocalization of the indicated LAP-MIS12-MPS1 proteins, and centromeres (CREST) in nocodazole-treated HeLa cells transfected with MPS1 siRNA for 48 hrs. M12, MIS12. DNA (DAPI) is in blue. Scale bar is 5 μm. A schematic representation of the LAP-MIS12-MPS1 protein is depicted. (**D**) Mitotic index from flow cytometric analysis as in (A). Graph represents averages of ≥2 independent experiments (± SEM), average for LAP-MPS1^{WT} reconstitution is set to 1.

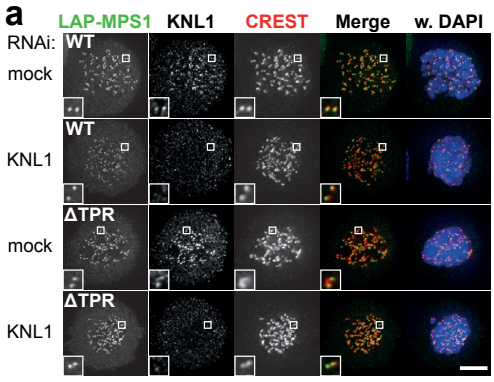
a
LAP-MPS1
KNL1
CREST
Merge
w. DAPI
RNAi:
mock
WT
KNL1
WT
mock
ΔTPR
KNL1
ΔTPR

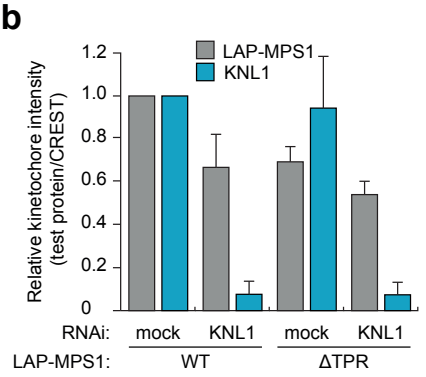
b
Relative kinetochore intensity
(test protein/CREST)
1.2
1.0
0.8
0.6
0.4
0.2
0
LAP-MPS1
KNL1
RNAi:
mock
KNL1
mock
KNL1
LAP-MPS1:
WT
ΔTPR

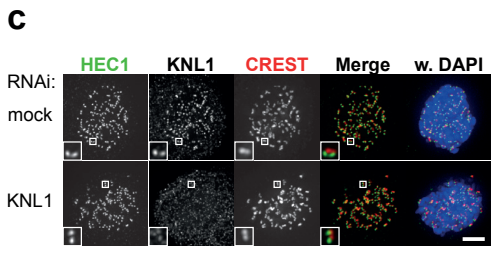
c
HEC1
KNL1
CREST
Merge
w. DAPI
RNAi:
mock
KNL1

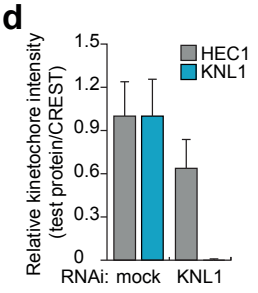
d
Relative kinetochore intensity
(test protein/CREST)
1.5
1.2
0.9
0.6
0.3
0
HEC1
KNL1
RNAi:
mock
KNL1

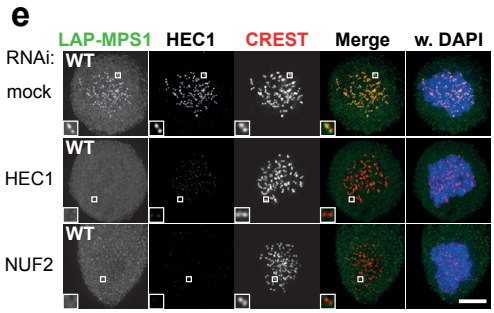
e
LAP-MPS1
HEC1
CREST
Merge
w. DAPI
RNAi:
mock
WT
HEC1
WT
NUF2
WT

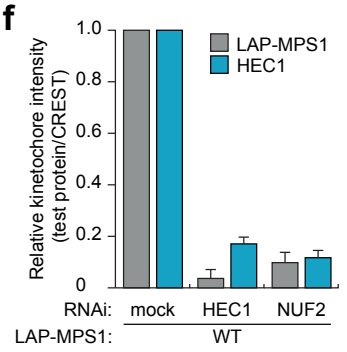
f
Relative kinetochore intensity
(test protein/CREST)
1.0
0.8
0.6
0.4
0.2
0
LAP-MPS1
HEC1
RNAi:
mock
HEC1
NUF2
LAP-MPS1:
WT

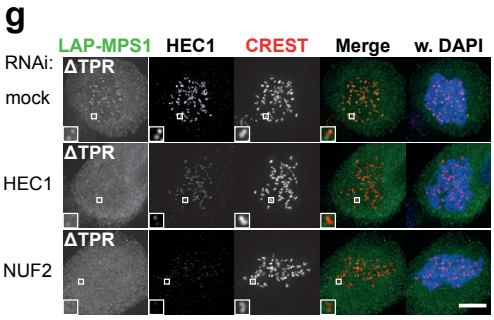
g
LAP-MPS1
HEC1
CREST
Merge
w. DAPI
RNAi:
mock
ΔTPR
HEC1
ΔTPR
NUF2
ΔTPR

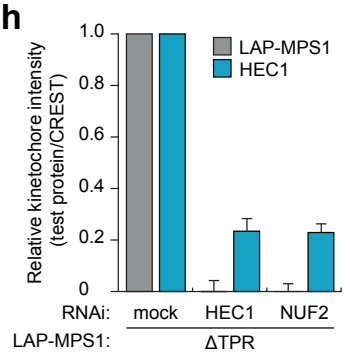
h
Relative kinetochore intensity
(test protein/CREST)
1.0
0.8
0.6
0.4
0.2
0
LAP-MPS1
HEC1
RNAi:
mock
HEC1
NUF2
LAP-MPS1:
ΔTPR

5B-D). Although GFP-HEC1$^{\Delta 207}$ was generally incorporated less efficiently than wild-type GFP-HEC1, even kinetochores containing high levels of GFP-HEC1$^{\Delta 207}$ were devoid of MPS1 (Figure 5D).

These results showed that residues 1-207 of HEC1 (encompassing the CH domain and tail) were necessary for MPS1 localization and checkpoint activity. To determine if HEC1 is also sufficient for MPS1 localization, we examined if HEC1 can recruit MPS1 when targeted to a non-kinetochore location. To this end, GFP-HEC1 was targeted to an array of *lac* operator (*lacO*) sequences in an arm of chromosome 1, by fusion to LacI. Indeed, accumulation of HEC1 on the *lacO* array was followed by recruitment of endogenous MPS1 to those sites (Figure 5E, F). Importantly, the ectopic recruitment of MPS1 depended on the microtubule-binding domains of HEC1, as MPS1 did not localize to *lacO* arrays decorated with GFP-HEC1$^{\Delta 207}$ (Figure 5E, F). Taken together, these data argue that the N-terminal, microtubule-binding region of HEC1 promotes efficient mitotic checkpoint activity by ensuring NTE-mediated localization of MPS1.

Control of MPS1 kinetochore localization by Aurora B is mediated by the TPR domain

Inhibition of Aurora B prevents the accumulation of MPS1 on unattached kinetochores and delays establishment of the mitotic checkpoint in early mitosis (*195*). Given the well-established regulation of the HEC1 N-terminal tail by Aurora B (*285*) and our finding that the HEC1 tail-CH region (1-207) is required to recruit MPS1, we hypothesized that Aurora B controls MPS1 localization by phosphorylating the HEC1 tail. To address this, MPS1 localization to kinetochores was assessed in HEC1-depleted cells reconstituted with GFP-HEC1$^{\Delta 80}$ (which lacks the HEC1 tail), GFP-HEC1^{9A} (lacking the Aurora B phosphorylation sites in the tail) or GFP-HEC1^{9D} (in which the Aurora B sites were substituted to aspartate residues to mimic phosphorylation; *50, 52, 109*). Surprisingly, all three HEC1 mutants were able to restore MPS1 kinetochore levels to the same extent as wild-type HEC1 (Figure S5A, B). We thus conclude that the regulation of MPS1 localization by Aurora B is not mediated by phosphorylation of the HEC1 tail.

We next asked if Aurora B controls the MPS1 localization module. As shown in Figure 6A, B, kinetochore-binding of MPS1$^{1\text{-}192}$ was abolished by treatment with ZM447439, showing that Aurora B affects MPS1 localization by regulating binding of this minimal domain to kinetochores. Strikingly, while ZM447439 strongly reduced the amounts of MPS1^{WT} at prometaphase kinetochores and abolished residual MPS1$^{\Delta 60}$ levels, it had no effect on kinetochore binding of MPS1$^{\Delta TPR}$ (Figure 6C, D). Consistently, while Aurora B inhibition weakened or abolished mitotic delays in nocodazole-treated cells expressing MPS1^{WT} (20% exit after 5h) or MPS1$^{\Delta 60}$ (82% exit after 5h), respectively, it left the (weakened) checkpoint in MPS1$^{\Delta TPR}$-expressing cells virtually unaffected (Figure 6E). Summarizing, removal of the TPR domain renders MPS1 localization independent of Aurora B activity. This suggests

Figure 4. **NTE-mediated MPS1 localization depends on the NDC80 complex**. (**A, B, E-H**) Representative images (A, E, G) and quantification (B, F, H) of immunolocalization of LAP-MPS1^{WT} or LAP-MPS1$^{\Delta TPR}$ and centromeres (CREST) in Flp-in HeLa cells transfected with siRNAs to MPS1 and Luciferase (mock), HEC1, NUF2 or KNL1 and treated with nocodazole and reversine. DNA (DAPI) is in blue. Scale bar is 5 µm. Insets were magnified by 300%. Graphs display total kinetochore intensities (± SEM) of the indicated proteins relative to centromeres (CREST). Data are from ≥21 cells from ≥2 independent experiments. Ratios for mock RNAi treated cells are set to 1. (**C, D**) Representative images (C) and quantification (D) of immunolocalization of HEC1, KNL1 and centromeres (CREST) in HeLa cells transfected with mock or KNL1 siRNAs and treated with nocodazole. DNA (DAPI) is in blue. Scale bar is 5 µm. Insets were magnified by 300%. Graph in B shows total kinetochore intensities (± SD) of HEC1 (gray bars) and KNL1 (blue bars) relative to centromeres. Data are from ≥13 cells and are representative of 3 experiments. Ratios for mock RNAi treated cells are set to 1.

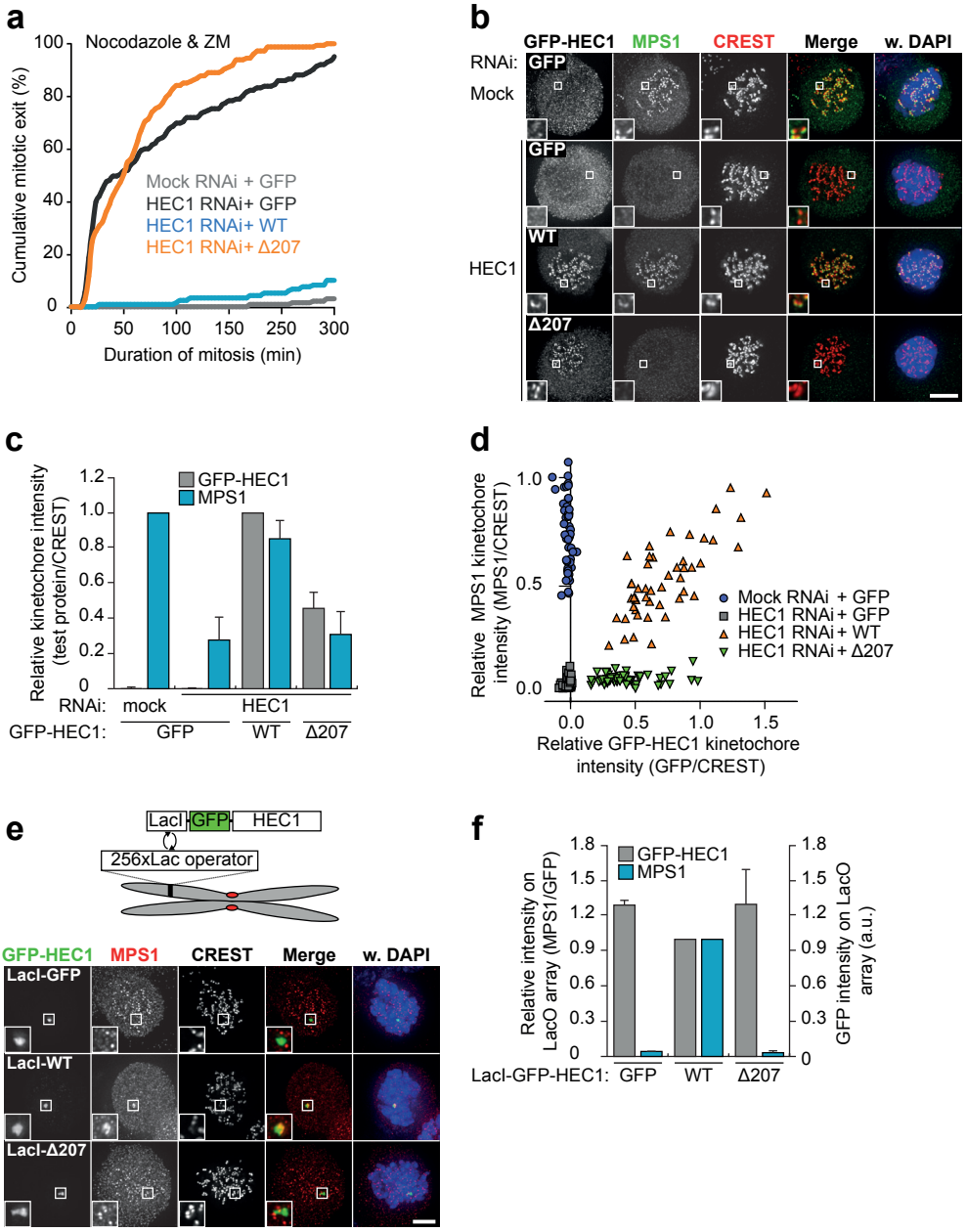

Figure 5. **The microtubule-binding domain of HEC1 directs MPS1 localization and function.** (**A**) Time-lapse analysis of duration of mitotic arrest in nocodazole- and ZM447439-treated Flp-in HeLa cells transfected with mock or HEC1 siRNA and expressing the indicated GFP-HEC1 proteins. Data indicate cumulative percentage of cells (from a total of ≥125 cells per treatment) that exit mitosis (scored as cell flattening) at the indicated times after NEB and are representative of 3 independent experiments. (**B-D**) Representative images (B) and quantification (C, D) of immunolocalization of MPS1, the indicated GFP-HEC1 proteins, and centromeres (CREST) in nocodazole-treated Flp-in HeLa cells transfected with mock or HEC1 siRNA. DNA (DAPI) is in blue. Scale bar is 5 μm. Insets were magnified by 300%. Graph in C displays total kinetochore intensities (± SEM) of the indicated proteins relative to centromeres (CREST). Data are from a total of ≥103 cells per treatment from

that the TPR domain normally prevents MPS1 localization, and this inhibitory effect is relieved by Aurora B (Figure 6F).

Discussion

Based on data presented in this study, we postulate that the mitotic checkpoint relies on the NTE-TPR module of MPS1 and that Aurora B-mediated control of the checkpoint impinges on this module. In our model (Figure 6F), MPS1 alternates between a localization-deficient and -proficient form, and the equilibrium can be driven to proficient by Aurora B activity. The TPR domain is important to maintain the deficient form, while the proficient form binds kinetochores predominantly through the NTE with some contribution from the TPR. Aurora B activity simultaneously inhibits the negative impact of the TPR domain on MPS1 localization and stimulates the contribution of the TPR domain to kinetochore binding. The model in figure 6F is consistent with present and previously published data. The model predicts that: i) deletion of the TPR domain renders localization and function of MPS1 solely dependent on NTE and independent of Aurora B activity (Figures 2 and 6); ii) deletion of the NTE allows weak but Aurora B-dependent MPS1 localization (Figures 2 and 6); iii) endogenous MPS1 can localize weakly in the absence of Aurora B activity. Indeed, we and others have shown that while MPS1 localization is potentiated by Aurora B activity (*195, 196*), it can weakly localize and eventually auto-activate without Aurora B (*195*).

Important questions are how the TPR domain prevents the NTE from localizing MPS1 to kinetochores and how Aurora B alleviates this. The most straightforward mechanism that we envision is one in which the NTE interacts with the TPR domain, inhibiting both NTE- and TPR-mediated kinetochore binding. In this scenario, release of this interaction is promoted (directly or indirectly) by Aurora B activity, rendering both the NTE and TPR available as kinetochore binding sites. Since Aurora B affects TPR functionality, both the release of NTE and the kinetochore affinity of TPR will depend on Aurora B. Aurora B could directly phosphorylate the NTE, the TPR, HEC1, or even an unknown kinetochore protein that directly binds MPS1 and whose function relies on HEC1. The Aurora B sites in the tail of HEC1 are not involved, and we have not been able to find Aurora B-dependent phosphorylation in the N-terminal domains of MPS1 or in the CH domain of HEC1. Aurora B may thus indirectly control MPS1 localization, for instance by causing a conformational change in HEC1 or MPS1 that exposes potential interaction sites, or by preventing PP1-dependent dephosphorylation of residues at the MPS1-kinetochore interface. Much work using cellular structure-function assays and *in vitro* interaction studies is needed to uncover the mechanism behind the regulation of MPS1 localization.

Catalytically inactive MPS1 accumulates on kinetochores to higher levels than active MPS1 (*210, 215*), suggesting that MPS1 kinase activity controls its own turnover at kinetochores. This accumulation

(Continued from previous page)

2 experiments. Ratios are set to 1 for mock RNAi treated cells (MPS1) and for GFP-HEC1^{WT} expressing cells (GFP-HEC1). Graph in D displays total kinetochore intensities of the indicated proteins relative to centromeres (CREST) for all cells of a single experiment. (**E-F**) Representative images (E) and quantification (F) of immunolocalization of MPS1, the indicated LacI-GFP-HEC1 proteins, and centromeres (CREST) in nocodazole-treated U2OS-LacO cells. DNA (DAPI) is in blue. Scale bar is 5 μm. Insets were magnified by 250%. Graph in F displays total intensities (± SEM) of MPS1 at LacO arrays relative to LacI-GFP-HEC1 (GFP) and total intensities of LacI-GFP-HEC1. Data are from a total of ≥17 cells from 2 experiments. Ratios for LacI-GFP-HEC1^{WT} expressing cells are set to 1.

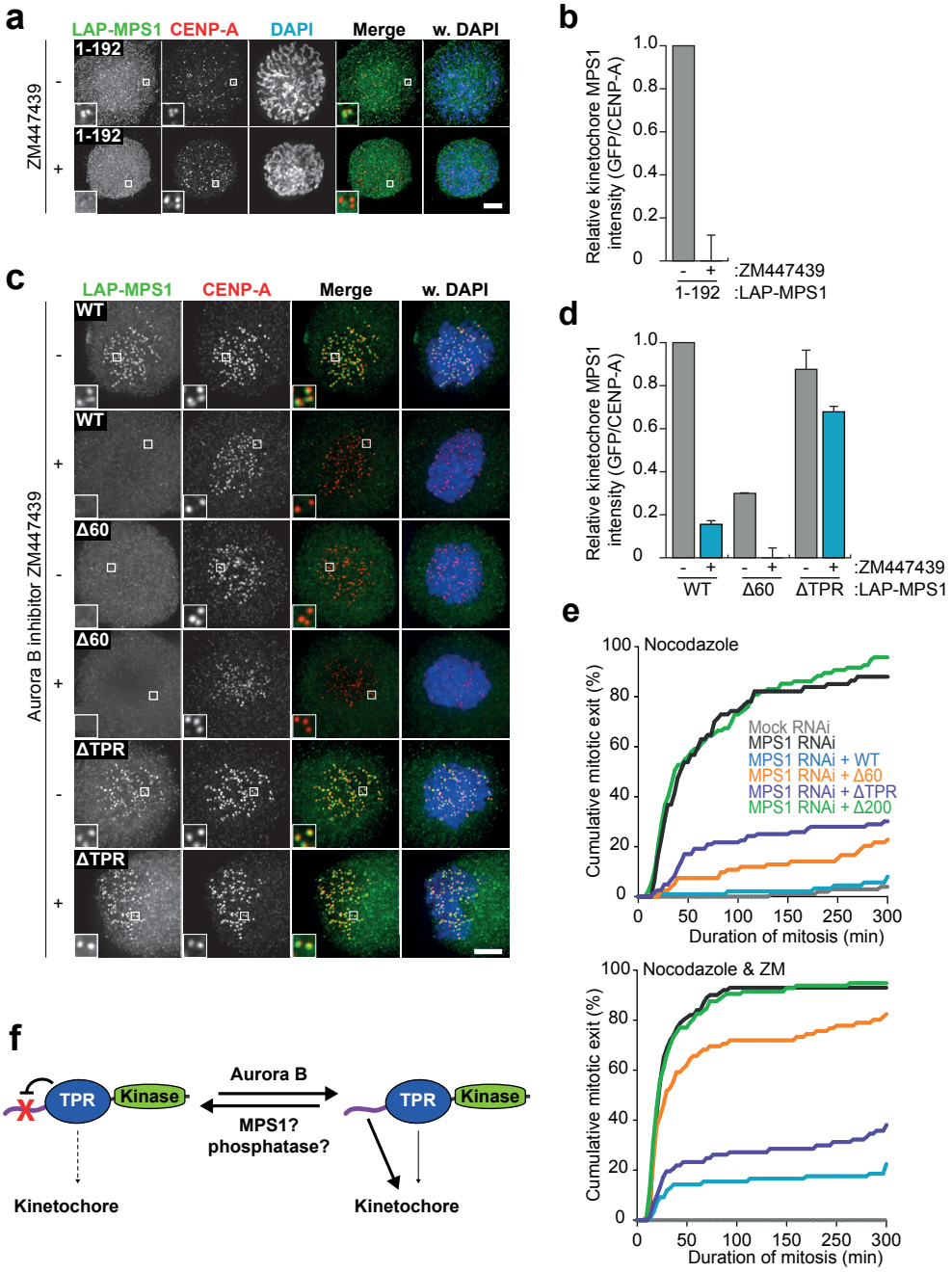

Figure 6. **Aurora B regulates MPS1 kinetochore localization by controlling function of the TPR domain.** (**A, B**) Representative images (A) and quantification (B) of immunolocalization of LAP-MPS1$^{1\text{-}192}$ and centromeres (CENPA) in prophase HeLaK FRT TetR cells depleted of MPS1 and treated with ZM447439, as indicated. (DAPI) is in blue. Scale bar is 5 µm. Insets were magnified by 390%. Graph in B shows total kinetochore intensities (± SEM) of MPS1 (gray bars) and GFP-HEC1 (blue bars) relative to centromeres. Data are from ≥38 cells from 2 experiments. Ratios for mock treated cells are

can at least in part be explained by postulating that inactivated MPS1 has increased residence time at kinetochores (*215*). MPS1 may also promote its turnover at kinetochores by counteracting the effects of Aurora B on TPR function, affecting in a more direct manner its own localization domain. MPS1 is autophosphorylated on multiple sites in the NTE as well as in the TPR domain (*125, 239-244*). This suggests that one or more of these phosphorylations either reduce the affinity of the NTE for its binding site at kinetochores or stimulate TPR-mediated inhibition of MPS1 localization. Detailing the mechanism by which MPS1 autoregulates its affinity for kinetochores will be an important future research effort.

The MPS1 localization module integrates the microtubule-attachment site, tension-dependent signaling, and mitotic checkpoint activity

Production of the MCC from a single kinetochore is inhibited upon engagement of this kinetochore with spindle microtubules, as exemplified by absence of MAD1 and MAD2 on attached kinetochores (*275*). Removal of these proteins is at least in part mediated by dynein-dependent poleward transport, but other, dynein-independent, mechanisms have been proposed. These include microtubule binding to the N-terminus of KNL1, attachment-dependent recruitment of phosphatases, and possibly an additional yet unresolved Spindly-controlled pathway (*275*). Any of these could, in principle, impinge on MPS1 kinetochore binding or regulation thereof by Aurora B. Our finding that MPS1 localization is dependent on the microtubule-binding domain of HEC1 offers a tentative alternative model. Although it is unclear if the molecular requirements of HEC1 to bind microtubules are the same as those that are required to promote MPS1 localization, the two functions of HEC1 could be mutually exclusive. In such a model, microtubule attachment would prevent MPS1 kinetochore binding, providing a direct mechanism of regulation. Absence of biorientation and the accompanying zone of Aurora B activity might continue to prime MPS1 kinetochore binding in case attachment is lost. This is consistent with asymmetric MPS1 localization on paired kinetochores during prometaphase and strongly reduced MPS1 levels on the attached sister kinetochore of a monotelic chromosome (Figure S5C, D), although dynein-dependent stripping could account for this behavior also. Further molecular insights into how the mitotic checkpoint machinery is integrated with the microtubule-attachment site and the error-correction machinery will be vital for understanding the coupling between attachment, tension and the cell-cycle responses to absence of either.

(Continued from previous page)

set to 1. (**C, D**) Representative images (C) and quantification (D) of immunolocalization of the indicated LAP-MPS1 proteins and centromeres (CENP-A) in MPS1-depleted HeLaK FRT TetR cells treated with nocodazole and reversine, with or without ZM447439. (DAPI) is in blue. Scale bar is 5 µm. Insets were magnified by 300%. Graph in D shows total kinetochore intensities (± SEM) of MPS1 relative to centromeres in DMSO-treated (gray bars) or ZM447439-treated (blue bars) cells. Data are from ≥32 cells from 2 experiments. Ratios for mock treated, LAP-MPS1^{WT} expressing cells are set to 1. (**E**) Time-lapse analysis of duration of mitotic arrest in HeLaK FRT TetR cells transfected with mock or MPS1 siRNA and expressing the indicated LAP-MPS1 proteins, and treated with nocodazole and DMSO (top panel) or nocodazole and ZM447439 (lower panel). Data indicate cumulative percentage of cells (from a total of ≥70 cells) that exit mitosis (scored as chromosomal decondensation) at the indicated times after NEB and are representative of ≥2 independent experiments. (**F**) Model of regulated MPS1 localization at unattached kinetochores. See Discussion for details.

Materials and methods

Protein expression and purification of MPS1$^{62-239}$

MPS1$^{62-239}$ was transformed in Rosetta2 (DE3) cells (Novagen). Cells were grown in LB medium at 30˚C until OD_{600nm}~0.6, then cooled down to 18˚C and induced at OD_{600nm}~0.8 for 16h with 1mM IPTG. For selenomethionine incorporation, the SelenoMet™ Medium (Molecular Dimensions Limited) was used according to the manufacturer instructions. Bacteria were harvested by centrifugation and resuspended in 100mL Buffer A (50mM Tris pH 7.5, 500 mM NaCl, 10mM Imidazole pH 8.0, 5 mM β-mercaptoethanol). Cells were lysed and cleared by high-speed centrifugation. The supernatant was treated with 2% streptomycin sulphate and further centrifuged. Finally the soluble extract was loaded on a 1 ml HisTrap affinity column (GE Healthcare) pre-charged with $NiCl_2$. After extensive washing with buffer A, the protein was eluted with a linear gradient of imidazole to 250 mM. The eluate was diluted 1:1 to reduce salt concentration, loaded on a 1 ml HiTrap Heparin column (GE Healthcare) and eluted with a linear gradient of NaCl to 2 M. The eluate was incubated with 3C protease for affinity tag cleavage, concentrated and loaded on a Superdex G75 16/60 Hi Load (GE Healthcare) equilibrated in Tris 25 mM pH 7.5, NaCl 150 mM, DTT 1 mM. The protein eluted as a monomer and was concentrated to 10 mg/ml and flash frozen in liquid nitrogen until further use.

Crystallization, data collection and structure solution

Crystals of MPS1$^{62-239}$ were grown in 0.1M MIB pH 5.0, 25% Peg1500 (Solution B2, PACT Screen, Qiagen; *286*) and were transferred into a cryoprotecting solution consisting of 25% glycerol before vitrification in liquid nitrogen. Data were collected at the ESRF on ID23-1 where the crystals diffracted to 2.2Å resolution in the space group $P2_12_12_1$ with cell dimensions a=79.9, b=80.1, c=142.2 Å. Phases were obtained by single wavelength anomalous dispersion (SAD), at the SLS beamline PX1. All data were integrated by MOSFLM (*287*) and scaled using SCALA (*288*). Since the a and b axes were very close to each other, many crystals appeared to belong to the primitive tetragonal rather than the primitive orthorhombic space group. Several datasets were collected, processed and analyzed using POINTLESS (*288*) and PHENIX.XTRIAGE (*289*). As the "more tetragonal" crystals appeared merohedrally twinned, we aimed to find orthorhombic crystals with minimal indications of twinning in the intensity distribution statistics. Such a dataset was identified with unit cell dimensions a=79.77 Å, b=79.81, c=139.2 Å, and a highly complete and redundant dataset was collected to 3.2 Å resolution. That crystal was used for phasing, using autoSHARP (*290*), based on the signal from the eight incorporated seleno-methionine residues resulting from four molecules within the asymmetric unit, two in each molecule. As the expected signal was rather low even in theory (2-3% at that resolution), the initial phases had a rather low FOM (0.22) which was improved after solvent flattening and two-fold non-crystallographic averaging to 0.86 (the four molecules were arranged in two pairs, as four-fold averaging was not useful in that case). These resulted in a good quality map that was used to build an initial model using BUCCANEER (*291*) and contained 582 residues (529 in sequence) dispersed in 8 discrete chains; this model however contained quite a few wrongly or out-of-register placed residues. A single molecule was manually isolated from that model using COOT (*292*), and was used as a search model to find the four copies in the related high resolution native dataset by molecular replacement using PHASER (*293*). The map from PHASER was subsequently used for running APR/wARP (*294*) to yield a model with 504 residues in 4 chains (405 in sequence), which contained no errors. That model was manually completed in COOT, with alternate rounds of refinement using REFMAC (*295*), followed by refinement in autoBUSTER (*296*) using autoncs and TLS refinement. The final model contained: residues 62-199, 62-195, 62-195 and 62-199 in the A, B, C and

D molecules respectively (preceded by residues GPG, which remained after protease cleavage); 229 water molecules, and several ordered components from the crystallization condition (11 glycerol, 5 PEG and 2 malonate molecules). Data collection and refinement statistics are shown in Table 1. The coordinates and structure factors have been deposited in the Protein Data Bank with accession no. 4B94.

Size-exclusion chromatography and multi-angle laser light scattering (SEC-MALLS) analysis

For quaternary structure determination of MPS1 constructs, 100µl of purified protein samples were injected (at 5mg/ml for $MPS1^{1-196}$, $MPS1^{9-255}$, $MPS1^{62-239}$ and at 15mg/ml for $MPS1^{1-239}$) into a Superdex S75 10/30 column connected to an ÄKTA FPLC (both GE Health Care) and coupled to a MiniDawn light scattering detector (Wyatt Technology). The measurements were performed in 20mM Hepes pH 7.4, 150 mM NaCl, 1mM TCEP and the elution profiles were monitored at 280 nm. Data was recorded and analyzed with the Astra 5 software (Wyatt Technology) using a differential index of refraction value of 0.185.

Ortholog definition and phylogenetic analyses

MPS1 orthologs were defined as described previously (*274*). In short: we performed BLAST (*297*) searches for hMPS1 against a local database comprised of genomes representative for all eukaryotic supergroups. The kinase domains of the resulting hits were aligned using MAFFT (*298*) with option LINSI. Positions with too many gaps (>20%) were excluded from the alignment. Subsequently, a RAxML (*299*) tree with 100 bootstraps was generated (option PROTGAMMAWAG). From the resulting tree a sub-cluster corresponding to the orthologous group of which hMPS1 is a member was delineated. Potential TPR domains in these homologs were searched for by constructing a HMMER3 profile (*300*) for the TPR domain of vertebrate MPS1 homologs. Significant sequences from additional MPS1 homologs were added to the profile in an iterative process until convergence. The domain topology (TPR, kinase) and resulting gene tree were visualized using iTOL (*301*).

Cell Culture and reagents

U2OS cells, HEK 293T cells and HeLa cells were grown in DMEM supplemented with 9% FBS, pen/strep (50 µg/ml) and L-glutamine (2 mM). All FRT HeLa cells stably expressing H2B-mRED, an HA-tagged Tet-repressor and doxycycline inducible MPS1 constructs were derived from the HeLaK FRT TetR cell line (*302*; a gift from U. Kutay; ETH Zurich, Switzerland) by transfection with pCDNA5/FRT/TO vector (Invitrogen) pOG44 (Invitrogen) and cultured in the same medium, but containing 9% Tet-approved FBS (Clontech), hygromycin (200 µg/ml) and puromycin (1 µg/ml). All HeLa Flp-in cells stably expressing a Tet-repressor and doxycycline-inducible MPS1 or HEC1 constructs were derived from the HeLa Flp-In cell line (*183*; gift from S. Taylor; University of Manchester, United Kingdom) as above and cultured in the same medium, but containing 9% Tet-approved FBS (Clontech), hygromycin (200 µg/ml) and blasticidin (4 µg/ml) instead. The U2OS-LacO cell line, bearing an array of 256 *lac* operator repeats on chromosome 1 (*303*) was a gift from I. Cheeseman (Whitehead Institute, Cambridge, USA). To induce protein expression in the inducible cell lines, doxycycline (1 ug/ml) was added for at least 8 hr. Thymidine (2 mM), nocodazole (830 nM), MG132 (10 µM), reversine (500 nM), doxycycline and puromycin (1 µg/ml) were all from Sigma. Hygromycin was from Roche. STLC (20 µM) and ZM447449 (2 µM) were both from Tocris Bioscience. Blasticidin was from PAA.

Immunoprecipitation and Immunoblotting

HEK 293T cells transfected with LAP-MPS1 (Figure S4E) or LAP-MPS1 and FLAG-MPS1 (Figure S1C)

were treated with thymidine for 24 hr and subsequently released into nocodazole for 16 hr. Cells were lysed in lysis buffer (50 mM Tris-Cl, pH 7.5, 150 mM NaCl, 5 mM EDTA, 1% Triton X-100, 0.1% SDS, 1mM β-glycerophosphate, 1mM NaF, 1 mM Na_3VO_4 and complete protease inhibitor [Roche]). LAP-MPS1 was bound to GFP-Trap agarose beads (ChromoTek) for 1 hr, washed four times in lysis buffer, after removal of all buffer sample buffer was added. Samples were separated by SDS-PAGE. Immunoblotting was done using standard protocols; the signal was visualized and analyzed on an ImageQuant LAS 4000 scanner (GE Healthcare) using enhanced chemiluminescence (Figures 2B, S1C, S4E) or analyzed on an Odyssey scanner (LI-COR Biosciences using fluorescently labeled secondary antibodies (Figures S3A, B).

Knockdown and reconstitution experiments with LAP-MPS1 and GFP-HEC1

For knockdown and reconstitution of MPS1 in HeLaK FRT TetR cell lines, cells were transfected with 10 nM MPS1 or mock siRNA for 16 hrs after which cells were arrested in early S-phase for 24 hrs by addition of thymidine. Subsequently, cells were released from thymidine for 8-10 hrs and arrested in prometaphase by the addition of nocodazole and (in MPS1 immunolocalization experiments) treated with reversine to accumulate MPS1 at kinetochores and MG132 to prevent mitotic exit. LAP-MPS1 expression was induced by the addition of doxycycline at the release from thymidine. For knockdown and reconstitution of MPS1 in HeLa Flp-in cells, cells were transfected with 20 nM MPS1 or mock siRNA and, in some experiments, 20 nM HEC1, NUF2 or KNL1 siRNA and subsequently treated as above. For knockdown and reconstitution of HEC1 in HeLa Flp-in cells, cells were transfected with 40 nM HEC1 or mock siRNA for 16 hrs after which cells were arrested S-phase for 24 hrs by addition of thymidine (2 mM). Subsequently, cells were released from thymidine and were transfected again with 40 nM HEC1 of mock siRNA. 8-10 hrs following the release, cells were arrested for a second time in S-phase for 14-16 hrs. Subsequently, cells were treated as above. GFP-HEC1 expression was induced by the addition of doxycycline at the time of the second thymidine addition. To compensate for less efficient incorporation of GFP-HEC1$^{\Delta 207}$ into kinetochores, its expression was induced at the time of the first thymidine addition. As a control, a cell line was used that inducibly expressed a full length mRNA encoding for GFP-HEC1 in which a stop codon was introduced to replace the first amino acid of HEC1 (GFP-HEC1^{STOP}), resulting in the expression of GFP.

Transfection and siRNA

For U2OS cells, plasmids were transfected using the calcium-phosphate method. Plasmids were transfected into HEK293T, HeLa and U2OS-LacO cells using Fugene 6 (Roche), according to the manufacturer's instructions. siRNAs used in this study were as follows: siRNAs used in this study were: si-HEC1 (5'-CCCUGGGUCGUGUCAGGAA-3', custom; Dharmacon), si-MPS1 (5'-GACAGAUGAUUCAGUUGUA-3', custom; Dharmacon), si-Mock (Luciferase GL2 duplex; Dharmacon/D-001100-01-20), si-NUF2 (5'-AAGCATGCCGTGAAACGTATA-3', custom; Dharmacon), siKNL1 (CASC5#5; Dharmacon/J-015673-05; 5'-GCAUGUAUCUCUUAAGGAA-3'). All siRNAs were transfected using Hiperfect (Qiagen) at 10, 20 or 40 nM (for HEC1 reconstitutions) according to manufacturer's instructions.

Antibodies

The following primary antibodies were used for immunofluorescence imaging and immunoblotting: MPS1-NT (Upstate), α-Tubulin (Sigma), CREST/ACA (Cortex Biochem), HEC1 (9G3; Abcam), GFP (custom rabbit polyclonal raised against full-length GFP as antigen; *205*), GFP (mouse monoclonal, Roche), CENP-A (3-19; Abcam), KNL1 (ab70537; Abcam), MAD2 (custom rabbit polyclonal raised

against full-length 6xHis-tagged MAD2 as antigen; *216*), pT676-MPS1 (custom rabbit polyclonal raised against the peptide CMQPDTpTSVVKDS coupled to KLH as antigen; *239*). Secondary antibodies were high-crossed goat-anti-human and anti-mouse Alexafluor647, goat-anti-rabbit and anti-mouse Alexafluor488 and Alexafluor568 (Molecular Probes) for immunofluorescence studies.

Live cell imaging, immunofluorescence and image quantification

For live cell imaging, cells were plated in 24-well glass bottom plates (MatTek), transfected and imaged in a heated chamber (37°C and 5% CO_2) using a 20X/0.5NA UPLFLN objective (Olympus) on an Olympus IX-81 microscope, controlled by Cell-M software (Olympus). Images were acquired using a Hamamatsu ORCA-ER camera and processed using Cell-M software. For imaging of H2B-mRed, multiple Z-layers were acquired and projected to a single layer by maximum intensity projection.

For immunofluorescence, cells, plated on 12-mm coverslips were pre-extracted with 0.1% Triton X-100 in PEM (100 mM PIPES, pH 6.8, 1 mM $MgCl_2$ and 5 mM EGTA) for 45 sec before fixation with 4% paraformaldehyde in PBS. Coverslips were washed with PBS and blocked with 3% bovine serum albumin (BSA) on PBS for 1 hr, incubated with primary antibodies for 2 to 4 hours at room temperature or 16 hours at 4°C, washed with PBS and incubated with secondary antibodies for an additional hour at room temperature. Coverslips were then incubated with DAPI for 2 minutes, washed and mounted using ProLong antifade (Molecular Probes). All images were acquired on a DeltaVision RT system (Applied Precision) with a 100X/1.40NA UPlanSAPO objective (Olympus) using SoftWorx software. Images are maximum intensity projections of deconvolved stacks. For quantification of immunostainings, all images of similarly stained experiments were acquired with identical illumination settings; cells expressing comparable levels of exogenous protein were selected for analysis and analyzed using ImageJ. An ImageJ macro was used to threshold and select all centromeres and all chromosome areas (excluding centromeres) using the DAPI and ACA channels as described previously (*195*). This was used to calculate the relative mean kinetochore intensity of various proteins ([centromeres-chromosome arm intensity (test protein)]/[centromeres-chromosome arm intensity (CREST/CENP-A)]. Immunostainings on LacO arrays were quantified as above, with the exception that the LacO dot was manually selected and that the relative mean LacO intensity of various proteins was calculated ([LacO-chromosome arm intensity (test protein)]/[LacO-chromosome arm intensity (GFP)].

Fluorescence recovery after photobleaching

Flp-in HeLa cells were grown in 8 well glass-bottom dishes (LabTek), depleted of endogenous MPS1 by transfection with MPS1 siRNA and induced to express $MPS1^{WT}$ or $MPS1^{\Delta TPR}$. The media was replaced with Leibovitz L-15 media (Invitrogen) supplemented with 10% FCS, 2 mM L-glutamine and 100 U/ml penicillin/streptomycin. Cells were treated with nocodazole (830 nM), MG132 (10 µM) and reversine (500 nM) 30 min before imaging. Cells expressing similar levels of LAP-MPS1 were selected for imaging. Samples were imaged on a personal DeltaVision system (Applied Precision) equipped with a heated chamber and lens warmer (both set at 37°C), with a 100X/1.40NA UPlanSAPO objective (Olympus) using SoftWorx software. Images were acquired using a CoolSNAP HQ2 (Photometrics) camera and processed using SoftWorx software and ImageJ. The EYFP-based LAP-tag of LAP-MPS1 was bleached using the 488-nM laser line of an Argon laser (max 20 mW) set to 100%. Areas centered on single kinetochore pairs were bleached once at 100% laser power for 200 ms. Fluorescence intensity of the entire cell was acquired for 3 pre-bleach iterations at a 500 ms interval and for 32 iterations post-bleach at an adaptive time interval (~600-800 ms). For each time point, the average

fluorescence intensity was measured in the area that encompassed kinetochore movement and in a similarly sized directly neighboring cytosolic area that was devoid of kinetochores throughout the experiment. Both areas were corrected for background and the mean fluorescence of the cytosolic area was substracted from the kinetochore area for each timepoint ($area_{(KT\text{-}cyto)}$). For each measurement, the average pre-bleach fluorescence intensity of the $area_{(KT\text{-}cyto)}$ was set to 100% and the measured post-bleach $area_{(KT\text{-}cyto)}$ signal was normalized to this value. Because a large volume of the cell was bleached, the total loss of YFP signal was calculated from the average fluorescence recovery in the cytosol at the last 3 timepoints (average fluorescence intensity post-bleach/average fluorescence intensity pre-bleach) and the post-bleach $area_{(KT\text{-}cyto)}$ measurements were normalized for this loss in total fluorescence ($area_{(KT\text{-}cyto)}$/[average fluorescence intensity post-bleach/average fluorescence intensity pre-bleach]). Recovery half-times (ln(2)/rate constant) and signal recovery were determined by non-linear curve fitting based on a one-phase association followed by a plateau using GraphPad Prism software.

Fluorescence assisted cell sorting

Cells were released from a 24 hr thymidine-induced block into nocodazole for 16 hr. All cells were harvested, washed once with PBS and fixed in 70% ice-cold ethanol for 2 hr. Cells were washed with PBS/0.1% Triton X-100 (PBST), incubated with anti-phospho-Ser/Thr-Pro antibody (MPM2; Millipore) in PBST for 1 h on ice and washed again in PBST. Incubation with Cy3-conjugated donkey-anti-mouse secondary antibody (Jackson Immunoresearch Laboratories) was for one hour on ice. After a final wash with PBST, DNA was stained with propidium iodide and cells were treated with RNAse A for 15 min and measured on a FACS Calibur flow cytometer (Becton Dickinson). Flow cytometric analysis of transfected cells was based on Spectrin-GFP expression. As control, a fraction of cells was lysed 48 hr post transfection and analyzed by immunoblotting for expression of exogenous MPS1.

Plasmids and cloning

pOG44 (Invitrogen) encodes a Flp recombinase expression vector. The pSuper-based shRNA plasmids used in this study were: Mock (AGATTCTAGCTAACTGTTC) and MPS1 (GACAGATGATTCAGTTGTA) as described previously (*205*). pCDNA3-LAP-$MPS1^{WT}$ and pCDNA3-LAP-$MPS1^{KD}$ encode full-length, N-terminally LAP-tagged and shRNA-insensitive (modified codons 288 and 289) wild-type or kinase-dead (D664A) MPS1, respectively and were described previously (*239*). pCDNA3-YFP-MIS12-$MPS1^{WT}$ and pCDNA3-YFP-MIS12-$MPS1^{KD}$ were created by inserting the full MIS12 sequence into pCDNA3-LAP-MPS1 and were described previously (215). pEGFP-$HEC1^{WT}$, a mammalian expression construct encoding N-terminally GFP-tagged full length wildtype HEC1, pEGFP-$HEC1^{9A}$ and pEGFP-$HEC1^{9D}$ (in which Ser4, Ser5, Ser8, Ser15, Ser55, Thr49, Ser55, Ser62 and Ser69 have been mutated to alanine or aspartic acid, respectively) have been described previously (*50*). pCDNA3-LAP-$MPS1^{\Delta 60}$ was created by introduction of an XhoI site at bases 174-179 of pCDNA3-LAP-$MPS1^{WT}$ and subsequent digestion with XhoI to excise bases 1-179 of MPS1. pCDNA3-LAP-$MPS1^{\Delta 100}$ was created by introduction of an XhoI site at bases 294-299 of pCDNA3-LAP-$MPS1^{WT}$ and subsequent digestion with XhoI to excise bases 1-299 of MPS1. pCDNA3-LAP-$MPS1^{\Delta 200}$ was created by introduction of an XhoI site at bases 594-599 of pCDNA3-LAP-$MPS1^{WT}$ and subsequent digestion with XhoI to excise bases 1-599 of MPS1. pCDNA3-LAP-$MPS1^{\Delta TPR}$ was generated by PCR of the LAP-tag and the first 186 bases of pCDNA3-LAP-$MPS1^{WT}$ using a reverse primer that contained a ClaI site and PCR of bases 577-1995 of MPS1 with a forward primer that contained a NarI site and ligation of ClaI site into the NarI site, creating a Ile-Ala linker. For generation of stable cell-lines, MPS1 and HEC1 cassettes were subcloned into pCDNA5/FRT/TO vector (Invitrogen). pCDNA5-FRT-TO-LAP-$MPS1^{WT}$ was created by ligation of the LAP-MPS1

module into the KpnI and ApaI sites of pCDNA5/FRT/TO. pCDNA5-FRT-TO-LAP-MPS1$^{1-192}$ was created by introduction of a stop codon at residue 193 of pCDNA3-LAP-MPS1^{WT} and subsequent cloning of the MPS1 cassette into pCDNA5-LAP-MPS1^{WT} with XhoI and ApaI. All other pCDNA5-FRT-TO-LAP-MPS1 constructs were created by ligation of the MPS1 cassette into the XhoI and ApaI restriction sites of pCDNA5-FRT-TO-LAP-MPS1^{WT}. All pCDNA5-FRT-TO-FLAG-MPS1 constructs were created by ligation of a double FLAG-tag into the BamHI and XhoI sites of pCDNA5/FRT/TO and subcloning of the MPS1 cassette into the XhoI and Apa I sites. All pCDNA3-YFP-MIS12-MPS1 constructs were created by ligation of the MPS1 cassette into the XhoI and ApaI restriction sites of pCDNA3-YFP-MIS12-MPS1^{WT}. pCDNA5-FRT-TO-GFP-HEC1^{WT} was created by digestion of pEGFP-HEC1^{WT}, a gift of J. DeLuca (Colorado State University, Fort Collins, USA), with NheI and ApaI and ligation of the GFP-HEC1^{WT} module into the XbaI and ApaI sites of pCDNA5/FRT/TO. pCDNA5-FRT-TO-GFP-HEC1^{STOP} was generated by mutagenesis of the HEC1 ATG to TAG by site directed mutagenesis. pCDNA5-FRT-TO-GFP-HEC1$^{\Delta 80}$ was created by looping out bases 1-237 of pCDNA5-FRT-TO-GFP-HEC1^{WT} by site directed mutagenesis. pCDNA5-FRT-TO-GFP-HEC1$^{\Delta 207}$ was created by looping out bases 1-618 of pCDNA5-FRT-TO-GFP-HEC1^{WT} by site directed mutagenesis. pCDNA5-FRT-TO-GFP-HEC1^{9A} was created by digestion of pEGFP-HEC1^{9A}, a gift of J. DeLuca (Colorado State University, Fort Collins, USA), with NheI and ApaI and ligation of the GFP-HEC1^{WT} module into the NheI and ApaI sites of pCDNA5-FRT-TO-GFP-HEC1^{WT}. pCDNA5-FRT-TO-GFP-HEC1^{9D} was created by site directed mutagenesis of pCDNA5-FRT-TO-GFP-HEC1^{WT} using the full length HEC1^{9D} gene, which was amplified by PCR from pEGFP-HEC1^{9D}-GFP, a gift of J. DeLuca (Colorado State University, Fort Collins, USA) as a mutagenesis primer. pLacI-LAP was created by a LacI PCR from pKG194 (a kind gift from I. Cheeseman and K. Gascoigne; Whitehead Institute, Cambridge, USA) and subsequent cloning into the Nhe1-site of pLAP (pIC113). All pLacI-GFP-HEC1 constructs were created by subcloning of the GFP-HEC1 cassette from pCDNA5-GFP-HEC1 constructs into the SacII and AgeI sites of pLacI-LAP. The sequence encoding for residues 62-239 of MPS1 was cloned into the pETNKI-His-3C-LIC-kan vector by ligation independent cloning. The resulting construct was fused N-terminally to the residues MAHHHHHHSAALEVLFQ-//-GPG, containing a HRV 3C protease cleavage site. All constructs were validated by sequencing of the full ORF.

Supplemental material

Figure S1 shows that MPS1 TPR lacks the characteristic KNL1-binding depression of BUB TPR domains and is monomeric in solution. Figure S2 shows the phylogenetic analysis of the MPS1 TPR domain. Figure S3 shows the expression of MPS1 and HEC1 in HeLa-FRT and HeLa Flp-in cell lines. Figure S4 shows that N-terminal MPS1 mutants retain kinase activity and display normal residence time at unattached kinetochores. Figure S5 shows that MPS1 localization is dependent on kinetochore-microtubule attachment status, but independent of Aurora B phosphorylation of the HEC1 tail.

Acknowledgments

We thank Tatjana Heidebrecht for assisting in some cloning and purification experiments, Jonathan Grimes for help in autoSHARP phasing, Jennifer DeLuca (Colorado State University) for GFP-HEC1 constructs, Stephen Taylor (University of Manchester) for the HeLa Flp-In cell line, Ulrike Kutay and Patrick Meraldi (ETH Zurich) for the HeLaK FRT TetR cells, Iain Cheeseman and Karen Gascoigne (Whitehead Institute) for the LacO/LacI system and the Kops, Lens, Medema and Rowland laboratories for insights and discussions. This work was supported by an ERC starting grant (KINSIGN, to GJPLK), by the Dutch Cancer Society (KWF UU2012-5427 to GJPLK), by EMBO (long-term fellowship to EC), and by the Swiss National Science Foundation (SNSF) PBBSP3-133408 (fellowship to EC).

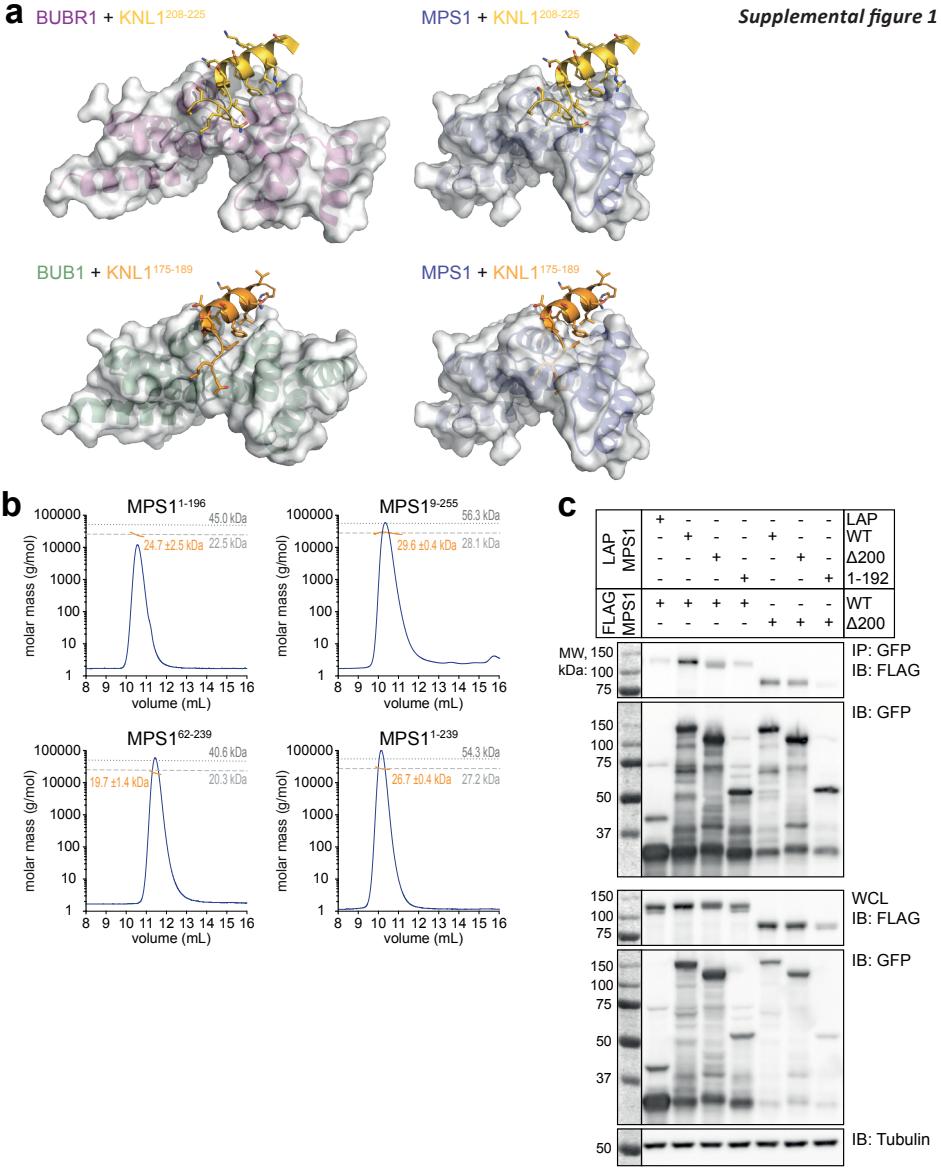

Figure S1: **MPS1 TPR lacks the characteristic KNL1-binding depression of BUB TPR domains and is monomeric in solution.** (**A**) Crystal structures of the BUB1 (PDB:4A1G) and BUBR1 (PDB:3SI5) TPR domains in complex with a KNL1 peptide, and structural superposition-based models of the binding of the MPS1 TPR domain to these peptides. The TPR domains are shown as cartoon diagrams in a semi-transparent surface as in Figure 1C. The orientation has been chosen to best illustrate the interaction interface with the KNL1 peptide, represented as a cartoon diagram with all side-chains shown as sticks. The superposition-based models for MPS1 illustrate the lack of the characteristic surface depression that facilitates KNL1 binding in the BUB TPR domains. (**B**) Size-exclusion chromatography and multiangle laser light scattering measurements of MPS1$^{1-196}$, MPS1$^{9-255}$, MPS1$^{62-239}$ and MPS1$^{1-239}$. The average Mr per volume unit (yellow dots) and the normalized UV_{280nm} elution profile (solid blue lines) are shown. The theoretical Mr values for the monomeric and dimeric forms are represented as dashed horizontal lines. (**C**) FLAG and GFP immunoblots (IB) of cell lysates (WCL; lower) or immunopurified (IP) FLAG-MPS1 (WT and Δ200; upper) from mitotic HEK 293T cells co-expressing FLAG-MPS1 and LAP-MPS1 variants (as indicated).

a

Supplemental figure 2

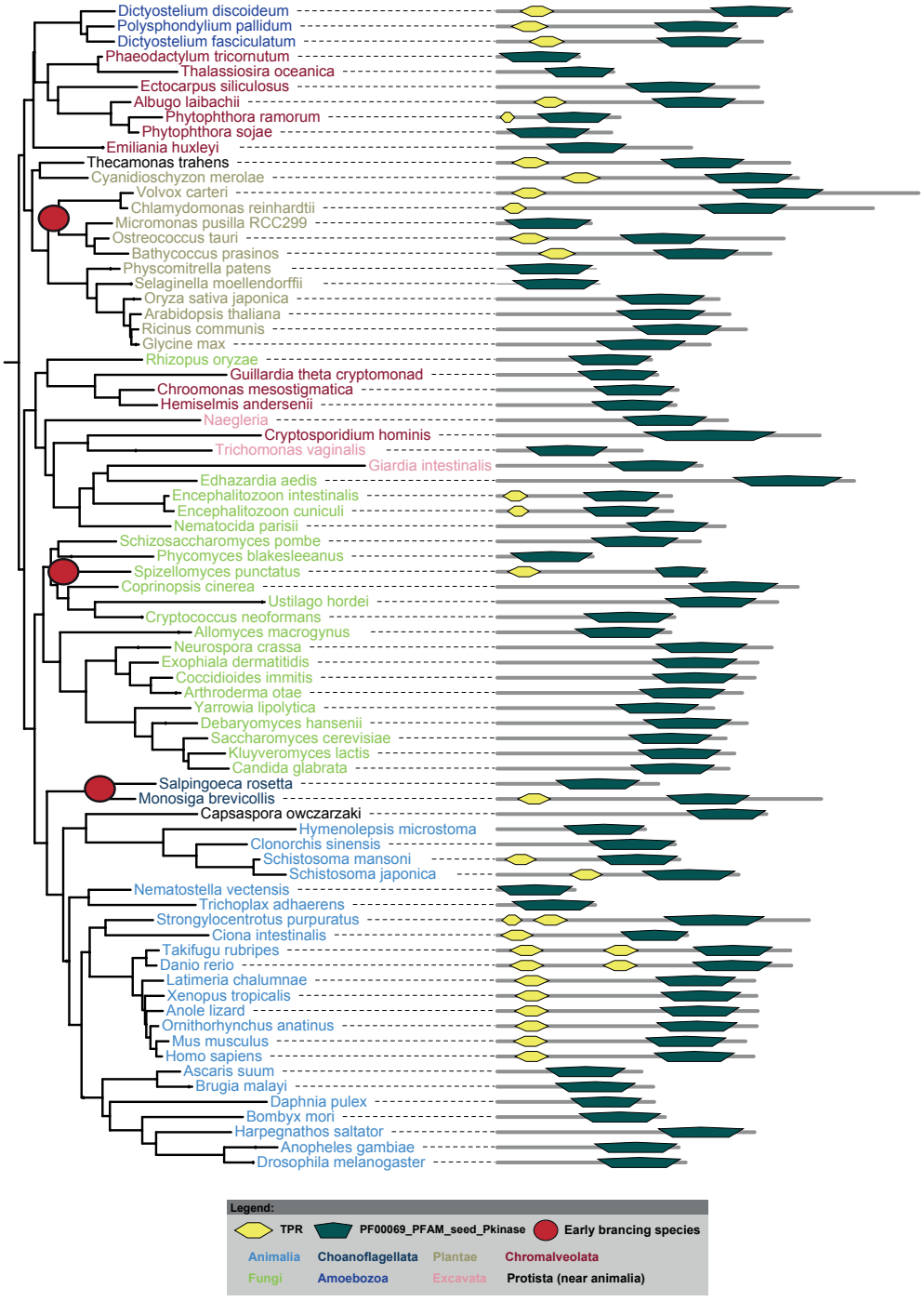

b

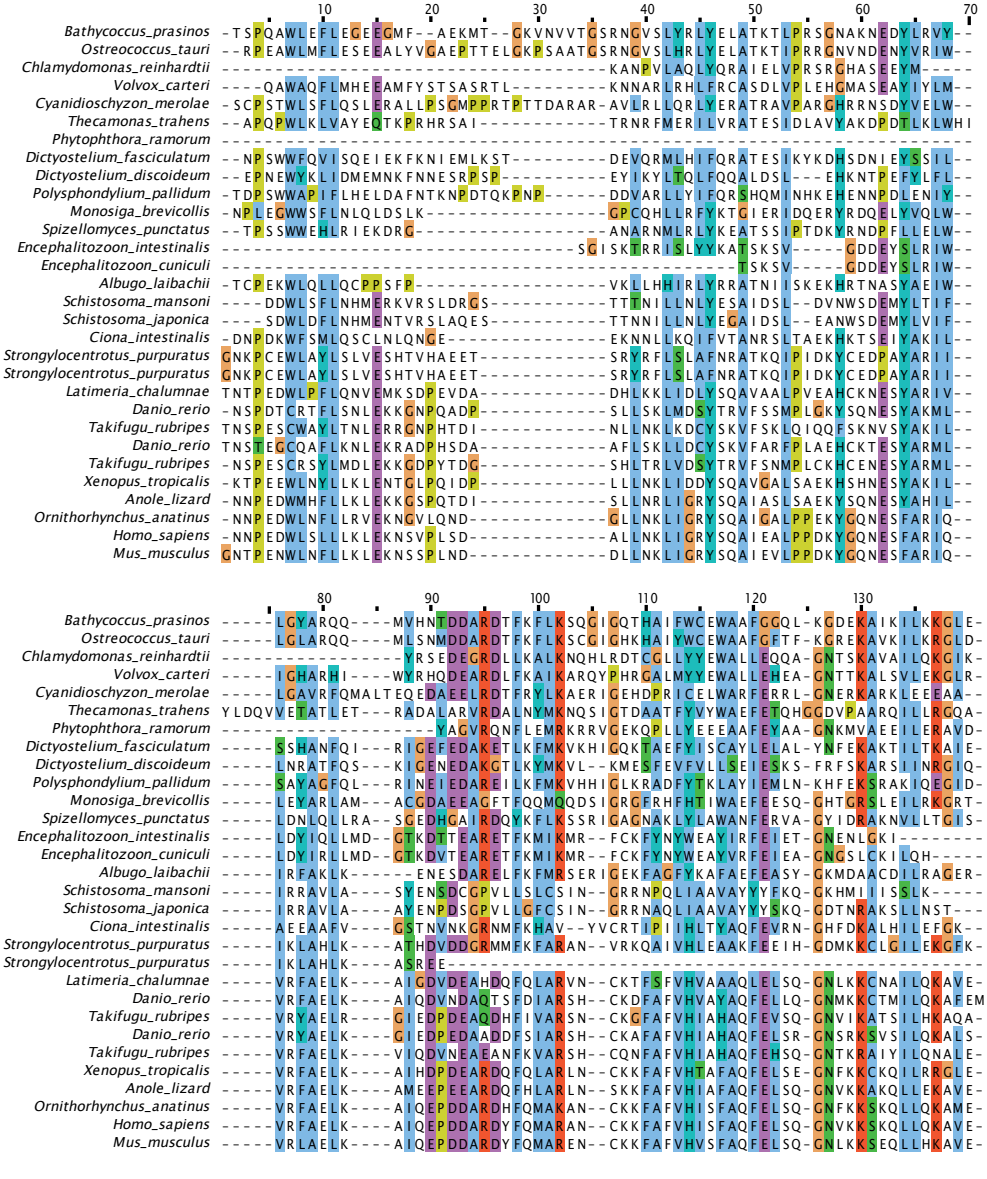

Figure S2: **Phylogenetic analysis of the MPS1 TPR domain.** (**A**) Phylogenetic tree of MPS1 homologs, based on the kinase domain. Differential coloring of major eukaryotic groups reveal clustering consistent with the eukaryotic species tree. Projection of the MPS1 domain topology onto the homolog tree shows a patchy distribution of the TPR domain, indicative of parallel evolution. Parallel loss is indicated by the presence of the TPR domain in species that branched off early relative to neighboring species in their major groups, e.g. algae versus plants and choanoflagellates versus animals (see red circles). Please note that we cannot formally exclude the possibility that incomplete gene annotation is an occasional reason for our inability to identify TPR domains in certain species (e.g. Salpingoeca rosetta, Nematostella vectensis, Trichoplax adhaerens and several chromaveolata). (**B**) Sequence alignment of the TPR domains of MPS1 homologs. Colors represent amino acid characteristics following the generally used clustal definition.

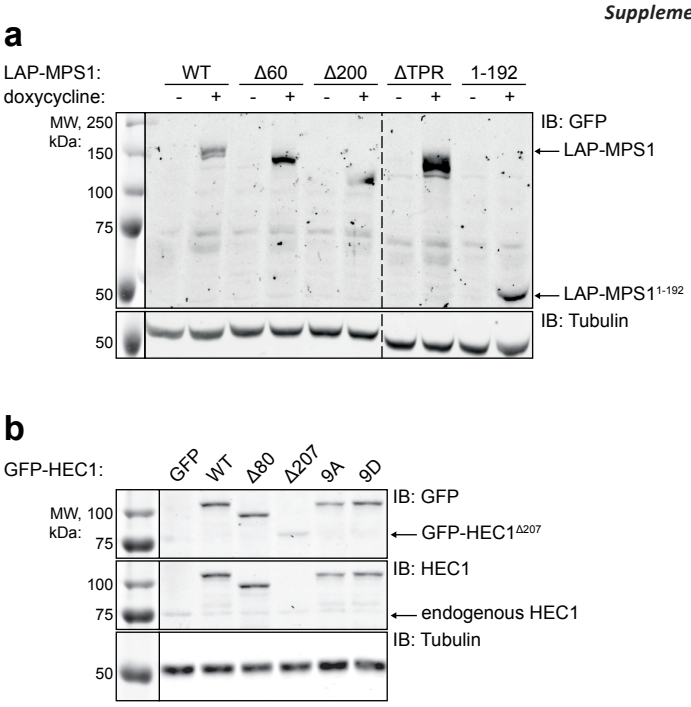

Figure S3: **HeLa-FRT LAP-MPS1 and HeLa Flp-in GFP-HEC1 cell lines.** (**A**) Immunoblot of whole cell lysates from mitotic HeLaK FRT TetR LAP-MPS1 cell lines that were induced (+ doxycycline) to express the indicated LAP-MPS1 proteins. Dotted line indicates excision of lanes. (**B**) Immunoblot of whole cell lysates from mitotic HeLa Flp-in GFP-HEC1 cell lines that were induced to express the indicated GFP-HEC1 proteins.

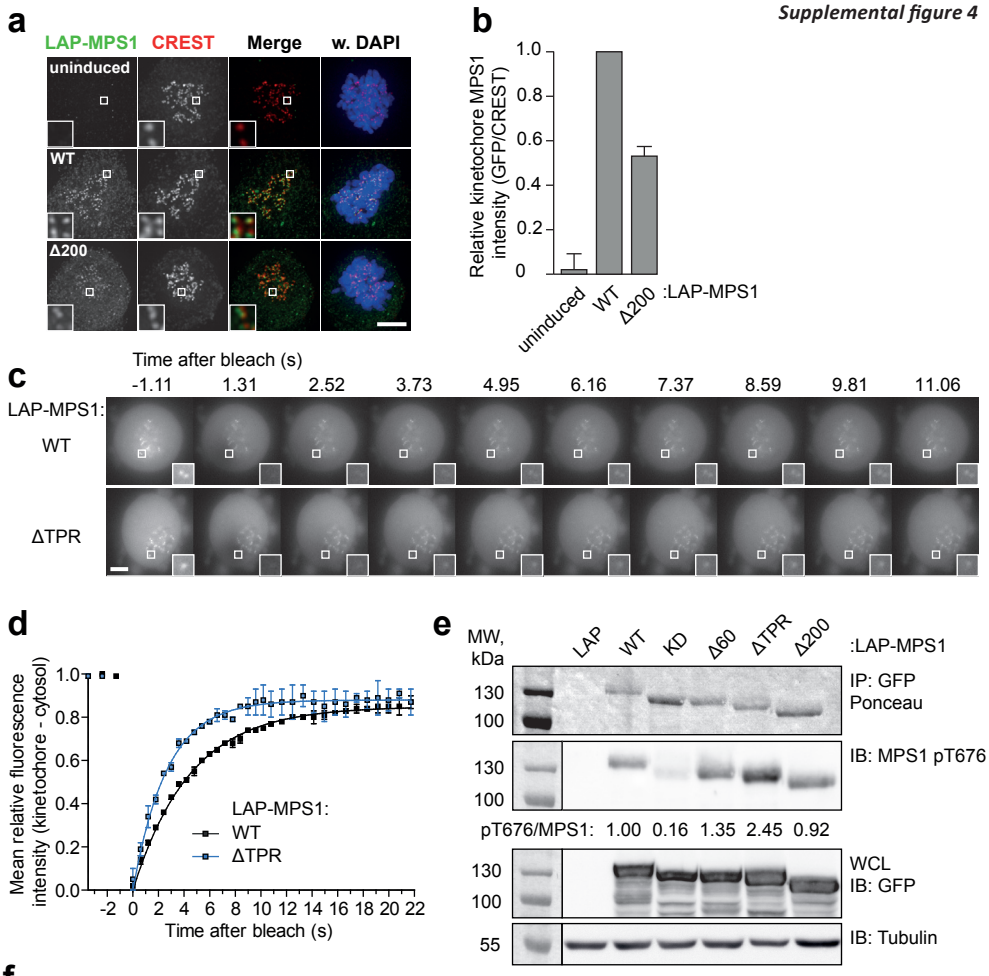

Figure S4: **N-terminal MPS1 mutants retain kinase activity and display normal residence time at unattached kinetochores.** (**A,B**) Representative images (A) and quantification (B) of immunolocalization of the indicated LAP-MPS1 proteins (GFP) and centromeres (CREST) in HeLaK FRT TetR cells treated with nocodazole, reversine (0.5 µM) and MG132. DNA (DAPI) is in blue. Scale bar is 5 µm. Insets were magnified by 390%. Graph in B shows total kinetochore intensities (± SEM) of LAP-MPS1 relative to centromeres. Data are from ≥19 cells from 2 experiments. Ratios for LAP-MPS1^{WT} expressing cells are set to 1. (**C, D**) Fluorescence recovery after photobleaching of LAP-MPS1^{WT} or LAP-MPS1$^{\Delta TPR}$-expressing Flp-in HeLa cells that were treated with nocodazole, MG132 and reversine (500 nM). Areas centered on single kinetochore pairs were bleached at t = 0 s. Scale bar is 5 µm. Insets were magnified by 300%. Graph in D shows the mean relative fluorescence intensities versus time (s) of the kinetochore regions from which intensities of neighboring cytosolic regions were substracted (± SEM). Data points have been fitted, yielding the curves shown (solid lines). LAP-MPS1^{WT} recovered with a $t_{½}$ of 3.0 s and a signal recovery of 0.85. LAP-MPS1$^{\Delta TPR}$ recovered with a $t_{½}$ of 1.8 s and a signal recovery of 0.88. Data are from 3 experiments and a total of ≥34 cells per condition. (**E, F**) Autophosphorylation assay of the indicated LAP-MPS1 proteins. MPS1 pT676 immunoblot (IB) and total protein levels are shown for immunopurified (IP) LAP-MPS1 from mitotic HEK 293T cells (upper); band intensity of MPS1 pT676/total protein relative to LAP-MPS1^{WT} is indicated. LAP-MPS1 (GFP) and tubulin immunoblots are shown for cell lysates (lower). Graph in F shows relative MPS1 pT676 intensity (± SD) relative to total protein. Data are from 3 experiments. Ratios for LAP-MPS1^{WT} are set to 1.

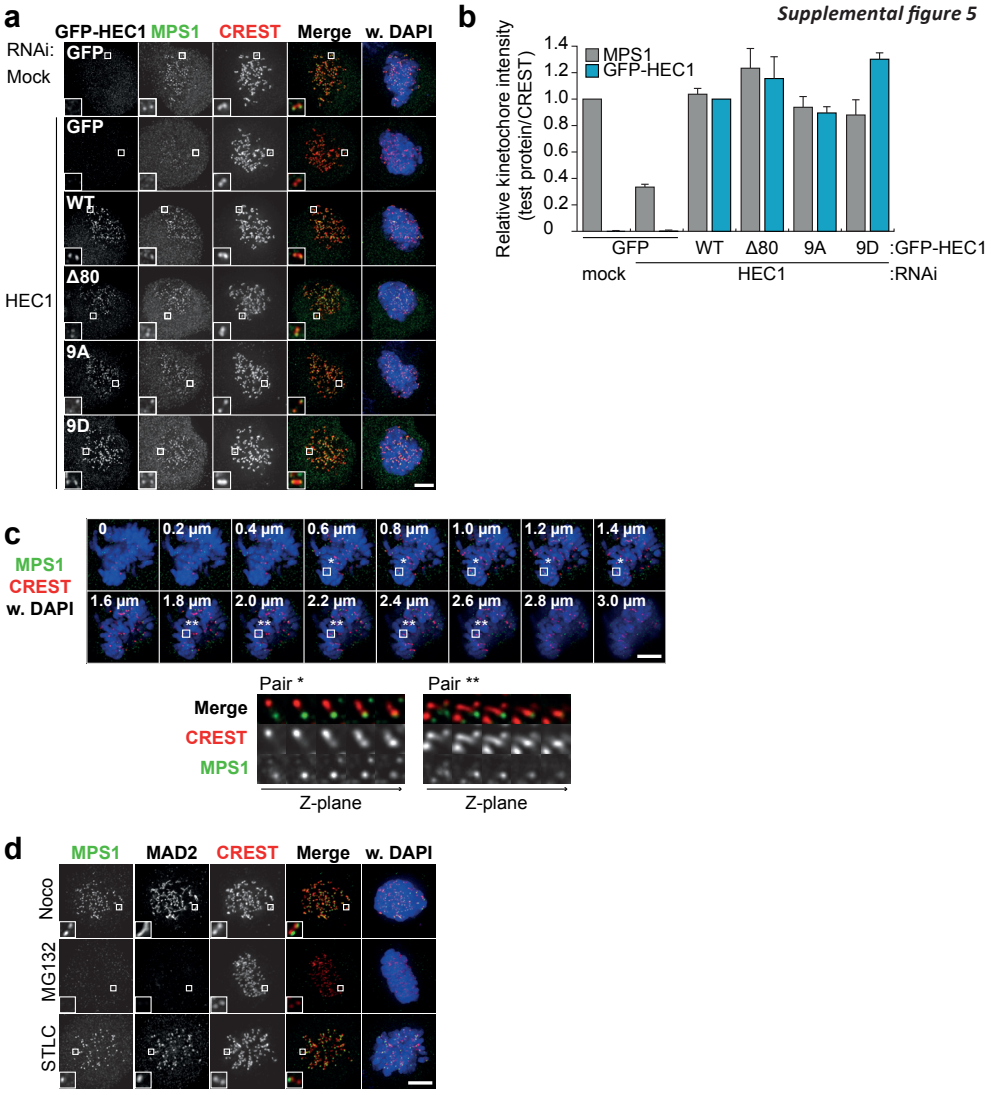

Figure S5: **MPS1 localization is dependent on kinetochore-microtubule attachment status, but independent of Aurora B phosphorylation of the HEC1 tail.** (**A, B**) Representative images (A) and quantification (B) of immunolocalization of the indicated GFP-HEC1 proteins and centromeres (CREST) in HeLa Flp-in cells transfected with mock or HEC1 siRNAs and treated with nocodazole and reversine (0.5 μM). DNA (DAPI) is in blue. Scale bar is 5 μm. Insets were magnified by 300%. Graph in B shows total kinetochore intensities (± SEM) of MPS1 (gray bars) and GFP-HEC1 (blue bars) relative to centromeres. Data are from ≥41 cells from 2 experiments. Ratios for mock RNAi treated cells are set to 1. Ratios of MPS1 localization are set to 1 for mock RNAi treated cells, or for GFP-HEC1 localization are set to 1 for GFP-HEC1^{WT} expressing cells. (**C**) Immunolocalization of MPS1 and centromeres (CREST) in an unperturbed prometaphase HeLa cell. Images show individual Z-planes at a 0.2 μm interval, as indicated. Asterisks indicate representative sister kinetochores pairs that are shown in blow-ups below. DNA (DAPI) is in blue. Scale bar is 5 μm. Lower panels were magnified by 400%. (**D**) Immunolocalization of MPS1 and centromeres (CREST) in HeLa cells that were treated with nocodazole (Noco), MG132 or S-trityl-l-cysteine (STLC) for 30 minutes. DNA (DAPI) is in blue. Scale bar is 5 μm. Insets were magnified by 300%.

Chapter 3

Exclusion of PP1 from kinetochores by Aurora B permits MPS1 localization and spindle assembly checkpoint activity

Wilco Nijenhuis[1,2] and Geert J.P.L Kops[1,2,3]

[1] Molecular Cancer Research and

[2] Department of Medical Oncology and

[3] Cancer Genomics Netherlands, University Medical Center Utrecht, 3584 CG, Utrecht, The Netherlands.

Manuscript in preparation

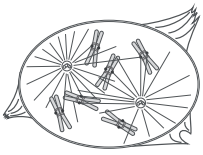

Abstract

The spindle assembly checkpoint (SAC) has evolved to delay chromosome segregation until all chromosomes have formed stable attachments to the mitotic spindle. Rapid SAC establishment and subsequent maintenance requires localization of the SAC kinase MPS1 to kinetochores of unattached chromosomes. MPS1 localization is regulated by Aurora B kinase activity by an unknown mechanism. Here, we show that Aurora B ensures MPS1 localization by excluding the phosphatase PP1 from kinetochores. Reducing kinetochore PP1, either by depletion or by mutating its binding site on the kinetochore scaffold KNL1, renders MPS1 kinetochore levels as well as SAC activity largely resistant to Aurora B inhibition. Conversely, allowing premature PP1 kinetochore binding by mutating the Aurora B phosphorylation site on KNL1 weakens the SAC. This SAC weakening can be overcome by artificially maintaining high levels of MPS1 at kinetochores. These data show that excluding PP1 from kinetochores is a prerequisite for establishing a robust SAC in human cells. Reversing this may be an important event in silencing the kinetochore-derived SAC signal upon microtubule attachment.

Introduction

Faithful chromosome segregation during mitosis is essential to maintain genomic stability. Two intertwined signaling networks have evolved to guard efficient and correct distribution of sister chromatids: The error-correction machinery destabilizes faulty kinetochore-microtubule interactions that arise quite frequently in early mitosis of human cells (*2, 98*), and the spindle assembly checkpoint (SAC) delays anaphase onset until all kinetochores are attached by spindle microtubules (*274*). The interplay between these two pathways ensures that the SAC is operating efficiently when error-correction takes place, and vice versa.

The core business of the SAC is inhibition of a multi-subunit E3-ubiquitin ligase called the anaphase promoting complex or cyclosome (APC/C) in order to maintain high levels of the key APC/C substrates Cyclin B and Securin (*274*). APC/C inhibition is accomplished by the mitotic checkpoint complex (MCC) that is formed by unattached kinetochores. The kinase MPS1 is a key contributor to this. Its localized activity at kinetochores promotes various aspects of SAC signaling, including kinetochore binding of a number of SAC proteins, MAD2 conformational activation, and MCC stabilization (reviewed in *277*). MPS1 recruitment to unattached kinetochores is dependent on the calponin-homology domain of the microtubule-binding protein HEC1 (*304*), but it is at present unclear if this represents a direct interaction.

Error-correction impinges on the 10-component KMN network, the main microtubule-binding site at kinetochores (*29, 116*). Aurora B phosphorylates multiple subunits within all three subcomplexes (MIS12, KNL1, NDC80), reducing microtubule binding affinity of the network. The two proteins within this network that directly interact with microtubules, HEC1 and KNL1, are phosphorylated by Aurora B in or near their microtubule-binding domains (*29, 43*). Phosphorylation of KNL1 occurs on pSer24 and pSer60 in N-terminal SSILK and RVSF motifs, respectively, and this, among others, excludes binding of the PP1 phosphatase to these motifs (*33, 36*). Due to PP1's ability to dephosphorylate Aurora B substrates, its exclusion from kinetochores in human cells allows error-correction (*36*). Subsequent relocalization of PP1 to kinetochores upon chromosome biorientation by dephosphorylation of these motifs is required to stabilize kinetochore-microtubule interactions. In C. *elegans* and fungi, however, kinetochore PP1 is involved in SAC silencing, but a role for Aurora B in regulating this was not reported in these species (*32, 257, 258*).

We and others recently established a role for Aurora B kinase activity in the recruitment of MPS1 to kinetochores, promoting MPS1 activation and thereby stimulating SAC activity (*195, 196, 215*). Aurora B-mediated control impinges on the N-terminus of MPS1 and likely drives MPS1 to a localization-proficient form (*304*). The present study set out to pinpoint the mechanism by which Aurora B regulates MPS1 kinetochore binding. Although HEC1 is critical for MPS1 localization and a premier substrate of Aurora B in error-correction, it is not the key effector of Aurora B with respect to MPS1 localization, since removing Aurora B phosphorylation sites on HEC1 does not impact MPS1 kinetochore binding (*304*). Instead, we here provide evidence that Aurora B regulates MPS1 localization indirectly, by preventing the binding of PP1 phosphatases to KNL1.

Results

PP1 depletion renders MPS1 localization and the SAC insensitive to Aurora B inhibition

To elucidate the mechanism by which Aurora B regulates MPS1 localization, we attempted to identify functionally relevant Aurora B phosphorylation sites. The two most likely candidate substrates in this regulation, HEC1 and MPS1, were excluded: The Aurora B sites in HEC1 are not involved in MPS1 recruitment (*304*) and while weak Aurora B-dependent *in vitro* phosphorylation of MPS1 was observed, mutation of the sites identified by mass spectrometry did not influence the kinetochore localization of MPS1 (data not shown). As Aurora B also regulates PP1 kinetochore binding (*36, 305*), we postulated that the regulation of MPS1 localization by Aurora B could be mediated by exclusion of PP1 from kinetochores. To examine this, we determined the effect of PP1 depletion on MPS1 localization. We chose to deplete the γ isoform, since PP1γ binds the outer kinetochore scaffold KNL1 in an Aurora B-dependent manner (*36, 306, 307*). Localization studies were performed in cells treated with the microtubule-depolymerizing drug nocodazole to exclude indirect effects of microtubules on MPS1 localization (Kops and Shah, 2012). Under such conditions, PP1γ kinetochore binding is expected to be minimal due to high Aurora B activity at the outer-kinetochore (*36, 109, 110*). In support of this, PP1γ depletion did not affect MPS1 or MAD2 localization in nocodazole-treated cells (Fig. 1A-C). In contrast, inhibition of Aurora B with the small molecule ZM447439 (*284*) reduced both MPS1 and MAD2 kinetochore levels (*195, 196, 304*) and this was significantly reversed by depletion of PP1γ (Fig. 1B-C).

Despite causing delocalization of MPS1, Aurora B inhibitors have no significant impact on the SAC response in nocodazole-treated cells. However, they weaken the SAC to the extent that it can be readily abrogated by low doses of the MPS1 inhibitor reversine (*195, 196, 304*; Fig. 1D). We used this sensitization of the SAC to further examine the role of PP1γ in SAC control by Aurora B. Live-cell imaging and measurements of the cumulative frequency of cells that exit mitosis at defined times after nuclear envelope breakdown showed that depletion of PP1γ delayed mitotic exit in ~20% of the cells after administration of ZM447439 and low reversine (Fig. 1D). The recovery of MPS1 localization and the improved SAC response upon PP1γ depletion support the hypothesis that PP1γ prevents MPS1 kinetochore binding when Aurora B is inactive.

N-terminal phosphorylation sites in KNL1 regulate PP1 kinetochore binding in human cells

PP1γ depletion may have numerous effects on cell division that could indirectly impair kinetochore function. To directly assess the role of kinetochore PP1 in MPS1 localization and SAC function, we next generated cell lines in which binding of PP1 to kinetochores was specifically impaired. PP1γ localizes to a region within the N-terminus of KNL1, consisting of a SSILK motif followed by a RVSF motif (Fig. 2A; *36*). Substitution of the RVSF motif for alanines ($KNL1^{4A}$) prevents PP1γ localization to metaphase kinetochores (*110*). Both motifs contain Aurora B phosphorylation sites at Ser24 (pSSILK) and Ser60 (RVpSF; *33*). Mutation of both serines to phospho-mimetic aspartic acids ($KNL1^{2SD}$) reduces the interaction of recombinant PP1γ with a KNL1 fragment *in vitro* (*36*). To directly study the role of the PP1-KNL1 interaction in Aurora B-mediated control of the SAC, we generated cell lines stably expressing siRNA-resistant full-length LAP-KNL1 variants carrying mutations that either abrogate PP1 localization (4A or 2SD) or that should permit PP1 localization even if Aurora B activity towards the KMN network is high (2SA). KNL1 was expressed from a doxycycline-inducible promoter in a

single integration site to ensure comparable genetic background and expression levels (Fig. 2B). All four LAP-KNL1 constructs (WT, 2SA, 2SD and 4A) were efficiently incorporated into kinetochores upon depletion of endogenous KNL1 by RNAi (Fig. 2C). For unknown reasons, we, like others (*36, 109, 306, 307*), were unable to detect endogenous PP1 at mitotic kinetochores with commercially available antibodies (not shown). We thus resorted to live-cell imaging of transiently expressed

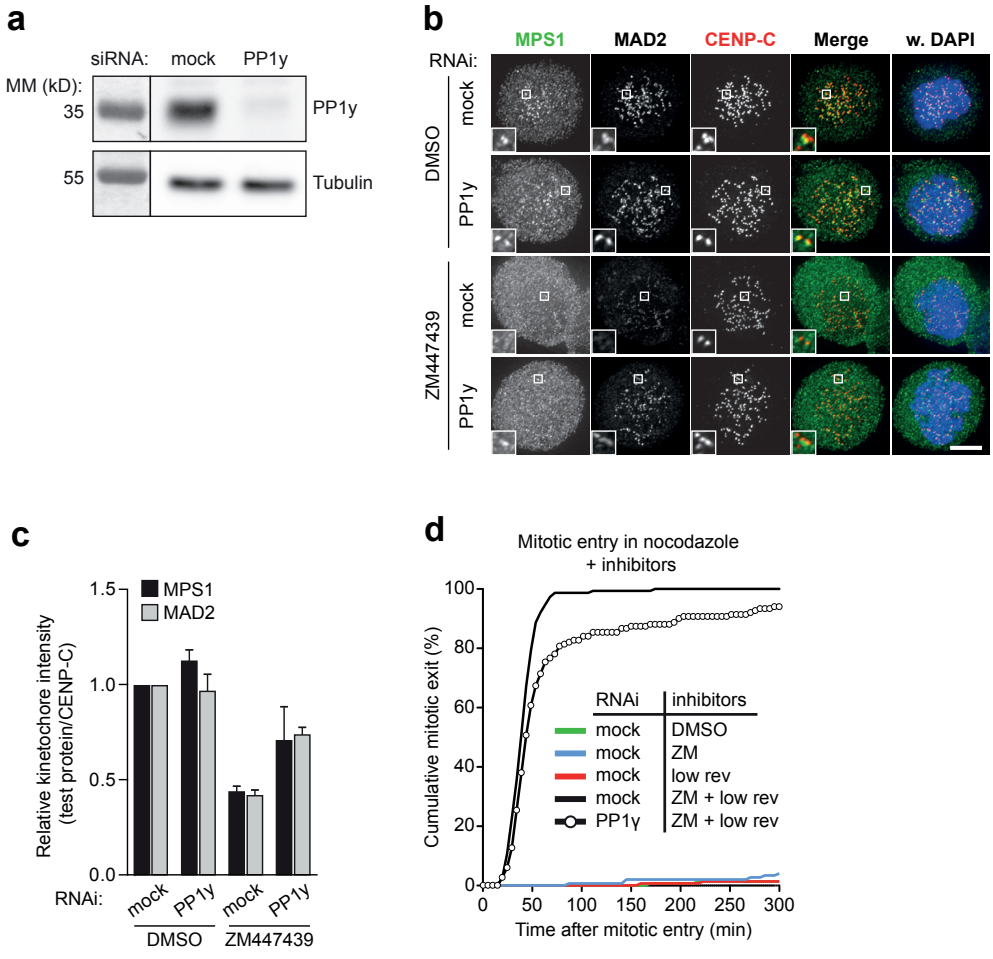

Figure 1. **Aurora B regulation of MPS1 localization is dependent on PP1.** (**A**) Immunoblot of whole-cell lysates from HeLa Flp-in cells that were transfected with mock or PP1γ siRNA. Boxes on left show molecular mass standard. MM, molecular mass. (**B and C**) Representative images (B) and quantification (C) of immunolocalization of MPS1, MAD2 and centromeres (CENP-C) in nocodazole and DMSO or ZM447439-treated Flp-in Hela cells transfected with mock or PP1γ siRNA. DNA (DAPI) is shown in blue. Insets show magnifications of the boxed regions. Graph in C displays total kinetochore intensities displays total kinetochore intensities (±SEM) of the indicated proteins relative to centromeres (CENP-C). Data are from a total of ≥30 cells per treatment from 2 experiments. Ratios are set to 1 for mock RNAi and DMSO-treated cells. (**D**) Time-lapse analysis of duration of mitotic arrest in nocodazole-treated Flp-in HeLa cells transfected with or PP1γ siRNA (indicated). Cells entered mitosis in the presence of DMSO, 125 nM of reversine (low rev), ZM447439 or a combination thereof (indicated). Data indicate cumulative percentage of cells (from a total of ≥150 cells) that exit mitosis (scored as cell flattening) at the indicated times after nuclear envelope breakdown and are representative of 3 independent experiments. Bars, 5 µm.

2xRFP-PP1γ in our KNL1 cell lines to determine the kinetochore PP1γ levels in our system (Fig. 2C-F). Quantification of 2xRFP-PP1γ levels on kinetochore pairs in live cells arrested in metaphase by the proteasome inhibitor MG132 for two hours revealed that 2xRFP-PP1γ was significantly enriched in cells expressing LAP-KNL1^{WT} whereas it was substantially reduced in cells expressing KNL1^{4A}, as expected (*36*). Interestingly, whereas 2xRFP-PP1γ recruitment to KNL1^{2SD} was almost as low as to KNL1^{4A}, recruitment to KNL1^{2SA} was increased to levels exceeding those of KNL1^{WT} cells. We thus conclude that, as predicted by Liu and colleagues, phosphorylation of Ser24 and Ser60 in KNL1 decreases the affinity of PP1γ for kinetochores. Reducing kinetochore PP1 levels has been reported to preclude the formation of stable kinetochore-microtubule attachments (*110*). In line with this, expression of KNL1^{2SD} or KNL1^{4A} impaired chromosome alignment (Fig. S1A-B): 41% and 51% of cells expressing KNL1^{2SD} or KNL1^{4A}, respectively, could not reach full alignment, compared to 16% of KNL1^{WT}-expressing cells. Likewise, premature PP1 localization by expression of KNL1^{2SA} also impaired alignment but to a lesser extent.

Preventing PP1 kinetochore binding renders MPS1 localization insensitive to Aurora B inhibitors

Since the Aurora B sites in KNL1 regulate PP1 kinetochore levels and given that Aurora B inhibition reduces kinetochore MPS1 in a PP1-dependent manner, we next wished to address if kinetochore-localized PP1 controls MPS1 kinetochore binding. To this end, endogenous MPS1 was detected by immunofluorescence in cells treated with nocodazole and the MPS1 inhibitor reversine to circumvent potential indirect effects of PP1 on MPS1 activity that are reflected in MPS1 kinetochore levels (*215, 304*). In nocodazole-treated cells, with high Aurora B activity, MPS1 was clearly detectable at kinetochores of cells expressing any of the KNL1 variants (Fig. 3A, C). Surprisingly, kinetochore MPS1 was not affected in cells expressing KNL1^{2SA} compared to those expressing KNL1^{WT}, KNL1^{2SD} or KNL1^{4A}. We show in figure 2F that KNL1^{2SA} recruits high levels of PP1γ to metaphase kinetochores. However, *in vitro* the 2SA mutation weakened the interaction between PP1γ and a KNL1 fragment (*36*). This suggests that in DMSO-treated cells, the KNL1^{2SA} mutant may not bind PP1γ as strongly as the unphosphorylated endogenous protein does in ZM447439-treated cells. Therefore, we determined if exclusion of PP1 from kinetochores could recover kinetochore localization of MPS1 when Aurora B was inhibited. Indeed, MPS1 displacement from kinetochores after Aurora B inactivation with ZM447439 was significantly rescued in KNL1^{2SD}- and KNL1^{4A}-expressing cells (Fig. 3B-C). This was further reflected in the levels of BUB1 at kinetochores: preventing the PP1-KNL1 association nearly completely recovered BUB1 kinetochore localization in ZM447439-treated cells (Fig. 3D-F). These data support the hypothesis that Aurora B-mediated disruption of the KNL1-PP1 interaction ensures high levels of MPS1 at kinetochores.

Figure 2. **Phosphorylation of Ser24 and Ser60 in KNL1 regulates PP1 kinetochore levels.** (**A**) Schematic representation of the various KNL1 mutants used in this study. (**B**) Immunoblot of whole cell lysates from mitotic HeLa Flp-in LAP-KNL1 cell lines that were transfected with mock or KNL1 siRNA and induced (+ doxycycline) to express the indicated LAP-KNL1 proteins. Boxes on left show molecular mass standard. MM, molecular mass. TFR, Transferrin receptor protein 1. (**C-F**) Representative images (C) and quantification (D-F) of the localization of the various LAP-KNL1 proteins and RFP-PP1γ in live MG132-treated KNL1-depleted Flp-in HeLa cells. Scale bar is 5 μm. Quantifications (E, F) were done as in D, for both channels lineplots of aligned sister kinetochores were drawn and transposed to center the inner centromere and after background substraction of each individual plot, averaged. Graph in E shows mean background-corrected LAP-KNL intensity of the various LAP-KNL1 proteins. Graph in F shows mean background-corrected RFP-PP1γ intensity in cells expressing the corresponding LAP-KNL1 proteins. Values from ≥30 lineplots and 6 cells per condition. Plot profile in gray shows LAP-KNL1^{WT} localization. Bars, 5 μm. WT, wild type.

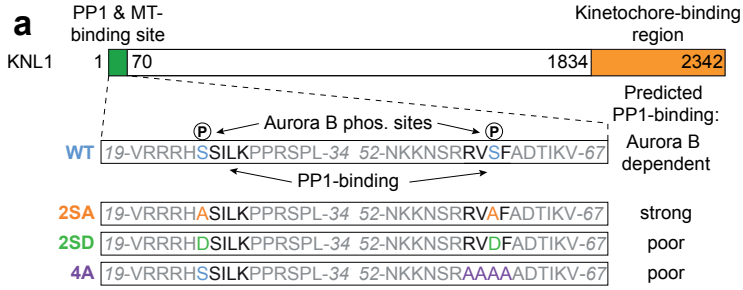
a
PP1 & MT-binding site
Kinetochore-binding region
KNL1
1
70
1834
2342
Predicted PP1-binding: Aurora B dependent
Aurora B phos. sites
WT 19-VRRRHSSILKPPRSPL-34 52-NKKNSRRVSFADTIKV-67
PP1-binding
2SA 19-VRRRHASILKPPRSPL-34 52-NKKNSRRVAFADTIKV-67 strong
2SD 19-VRRRHDSILKPPRSPL-34 52-NKKNSRRVDFADTIKV-67 poor
4A 19-VRRRHSSILKPPRSPL-34 52-NKKNSRAAAAADTIKV-67 poor

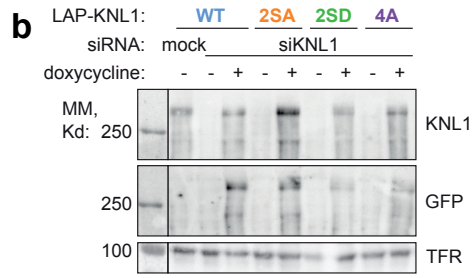
b
LAP-KNL1: WT 2SA 2SD 4A
siRNA: mock siKNL1
doxycycline: - - + - + - + - +
MM, Kd: 250
KNL1
250
GFP
100
TFR

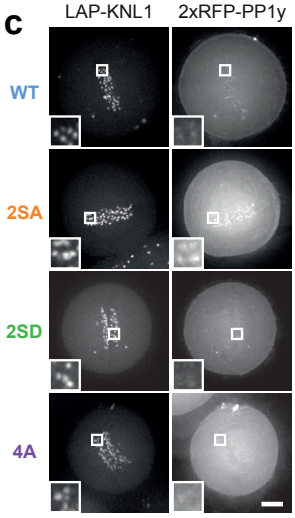
c
LAP-KNL1
2xRFP-PP1y
WT
2SA
2SD
4A

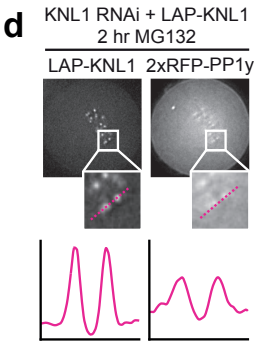
d
KNL1 RNAi + LAP-KNL1
2 hr MG132
LAP-KNL1
2xRFP-PP1y

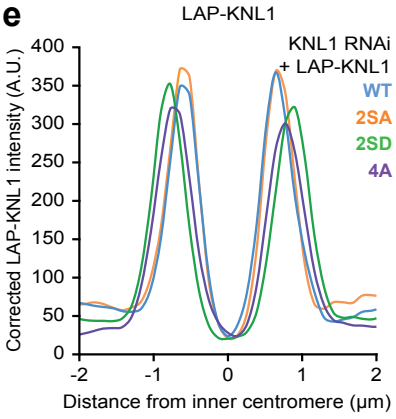
e
LAP-KNL1
KNL1 RNAi + LAP-KNL1
WT
2SA
2SD
4A
Corrected LAP-KNL1 intensity (A.U.)
400
350
300
250
200
150
100
50
0
-2
-1
0
1
2
Distance from inner centromere (µm)

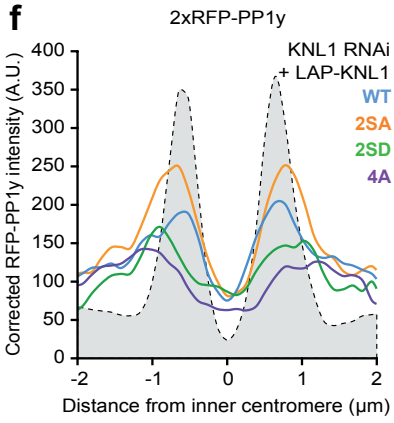
f
2xRFP-PP1y
KNL1 RNAi + LAP-KNL1
WT
2SA
2SD
4A
Corrected RFP-PP1y intensity (A.U.)
400
350
300
250
200
150
100
50
0
-2
-1
0
1
2
Distance from inner centromere (µm)

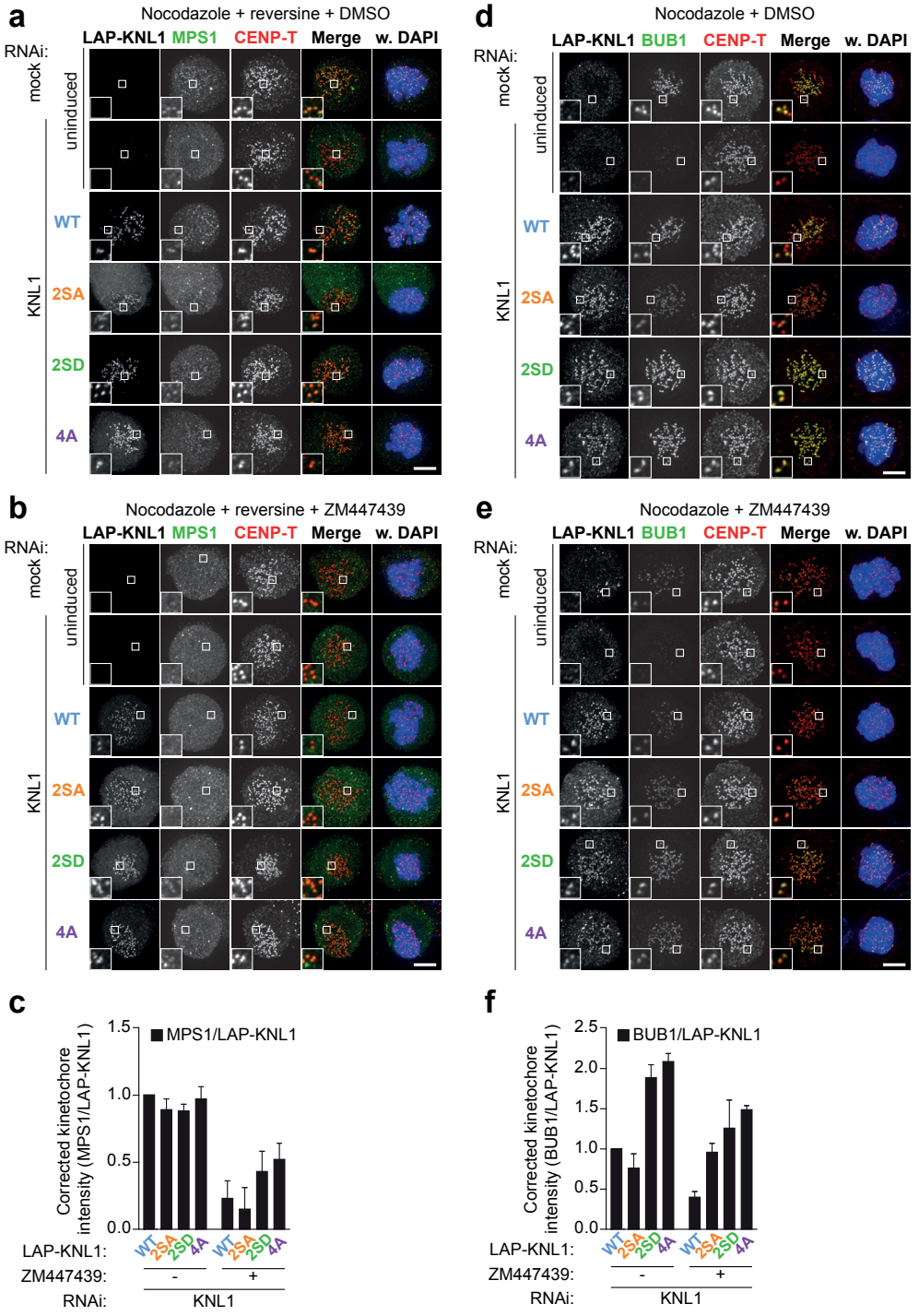
a
Nocodazole + reversine + DMSO
LAP-KNL1 MPS1 CENP-T Merge w. DAPI
RNAi:
mock
uninduced
KNL1
WT
2SA
2SD
4A
d
Nocodazole + DMSO
LAP-KNL1 BUB1 CENP-T Merge w. DAPI
b
Nocodazole + reversine + ZM447439
e
Nocodazole + ZM447439
c
MPS1/LAP-KNL1
Corrected kinetochore intensity (MPS1/LAP-KNL1)
1.5
1.0
0.5
0.0
LAP-KNL1:
ZM447439:
RNAi:
-
+
KNL1
f
BUB1/LAP-KNL1
Corrected kinetochore intensity (BUB1/LAP-KNL1)
2.5
2.0

Precocious PP1 kinetochore binding weakens the SAC response

Our data thus far predict that alterations in PP1 levels at kinetochores should affect the SAC response: elevated levels (2SA) are predicted to weaken the SAC, while reduced levels (2SD and 4A) are predicted to strengthen the SAC or at least delay its efficient silencing. This is true in budding yeast, where a RVSF to RASA mutant that perturbed the Spc105/KNL1-PP1 interaction prevented SAC silencing (*257*). In agreement with this, PP1 localization to kinetochores in human cells is maximal in metaphase but weak in prometaphase and in nocodazole-treated cells (*36, 109*). To determine the influence of PP1 localization, the SAC response to nocodazole was measured in cells in which endogenous KNL1 was reconstituted with the various LAP-KNL1 mutants. In our hands, KNL1 depletion did not potently abolish the SAC, presumably due to lack of RNAi penetrance. We therefore sensitized the SAC by adding a low dose of reversine (250 nM) before cells entered mitosis. Under these conditions, nocodazole-treated cells depleted of KNL1 rapidly exited mitosis (70% exit after 40 minutes, 100% exit after 250 minutes) while mock-depleted cells maintained a mitotic arrest for many hours (4% exit after 250 minutes; Fig. 4A). Replacement of endogenous KNL1 with KNL1^{WT} restored the SAC response (17 % exit after 250 minutes), as did expression of KNL1^{2SD} (28 % exit after 250 minutes) or KNL1^{4A} (11% exit after 250 minutes; Fig. 4A). Strikingly, however, cells expressing LAP-KNL1^{2SA} exited as rapidly as cells from which KNL1 had been depleted (84% exit after 40 minutes, 100% exit after 250 minutes; Fig. 4A), suggesting that precocious binding of PP1 to KNL1 at the onset of mitosis synergizes with MPS1 inhibition, together potently preventing SAC activation. In support of this, efficient depletion of PP1α, PP1γ or both partially restored the SAC response in KNL1^{2SA}-expressing cells (Fig. 4B, C).

We next asked if PP1-binding mutants of KNL1 also affected SAC silencing. To this end, low dose of reversine was added to nocodazole-arrested mitotic cells that had already engaged the SAC, and mitotic exit was monitored by timelapse imaging. Under these conditions, both mock-depleted and KNL1^{WT}-expressing cells showed significant SAC silencing (50% exit after respectively 114 and 120 minutes), which was enhanced by depletion of KNL1 (50% exit after 58 min; Fig. 4D). Similar to effects on SAC establishment, cells expressing LAP-KNL1^{2SA} were unable to delay mitotic exit to any extent (50% exit after 56 min; Fig. 4D). Interestingly, expression of LAP-KNL1^{2SD} and especially LAP-KNL1^{4A} significantly prevented mitotic exit beyond that achieved by KNL1^{WT} (50% exit after 180 min and >250 min, respectively; Fig 4D).

Exclusion of PP1 from kinetochores maintains a SAC response in the absence of Aurora B activity

Similar to KNL1, functionality of Aurora B in the SAC can be visualized by our sensitized SAC assay. Addition of 125 nM reversine or ZM447439 to nocodazole-treated cells has little effect on ability of the SAC to delay mitosis for hours, but co-administration of both inhibitors potently abrogates the

Figure 3. **Preventing PP1 kinetochore binding renders MPS1 and BUB1 localization insensitive to Aurora B inhibitors.** (**A-C**) Representative images (A, B) and quantification (C) of immunolocalization of the various LAP-KNL1 proteins, MPS1 and centromeres (CENP-T) in nocodazole, MG132, reversine and DMSO (A) or ZM447439-treated (B) Flp-in HeLa cells transfected with mock or KNL1 siRNA. Graph in C displays kinetochore intensities (±SEM) of MPS1 relative to LAP-KNL1. Data are from a total of ≥41 cells per treatment from ≥3 experiments. (**D-F**) Representative images (D, E) and quantification (F) of immunolocalization of the various LAP-KNL1 proteins, BUB1 and centromeres (CENP-T) in nocodazole, MG132 and DMSO (D) or ZM447439-treated (E) Flp-in HeLa cells transfected with mock or KNL1 siRNA. Graph in F shows kinetochore intensities (±SEM) of BUB1 relative to LAP-KNL1. Data are from a total of ≥25 cells per treatment from ≥2 experiments. DNA (DAPI) is shown in blue. Ratios are set to 1 for LAP-KNL1^{WT}-expressing in DMSO treated cells. Insets show magnifications of the boxed regions. Bars, 5 μm. WT, wild type.

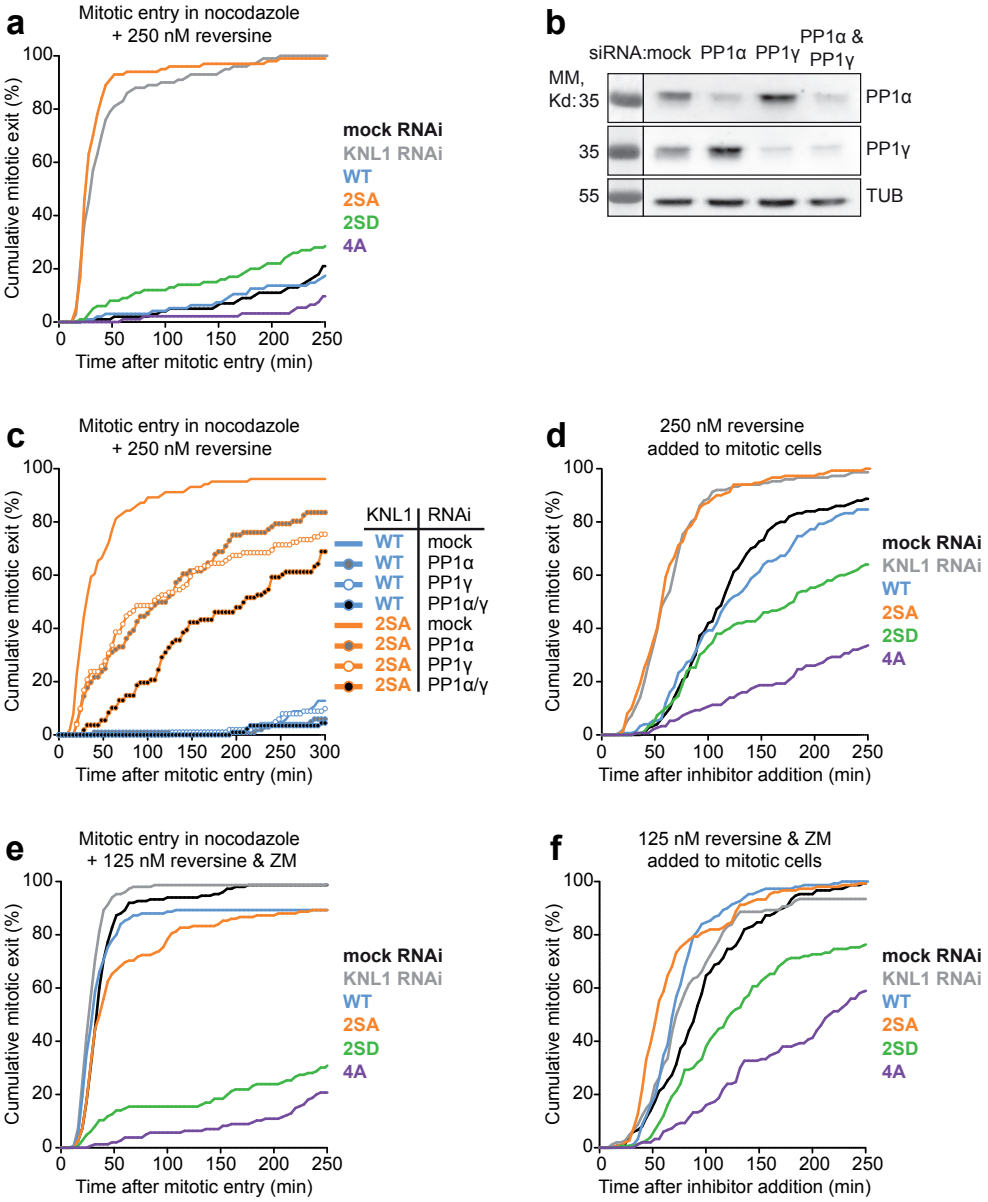

Figure 4. **Kinetochore PP1 modulates establishment and silencing of SAC signaling.** (**A**) Time-lapse analysis of duration of mitotic arrest in nocodazole-treated Flp-in HeLa cells transfected with mock or KNL1 siRNA and expressing the indicated LAP-KNL1 proteins. Cells entered mitosis in the presence of 250 nM of reversine. Data indicate cumulative percentage of cells (from a total of 100 cells) that exit mitosis (scored as cell flattening) at the indicated times after nuclear envelope breakdown and are representative of 2 independent experiments. (**B**) Immunoblot of whole-cell lysates from HeLa Flp-in cells that were transfected with mock, PP1α, PP1γ or a combination thereof (indicated). Boxes on left show molecular mass standard. MM, molecular mass. TUB, α-Tubulin. (**C**) Time-lapse analysis as in A. Nocodazole-treated Flp-in HeLa cells expressing the indicated LAP-KNL1 proteins were transfected with KNL1 siRNA and a combination of mock, PP1α and PP1γ siRNA (indicated). Data (from a total of ≥77 cells) are representative of at least 2 independent experiments. (**D**) Time-

SAC (*195, 304*; Fig. 1D). Inactivation of the SAC by ZM447439 under these conditions is dependent on delocalization of MPS1, as artificially tethering MPS1 to kinetochores recovers the SAC response (*195, 304*). Given our observation that KNL1^{2SA} weakened the SAC response and that KNL1^{2SD} and KNL1^{4A} significantly prevented MPS1 delocalization upon Aurora B inhibition, we therefore next asked if expression of mutants that prevent PP1 kinetochore recruitment would recover SAC activation when cells were treated with a combination of Aurora B inhibitor and a low dose of MPS1 inhibitor (Fig. 4E). As expected, control cells as well as cells treated with KNL1 siRNA, and cells expressing KNL1^{WT} or KNL1^{2SA} failed to mount a significant SAC response when treated with low reversine and ZM447439. Importantly, and in agreement with significant maintenance of MPS1 at kinetochores (Fig. 3C), KNL1^{2SD} or KNL1^{4A} enabled effective and prolonged activation of the SAC. Moreover, when mitotic cells that had already established a SAC response were challenged with low reversine and ZM447439, KNL1^{2SD}- and KNL1^{4A}-expressing cells maintained their mitotic states far longer than KNL1^{2SA} or KNL1^{WT}-expressing cells (Fig. 4F). Together, these data show that preventing PP1-KNL1 association contributes to the establishment and maintenance of the SAC by Aurora B activity.

If excluding PP1 from kinetochores is an important mechanism by which Aurora B impacts MPS1 kinetochore binding and thus the SAC, recovering MPS1 on kinetochores in conditions of elevated kinetochore PP1 should significantly strengthen the SAC. Indeed, artificially tethering MPS1 to kinetochores by transient expression of MIS12-MPS1 (*215*) almost fully restored the SAC in approximately 50% of KNL1^{2SA}-expressing cells, whereas a kinase-deficient version of MIS12-MPS1 could not (Fig. 5A). Detectable MIS12-MPS1 expression in our transient assay was seen in only roughly half of the cells, and therefore the non-responsive fraction likely represents cells that had not achieved significant MIS12-MPS1 expression. In conclusion, these data show that the SAC defect induced by precocious PP1 localization is due to delocalization of MPS1.

Discussion

The data presented here demonstrate that exclusion of PP1 from kinetochores by Aurora-B mediated phosphorylation of KNL1 is required to protect MPS1 localization and the SAC. In our model (Fig. 5B), the kinetochore localization of MPS1 is stimulated by a yet unknown kinase, activity of which is opposed by kinetochore PP1. Aurora B in turn stimulates MPS1 localization by preventing the PP1-KNL1 association.

PP1-binding sites can be identified in most eukaryotic KNL1 homologs (*274*), and the here described mechanism may therefore be a more widely conserved principle in evolution. For example, in fission yeast, inhibition of the Aurora kinase Ark1 delocalizes the MPS1 homolog Mph1 from unattached kinetochores and drives rapid mitotic exit despite absence of kinetochore-microtubule interactions (*255*). In agreement with what we have shown here, Ark1 activity is superfluous in SAC maintenance upon deletion of the PP1 homolog Dis2 (*255*), and efficient SAC silencing after Ark1 inhibition

(Continued from previous page)

lapse analysis as in A. Nocodazole-arrested cells were treated with 250 nM of reversine. Data (from a total of 150 cells) are representative of 3 independent experiments. (**E**) Time-lapse analysis as in A. Cells entered mitosis in the presence of 125 nM of reversine and ZM447439. Data (from a total of 150 cells) are representative of 3 independent experiments. (**F**) Time-lapse analysis as in A. Nocodazole-arrested cells were treated with 125 nM of reversine and ZM447439. Data (from a total of 150 cells) are representative of 3 independent experiments.

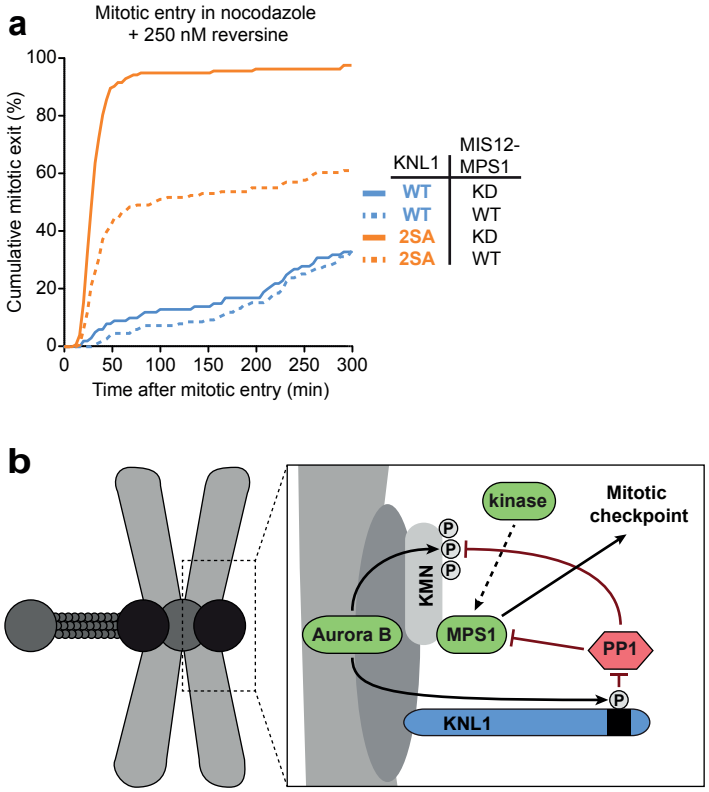

Figure 5. **SAC defects by premature kinetochore binding of PP1 are due to MPS1 delocalization.** (**A**) Time-lapse analysis of duration of mitotic arrest in nocodazole-treated Flp-in HeLa cells transfected with KNL1 siRNA and expressing wildtype (WT) or kinase dead LAP-MIS12-MPS1 and the indicated LAP-KNL1 proteins. Cells entered mitosis in the presence of 250 nM of reversine. Data indicate cumulative percentage of cells (from a total of ≥100 cells) that exit mitosis (scored as cell flattening) at the indicated times after nuclear envelope breakdown and are representative of at least 2 independent experiments. Bars, 5 µm. WT, wild type. (**B**) Model of regulated MPS1 localization by PP1 and Aurora B.

depends on association of Dis2 with the KNL1 homolog Spc7 (*258*). Moreover, like in human cells, artificial tethering of Mph1 to kinetochores renders the SAC independent of Ark1 (*102*). In contrast, in budding yeast, Mps1 localization is independent of the Aurora kinase Ipl1 (*222*), and phosphorylation of the RVSF motif is reported to be dispensable for SAC maintenance (*257*). Likely, therefore, an Aurora B-PP1-MPS1-like pathway does not exist in budding yeast.

Does Aurora B regulate the SAC exclusively via PP1 exclusion?

We show here that upon mitotic entry the exclusion of PP1 from KNL1 is sufficient to overcome the effects of Aurora B inhibition on the SAC (Fig. 4A). However, when nocodazole-arrested cells were treated with the combination of ZM447439 and low reversine, the SAC was not completely rescued by expression of LAP-KNL1^{4A} (Fig. 4B). Therefore, it remains possible that other Aurora-B dependent kinetochore pools of PP1, such as PP1-CENP-E (kinesin-7; *305*) are involved in SAC regulation. Indeed expression of LAP-KNL1^{2SA} did not affect the SAC as strongly as Aurora B inhibition itself: While Aurora B inhibition drove mitotic exit in combination with 125 nM reversine, the addition of 250 nM

of reversine was required to drive mitotic exit in LAP-KNL1^{2SA}-expressing cells. Moreover, expression of LAP-KNL1^{4A} did not completely recover kinetochore MPS1 when Aurora B was inhibited. Although this may be due to inefficient knockdown of KNL1 in our experiments, leaving residual endogenous KNL1 at kinetochores, it is equally possible that Aurora B has additional means of regulating kinetochore MPS1.

Phosphorylation-dependent localization of MPS1

Our observation that the regulation of MPS1 localization by Aurora B is predominantly indirect and mediated via the exclusion of PP1 from kinetochores begs the question what the kinase is that recruits MPS1 to kinetochores, and how does it do so? Several kinases have been suggested to regulate MPS1 kinetochore localization, including MAPK (*245*), NEK2 (*308*), Polo in *Drosophila* (*309*) and MPS1 itself (*243*). However, we and others have shown that MPS1 inhibition allows potent MPS1 localization (*204, 210, 215, 217*), NEK2 is degraded in early mitosis (*310, 311*), and our unpublished data do not support a role for PLK1 in MPS1 localization (T. Sliedrecht and GJPLK). Since multiple reported phosphorylation sites on MPS1 fit the CDK1 consensus motif, we consider CDK1 the prime candidate regulator of MPS1 kinetochore binding (*125, 126, 215, 228, 238, 239, 242, 243, 245*). Constitutive CDK1-dependent activation of MPS1 could allow SAC signaling to be active by default at the onset of mitosis. Regulated inactivation of MPS1, by delocalization upon kinetochore attachment and further suppression of MPS1 signaling upon biorientation could then be sufficient for dynamic regulation of MPS1 function. A thorough investigation of this possibility will require identification of the direct receptor for MPS1 at kinetochores. Given that ectopic localization of HEC1 to LacO arrays on the arm of chromosome 1 is sufficient to recruit MPS1 to those ectopic sites (*304*), the NDC80 complex is the most likely candidate for such an MPS1 receptor. Biochemical reconstitution of a potential interaction may further facilitate examination of the contribution of kinases and PP1 to the regulation of MPS1 localization.

Methods

Cell culture and reagents

HeLa Flp-in cells (gift from S. Taylor, University of Manchester, Manchester, England, UK) stably expressing a TetR, were cultured in DMEM supplemented with 9% tetracycline-approved FBS, 50 µg/ml penicillin/streptomycin and 2 mM L-glutamine. All HeLa Flp-in cells stably expressing a doxycycline-inducible KNL1 construct were derived from the HeLa Flp-in cell line by transfection with pCDNA5/FRT/TO vector (Invitrogen) and pOG44 (Invitrogen) and cultured in the same medium but containing 200 µg /ml hygromycin and 4 µg /ml blasticidin. To induce protein expression in the inducible cell lines, 1 µg/ml doxycycline was added for ≥36 h. Thymidine (2 mM), nocodazole (830 nM), MG132 (10 µM), reversine, doxycycline and puromycin (1 µg/ml) were all obtained from Sigma-Aldrich. Hygromycin was purchased from Roche. ZM447439 was obtained from Tocris Bioscience. Blasticidin was obtained from PAA Laboratories.

Knockdown and reconstitution experiments with LAP-KNL1

For knockdown and reconstitution of KNL1 in HeLa Flp-in cells, cells were transfected with 20 nM KNL1 or mock siRNA and, in some experiments, 20-40 nM additional mock, PP1α, PP1γ or PP1α and PP1γ siRNA for 16 h after which the cells were arrested in early S phase for 24 h by addition of thymidine. Subsequently, cells were release from thymidine for 8-10 h and arrested by the addition of nocodazole and (in MPS1 immunolocalization experiments) treated with reversine to accumulate MPS1 at kinetochores and MG132 to prevent mitotic exit. For alignment assays, cells were arrested by the addition of MG132 for 30 min. LAP-KNL1 expression was induced by the addition of doxycycline during the thymidine block.

Transfection and siRNA

Plasmids were transfected into HeLa Flp-in cells using Fugene 6 (Roche) according to the manufacturer's instructions. siRNAs used in this study were as follows: si-mock (Luciferase GL2 duplex; D001100-01-20; Thermo Fisher Scientific); siKNL1, 5'-GCAUGUAUCUCUUAAGGAA-3' (CASC5#5; J-015673-05; Thermo Fisher Scientific); siPP1α, 5'-CCGCAUCUAUGGUUUCUAC-3' (custom, Thermo Fisher Scientific) and PP1γ 5'-GCAUGAUUUGGAUCUUAUA-3' (custom, Thermo Fisher Scientific). All siRNAs were transfected using HiPerFect (Qiagen) at 20 nM according to the manufacturer's instructions.

Immunoblotting

Immunoblotting was performed using standard protocols; the signal was visualized and analyzed on a scanner (ImageQuant LAS 4000; GE Healthcare) using enhanced chemiluminescence.

Antibodies

The following primary antibodies were used for immunofluorescence imaging and immunoblotting: MPS1-N terminal (EMD Millipore), α-tubulin (Sigma-Aldrich), BUB1 (A300-373A; Bethyl), transferrin-receptor (13-6890; Invitrogen), CENP-C (PD030; MBL), CENP-T (D286-3; MBL), PP1α C19 (sc6104; Santa Cruz), PP1γ (A300-906A; Bethyl), KNL1 (ab70537; Abcam), MAD2 (custom rabbit polyclonal raised against full-length 6xHis-tagged MAD2 as antigen; *216*). Secondary antibodies were goat anti-rat Alexa Fluor 647, high-crossed goat anti-guinea pig Alexa Fluor 647, goat anti-rabbit and anti-mouse Alexa Fluor 488 and Alexa Fluor 568 (Molecular Probes) for immunofluorescence experiments.

Live-cell imaging, immunofluorescence and image quantification

For live-cell imaging for time-lapse analysis, cells were plated in 24-well glass-bottom plates (MatTek Corporation), transfected, and imaged in a heated chamber (37°C and 5% CO_2) using a 20x/0.5 NA UPLFLN objective (Olympus) on a microscope (IX-81; Olympus) controlled by Cell-M software (Olympus). Images were acquired using a camera (ORCA-ER; Hamamatsu Photonics) and processed using Cell-M software.

For live-cell imaging of RFP-PP1γ and LAP-KNL1, cells were grown in 8 well glass-bottom dishes (LabTek Corporation), depleted of endogenous KNL1 by transfection with KNL1 siRNA and induced to express the various LAP-KNL1 alleles for 6 h, subsequently cells were transfected to express RFP-PP1γ for 36 h. The media were replaced with Leibovitz L-15 media (Invitrogen) supplemented with 10% FCS, 2 mM L-glutamine and 100 U/ml penicillin and streptomycin. Cells were treated with 10 µM MG132 2 h before imaging. Samples were imaged on a personal DeltaVision system equipped with a heated chamber and lens warmer (both set at 37°C), with a 100x/1.40 NA U Plan S Apochromat objective using softWoRx software. Images were acquired using a camera (CoolSNAP HQ2; Photometrics) and processed using softWorx software and ImageJ. RFP-PP1γ and LAP-KNL1 intensities were plotted along a line crossing through the center of 2 aligned sister kinetochores in a single Z-plane. Individual plots were subjected to background subtraction using the minimal intensity value between the two peak values in the LAP-KNL1 channel (corresponding to kinetochores), transposed along the distance axis to be centered at the inner centromere and subsequently averaged.

For immunofluorescence, cells plated on 12-mm coverslips were pre-extracted with 0.1% Triton X-100 in PEM (100 mM Pipes, pH 6.8, 1 mM $MgCl_2$ and 5 mM EGTA) for 45s before fixation with 4% paraformaldehyde in PBS for 10 min. Coverslips were washed with PBS and blocked with 3% BSA in PBS for 30 min, incubated with primary antibodies for 2-4 h at room temperature or 16 h at 4°C, washed with PBS and incubated with secondary antibodies for an additional hour at room temperature. Coverslips were then incubated with DAPI for 2 min, washed and mounted using antifade (ProLong; Molecular Probes). For alignment assays, cells were treated as before, but were fixed with 3.7% Shandon Zinc Formal-Fixx (Thermo Scientific) for 10 min and subsequently washed with PBS and permeabilized with 0.5% Triton X-100 for 15 min. All images were acquired on a deconvolution system (Deltavision RT; Applied Precision) with a 100x/1.40 NA U Plan S Apochromat objective (Olympus) using softWoRx software (Applied precision). Images are maximum intensity projections of deconvolved stacks. For quantification of immunostainings, all images of similarly stained experiments were acquired with identical illumination settings; cells expressing comparable levels of exogenous protein were selected for analysis and analyzed using ImageJ (National Institutes of Health). An ImageJ macro was used to threshold and select all centromeres and all chromosome areas (excluding centromeres) using the DAPI and anti-centromere antibodies channels as described previously (*195*). This was used to calculate the relative mean kinetochore intensity of various proteins ([centromeres-chromosome arm intensity (test protein)]/[centromeres-chromosome arm intensity (CENP-C/CENP-T)].

Plasmids and cloning

pOG44 (Invitrogen) encodes a FLP recombinase expression vector. pCDNA3-YFP-MIS12-MPS1^{WT} and pCDNA3-YFP-MIS12-MPS1^{KD} were described previously (*215*). pCDNA5-LAP-KNL1^{WT} encodes full length, N-terminally LAP-tagged and siRNA-resistant wildtype KNL1 (modified codons 258 and 259) and was created by digestion of pEYFP-LAP-KNL1^{WT} , a gift from I. Cheeseman (Whitehead Institute,

Cambridge, USA) with XhoI and HpaI to isolate the full length KNL1^{WT} cassette, which was ligated into the XhoI and PmeI sites of pCDNA5/FRT/TO (invitrogen). An N-terminal LAP-tag was introduced by subcloning the LAP-tag cassette from pCDNA3-LAP-MPS1$^{\Delta 200}$ (*304*) into the KpnI and XhoI sites of the resulting plasmid. pCDNA5-LAP-KNL1^{2SA} and pCDNA5-LAP-KNL1^{2SD} were created by subcloning the KNL1 N-terminus from pEYFP-LAP-KNL1^{2SA} and pEYFP-LAP-KNL1^{2SD} (also gifts from I. Cheeseman) into pCDNA5-LAP-KNL1^{WT} via the XhoI and EcoRV restriction sites. pCDNA5-LAP-KNL1^{4A} was created by site-directed mutagenesis of pCDNA5-LAP-KNL1^{WT}.pCDNA3-puro-2xRFP-PP1γ was created by PCR of a tandem of tagRFP inserts from pPA-TAGRFP-H2B (Evrogen) and ligation into the BamHI and NotI restriction sites of the N-terminal LAP-tag of pLAP-PP1γ (a gift from I. Cheeseman). The resulting RFP-RFP-PP1γ cassette was subcloned the BamHI and EcoRI restriction sites of pCDNA3-puro.

Supplemental Material

Figure S1 shows that dysregulation of PP1 kinetochore recruitment causes chromosomal alignment defects.

Acknowledgements

We thank Iain Cheeseman for GFP-KNL1 and LAP-PP1γ constructs, Stephen Taylor for the HeLa Flp-in cell line and the Kops and Lens labs for insights and discussions. This work was supported by an European Research Council starting grant (KINSIGN; to G.J.P.L. Kops) and by the Dutch Cancer Society (KWF Kankerbestrijding; UU2012-5427; to G.J.P.L. Kops).

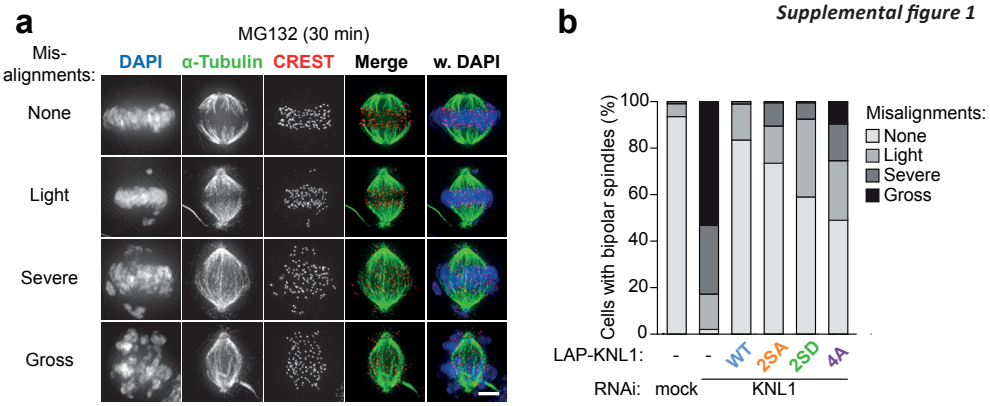

Figure S1: **Abnormal kinetochore PP1 levels result in mild chromosomal alignment defects.** (**A-B**) Representative images (A) and quantification (B) of chromosome alignment in Flp-in HeLa that were transfected with mock or KNL1 siRNA, induced to express the various LAP-KNL1 proteins and treated with MG132 for 30 min. Graph (B) indicates incidence of chromosomal misalignments in cells with bipolar spindles. Data are from a total of ≥100 cells per treatment from 2 experiments. Bars, 5 µm. WT, wild type.

Chapter 4

Negative feedback between kinetochore phosphatases regulates the spindle assembly checkpoint

Wilco Nijenhuis[1,2], Antoinette Teixeira[1,2], Adrian T. Saurin[4] and Geert J.P.L Kops[1,2,3,4]

[1] Molecular Cancer Research and

[2] Department of Medical Oncology and

[3] Cancer Genomics Netherlands, University Medical Center Utrecht, 3584 CG, Utrecht, The Netherlands.

[4] These authors have contributed equally

Manuscript in preparation

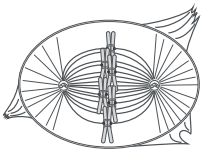

Abstract

Error-free chromosome segregation during mitosis is ensured by the concerted activities of the spindle assembly checkpoint (SAC) and the attachment error correction machinery. Both processes are regulated at kinetochores by the activities of kinases, most notably Aurora B, MPS1 and BUB1, as well as phosphatases. Efficient error-correction requires kinetochore-localized PP2A-B56, while stabilization of attachments and SAC silencing at metaphase require kinetochore-localized PP1. How the localized activities of these phosphatases are regulated is, however, unclear. Here, we demonstrate that PP1 and PP2A-B56 are involved in a negative feedback loop that serves to reduce their levels at kinetochores. Using a PP1 docking mutant of the kinetochore scaffold KNL1, we show that PP1 suppresses kinetochore localization of PP2A-B56 by dephosphorylation of its docking site in BUBR1. In turn, PP2A-B56 dephosphorylates the PP1-binding motifs in KNL1, causing PP1 localization and subsequent removal of SAC kinases from kinetochores. Efficient SAC silencing thus requires kinetochore localization of both PP1 and PP2A-B56, and we show that tethering the PP2A-B56-binding motif of BUBR1 to kinetochores can force mitotic exit by permitting kinetochore-binding of PP1. We thus propose that PP1 and PP2A-B56 are in a localized negative feedback that ensures low levels of SAC-silencing phosphatase activity at kinetochores in prometaphase.

Introduction

The accurate distribution of chromosomes at the end of mitosis is essential to maintain genomic stability and cellular viability. The spindle assembly checkpoint (SAC) has evolved to ensure that anaphase onset is delayed until all kinetochores have been productively attached by spindle microtubules (*274*). The error-correction machinery promotes biorientation of sister chromatids by destabilizing kinetochore-microtubule attachments that are not under tension (*98*), which are common in early prometaphase (*2*). These two separate processes are functionally interdependent: the SAC allows time for the error-correction machinery to destabilize improper kinetochore-microtubule attachments, and unattached kinetochores that result from error-correction in turn elicit a SAC response.

The SAC delays anaphase onset by inhibition of the anaphase promoting complex, a multi-subunit E3 ubiquitin ligase that targets cyclin B and securin for proteasomal destruction, by generating a diffusible inhibitor termed the mitotic checkpoint complex (MCC; reviewed in *276*). SAC signaling requires the activity of the mitotic kinases BUB1 and MPS1, which are functionally dependent on their recruitment to kinetochores (*183, 195, 198, 208, 215, 304, 312*). At kinetochores, MPS1 stimulates the kinetochore localization of other SAC proteins, including MAD1, MAD2, BUBR1 (reviewed in *277*). Additionally, MPS1 promotes the kinetochore recruitment of BUB1 via phosphorylation of the MELT motifs in KNL1 (*39, 41, 42*). Although not required *in vitro* (*177*), MPS1 is also needed for MAD2 dimerization in cells (*210*). At the heart of the error-correction machinery is the kinase Aurora B, the enzymatic component of the chromosomal passenger complex. Aurora B reduces affinity of kinetochores for microtubules by phosphorylating multiple components of the KNL1-MIS12-NDC80 (KMN) network that composes the main microtubule-binding site of kinetochores (*29, 43, 116*).

The activity of kinetochore-based kinases is opposed by at least two phosphatases. PP1γ and a pool of PP2A that is associated with regulatory subunits of the B56 family (PP2A-B56) are both required for the stabilizing kinetochore-microtubule interactions by countering Aurora B activity at the outer kinetochore (*36, 100, 119, 120, 122*). The phase of mitosis at which they do so is, however, different. PP2A levels at kinetochores are high in prometaphase, when its activity dampens Aurora B activity in order to allow establishment of attachments. PP2A levels subsequently decrease at metaphase, when its kinetochore recruiter BUBR1 is delocalized from kinetochores. In contrast, PP1 levels are low in prometaphase but increase at metaphase, at which point it dephosphorylates Aurora B substrates to ensure that attachments are sufficiently stable for chromosome segregation during anaphase. Additionally, PP1γ is required for SAC silencing in fungi and nematodes (*32, 255, 256*). PP1 may accomplish this by countering activity of the main SAC kinase MPS1, since in budding yeast Glc7/PP1 is required to dephosphorylate the MELT motifs of Spc105/KNL1.

The activities of PP1γ and PP2A-B56 are dependent on their localization to kinetochores. PP1γ is recruited to two PP1-binding SILK and RRVSF motifs in the N-terminus of KNL1, a large scaffold and member of the KMN network (*32, 36, 257, 258*). Binding of PP1γ to KNL1 is suppressed by Aurora B-dependent phosphorylation of the serines in either motif (*33, 36*; chapter 3 of this thesis). PP2A-B56 is localized to kinetochores by a direct interaction with the KARD domain of BUBR1 (*121-123*). This interaction depends on phosphorylation of the KARD by CDK1 and PLK1 (*122*). Thus, while phosphorylation of the KARD is required to localize PP2A-B56, dephosphorylation of KNL1 is required to localize PP1. Given the role of PP1 in the SAC (chapter 3 of this thesis), efficient SAC silencing and the formation of stable kinetochore-microtubule attachments may thus require reduced phospho-

occupancy of the PP1 docking sites in KNL1. Here, we report that PP2A-B56 promotes PP1-dependent SAC silencing by dephosphorylating KNL1. Moreover, PP1 prevents PP2A-B56 kinetochore binding by dephosphorylating the KARD motif of BUBR1. As a result, PP1 and PP2A-B56 create a negative feedback loop that integrates upstream signaling from MPS1, Aurora B and PLK1 to regulate activation and silencing of the SAC.

Results

Suppression of BUB1 kinetochore localization by KNL1-associated PP1

We hypothesized that PP1 and PP2A operate in a negative feedback loop (Fig. 1A). This is based on four reported observations: First, PP2A-B56 depletion enhances phosphorylation of the PP1-docking SILK motif in KNL1 (*120*); Second, the budding yeast PP1 homolog Glc7 counters Bub1 kinetochore binding which depends on phosphorylation of MELT-like motifs in Spc105/KNL1; Third, BUB1 is needed for BUBR1 localization; Fourth, BUBR1, when phosphorylated on its KARD domain, recruits PP2A-B56 to kinetochores. To test whether reciprocal control of PP1 and PP2A-B56 exists and how this affects chromosome segregation, we first examined if the kinetochore-bound pool of PP1 countered BUB1 localization in human cells. For this, we made use of a set of isogenic HeLa Flp-in cell lines that inducibly expressed siRNA-resistant LAP-tagged KNL1 mutants from a single genomic locus (chapter 3 of this thesis; Fig. 1B). This system allowed modulation of the kinetochore PP1 levels by replacing endogenous KNL1 with alleles that were mutated in the PP1-binding motifs. The three mutant KNL1 variants were KNL1^{4A,} KNL1^{2SA} and KNL1^{2SD} (Fig. 1B). KNL1^{4A} carries alanine substitutions of the RVSF motif, thus preventing PP1γ localization to metaphase kinetochores (*36*; chapter 3 of this thesis). KNL1^{2SD} carries aspartic acid substitutions of the Aurora B phosphorylation sites at Ser24 (pSSILK) and Ser60 (RRVpSF) that reduce the interaction with recombinant PP1γ with a KNL1 fragment *in vitro* (*33, 36*) and reduce PP1γ localization to metaphase kinetochores (chapter 3 of this thesis). Conversely, KNL1^{2SA} carries alanine substitutions of the same residues, causing high levels of PP1γ to kinetochores (chapter 3 of this thesis) and should permit PP1γ localization even if Aurora B activity towards the KMN network is high.

Preventing kinetochore recruitment of PP1 by replacement of endogenous KNL1 with LAP-KNL1^{4A} increased BUB1 at the kinetochores of cells that were arrested in mitosis by treatment with the microtubule destabilizing drug nocodazole (Fig. 1 C, D, G). To examine if this increase is due to elevated phosphorylation of MELT motifs by MPS1, we inhibited MPS1 kinase activity with reversine (*217*) in nocodazole-arrested cells that were additionally treated with the proteasome inhibitor MG132 to prevent mitotic exit. Whereas MPS1 inhibition largely delocalized BUB1 in KNL1^{WT}-expressing cells

Figure 1: **Kinetochore PP1 suppresses MPS1-dependent kinetochore localization of BUB1.** (**A**) Model of hypothetical negative feedback control of PP1 and PP2A-B56 kinetochore localization. (**B**) Schematic representation of the various KNL1 mutants used in this study. Aurora B phosphorylation sites (blue) within the PP1-binding motifs (bold) are indicated. (C-I) Representative images (**C, E, H**) and quantification (**D, F, G, I**) of immunolocalization of the various LAP-KNL1 proteins (GFP), BUB1 and centromeres (CREST or CENP-T) in Flp-in HeLa cells transfected with siRNAs to KNL1 and luciferase (mock) and treated with nocodazole, MG132 and DMSO (C, D, H and I) or reversine (500 nM; E and F). Graphs in D, F and I display total kinetochore intensities (±SEM) of the indicated proteins relative to centromeres. Graph in G shows relative kinetochore intensities of BUB1 relative to LAP-KNL1 as plotted in D and F. The data depicted in H and I are also shown in chapter 3 (Figure 3D,F). Data are from a total of ≥19 cells per treatment from 2 independent experiments. Ratios are set to 1 for DMSO-treated LAP-KNL1^{WT}-expressing cells. DNA (DAPI) is shown in blue. Insets show magnifications of the boxed regions. Bars, 5 µm.

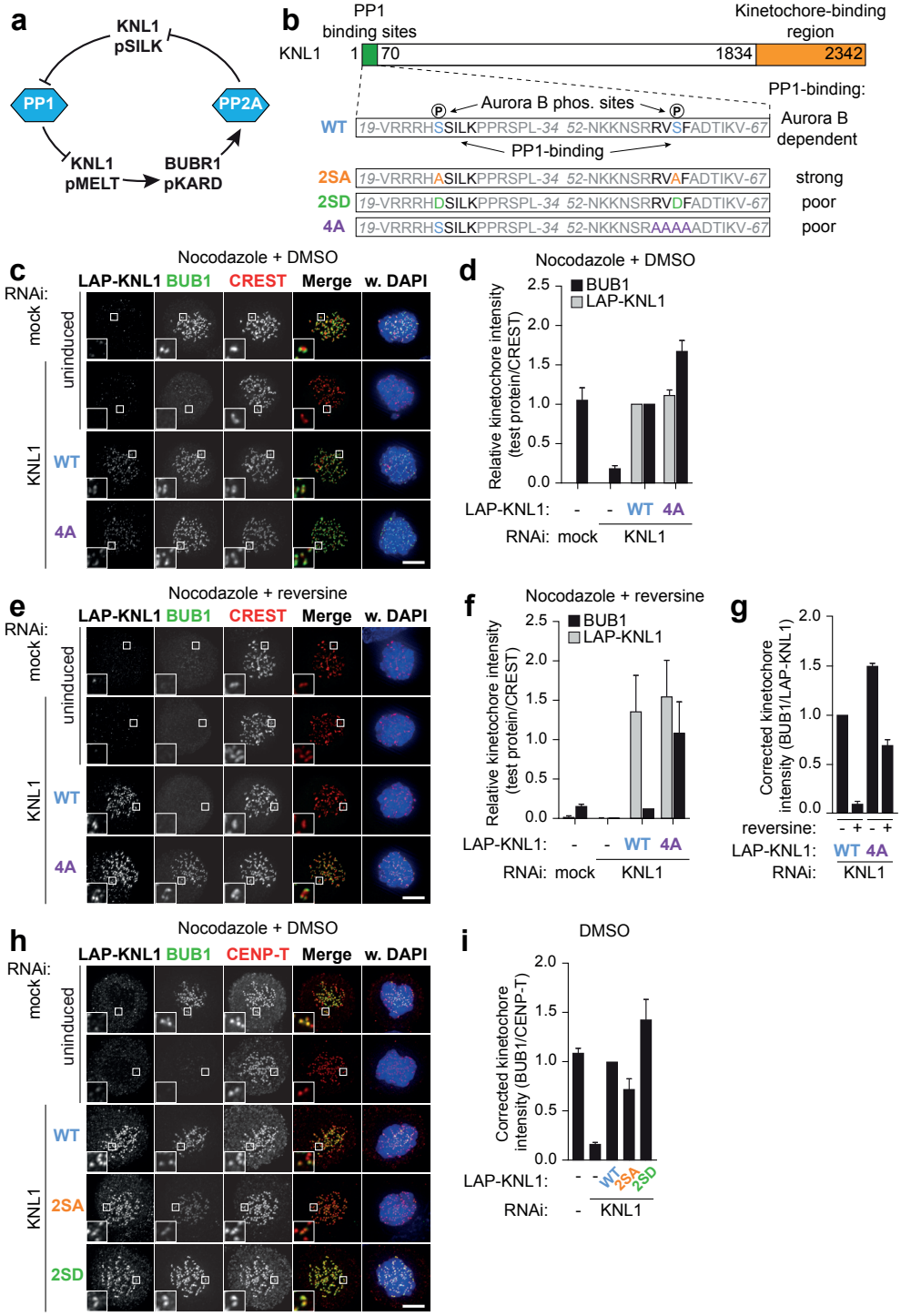
a
KNL1
pSILK
PP1
PP2A
KNL1
pMELT
BUBR1
pKARD
b
PP1
binding sites
Kinetochore-binding
region
KNL1
1
70
1834
2342
PP1-binding:
Aurora B phos. sites
WT
19-VRRRHSSILKPPRSPL-34 52-NKKNSRRVSFADTIKV-67
Aurora B
dependent
PP1-binding
2SA
19-VRRRHASILKPPRSPL-34 52-NKKNSRRVAFADTIKV-67
strong
2SD
19-VRRRHDSILKPPRSPL-34 52-NKKNSRRVDFADTIKV-67
poor
4A
19-VRRRHSSILKPPRSPL-34 52-NKKNSRAAAAADTIKV-67
poor
c
Nocodazole + DMSO
LAP-KNL1 BUB1 CREST Merge w. DAPI
RNAi:
mock
uninduced
KNL1
WT
4A
d
Nocodazole + DMSO
BUB1
LAP-KNL1
Relative kinetochore intensity
(test protein/CREST)
2.5
2.0
1.5
1.0
0.5
0.0
LAP-KNL1: - - WT 4A
RNAi: mock KNL1
e
Nocodazole + reversine
LAP-KNL1 BUB1 CREST Merge w. DAPI
RNAi:
mock
uninduced
KNL1
WT
4A
f
Nocodazole + reversine
BUB1
LAP-KNL1
Relative kinetochore intensity
(test protein/CREST)
2.5
2.0
1.5
1.0
0.5
0.0
LAP-KNL1: - - WT 4A
RNAi: mock KNL1
g
Corrected kinetochore
intensity (BUB1/LAP-KNL1)
2.0
1.5
1.0
0.5
0.0
reversine: - + - +
LAP-KNL1: WT 4A
RNAi: KNL1
h
Nocodazole + DMSO
LAP-KNL1 BUB1 CENP-T Merge w. DAPI
RNAi:
mock
uninduced
KNL1
WT
2SA
2SD
i
DMSO
Corrected kinetochore
intensity (BUB1/CENP-T)
2.0
1.5
1.0
0.5
0.0
LAP-KNL1: - - WT 2SA 2SD
RNAi: - KNL1

(9% remaining), BUB1 levels remained high in cells expressing KNL1^{4A} (69% remaining; Fig. 1E, F, G). To further examine if kinetochore levels of BUB1 were regulated by phosphorylation of the PP1 docking motif, we analyzed BUB1 levels in cells expressing KNL1^{2SA} or KNL1^{2SD}. As seen in figures 1H and 1I KNL1^{2SA} recruited significantly less BUB1 than KNL1WT while KNL1^{2SD} recruited considerably more. Moreover, while BUB1 is normally removed from kinetochores upon biorientation (*313, 314*), expression of KNL1^{4A} retained BUB1 localization on metaphase kinetochores (Fig. S1). From these data we concluded that kinetochore PP1 suppresses the MPS1-dependent kinetochore localization of BUB1 in mammalian cells, and that this is regulated by phosphorylation of the PP1 docking motifs in KNL1**.**

Efficient activation and silencing of the SAC is controlled by kinetochore PP1.

The observation that preventing kinetochore localization of PP1 caused resistance of BUB1 kinetochore binding to MPS1 inhibition prompted us to examine whether this was true also for the SAC response. Establishment and maintenance of the SAC was determined by live-cell imaging of nocodazole-treated cells and analysis of the time from nuclear envelope breakdown to mitotic exit. When faced with a high dose of reversine, cells expressing KNL1^{WT} or KNL1^{2SA} failed to establish a functional SAC (70% exit after 50 and 24 minutes, respectively; Fig. 2A). However, expression of KNL1^{2SD} (29% exit after 120 minutes) or KNL1^{4A} (13% exit after 120 minutes) allowed establishment of a SAC response that persisted for several hours despite strongly reduced MPS1 activity. This was supported by the observation that while the kinetochore loading of MAD1 was prevented by inhibition of MPS1 before mitotic entry in control cells, MAD1 was still potently recruited in MPS1-inhibited cells expressing KNL1^{2SD} or KNL1^{4A} (Fig. 2B-D). Mitotic delays in KNL1^{4A}- and KNL1^{2SD}-expressing cells upon treatment with reversine were due to persistent SAC response and not caused by additional defects in mitotic exit since additional depletion of MAD2 prevented these delays (Fig. S2A). Of note: depletion of MPS1 reverted the delays also, indicating that SAC establishment in the presence of 500 nM reversine can be achieved by low residual MPS1 activity. Together, these data support the hypothesis that PP1 needs to be excluded from kinetochores for efficient SAC establishment.

To examine if PP1 binding to KNL1 is required also for SAC silencing, we inhibited MPS1 after cells had been allowed to establish the SAC. Addition of reversine to cells arrested in mitosis by nocodazole caused rapid exit of control cells and cells expressing KNL1^{WT} (Fig. S2B). In contrast, exit was significantly delayed in cells expressing KNL1^{2SD} or KNL1^{4A} (50% exit after 122 and 194 minutes, respectively). This correlated with persistent stability of the SAC effector complex MCC: while the MAD2-CDC20 interaction was substantially reduced by MPS1 inhibition of nocodazole-treated control cells, it was partially retained in KNL1^{2SD} or KNL1^{4A}-expressing cells (Fig. S2C). Additionally, MPS1 inhibition in KNL1^{WT}-expressing cells was accompanied by increased mobility of BUBR1 on gel, suggestive of BUBR1 dephosphorylation, but this was largely prevented by expression of KNL1^{2SD} and KNL1^{4A}.

Phosphorylation of the BUBR1 KARD is opposed by KNL1-associated PP1

Our observation that kinetochore PP1 affects BUBR1 phosphorylation (see Fig. S2C) raised the possibility that PP1 controls phosphorylation of the BUBR1 KARD and thereby kinetochore levels of PP2A-B56. As expected from its dependency on BUB1, kinetochore levels of BUBR1 were elevated about 1.5 fold in cells expressing KNL1^{4A} or LAP-KNL1^{SD} (Fig. 3A-C). Strikingly, however, phosphorylation of Thr680 in the KARD of BUBR1 showed a much more pronounced response to kinetochore levels of PP1: exclusion of PP1 from kinetochores by expression of KNL1^{2SD} or KNL1^{4A} increased KARD phosphorylation by 2.5 and 3 fold, respectively (Fig. 3D, E, F). In contrast, increased PP1 recruitment by expression of KNL1^{2SA} reduced the kinetochore pT680 signal by ~30%. In support of this, pThr680 levels were sensitive to

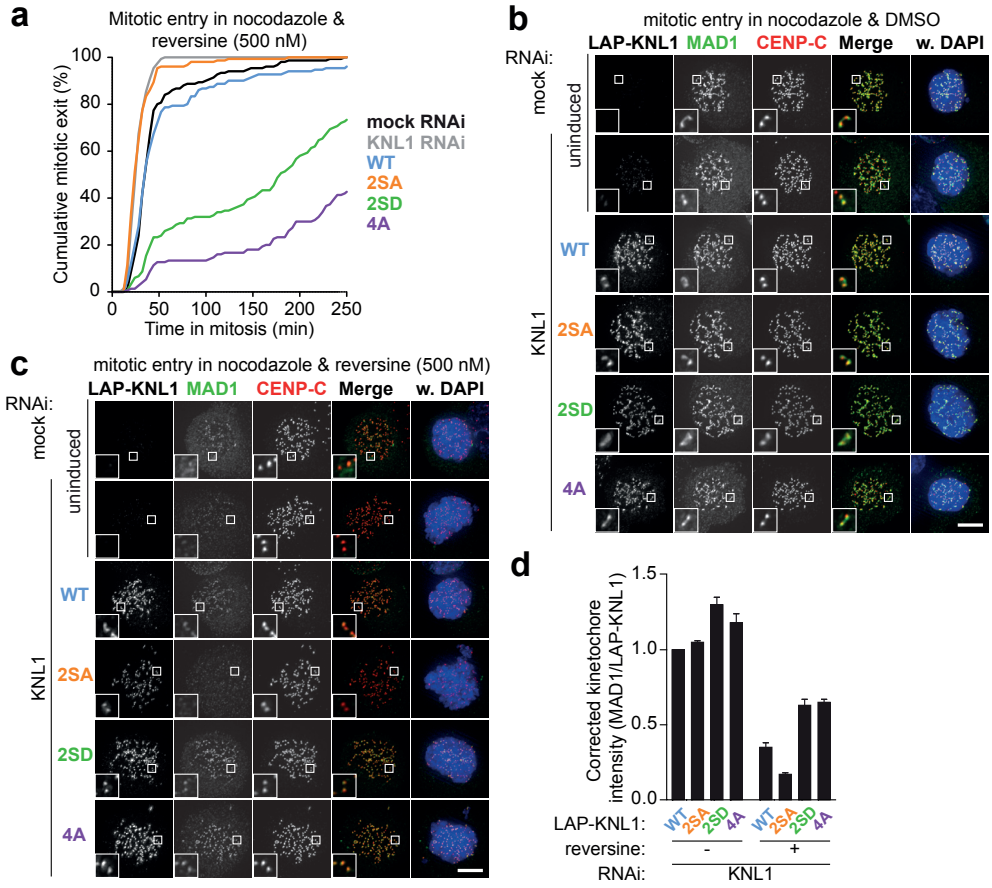

Figure 2: **Preventing PP1 kinetochore binding potentiates SAC establishment upon MPS1 inhibition.** (**A**) Time-lapse analysis of duration of mitotic arrest in nocodazole-treated Flp-in HeLa cells transfected with mock or KNL1 siRNA and expressing the indicated LAP-KNL1 proteins. Cells entered mitosis in the presence of 500 nM of reversine. Data indicate cumulative percentage of cells (from a total of 150 cells) that exit mitosis (scored as cell flattening) at the indicated times after nuclear envelope breakdown (NEB) and are representative of 3 independent experiments. (**B-D**) Representative images (B, C) and quantification (D) of immunolocalization of the various LAP-KNL1 proteins (GFP), MAD1 and centromeres (CENP-C) in Flp-in HeLa cells transfected with siRNAs to KNL1 and luciferase (mock). Cells entered mitosis in the presence of nocodazole of DMSO (B) or reversine (500 nM; C) and were subsequently treated with MG132. Graph in D display total kinetochore intensities (±SEM) of MAD1 relative to centromeres (LAP-KNL1). Data are from a total of ≥26 cells per treatment from 2 independent experiments. Ratios are set to 1 for DMSO-treated LAP-KNL1^{WT}-expressing cells. DNA (DAPI) is shown in blue. Insets show magnifications of the boxed regions. Bars, 5 µm.

addition of Aurora B inhibitors but were resistant to Aurora B inhibition when cells expressed KNL1^{4A} or KNL1^{2SD} (Fig. S2A-F). These data thus support the hypothesis that phosphorylation of the KARD is normally suppressed by PP1-KNL1 during prometaphase .

PP2A-B56 opposes phosphorylation of the KNL1 MELT motif via phosphoregulation of PP1-KNL1 binding

Having established that PP1 opposes phosphorylation of the PP2A recruitment motif at kinetochores,

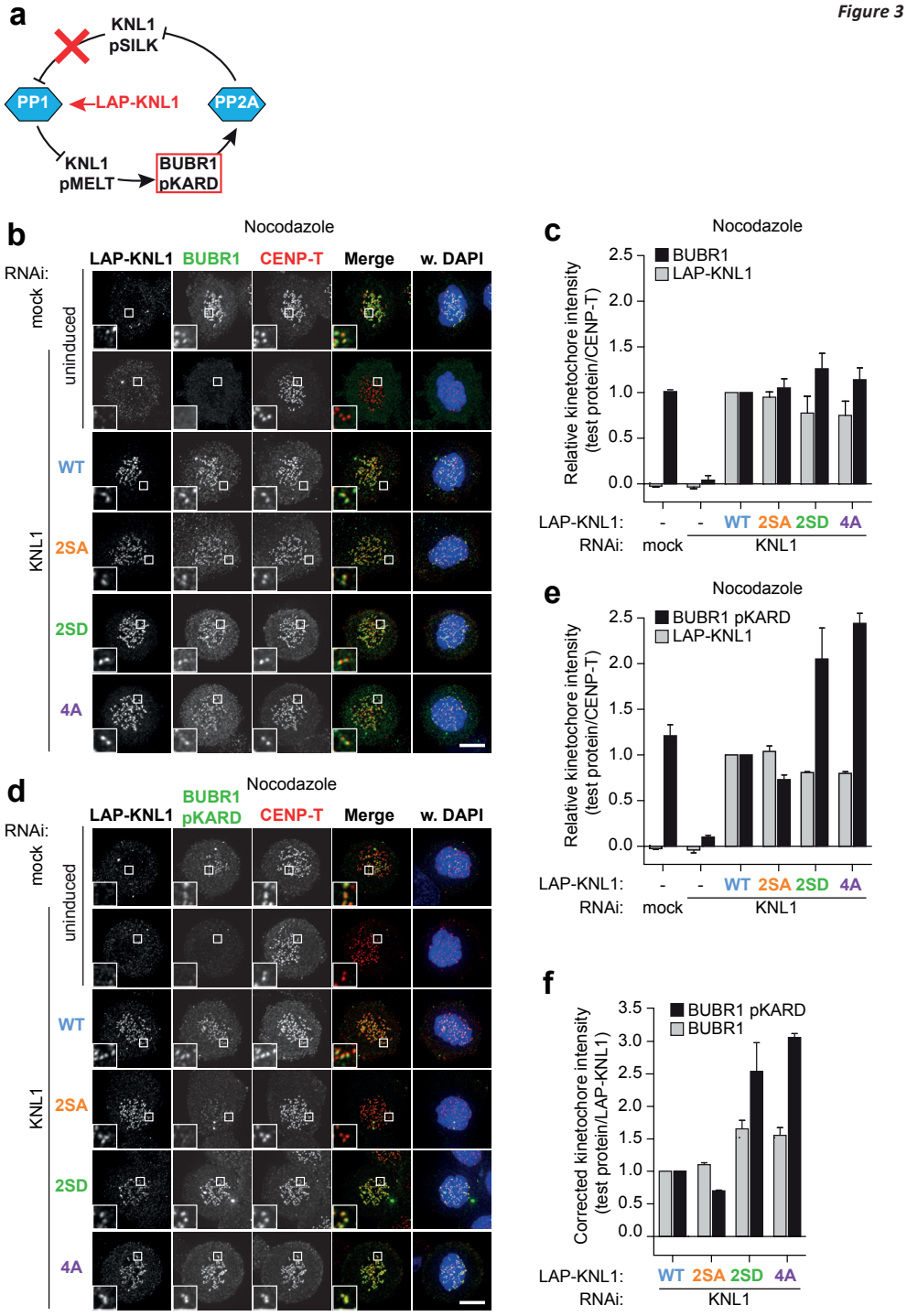
a
KNL1
pSILK
PP1
LAP-KNL1
PP2A
KNL1
pMELT
BUBR1
pKARD
b
Nocodazole
LAP-KNL1
BUBR1
CENP-T
Merge
w. DAPI
RNAi:
mock
uninduced
KNL1
WT
2SA
2SD
4A
c
Nocodazole
BUBR1
LAP-KNL1
Relative kinetochore intensity
(test protein/CENP-T)
2.5
2.0
1.5
1.0
0.5
0.0
LAP-KNL1:
- - WT 2SA 2SD 4A
RNAi:
mock
KNL1
d
Nocodazole
LAP-KNL1
BUBR1
pKARD
CENP-T
Merge
w. DAPI
RNAi:
mock
uninduced
KNL1
WT
2SA
2SD
4A
e
Nocodazole
BUBR1 pKARD
LAP-KNL1
Relative kinetochore intensity
(test protein/CENP-T)
2.5
2.0
1.5
1.0
0.5
0.0
LAP-KNL1:
- - WT 2SA 2SD 4A
RNAi:
mock
KNL1
f
BUBR1 pKARD
BUBR1
Corrected kinetochore intensity
(test protein/LAP-KNL1)
3.5
3.0
2.5
2.0
1.5
1.0
0.5
0.0
LAP-KNL1:
WT 2SA 2SD 4A
RNAi:
KNL1

Figure 3: **Kinetochore PP1 opposes phosphorylation of the BUBR1 KARD domain.** (**A**) Scheme of perturbations performed in this figure. (**B and C**) Representative images (B) and quantification (C) of immunolocalization of the various LAP-KNL1 proteins (GFP), BUBR1 and centromeres (CENP-T) in Flp-in HeLa cells transfected with siRNAs to KNL1 and luciferase (mock) and treated with nocodazole, MG132 and DMSO. Graph in C displays total kinetochore intensities (±SEM) of the indicated proteins relative to centromeres (CENP-T). Data are from a total of ≥21 cells per treatment from 3 independent experiments. (**D and E**) Representative images (D) and quantification (E) of immunolocalization of various LAP-KNL1 proteins (GFP), pKARD-BUBR1 (pT680) and centromeres (CENP-T) in Flp-in HeLa cells treated as in B. Graph in E displays total kinetochore intensities (±SEM) of the indicated proteins relative to centromeres (CENP-T). Data are from a total of ≥38 cells per treatment from 2 independent experiments. (**F**) Graph shows relative kinetochore intensities of BUBR1 and pKARD BUBR1 relative to LAP-KNL1 as plotted in C and E. Ratios are set to 1 for DMSO-treated LAP-KNL1^{WT}-expressing cells. DNA (DAPI) is shown in blue. Insets show magnifications of the boxed regions. Bars, 5 µm.

Figure 4

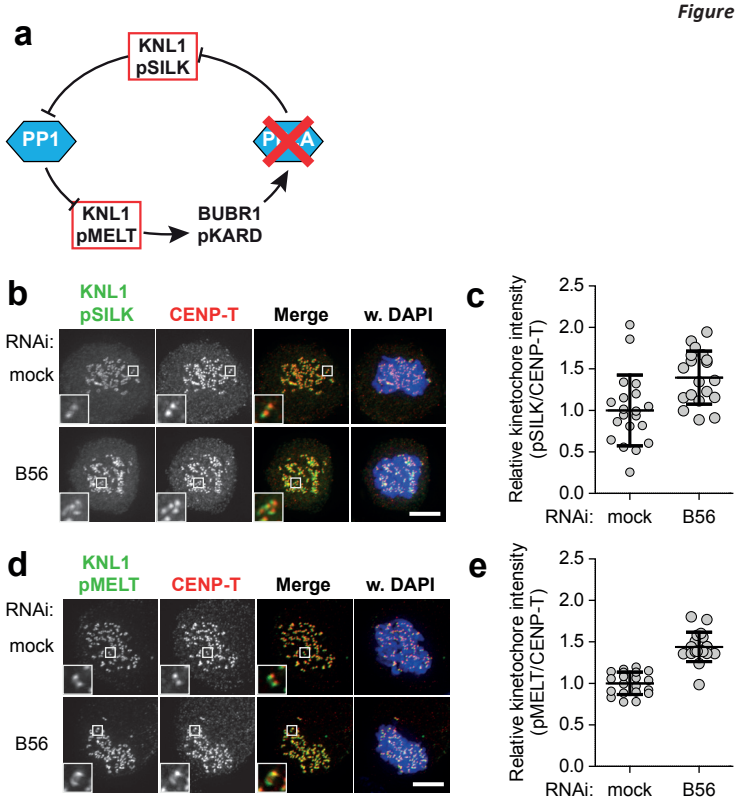

Figure 4: **PP2A-B56 antagonizes phosphorylation of KNL1 SILK and MELT motifs.** (**A**) Scheme of perturbations performed in this figure. (**B-E**) Representative images (B, D) and quantification (C, E) of immunolocalization of pSILK-KNL1 (pSer24; B and C) or pMELT-KNL1 (pThr943/pThr1155; D and E) and centromeres (CENP-T) in nocodazole and MG132-treated Flp-in HeLa cells transfected with mock siRNA or a PP2A-B56 siRNA pool. Graphs display total kinetochore intensities (±SD) of the indicated proteins relative to centromeres (CENP-T). Ratios for mock siRNA-treated cells are set to 1. One dot represents on cell. DNA (DAPI) is shown in blue. Insets show magnifications of the boxed regions. Bars, 5 µm.

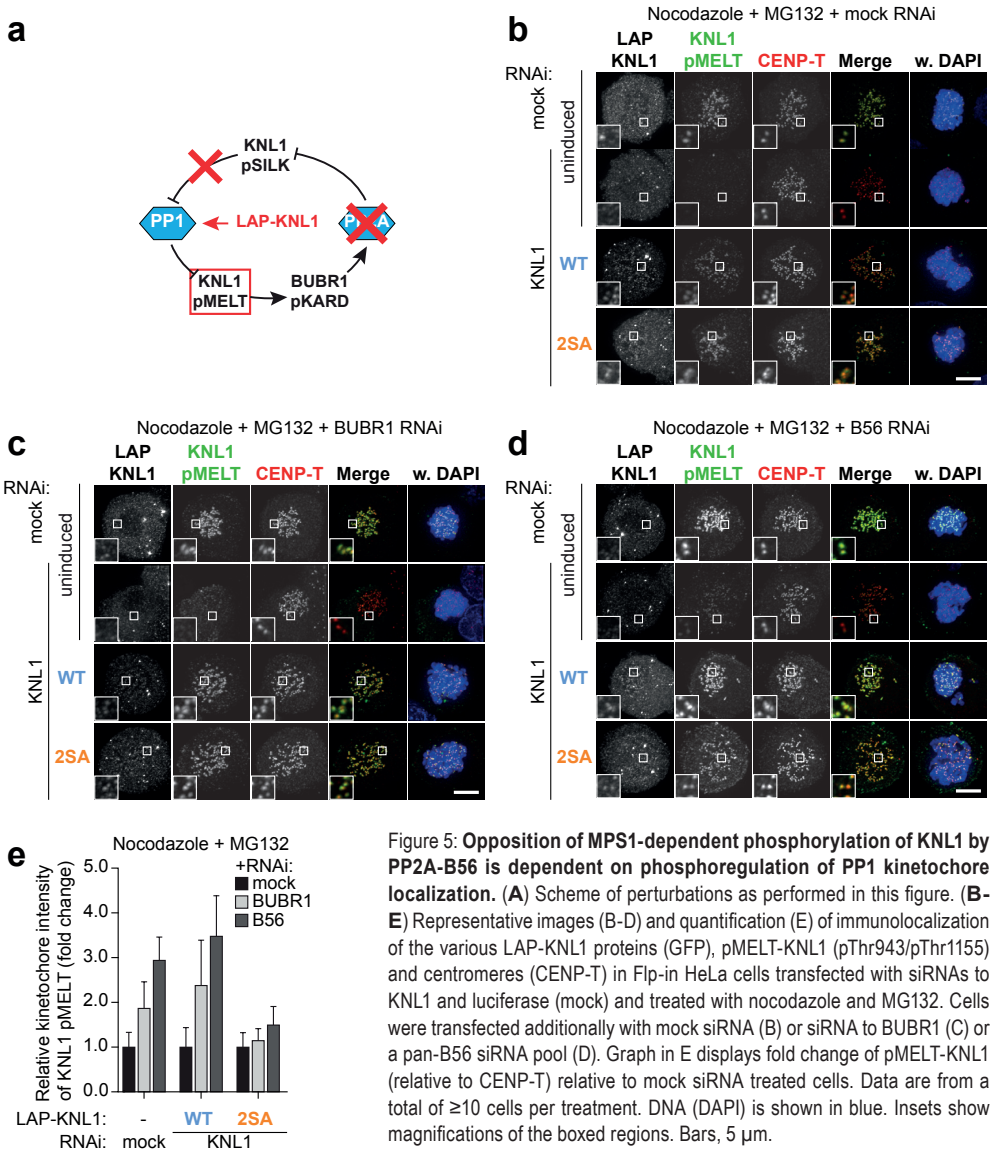

Figure 5: **Opposition of MPS1-dependent phosphorylation of KNL1 by PP2A-B56 is dependent on phosphoregulation of PP1 kinetochore localization.** (**A**) Scheme of perturbations as performed in this figure. (**B-E**) Representative images (B-D) and quantification (E) of immunolocalization of the various LAP-KNL1 proteins (GFP), pMELT-KNL1 (pThr943/pThr1155) and centromeres (CENP-T) in Flp-in HeLa cells transfected with siRNAs to KNL1 and luciferase (mock) and treated with nocodazole and MG132. Cells were transfected additionally with mock siRNA (B) or siRNA to BUBR1 (C) or a pan-B56 siRNA pool (D). Graph in E displays fold change of pMELT-KNL1 (relative to CENP-T) relative to mock siRNA treated cells. Data are from a total of ≥10 cells per treatment. DNA (DAPI) is shown in blue. Insets show magnifications of the boxed regions. Bars, 5 µm.

we next asked if PP2A-B56 could in turn regulate the localization of PP1. The binding of PP1 to KNL1 is prevented by Aurora B-dependent phosphorylation of the PP1-binding motifs at Ser24 (KNL1 pSILK) and Ser60. In line with published data (*120*), depletion of all five B56 isoforms increased phosphorylation of the KNL1 SILK motif by ~40% (Fig. 4A-C). This was accompanied by increased phosphorylation of a KNL1 MELT motif (pThr943/pThr1155) by ~43% (Fig. 4D, E), suggesting that B56 normally enables PP1 kinetochore binding. To examine this further, we uncoupled PP1 localization from phosphoregulation by expressing KNL1^{2SA} (Fig. 5A). As in control cells, depletion of B56 or BUBR1 increased MELT phosphorylation substantially in KNL1^{WT}-expressing cells (Fig. 5B-E). Importantly,

this was largely prevented by expression of KNL1^{2SA} (Fig. 5B-E), showing that suppression of MELT phosphorylation by B56 is dependent on phosphoregulation of PP1 localization. Together, these data show that PP2A-B56 opposes phosphorylation of the PP1-binding motifs of KNL1 and thereby enables dephosphorylation of the KNL1 MELT-like motifs. Together with the observation that kinetochore PP1 suppresses the phosphorylation of the BUBR1 KARD domain (Fig. 2), these data lead us to conclude that PP1 and PP2A-B56 regulate each other in a negative feedback cycle that suppresses the kinetochore localization of both phosphatases (Fig. 1A).

PP2A-B56 contributes to SAC silencing by enabling PP1 kinetochore binding

If PP2A-B56 and PP1 are in a negative feedback loop, kinetochore PP2A-B56 should affect the SAC response. The contribution of PP2A-B56 to SAC signaling was addressed by allowing cells to enter mitosis in the presence of nocodazole and an intermediate (250 nM) or high (500 nM) dose of reversine. Mock RNAi-treated cells that entered mitosis in 250 nM of reversine arrested for several hours (Fig. 6A), but slowly exited thereafter (18% exit after 240 minutes). This slow exit was prevented by B56 depletion (Fig. 6A). The SAC could not efficiently establish in control cells treated with high reversine, but strikingly SAC establishment was permitted in high reversine in the absence of B56 (11% exit after 240 minutes; Fig. 6B). In agreement with a role of Aurora B in opposing PP1 localization, SAC establishment in B56-depleted cells depended on Aurora B activity (Fig. 6C).

To directly test if kinetochore PP2A-B56 can prevent SAC establishment by promoting PP1 localization, we artificial tethered PP2A to kinetochores by expressing a MIS12 fusion of the KARD domain carrying phosphomimetic substitutions (MIS12-KARD^{3D}; Fig. 6D; *122*). Overexpression of MIS12-KARD^{3D} but not of the unphosphorylatable MIS12-KARD^{3A} prevented SAC activation in a significant fraction of KNL1^{WT}-expressing cells when the SAC was weakened by partial MPS1 inhibition with 250 nM reversine (Fig. 6E). We suspect that the responsive fraction represented cells that were efficiently transfected. Importantly, overexpression of MIS12-KARD^{3D} no longer prevented SAC establishment in cells expressing KNL1^{4A}, showing that SAC silencing by kinetochore PP2A depends on kinetochore PP1.

Discussion

We have shown that PP1 and PP2A-B56 are involved in negative feedback regulation: PP1 reduces PP2A-B56 kinetochore levels while PP2A-B56 enhances PP1 kinetochore levels (Fig. 6F). This negative feedback signaling may ensure dampened PP1 and PP2A-B56 activity at unattached kinetochores. We envision that whenever KNL1-bound PP1 exceeds a threshold, its levels are quickly reduced by its effect on kinetochore PP2A, and vice versa. Such mutual phosphatase control may allow sufficient levels of phosphatase localization to allow the dynamic turnover of Aurora B-dependent phosphorylations, while protecting the kinetochore localization of BUB1 and BUBR1. The switch to high PP1 localization in metaphase may subsequently be initiated by reduced Aurora B-dependent phosphorylation of the PP1 docking sites. Removal of the kinase combined with (low) activity of PP2A will allow rapid accumulation of PP1 that subsequently can supplant PP2A-B56 as the main kinetochore phosphatase, and initiate SAC silencing.

Which phosphatase opposes Aurora B phosphorylations?

Aurora B regulates kinetochore-microtubule stability by phosphorylation of the microtubule-binding interfaces of the KMN network (*29, 43, 116*), which decreases the affinity of the basic microtubule

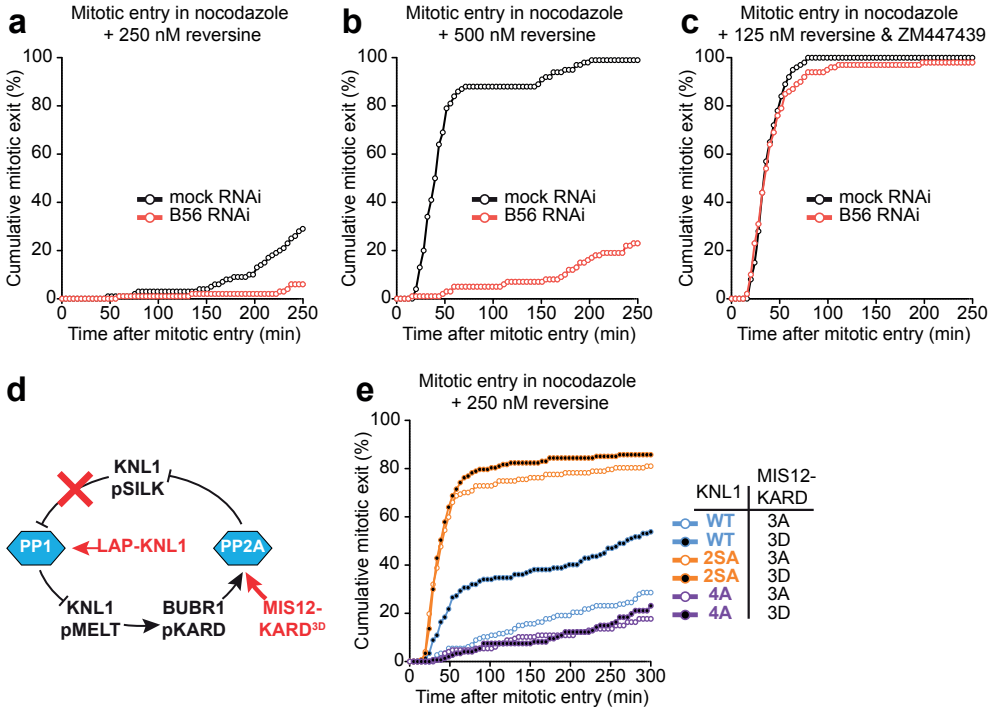

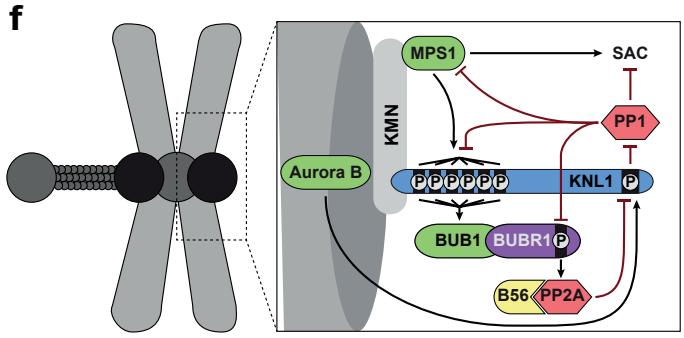

Figure 6: **PP2A-B56 contributes to SAC silencing by enabling PP1 kinetochore binding. (A-C)** Time-lapse analysis of duration of mitotic arrest in Flp-in HeLa cells transfected with siRNA to luciferase (mock) or a or a PP2A-B56 siRNA pool and entered mitosis in the presence of nocodazole and an intermediate (250 nM; A) or high (500 nM; B) dose of reversine or a low (125 nM) dose of reversine and ZM447439 (C). Data indicated cumulative percentage of cells (from a total of 100 cells) that exit mitosis (scored as cell flattening) at the indicated times after nuclear envelope breakdown (NEB) and are representative of 2 independent experiments. (**D**) Scheme of perturbations as performed in E. (**E**) Time-lapse analysis as in A. Flp-in HeLa cells were transfected with KNL1 siRNA and induced to express the indicated LAP-KNL1 proteins. Cells were additionally transfected to express YFP-tagged MIS12-BUBR1 KARD^{3A} or MIS12-BUBR1 KARD^{3D}. (**F**) Model of negative feedback regulation of PP1 and PP2A-B56 at unattached kinetochores. See discussion for details.

binding sites for the acidic microtubules. Formation of stable kinetochore-microtubule thus requires dephosphorylation of these sites. An activity gradient of Aurora B emanates from its residence at the inner centromere and spreads out to include the outer kinetochore (*108*). Although recently disputed by studies in budding yeast (*115*), the current model for stabilization of kinetochore-microtubule connections in human cells is that upon biorientation, kinetochore stretching spatially places the outer kinetochore outside of the sphere of influence of Aurora B, which allows for dephosphorylation of

Aurora B substrates by PP1 (*110*). However, initial kinetochore-microtubule attachments are formed before chromosome biorientation has been achieved. This creates a conceptual paradox: how are the initial attachments maintained despite proximity to Aurora B activity? A recent solution proposed by Foley et al. is that PP2A-B56 dampens Aurora B-dependent phosphorylations of the KMN network. This is in line with its localization to kinetochores during prometaphase (*120*). However, since PP1 also opposes Aurora B phosphorylations (*36*) and given our present data that PP2A-B56 enables kinetochore PP1, it is possible that the observed lack of dephosphorylation of Aurora B substrates in B56-depleted cells in prometaphase is due to absence of kinetochore PP1. This is seemingly inconsistent with the observation that PP1 is most prominently localized to kinetochores in metaphase. However, PP1 does localize weakly to kinetochores in prometaphase (*109, 110*), and this may be sufficient to counter Aurora B activity to such an extent as to allow initial formation of kinetochore-microtubule attachments. It will be of interest to examine whether the enhanced KMN network phosphorylations in B56-depleted cells are due to PP1 activity.

The impact of phosphatases on SAC establishment and silencing

Absence of PP1 and PP2A-B56 affects the localization of several SAC proteins, including MPS1, BUB1, BUBR1 and MAD1, to kinetochores of nocodazole-treated cells. Thus, these phosphatases normally prevent accumulation of maximal amounts of SAC proteins at individual unattached kinetochores and may therefore modulate SAC signaling strength. A possible result of loss of phosphatase activity is that it could conceivably result in SAC hyperactivation. Although this was not reflected in MCC levels in KNL1^{4A} cells, it may be difficult to distinguish SAC hyperactivation from defects in SAC silencing. If MCC levels are maximal in nocodazole-treated cells, hyperactivation may only be apparent when SAC signaling is weakened, for instance by low reversine or, in a physiological prometaphase, by few unattached kinetochores. We observed persistent SAC activity in cells expressing KNL1^{4A}, which is in agreement with data from budding yeast (*257*) and fission yeast (*258*). Additionally, cells expressing KNL1^{4A} or depleted of B56 efficiently established a SAC response when MPS1 was inhibited with reversine doses that normally drive mitotic exit. Thus, PP1 and PP2A-B56 clearly oppose SAC activity at unattached kinetochores. Differentiating between SAC hyperactivity or defects in SAC silencing will require mechanistic insights into the molecular events that silence MCC production at kinetochores upon microtubule attachment and biorientation.

Together, kinetochore PP1 and PP2A-B56 mediate the dephosphorylation of numerous substrates in the outer kinetochore. These include the BUBR1-KARD, DSN1 and the SILK and MELT motifs of KNL1 (*120, 122*; this study). These phosphatases furthermore oppose the kinetochore localization of PLK1, possibly via dephosphorylation of BUB1 (*120, 315*; chapter 3 of this thesis). Most of these phosphorylations directly or indirectly affect the kinetochore localization of PP2A-B56 and PP1 and thereby impinge on SAC signaling. It is however unknown which phosphorylations need to be removed to halt MCC production. Perturbing the kinetochore localization of PP2A-B56 and PP1 not only allows the mapping of regulated kinetochore phosphorylation sites, but also enables dephosphorylation events to be assigned to the activities of individual phosphatases. Therefore, quantitative phosphoproteomics of SAC proteins and the KMN network in KNL1^{4A} and BUBR1$^{\Delta KARD}$-expressing cells will be instrumental in unraveling the network of phosphorylations that regulate SAC signaling. When combined with the selective inactivation of SAC kinases, such approaches may also permit the identification of the dephosphorylation events that trigger SAC silencing. It will be of exceeding interest to determine which phosphorylations persist in KNL1^{4A}-expressing cells following the inhibition of MPS1.

Negative phosphatase feedbacks in mitosis

Ser/Thr phosphatases are functionally defined by their interactions with regulatory subunits and subcellular localization. The primary PP1 docking motif [K/R]-]K/R]-[V/I]-x-[F/W] is present in 70% of all PP1 interacting proteins (*316*). When the x in this motif is a serine or threonine, it is also the consensus motif of Aurora B phosphorylation sites (R-[R/K]-x-[S/T]-F; *317*). Suppression of PP1 docking by Aurora B may thus be a common theme in mitosis. Indeed, in addition to KNL1, Aurora B also regulates the docking of PP1 to the kinesin CENP-E (*305*) and possibly to the chromatin protein Repo-Man (*318*). Although less-well characterized, interaction of PP2A-B56 isoforms with recruiting proteins may also have a common theme: the KARD domain of BUBR1 shares a LSPI motif with the B56 docking motif of Repo-Man (*122, 318*). Considering that suppressive phosphorylations in PP1 docking motifs also need to be removed for dynamic regulation of PP1 docking, negative feedback between PP1 and PP2A-B56 localization might prove a common regulatory mechanism in mitosis.

Methods

Cell culture and reagents

HeLa Flp-in cells (a gift from S. Taylor, University of Manchester, Manchester, England, UK), stably expressing a TetR, were cultured in DMEM supplemented with 9% tetracycline-approved FBS, 50 µg/ml penicillin/streptomycin and 2 mM L-glutamine. HeLa Flp-in cells stably expressing a doxycycline-inducible, siRNA-resistant, LAP-tagged KNL1 construct were described previously (chapter 3 of this thesis) and maintained in the same medium but containing 200 µg/ml hygromycin and 4 µg/ml blasticidin. To induce protein expression in the inducible cell lines, 1 µg/ml doxycycline was added for ≥36 h. Thymidine (2 mM), nocodazole (830 nM), MG132 (10 µM), reversine, doxycycline and puromycin (1 µg/ml) were all obtained from Sigma-Aldrich. Hygromycin was purchased from Roche. ZM447439 was obtained from Tocris Bioscience. Blasticidin was obtained from PAA Laboratories.

Knockdown and reconstitution experiments with LAP-KNL1

For knockdown and reconstitution of KNL1 in HeLa Flp-in cells, cells were transfected with 20 nM KNL1 or mock siRNA and, in some experiments, 20 nM additional mock, MPS1 or MAD2 siRNA for 16 h after which the cells were arrested in early S phase for 24 h by addition of thymidine. Subsequently, cells were release from thymidine for 8-10 h and arrested by the addition of nocodazole and (for immunolocalization experiments) subsequently treated with MG132 to prevent mitotic exit and (in some experiments) reversine, ZM447439 or DMSO for 20-30 minutes. LAP-KNL1 expression was induced by the addition of doxycycline during the thymidine block.

Transfection, plasmids and siRNA

Plasmids were transfected into Flp-in HeLa cells using Fugene HD (Promega) according to the manufacturer's instructions. pLAP-MIS12-KARD^{3A} and pLAP-MIS12-KARD^{3D} encode LAP-MIS12 tagged variants of the BUBR1 KARD domain (amino acids 647-697) in which Ser670, Ser676 and Thr680 were mutated to alanines (KARD^{3A}) or phosphomimetic aspartic acids (KARD^{3D}) and have been described before (*122*).

siRNAs used in this study were as follows: si-MPS1, 5'-GACAGAUGAUUCAGUUGUA-3' (custom; Thermo Fisher Scientific); si-mock (Luciferase GL2 duplex; D-001100-01-20; Thermo Fisher Scientific); siKNL1, 5'-GCAUGUAUCUCUUAAGGAA-3' (CASC5#5; J-015673-05; Thermo Fisher Scientific); si-BUBR1, 5'-AGAUCCUGGCUAACUGUUC-3' (custom; Thermo Fisher Scientific); siBUB1, 5'-CCUGAUAUUUCUGAUGACA-3' (custom; Thermo Fisher Scientific); siMAD2, 5'-UACGGACUCACCUUGCUUG-3' (custom; Thermo Fisher Scientific). The B56 family siRNA pool was composed of 5 individual siRNAs that together targeted all B56 isoforms as described previously (*120*). The siRNAs were mixed at an equimolar ratio and transfected at a total concentration of 20 nM. The siRNAs used (all from Thermo Fisher Scientific) were B56α (PPP2R5A), 5'-UGAAUGAACUGGUUGAGUA-3'; B56β (PPP2R5B), 5'-GAACAAUGAGUAUAUCCUA-3'; B56γ (PPP2R5C), 5'-GGAAGAUGAACCAACGUUA-3'; B56δ (PPP2R5D), 5'-UGACUGAGCCGGUAAUUGU-3'; B56ε (PPP2R5E), 5'-GCACAGCUGGCAUAUUGUA-3'. All siRNAs were transfected using HiPerFect (Qiagen) at 20 nM according to the manufacturer's instructions.

Immunoprecipitation and immunoblotting

Flp-in HeLa cells in which KNL1 was depleted and reconstituted with LAP-KNL1 were treated with thymidine for 24 h and subsequently released into nocodazole for 14 h. Cells were treated with reversine

(500 nM) or DMSO and MG132 to prevent mitotic exit for 1 hour. Mitotic cells were isolated by mitotic shake off and lysed in lysis buffer (50 mM Tris-Cl, pH 7.5, 150 mM NaCl, 1% TX-100, 2mM $MgCl_2$, 5 mM EDTA, supplemented with protease inhibitors and phosphatase inhibitors) on ice. The cleared extract was incubated with 10% protein A-agarose beads (Roche)/antibody mix for 2 hours at 4°C on a rotating wheel. The beads were washed four times with lysis buffer. Supernatant and beads were processed for SDS-PAGE and the proteins were transferred to nitrocellulose membranes for immunoblotting. Immunoblotting was performed using standard protocols; the signal was visualized and analyzed on a scanner (ImageQuant LAS 4000; GE Healthcare) using enhanced chemiluminescence.

Antibodies

The pMELT-KNL1 antibody, directed against Thr943 and Thr1155 of human KNL1, was raised in rabbits using the peptide MEI-pT-RSHTTALEC coupled to KLH as antigen and affinity purified using the described peptide (Covance). The antibody was used in the presence of nonphosphorylated peptide (1 ng/ml) in all experiments.

The following primary antibodies were used for immunofluorescence imaging and immunoblotting: α-tubulin (T5168, Sigma-Aldrich), BUB1 (A300-373A; Bethyl), BUBR1 (A300-386A; Bethyl), BUBR1 (custom sheep polyclonal), CENP-C (PD030; MBL), CENP-T (D286-3; MBL), CREST (Cortex Biochem), CDC20 (E7; SantaCruz Biotechnology), GFP (mouse monoclonal; Roche), GFP (custom rabbit polyclonal; *205*), MAD1 (custom mouse monoclonal) was a gift from A. Musacchio (MPI, Dortmund, Germany; *175*), MAD2 (custom rabbit polyclonal raised against full-length 6xHis-tagged MAD2 as antigen; *216*). pT680-BUBR1 (custom rabbit polyclonal; *122*), pS24-KNL1 (custom rabbit polyclonal) was a gift from I. Cheeseman (Whitehead Institute, Cambridge, MA, USA (*33*). Secondary antibodies were goat anti-rat Alexa Fluor 647, high-crossed goat anti-guinea pig and anti-human Alexa Fluor 647, donkey anti-sheep Alexa Fluor 568 and goat anti-rabbit and anti-mouse Alexa Fluor 488 and Alexa Fluor 568 (Molecular Probes) for immunofluorescence experiments.

Live-cell imaging, immunofluorescence and image quantification

For live-cell imaging for time-lapse analysis, cells were plated in 24-well glass-bottom plates (MatTek Corporation), transfected, and imaged in a heated chamber (37°C and 5% CO_2) using a 20x/0.5 NA UPLFLN objective (Olympus) on a microscope (IX-81; Olympus) controlled by Cell-M software (Olympus). Images were acquired using a camera (ORCA-ER; Hamamatsu Photonics) and processed using Cell-M software.

For immunofluorescence, cells plated on 12-mm coverslips were pre-extracted with 0.1% Triton X-100 in PEM (100 mM Pipes, pH 6.8, 1 mM $MgCl_2$ and 5 mM EGTA) for 45s before fixation with 4% paraformaldehyde in PBS for 10 min. Coverslips were washed with PBS and blocked with 3% BSA in PBS for 30 min, incubated with primary antibodies for 2-4 h at room temperature or 16 h at 4°C, washed with PBS and incubated with secondary antibodies for an additional hour at room temperature. Coverslips were then incubated with DAPI for 2 min, washed and mounted using antifade (ProLong; Molecular Probes). For alignment assays, cells were treated as before, but were fixed with 3.7% Shandon Zinc Formal-Fixx (Thermo Scientific) for 10 min and subsequently washed with PBS and permeabilized with 0.5% Triton X-100 for 15 min. All images were acquired on a deconvolution system (Deltavision RT; Applied Precision) with a 100x/1.40 NA U Plan S Apochromat objective (Olympus) using softWoRx software (Applied precision). Images are maximum intensity projections of deconvolved stacks. For

quantification of immunostainings, all images of similarly stained experiments were acquired with identical illumination settings; cells expressing comparable levels of exogenous protein were selected for analysis and analyzed using ImageJ (National Institutes of Health). An ImageJ macro was used to threshold and select all centromeres and all chromosome areas (excluding centromeres) using the DAPI and anti-centromere antibodies channels as described previously (*195*). This was used to calculate the relative mean kinetochore intensity of various proteins ([centromeres-chromosome arm intensity (test protein)]/[centromeres-chromosome arm intensity (CENP-C/CENP-T/CREST)].

Supplemental Material

Fig. S1 shows that the removal of BUB1 from bioriented kinetochores is dependent on kinetochore PP1. Fig. S2 shows that the localization of PP1 to KNL1 is a prerequisite for efficient SAC silencing. Fig. S3 shows that the exclusion of PP1 from kinetochores renders BUBR1 kinetochore localization insensitive to Aurora B inhibition.

Acknowledgements

We thank Mathijs Vleugel for help with the pMELT-KNL1 antibody, Iain Cheeseman for the pSer24-KNL1 antibody, Andrea Musacchio and Anna de Antoni for the MAD1 antibody, Stephen Taylor for the HeLa Flp-in cell line and the Kops and Lens laboratories for insights and discussions. This work was supported by an European Research Council starting grant (KINSIGN; to G.J.P.L. Kops) and by the Dutch Cancer Society (KWF Kankerbestrijding; UU2012-5427; to G.J.P.L. Kops).

Supplemental figure 1

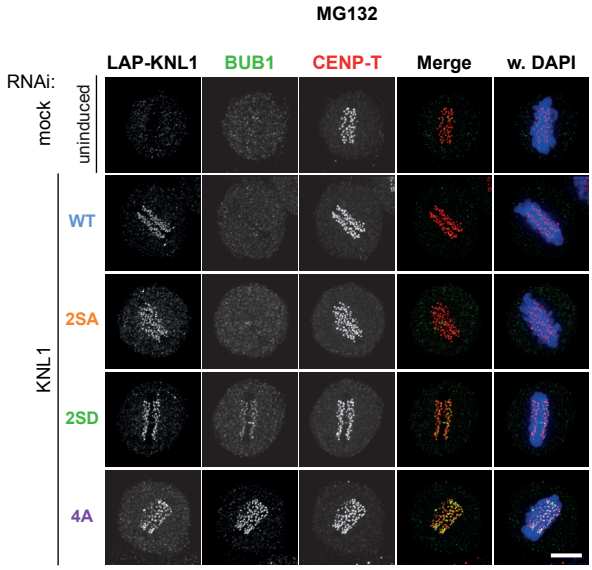

Figure S1: **Kinetochore exclusion of PP1 maintains BUB1 localization to metaphase kinetochores.** Representative images of immunolocalization of the various LAP-KNL1 proteins, BUB1 and centromeres (CENP-T) in Flp-in HeLa cells transfected with siRNAs to KNL1 and luciferase (mock) and treated with MG132. DNA (DAPI) is shown in blue. Bars, 5 µm.

Supplemental figure 2

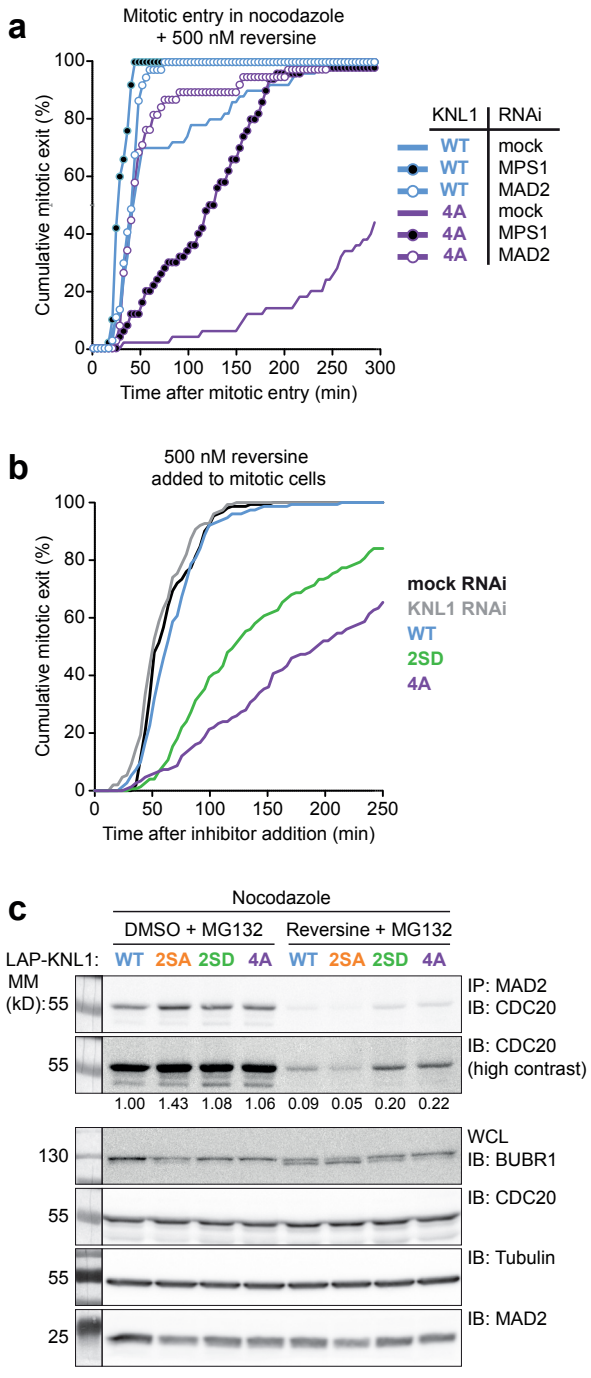

Figure S2: **Kinetochore binding of PP1 allows efficient SAC silencing.** (**A**) Time-lapse analysis of duration of mitotic arrest in nocodazole-treated Flp-in HeLa cells transfected with KNL1 siRNA and expressing the indicated LAP-KNL1 proteins. Cells entered mitosis in the presence of 500 nM of reversine. Cells were additionally transfected with siRNAs to luciferase (mock), MPS1 or MAD2. Data are from a total of 50 cells per treatment. (**B**) Time-lapse analysis of duration of mitotic arrest in Flp-in HeLa cells transfected with mock or KNL1 siRNA and expressing the indicated LAP-KNL1 proteins. Nocodazole-arrested cells were treated with 500 nM of reversine. Data are from a total of 150 cells per treatment and are representative of 3 independent experiments. (**C**) MAD2, CDC20, Tubulin and BUBR1 immunoblots (IB) of whole-cell lysates and CDC20 immunoblots of immunopurified (IP) MAD2 from mitotic Flp-in HeLa cells transfected with KNL1 siRNA and expressing the indicated LAP-KNL1 variants. Nocodazole-arrested cells were treated with MG132 and DMSO or reversine (500 nM). Band intensity of CDC20 in MAD2 IPs is indicated. Boxes on left show molecular mass standard. MM, molecular mass.

Figure S3: **Kinetochore exclusion of PP1 allows persistent BUBR1 localization and BUBR1-KARD phosphorylation in the absence of Aurora B activity.** (**A**) Scheme of perturbations as performed in this figure. (**B and C**) Representative images (B) and quantification (C) of immunolocalization of the various LAP-KNL1 proteins (GFP), BUBR1 and centromeres (CENP-T) in Flp-in HeLa cells transfected with siRNAs to KNL1 and luciferase (mock) and treated with nocodazole, MG132 and ZM447439. Graph in C displays total kinetochore intensities (±SEM) of the indicated proteins relative to centromeres (CENP-T). Data are from a total of ≥19 cells per treatment from 2 independent experiments. (**D and E**) Representative images (D) and quantification (E) of immunolocalization of various LAP-KNL1 proteins (GFP), pKARD-BUBR1(pT680) and centromeres (CENP-T) in Flp-in HeLa cells treated as in B. Graph in E displays total kinetochore intensities (±SEM) of the indicated proteins relative to centromeres (CENP-T). Data are from a total of ≥28 cells per treatment from ≥2 independent experiments. (**F**) Graph of relative kinetochore intensities of BUBR1 and pKARD BUBR1 relative to LAP-KNL1 as plotted in C and E. Ratios are set to 1 for DMSO-treated LAP-KNL1^{WT}-expressing cells. DNA (DAPI) is shown in blue. Insets show magnifications of the boxed regions. Bars, 5 µm.

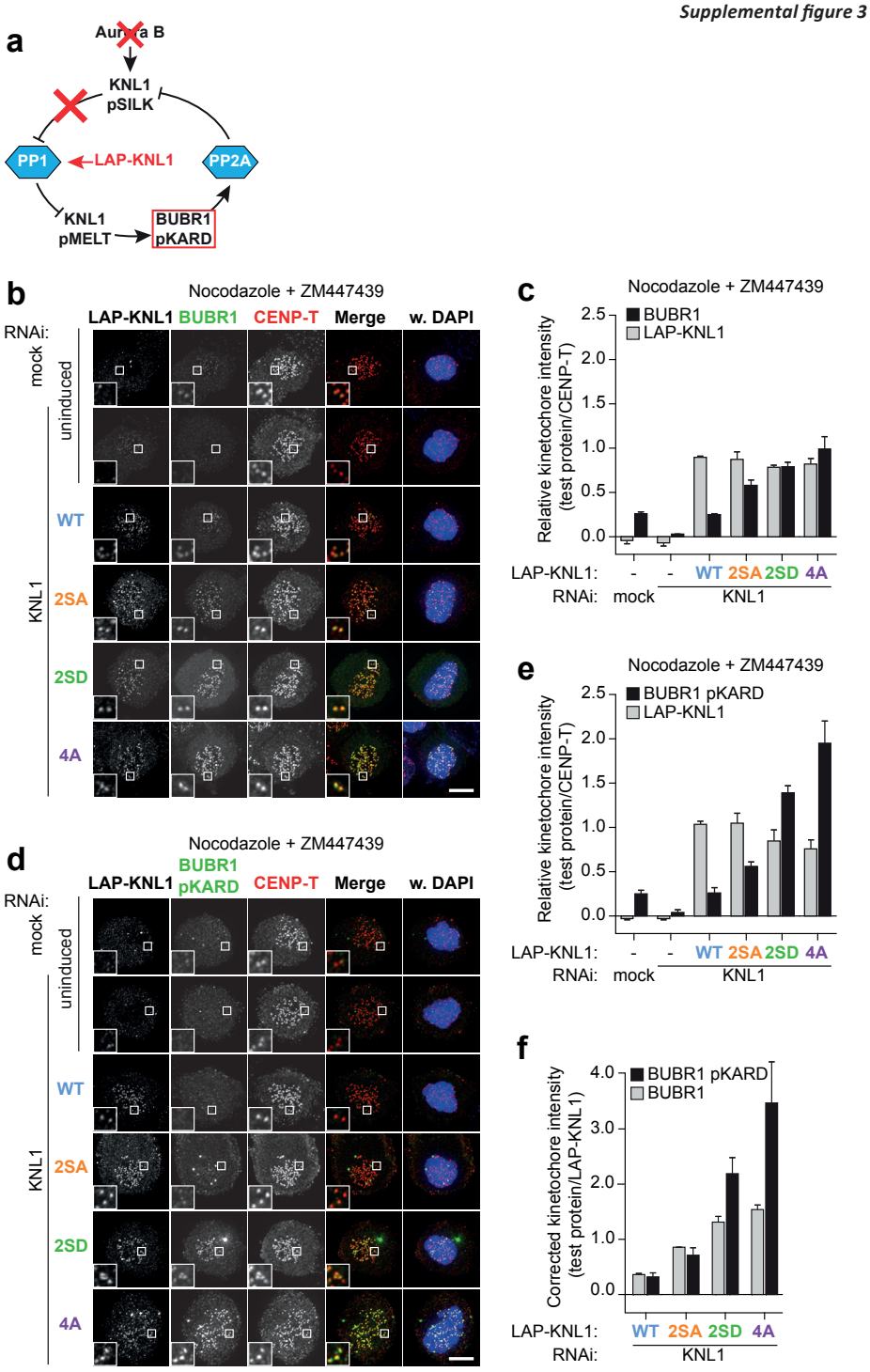
a
Aurora B
KNL1
pSILK
PP1
LAP-KNL1
PP2A
KNL1
pMELT
BUBR1
pKARD
b
Nocodazole + ZM447439
LAP-KNL1 BUBR1 CENP-T Merge w. DAPI
RNAi:
mock
uninduced
KNL1
WT
2SA
2SD
4A
c
Nocodazole + ZM447439
BUBR1
LAP-KNL1
Relative kinetochore intensity
(test protein/CENP-T)
2.5
2.0
1.5
1.0
0.5
0.0
LAP-KNL1: - - WT 2SA 2SD 4A
RNAi: mock KNL1
d
Nocodazole + ZM447439
LAP-KNL1 BUBR1 pKARD CENP-T Merge w. DAPI
RNAi:
mock
uninduced
KNL1
WT
2SA
2SD
4A
e
Nocodazole + ZM447439
BUBR1 pKARD
LAP-KNL1
Relative kinetochore intensity
(test protein/CENP-T)
2.5
2.0
1.5
1.0
0.5
0.0
LAP-KNL1: - - WT 2SA 2SD 4A
RNAi: mock KNL1
f
BUBR1 pKARD
BUBR1
Corrected kinetochore intensity
(test protein/LAP-KNL1)
4.0
3.0
2.0
1.0
0.0
LAP-KNL1: WT 2SA 2SD 4A
RNAi: KNL1

Chapter 5

Summary and Discussion

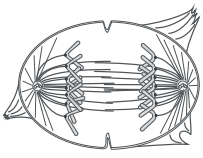

Summary

Error-free chromosome segregation in mitosis depends on the concerted activities of the spindle assembly checkpoint (SAC) and the error-correction machinery. Both the SAC and chromosome biorientation critically depend on the activities of MPS1 kinase. Prior to the work in this thesis, it had been demonstrated that the recruitment of MPS1 to kinetochores was functionally important and that this depended on Aurora B signaling, but it was poorly understood which molecular mechanisms governed MPS1 kinetochore localization. We find that the kinetochore-binding region of MPS1 is composed of a TPR domain, of which we resolved the structure, and an N-terminal extension (NTE). We show that MPS1 kinetochore binding is predominantly mediated by the NTE and that this is regulated by the TPR domain. Moreover, we demonstrate that the kinetochore localization of MPS1 is dependent on the calponin homology (CH) domain of HEC1, which leads us to propose that the kinetochore localization of MPS1 may be directly prevented by the formation of kinetochore-microtubule attachments (Chapter 2). When studying the regulation of MPS1 kinetochore localization by Aurora B, we show that Aurora B enables MPS1 localization by relieving the suppression of the NTE by the TPR domain (Chapter 2). We furthermore showed that Aurora B predominantly regulates MPS1 kinetochore localization in an indirect manner, by inhibiting kinetochore binding of the phosphatase PP1 through phosphorylation of its docking motifs in the kinetochore scaffold KNL1 (Chapter 3). In chapter 4, we show that these motifs are dephosphorylated by PP2A-B56, thus implicating PP2A-B56 in PP1 kinetochore localization and inhibition of SAC signaling. Furthermore, we demonstrate that PP2A-B56 and PP1 control each other's localization to kinetochores by negative feedback signaling (Chapter 4). We propose that such negative phosphatase feedback may serve to maintain the right level of SAC signaling and enable rapid SAC silencing at metaphase.

Discussion

1. Kinetochore localization of MPS1 and the SAC

MPS1 has long been established to bind unattached kinetochores (*198, 208, 209*). Prior to the work presented in this thesis, the relevance of this localization for MPS1 function and the SAC was not well understood. Partially, this resulted from the technical challenges that complicate the study of MPS1 localization mechanisms. Firstly, the kinetochore localization of endogenous MPS1 is difficult to detect. A main cause of this is that kinetochore-bound MPS1 represents only a small, highly dynamic, pool of all MPS1 molecules in a cell (*215, 319*). Moreover, the abundance of MPS1 at kinetochores is variable during mitotic progression. Kinetochore levels of MPS1 are highest during prophase and drop progressively during a prolonged prometaphase arrest (*195*). Additionally, structure-function analyses of MPS1 localization have suffered from an insufficient understanding of the structural organization of the kinetochore-binding domain of MPS1.

Prior to the work presented in this thesis, overexpression of N-terminal MPS1 fragments had been shown to delocalize endogenous MPS1 and weaken the SAC (*208, 211*). It was therefore concluded that kinetochore localization of MPS1 is involved in SAC signaling. However, it had also been suggested that MPS1 kinetochore localization may not be required to maintain a mitotic arrest. This followed from the observation that a localization-deficient MPS1 mutant, MPS1$^{\Delta 100}$, could maintain a SAC response to nocodazole (*218*). However, due to the technicalities of how that experiment was performed, it is likely that MPS1$^{\Delta 100}$ was weakly localized to kinetochores via dimerization with inactive, localization-proficient MPS1 and could thereby activate the SAC. This would be in line with similar observations during meiosis in mouse oocytes (*212*).

In chapter 2, we addressed the involvement of MPS1 kinetochore localization in SAC signaling by structure-function analysis of the N-terminal region of MPS1. We demonstrated that the non-localizing mutant MPS1$^{\Delta 200}$ was unable to generate a SAC response to nocodazole. Importantly, this mutation did not affect MPS1 dimerization or kinase activity. Moreover, MPS1$^{\Delta 200}$ could activate the SAC when it was artificially tethered to kinetochores. These data strongly suggest that the kinetochore localization of MPS1 is required for the SAC.

2. Mechanisms of MPS1 kinetochore localization

2.1 Identification of the kinetochore recruiter of MPS1

In chapter 2, we demonstrate that MPS1 kinetochore binding is dependent on the calponin homology (CH) domain of HEC1. This is in line with the previous observation that budding yeast Mps1 interacted directly with an N-terminal fragment of Ndc80/HEC1 when co-expressed in *E. coli* (*221*). It however remains unknown if MPS1 directly binds HEC1 in mammals and if so, how this is regulated. Importantly, several lines of evidence suggest that the HEC1 CH domain is insufficient to recruit MPS1 in cells. Whereas MPS1 was recruited to *lacO* arrays decorated with LacI-HEC1^{WT}, we did not detect MPS1 localization to LacI-HEC1$^{1\text{-}207}$ foci (not shown). Moreover, the kinetochore localization of MPS1 in nocodazole-treated cells was not enhanced when the HEC1 CH domain was artificially tethered to kinetochores by overexpression of MIS12-HEC1$^{80\text{-}207}$ (not shown). As HEC1 forms obligate heterodimers with NUF2, human MPS1 may interact with the N-terminal regions of both HEC1 and NUF2 (see chapter 1, Fig. 2). It is additionally possible that MPS1 solely interacts with NUF2 and that HEC1$^{\Delta 207}$ caused structural aberrations in NUF2 that prevented the recruitment of MPS1. Finally, it

remains a possibility that the HEC1/NUF2-MPS1 interaction is indirect, but more on that below.

To understand how MPS1 is recruited to kinetochores, it is essential to validate if the interaction between MPS1 and the Ndc80 complex is direct. An important tool to study MPS1-Ndc80 binding *in vitro* will be the Ndc80^{bonsai} complex, an engineered version of the Ndc80 complex that consists of a heterodimer of HEC1-SPC25 and NUF2-SPC24 chimaera's (*49*). These constructs lack the long coiled coils of the native complex and are efficiently expressed in bacteria. Ndc80^{bonsai} encompasses the complete CH domains of both HEC1 and NUF2, as well as the N-terminal tail of HEC1 and is therefore likely to fit the molecular requirements to bind MPS1. Furthermore, MPS1-Ndc80 interaction studies are likely to benefit from the use of full-length MPS1 instead of the N-terminal fragments that were used for biophysical analyses in chapter 2. While the N-terminal MPS1$^{1-192}$ fragment did localize to kinetochores, it did so weakly and could be detected there exclusively in prophase. Therefore, if a direct interaction between the NTE-TPR module and the Ndc80 complex exists, it is likely that it is stabilized by other regions of MPS1.

Whereas the Ndc80 complex is loaded onto kinetochores in G2, MPS1 is not recruited until prophase. MPS1 may not be recruited earlier because its localization requires the establishment of mitotic phosphorylations. This is supported by the observation that premature activation of Aurora B, by artificially tethering INCENP to kinetochores, allows MPS1 localization in G2 (*195*), and by our observation that LacI-HEC1 was able to recruit MPS1 to *lacO* arrays only in mitosis but not in interphase (not shown). MPS1 may thus not interact efficiently with unphosphorylated Ndc80 complex. Prephosphorylation of Ndc80 with a panel of mitotic kinases, including Aurora B, BUB1, CDK1 and PLK1 may therefore be required to allow an interaction between MPS1 and the Ndc80 complex *in vitro*.

It remains possible that MPS1 does not interact directly with the Ndc80 complex in mammals. If so, it is not immediately obvious which other kinetochore proteins could be the kinetochore receptor for MPS1. Depletion of most outer-kinetochore proteins had no effect on MPS1 kinetochore levels, except HEC1/NUF2 (*47, 209*). In addition, MPS1 has not been identified as a binding partner by mass spectrometry of purified kinetochore proteins, and vice versa (*320*). Such approaches are troubled by the high turnover of MPS1 at kinetochores (*215, 319*) which likely allows MPS1-containing complexes to dissociate during purification. This is exacerbated by the stringent purification protocols that are required to isolate kinetochore complexes. These problems may be circumvented by limited chemical crosslinking of mitotic cells, which may allow sufficient MPS1 to be covalently linked to kinetochores to be detected in complex with kinetochore proteins by pulldown and mass spectrometry. Nevertheless, we consider it highly likely that the direct recruiter of MPS1 is the Ndc80 complex, and efforts are currently underway in the lab to test this.

2.2 Regulatory mechanisms of MPS1 kinetochore localization

Regulation by kinetochore-microtubule attachments

In chapter 2, we showed that MPS1 localization is strongly reduced on the attached sister kinetochore of a monotelic chromosome. This suggests that MPS1 is specifically removed from kinetochores upon attachment by spindle microtubules. As MPS1 localization is dependent on the microtubule-binding CH domain of HEC1, we proposed that MPS1 and microtubules could interact with the same surface of HEC1 in a mutually exclusive manner. If so, kinetochore-microtubule attachments would directly delocalize MPS1 by competitive binding to HEC1. This would then integrate SAC signaling

with kinetochore-microtubule attachments and could potentially be the initial step that triggers SAC silencing (Fig. 1A). Addressing this model will be important, but technically challenging. If direct binding between MPS1 and the Ndc80 complex can be detected *in vitro*, and Ndc80 utilizes the same surface to bind microtubules and MPS1, then this interaction should be sensitive to the presence of purified tubulin.

The delocalization of MPS1 from attached kinetochores in cells may be caused by direct competition with microtubules, or by other regulatory mechanisms, such as dynein-dependent stripping. An approach to distinguish between these possible modes of MPS1 removal from kinetochores is the use of cells expressing the spindly-box mutant of Spindly. This mutant prevents dynein recruitment to kinetochores and stripping of MAD1 and MAD2 (*249, 253*). If MPS1 is still delocalized from kinetochores in spindly-box mutant-expressing cells, this proves that MPS1 removal can occur independent of dynein. It would additionally be informative to determine if MPS1 recruitment to Ndc80 complexes is sensitive to microtubule attachment in a non-kinetochore environment, such as at LacI-HEC1 foci. The expression of LacI-CENP-T allows the assembly of ectopic kinetochore-like structures at *LacO* foci (*26*). These foci stably attach to spindle microtubules, likely because they accumulate high levels of HEC1. LacI-HEC1 foci may therefore attach to spindle microtubules in a similar manner. If the localization of MPS1 to LacI-HEC1 foci is mutually exclusive with the attachment of these foci by spindle microtubules, that would be highly suggestive that MPS1 kinetochore localization is directly controlled by kinetochore-microtubules.

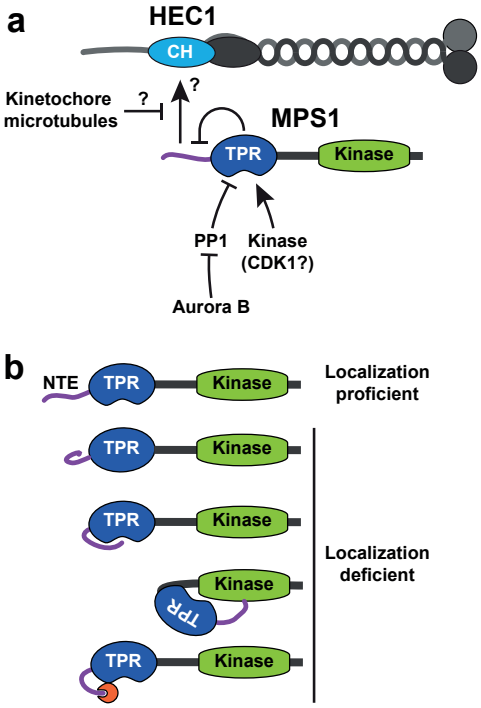

Figure 1: **Mechanisms and regulation of MPS1 kinetochore localization.** (**A**) Schematic model of the regulation of MPS1 kinetochore localization. CH: calponin homology domain. See section 2 for details. (**B**) Schematic model of possible mechanisms of NTE inhibition by the TPR domain. See section 2.2: "conformational regulation by the TPR domain" for details.

This can be further explored by mutagenesis of the microtubule-binding interface of the Ndc80 complex. This interface of the Ndc80 complex is well characterized, and the residues in the CH domains of HEC1 and NUF2 that critically contribute to microtubule binding have been mapped (*49*). If this surface is additionally utilized for MPS1 recruitment, then mutations in this interface that perturb microtubule-binding may prevent MPS1 localization to kinetochores or LacI-HEC1 foci in a similar way as HEC1$^{\Delta 207}$ does.

Regulation by phosphorylation

As discussed above, we expect the interaction between the Ndc80 complex and MPS1 to be dependent on mitotic phosphorylation. It is well established that MPS1 kinetochore localization

critically depends on the activity of Aurora B (*195, 217*). However, we show in chapter 3 that Aurora B predominantly impinges on MPS1 kinetochore localization in an indirect manner, via regulation of the kinetochore localization of PP1. Aurora B may still promote MPS1 localization via an additional pathway, independently of PP1 regulation, as uncoupling of PP1 localization from phosphoregulation by Aurora B did not fully recover MPS1 localization upon inhibition of Aurora B (chapter 3). Nevertheless, such an additional pathway is unlikely to dominantly regulate MPS1 kinetochore localization. The unexpected finding that the control of MPS1 localization by Aurora B is mediated by inhibition of a phosphatase poses the question which kinase then drives the kinetochore localization of MPS1 (Fig. 1A). Essentially all mitotic kinases may be involved, but BUB1, PLK1 and MPS1 are unlikely candidates. BUB1 is not required for MPS1 localization, since its depletion enhances the amount of MPS1 at kinetochores (not shown and *209*). Also, MPS1 kinetochore localization is not reduced by the inhibition of PLK1 (Tale Sliedrecht, personal communication and *209*). Finally, MPS1 has been suggested to mediate its own localization, as MPS1 recruitment has been reported to require (auto)phosphorylation of the NTE at Thr12 and Ser15 (*243*). However, it has thereafter been established that the kinase activity of MPS1 is not required for its localization (*210, 215, 217*). The kinase most likely to drive MPS1 kinetochore recruitment appears to be CDK1. Multiple reported phosphorylation sites on MPS1 fit the CDK1 consensus motif (S/T-P; *125, 126, 215, 228, 238, 239, 242, 243, 245*). Of these, phosphorylation of Ser821 has been suggested to contribute to MPS1 kinetochore localization (*243*), although another report has found Ser821 as an autophosphorylation site (*239*). Moreover, preliminary data suggests that the kinetochore localization of MPS1 is rapidly lost from unattached kinetochores after CDK1 inhibition (not shown). CDK1-dependent recruitment of MPS1 is also conceptually attractive, as it would allow the SAC to be activated by default following mitotic entry. Regardless of the kinase, it will be of interest to identify the phospho-residue(s) important for MPS1 localization. These residues may reside at the Ndc80 complex, at MPS1 itself or at a currently unidentified intermediator. Quantitative phosphoproteomics of MPS1 and the KMN network will be invaluable to screen for phosphorylations that control MPS1 kinetochore recruitment. In such screens, Aurora B-dependent phosphorylations of the MPS1 NTE-TPR module and the Ndc80 complex that fit the CDK1 consensus motif will be prime candidates for further analysis.

Conformational regulation by the TPR domain

In chapter 2 we showed that NTE-dependent kinetochore localization of MPS1 is regulated by an N-terminal TPR domain. We suggested that the TPR domain ($MPS1^{62-192}$) imposes an inhibitory conformation on the NTE ($MPS1^{1-60}$) and that this was relieved by the activity of Aurora B. However, we did not experimentally address this hypothesis. Much structural and biophysical work is still needed to unravel the function of the MPS1 TPR domain. Central in our hypothesis is the concept that MPS1 can adopt a localization proficient form, in which the NTE is available to mediate kinetochore binding and a localization deficient form, in which the NTE is blocked under influence of the TPR domain.

There are several ways in which MPS1 can adopt such a localization-deficient conformation (Fig. 1B). In one scenario, structural rearrangements of the TPR domain induce a conformational change of the NTE that frees it for kinetochore binding. Such structural rearrangements of the TPR could potentially be mediated by ligand binding or phosphorylation. However, this is unlikely as TPR domains are stable and ligand binding generally induces little or no structural rearrangements (*321*). Alternatively, the TPR may interact with the NTE directly. In such an interaction, the NTE could bind the ligand binding groove of the TPR, as is typical for TPR-ligand interactions, or fold back onto the convex surface in a manner that is reminiscent of interactions of BUB TPR domains and the KI motifs

of KNL1 (*37, 38*). If such an interaction within the NTE-TPR module exists, it should be perturbed by mutations of the TPR ligand-binding groove or convex backside. Such mutations would relieve the NTE from inhibition by the TPR domain and should therefore allow MPS1 to localize kinetochores in the absence of Aurora B activity, in a similar way as MPS1$^{\Delta TPR}$. It is also possible that the NTE interacts with other regions of MPS1, such as the kinase domain. In this scenario, the TPR could allow this interaction by functioning as linker that bridges the distance between the NTE and the C-terminal kinase. By interacting with the kinase domain, the NTE could also function to regulate activation of the kinase domain, either allosterically or by functioning as a pseudosubstrate (*322*). A role for the TPR domain in regulating activity of the kinase domain is supported by the observation that MPS1$^{\Delta TPR}$ displayed elevated levels of autophosphorylation. To differentiate between these possibilities, *in vitro* binding studies using recombinant TPR domain, kinase domain and NTE peptides would be instrumental. Finally, it is possible that inhibition of the NTE by the TPR domain is mediated by another, currently unidentified, protein. For example, an inhibitor of the NTE could bind to MPS1 in an TPR-dependent manner. However, as no stable interactors of MPS1 have been identified, there are at present no likely candidate proteins to mediate this function.

The role of dimerization

MPS1 forms dimers in cells (*210, 212* and chapter 2). *In vitro*, induced dimerization of MPS1 enhances transactivation of the kinase (*238*), but it remains unclear if MPS1 dimerization is functionally relevant for its localization to kinetochores and for the SAC. Further functional characterization MPS1 dimerization requires identification of the molecular properties of MPS1 that allow its dimerization. In a recent study by Thebault and coworkers MPS1$^{1-239}$ was found to dimerize *in vitro* by analytical ultracentrifugation. As the shorter MPS1$^{55-210}$ fragment was exclusively found as a monomer in solution, this led to the proposition that MPS1 dimerization requires the NTE (*323*). However, in our hands, four N-terminal MPS1 fragments, including MPS1$^{1-239}$, were monomers in solution (chapter 2) as analyzed by multi-angle laser light scattering analysis. Moreover, MPS1$^{1-200}$ was not required for MPS1 dimerization in cells. Therefore, we consider it unlikely that the NTE or the TPR domain mediate MPS1 dimerization. Instead, MPS1 dimerization appears to be mediated via its C-terminal regions.

3. Regulation of the NTE-TPR module by PP1

MPS1 kinetochore localization is dependent on the kinase activity of Aurora B (*195, 196*). In chapter 2 we demonstrated that Aurora B impinges on MPS1 localization via the TPR domain, since deleting the TPR domain from MPS1 renders its localization insensitive to Aurora B inhibition. In chapter 3, we however showed that the influence of Aurora B on MPS1 is predominantly indirect, by preventing the kinetochore localization of MPS1. This led us to propose that MPS1 kinetochore localization is controlled by an Aurora B-PP1-MPS1 pathway. Integration of these observations leads to a model in which PP1 regulates MPS1 localization by opposing the activity of a kinase that relieves TPR-dependent inhibition of the NTE, by phosphorylation of the NTE-TPR module, the Ndc80 complex, or an unknown intermediator, as discussed above.

If PP1 impinges on MPS1 localization via the TPR domain, then deletion of the TPR should desensitize MPS1 kinetochore localization to increased kinetochore levels of PP1. However, expression of KNL1^{2SA}, which accumulates PP1 on metaphase kinetochores, did not reduce the kinetochore localization of MPS1 in nocodazole-arrested cells. Therefore, we could not address if PP1 impinged on MPS1 localization via the TPR domain by testing the sensitivity of MPS1$^{\Delta TPR}$ to kinetochore levels

of PP1. Since KNL1^{2SA} did give functional SAC defects, a solution may be to examine whether MPS1$^{\Delta TPR}$ can improve the SAC response to nocodazole in KNL1^{2SA}-expressing cells. It would furthermore be informative to determine the kinetochore localization of MPS1 in late G2. Artificial tethering of INCENP to kinetochores enables precocious activation of Aurora B and permits the kinetochore localization of MPS1 in G2 (*195*). If inhibition of MPS1 localization by the TPR domain is dependent on suppression of CDK1-dependent phosphorylation by PP1, then MPS1$^{\Delta TPR}$ should be recruited to kinetochores in G2 in a similar manner. Endogenous MPS1 should then also be recruited to kinetochores in G2 by expression of KNL1^{4A}, which prevents the kinetochore localization of PP1.

4. SAC activation by Aurora B via phosphoregulation of PP1 kinetochore localization

In chapters 3 and 4, we demonstrate that SAC signaling is regulated by kinetochore PP1. We show that kinetochore PP1 opposes the phosphorylation of KNL1 MELT motifs and the BUBR1 KARD and thereby antagonizes the kinetochore localization of BUB1, BUBR1 and PP2A-B56. Moreover, we show that the kinetochore recruitment of PP1 is a prerequisite for efficient silencing of the SAC.

Aurora B has previously been shown to drive SAC activation by stimulating the kinetochore localization of MPS1, BUB1 and BUBR1 (*101, 194-196, 284*). In this thesis, all effects of Aurora B inhibition on the SAC could be at least largely recovered when the kinetochore localization of PP1 was prevented by the expression of KNL1^{4A}. This suggests that Aurora B impinges on the SAC predominantly by the regulation of PP1 kinetochore localization. However, throughout our experiments, premature kinetochore recruitment by expression of KNL1^{2SA} failed to completely phenocopy Aurora B inhibition. For example, in chapter 3, we determined the sensitivity of BUB1 localization to kinetochore PP1 levels. Increasing kinetochore PP1 levels by expression of KNL1^{2SA} subtly reduced BUB1 kinetochore localization, by ~24%. However, inhibition of Aurora B reduced BUB1 localization by ~60%. This difference could suggest that Aurora B impinges on BUB1 localization via additional pathways, such as by the regulation of MPS1 localization. However, when Aurora B was inhibited in KNL1^{2SA}-expressing cells, BUB1 was not removed from kinetochores. This recovery of BUB1 localization by KNL1^{2SA} strongly suggests that the dephosphorylation of PP1 docking motifs is a prerequisite for the delocalization of BUB1 following Aurora B inhibition. Importantly, this result also suggests that the variation between the effects of Aurora B inhibition and KNL1^{2SA} expression results from subtle differences in the level of PP1 recruitment between these two conditions. *In vitro*, the binding of PP1γ to an unphosphorylated fragment of KNL1 is reduced by ~20% by the substitution of Ser24 and Ser60 for alanines (*36*). Therefore, whereas KNL1^{2SA} increases PP1 localization in an unperturbed mitosis as we show in chapter 3, it is likely that this mutant does not recruit PP1 as effectively as the unphosphorylated wildtype protein when Aurora B is inhibited before mitotic entry.

These subtle differences in kinetochore PP1 levels may have a profound effect on SAC signaling. Therefore, it is necessary to carefully quantity kinetochore PP1 levels in nocodazole arrested cells. It will be important to quantitatively assess how PP1 recruitment is regulated by Aurora B and PP2A-B56 and how this is affected by mutations of the PP1-binding sites in KNL1. Additionally, it will be important to validate that the binding of PP1γ to a recombinant KNL1 fragment *in vitro* is reduced by phosphorylation by Aurora B.

5. Integration of mitotic kinase signaling by kinetochore phosphatases during mitotic progression

In chapter 4, we show that PP1 and PP2A-B56 are involved in negative feedback regulation: PP1

reduces PP2A-B56 kinetochore levels while PP2A-B56 enhances PP1 kinetochore levels. Such negative feedback regulation serves to recruit sufficient PP1 to prometaphase kinetochores to allow dynamic turnover of Aurora B-dependent phosphorylations while protecting the localization of BUB1 and BUBR1. Subsequently, at metaphase, low activity of PP2A-B56 combined with inactivation of Aurora B allow accumulation of PP1, which can replace PP2A-B56 as the main kinetochore phosphatase and initiate SAC signaling.

An important remaining question is how the activities of PP1 and PP2A-B56 are concerted to allow rapid SAC activation in prophase and efficient SAC silencing in metaphase. To better understand these mechanisms it is important to determine how this signaling network switches from a PP1-dominant to a PP2A-dominant state upon mitotic entry and vice versa upon biorientation. Computational modeling of these events may help to predict what response is generated after which alteration to the system. Such modeling requires identification of external stimuli that feed into the network and a molecular understanding of how changes in individual stimuli are affect signaling throughout the network.

An integrated model of kinetochore-based kinase and phosphatase signaling in the SAC.

Based on published data and the work described in this thesis, I propose an integrated model of a PP2A-B56 and PP1-dependent signaling network at kinetochores (Fig. 2A-D). In this model, the kinetochore localization of PP2A-B56 and PP1 phosphatases is controlled by a network of kinetochore-based mitotic kinases. This network is densely interconnected and contains several feedback loops, but the main regulatory nodes are Aurora B, MPS1, PP1 and PP2A-B56.

Aurora B provides two major inputs: it antagonizes the localization of PP1γ by phosphorylation of the PP1-docking sites in KNL1 (*33, 36* and chapter 3) and it reduces the microtubule-binding affinity of the KMN network (*29, 43*). Aurora B is activated by stimuli from CDK1, BUB1 and MPS1 and silenced upon biorientation, possibly by spatial separation from its substrates by kinetochore stretching (*105, 106, 110, 205*).

PP1 has multiple functions, all of which contribute to SAC silencing: (1) dephosphorylation of the KNL1 MELT motifs, thereby opposing the kinetochore localization of BUB1 and BUBR1 (*39* and chapter 4); (2) preventing the recruitment of PP2A-B56, by dephosphorylation of the BUBR1 KARD (chapter 4); (3) preventing the kinetochore localization of MPS1, likely by enabling TPR-dependent blocking of NTE-dependent kinetochore binding (chapters 2 and 3); and finally (4) PP1 likely stabilizes microtubule attachments at metaphase by removing Aurora B dependent-phosphorylations in the KMN network (*36*). PP1 kinetochore localization is suppressed by phosphorylation of the PP1-docking sites in KNL1 and promoted by dephosphorylation of these sites by PP2A-B56 (*33, 36, 120* and chapters 3 and 4).

MPS1 feeds into the BUB1-BUBR1-PP2A pathway by phosphorylating the KNL1 MELT motifs (*39, 41, 42*). Additionally, MPS1 stimulates the activation of Aurora B (*194, 205*). NTE-dependent kinetochore binding of MPS1 is inhibited by the TPR domain (chapter 2). It is likely that this inhibition is relieved upon phosphorylation by an unknown kinase and this is opposed by PP1γ (chapter 3). Additionally, MPS1 is delocalized from kinetochore by attached microtubules (chapter 2).

Finally, PP2A-B56 promotes the kinetochore localization of PP1γ by removing Aurora B-dependent

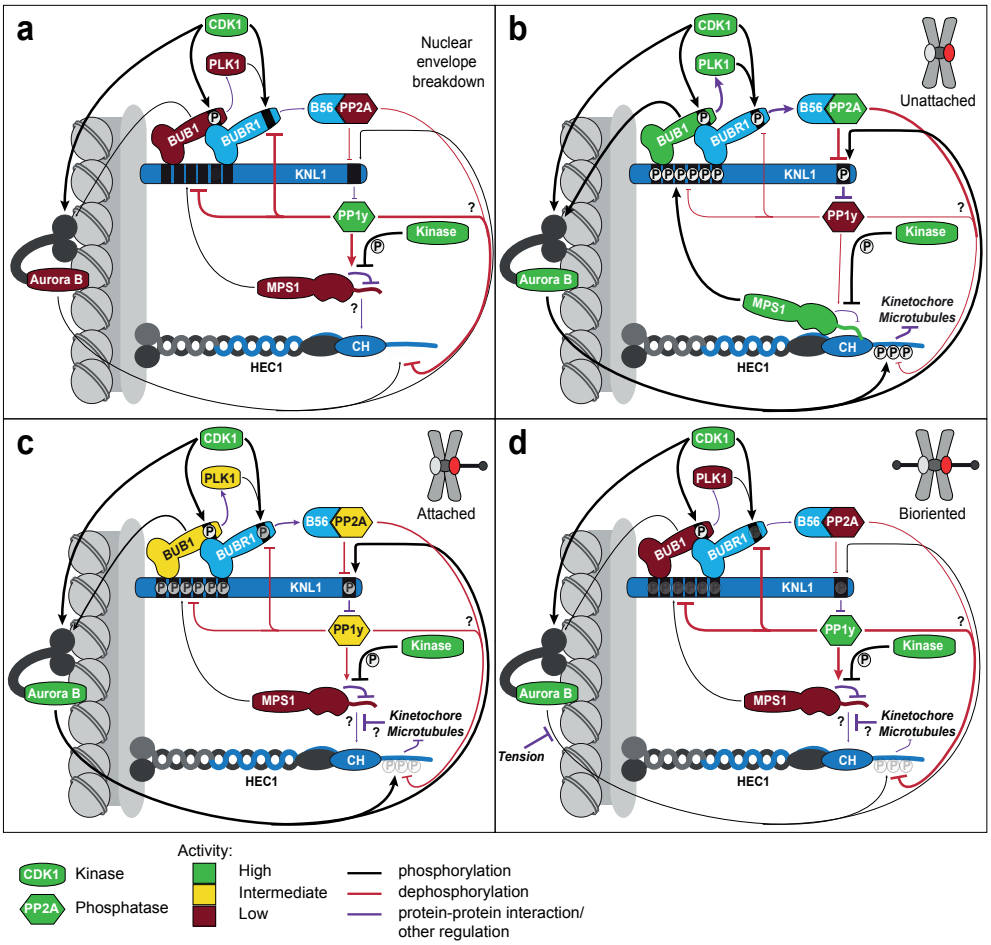

Figure 2: **An integrated model of kinetochore-based kinase and phosphatase signaling in the SAC.** (**A-D**) Schematic model of the subcellular localization and activity of kinetochore-based kinases and phosphatases in relation to SAC regulation on an individual kinetochore (red) during mitotic progression. P: phosphorylation. Thickness of lines is indicates level of activity. Scaffold proteins are in blue. See section 5 for details.

phosphorylations of the PP1-docking motifs (*120* and chapter 4). Additionally, PP2A-B56 may enable the initial formation of kinetochore-microtubule attachments by suppressing Aurora B-dependent phosphorylation of the KMN network in prometaphase (*120-123*). PP2A-B56 is recruited to its BUBR1 scaffold by CDK1 and PLK1-dependent phosphorylation of the KARD and this is opposed by PP1 (*121-123* and chapter 4).

Like the PP1-PP2A feedback discussed above, this network of feedbacks may be best understood through computational modeling. Since we know much about SAC responses to specific perturbations within this network, and since we have many tools to test various other perturbations and responses, it may be interesting to use the data to guide design and verification of a computational model. If successful, such a model may be able to answer questions related to robustness, sensitivity and switch-like behaviour of the SAC network.

Activation of mitotic kinases in prophase

I envision that at nuclear envelope breakdown, the network is dominated by the activities of CDK1 and PP1 (Fig. 2A). Uninhibited by Aurora B activity, PP1 is likely recruited to high levels in G2. Such high PP1 levels likely suppress the kinetochore localization of BUB1, BUBR1, MPS1, PLK1 and PP2A-B56 before prophase. Subsequently, in early prophase, CDK1 drives the transactivation of Aurora B and primes PLK1 localization by phosphorylation of BUB1 (*315*). As the Aurora B-dependent phosphorylation of the PP1 docking motifs in KNL1 is at this point unopposed by PP2A-B56, Aurora B activation rapidly delocalizes PP1.

Prometaphase

The coupling of Aurora B activation and PP1 inactivation in prophase has several consequences (Fig. 2B). Whereas MPS1 kinetochore localization was previously prevented by PP1, the inhibition of NTE-dependent binding by the TPR domain is now relieved by the activity of an unknown kinase, which allows high levels of MPS1 localization. Subsequently, MPS1-dependent phosphorylation of the MELT motifs activates the BUB1-BUBR1-PP2A pathway. This results in the accumulation of PP2A at kinetochores, and dephosphorylation of the PP1 docking motifs in KNL1, which enables low levels of PP1 recruitment and engages a negative feedback cycle as described in chapter 4. This negative feedback loop moderates SAC activation and allows dynamic phosphorylation of the KMN network. Additionally, the kinetochore localization of MPS1 and BUB1 allows further activation of Aurora B, which creates a positive feedback cycle that accelerates SAC activation in prophase and early prometaphase (*194, 195*).

Monotelic attachment

The formation of a monotelic kinetochore-microtubule attachment impacts on the network by delocalizing MPS1 from the attached sister kinetochore (Fig. 2C). In combination with low kinetochore levels of PP1, this loss of MPS1 activity likely reduces phosphorylation of the MELT motifs, which would partially delocalize BUB1, BUBR1, PLK1 and PP2A-B56. As Aurora B remains active under these conditions, a drop in PP2A-B56 will probably not result in the accumulation of high kinetochore levels of PP1 (*33*). However, in combination with the loss of localized MPS1 activity, even a small increase in PP1 could have profound effects on KMN network phosphorylation.

Biorientation

Upon biorientation, Aurora B activity towards the outer kinetochore is reduced, at least in part as a result of spatial separation from it substrates (*36*). The loss of Aurora B activity, coupled with residual localization of PP2A-B56 on a bioriented kinetochore likely results in rapid dephosphorylation of the PP1-binding motifs in KNL1 (Fig. 2D). The subsequent accumulation of PP1 at kinetochores drives dephosphorylation of the KARD and MELT motifs, the delocalization of BUB1, BUBR1, PLK1 and PP2A-B56. This may enable terminal silencing of kinetochore-based SAC signaling. Furthermore, the combined inactivation of Aurora B and activation of PP1 allows stabilization of kinetochore-microtubule attachments.

Validation

Most of the individual kinetochore binding events and regulatory phosphorylations in our model have been characterized to some extent. However, it is not well defined how the subcellular localization and phosphorylation of individual proteins is affected by signaling events upstream or downstream in the network. Therefore, validation of this model requires careful systematic and quantitative

analysis of how perturbations of individual network nodes affect signaling throughout the network.

Concluding remarks

The work presented in this thesis provides new mechanistic insights into the regulation of SAC signaling at kinetochores. In particular, this work has revealed how the localization of MPS1 to kinetochores is controlled by multiple layers of regulation. We also demonstrated how activation and silencing of the SAC is regulated by the finely tuned activities of kinetochore phosphatases. These findings further elucidate how SAC signaling is controlled by kinetochore-microtubule interactions and tension-dependent signaling and thereby contribute to the understanding of the fundamental aspects that dictate mitotic regulation.

References

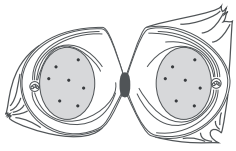

1. K. Nasmyth, Cohesin: a catenase with separate entry and exit gates? *Nat Cell Biol* **13**, 1170 (Oct, 2011).
2. V. Magidson *et al.*, The spatial arrangement of chromosomes during prometaphase facilitates spindle assembly. *Cell* **146**, 555 (Aug 19, 2011).
3. A. Suzuki *et al.*, Spindle microtubules generate tension-dependent changes in the distribution of inner kinetochore proteins. *J Cell Biol* **193**, 125 (Apr 4, 2011).
4. B. F. McEwen, A. B. Heagle, G. O. Cassels, K. F. Buttle, C. L. Rieder, Kinetochore fiber maturation in PtK1 cells and its implications for the mechanisms of chromosome congression and anaphase onset. *J Cell Biol* **137**, 1567 (Jun 30, 1997).
5. B. R. Brinkley, E. Stubblefield, The fine structure of the kinetochore of a mammalian cell in vitro. *Chromosoma* **19**, 28 (1966).
6. P. T. Jokelainen, The ultrastructure and spatial organization of the metaphase kinetochore in mitotic rat cells. *Journal of ultrastructure research* **19**, 19 (Jul, 1967).
7. L. S. Burrack, J. Berman, Flexibility of centromere and kinetochore structures. *Trends in genetics : TIG* **28**, 204 (May, 2012).
8. K. H. Choo, B. Vissel, A. Nagy, E. Earle, P. Kalitsis, A survey of the genomic distribution of alpha satellite DNA on all the human chromosomes, and derivation of a new consensus sequence. *Nucleic Acids Res* **19**, 1179 (Mar 25, 1991).
9. H. Masumoto, H. Masukata, Y. Muro, N. Nozaki, T. Okazaki, A human centromere antigen (CENP-B) interacts with a short specific sequence in alphoid DNA, a human centromeric satellite. *J Cell Biol* **109**, 1963 (Nov, 1989).
10. W. C. Earnshaw, N. Rothfield, Identification of a family of human centromere proteins using autoimmune sera from patients with scleroderma. *Chromosoma* **91**, 313 (1985).
11. W. C. Earnshaw, P. S. Machlin, B. J. Bordwell, N. F. Rothfield, D. W. Cleveland, Analysis of anticentromere autoantibodies using cloned autoantigen CENP-B. *Proc Natl Acad Sci U S A* **84**, 4979 (Jul, 1987).
12. D. Hasson *et al.*, The octamer is the major form of CENP-A nucleosomes at human centromeres. *Nat Struct Mol Biol* **20**, 687 (Jun, 2013).
13. D. K. Palmer, K. O'Day, H. L. Trong, H. Charbonneau, R. L. Margolis, Purification of the centromere-specific protein CENP-A and demonstration that it is a distinctive histone. *Proc Natl Acad Sci U S A* **88**, 3734 (May 1, 1991).
14. D. K. Palmer, K. O'Day, M. H. Wener, B. S. Andrews, R. L. Margolis, A 17-kD centromere protein (CENP-A) copurifies with nucleosome core particles and with histones. *J Cell Biol* **104**, 805 (Apr, 1987).
15. H. Tachiwana *et al.*, Crystal structure of the human centromeric nucleosome containing CENP-A. *Nature* **476**, 232 (Aug 11, 2011).
16. T. Nishino *et al.*, CENP-T-W-S-X forms a unique centromeric chromatin structure with a histone-like fold. *Cell* **148**, 487 (Feb 3, 2012).
17. T. Hori *et al.*, CCAN makes multiple contacts with centromeric DNA to provide distinct pathways to the outer kinetochore. *Cell* **135**, 1039 (Dec 12, 2008).
18. B. A. Sullivan, G. H. Karpen, Centromeric chromatin exhibits a histone modification pattern that is distinct from both euchromatin and heterochromatin. *Nat Struct Mol Biol* **11**, 1076 (Nov, 2004).
19. S. A. Ribeiro *et al.*, A super-resolution map of the vertebrate kinetochore. *Proc Natl Acad Sci U S A* **107**, 10484 (Jun 8, 2010).
20. M. Perpelescu, T. Fukagawa, The ABCs of CENPs. *Chromosoma* **120**, 425 (Oct, 2011).

21. C. W. Carroll, K. J. Milks, A. F. Straight, Dual recognition of CENP-A nucleosomes is required for centromere assembly. *J Cell Biol* **189**, 1143 (Jun 28, 2010).
22. C. W. Carroll, M. C. Silva, K. M. Godek, L. E. Jansen, A. F. Straight, Centromere assembly requires the direct recognition of CENP-A nucleosomes by CENP-N. *Nat Cell Biol* **11**, 896 (Jul, 2009).
23. D. Fachinetti *et al.*, A two-step mechanism for epigenetic specification of centromere identity and function. *Nat Cell Biol* **15**, 1056 (Sep, 2013).
24. H. Kato *et al.*, A conserved mechanism for centromeric nucleosome recognition by centromere protein CENP-C. *Science* **340**, 1110 (May 31, 2013).
25. E. Screpanti *et al.*, Direct binding of Cenp-C to the Mis12 complex joins the inner and outer kinetochore. *Curr Biol* **21**, 391 (Mar 8, 2011).
26. K. E. Gascoigne *et al.*, Induced ectopic kinetochore assembly bypasses the requirement for CENP-A nucleosomes. *Cell* **145**, 410 (Apr 29, 2011).
27. M. R. Przewloka *et al.*, CENP-C is a structural platform for kinetochore assembly. *Curr Biol* **21**, 399 (Mar 8, 2011).
28. T. Nishino *et al.*, CENP-T provides a structural platform for outer kinetochore assembly. *EMBO J* **32**, 424 (Feb 6, 2013).
29. I. M. Cheeseman, J. S. Chappie, E. M. Wilson-Kubalek, A. Desai, The conserved KMN network constitutes the core microtubule-binding site of the kinetochore. *Cell* **127**, 983 (Dec 1, 2006).
30. I. M. Cheeseman *et al.*, A conserved protein network controls assembly of the outer kinetochore and its ability to sustain tension. *Genes Dev* **18**, 2255 (Sep 15, 2004).
31. A. Desai *et al.*, KNL-1 directs assembly of the microtubule-binding interface of the kinetochore in C. elegans. *Genes Dev* **17**, 2421 (Oct 1, 2003).
32. J. Espeut, D. K. Cheerambathur, L. Krenning, K. Oegema, A. Desai, Microtubule binding by KNL-1 contributes to spindle checkpoint silencing at the kinetochore. *J Cell Biol* **196**, 469 (Feb 20, 2012).
33. J. P. Welburn *et al.*, Aurora B phosphorylates spatially distinct targets to differentially regulate the kinetochore-microtubule interface. *Mol Cell* **38**, 383 (May 14, 2010).
34. T. Kiyomitsu, H. Murakami, M. Yanagida, Protein interaction domain mapping of human kinetochore protein Blinkin reveals a consensus motif for binding of spindle assembly checkpoint proteins Bub1 and BubR1. *Mol Cell Biol* **31**, 998 (Mar, 2011).
35. T. Kiyomitsu, C. Obuse, M. Yanagida, Human Blinkin/AF15q14 is required for chromosome alignment and the mitotic checkpoint through direct interaction with Bub1 and BubR1. *Dev Cell* **13**, 663 (Nov, 2007).
36. D. Liu *et al.*, Regulated targeting of protein phosphatase 1 to the outer kinetochore by KNL1 opposes Aurora B kinase. *J Cell Biol* **188**, 809 (Mar 22, 2010).
37. V. Krenn, A. Wehenkel, X. Li, S. Santaguida, A. Musacchio, Structural analysis reveals features of the spindle checkpoint kinase Bub1-kinetochore subunit Knl1 interaction. *J Cell Biol* **196**, 451 (Feb 20, 2012).
38. V. M. Bolanos-Garcia *et al.*, Structure of a Blinkin-BUBR1 complex reveals an interaction crucial for kinetochore-mitotic checkpoint regulation via an unanticipated binding Site. *Structure* **19**, 1691 (Nov 9, 2011).
39. N. London, S. Ceto, J. A. Ranish, S. Biggins, Phosphoregulation of Spc105 by Mps1 and PP1 Regulates Bub1 Localization to Kinetochores. *Curr Biol*, (Apr 17, 2012).
40. I. Primorac *et al.*, Bub3 reads phosphorylated MELT repeats to promote spindle assembly

checkpoint signaling. *eLife* **2**, e01030 (2013).
41. L. A. Shepperd *et al.*, Phosphodependent Recruitment of Bub1 and Bub3 to Spc7/KNL1 by Mph1 Kinase Maintains the Spindle Checkpoint. *Curr Biol*, (Apr 17, 2012).
42. Y. Yamagishi, C. H. Yang, Y. Tanno, Y. Watanabe, MPS1/Mph1 phosphorylates the kinetochore protein KNL1/Spc7 to recruit SAC components. *Nat Cell Biol*, (Jun 3, 2012).
43. J. G. DeLuca *et al.*, Kinetochore microtubule dynamics and attachment stability are regulated by Hec1. *Cell* **127**, 969 (Dec 1, 2006).
44. M. L. McCleland *et al.*, The vertebrate Ndc80 complex contains Spc24 and Spc25 homologs, which are required to establish and maintain kinetochore-microtubule attachment. *Curr Biol* **14**, 131 (Jan 20, 2004).
45. P. A. Wigge, J. V. Kilmartin, The Ndc80p complex from Saccharomyces cerevisiae contains conserved centromere components and has a function in chromosome segregation. *J Cell Biol* **152**, 349 (Jan 22, 2001).
46. J. G. DeLuca, B. Moree, J. M. Hickey, J. V. Kilmartin, E. D. Salmon, hNuf2 inhibition blocks stable kinetochore-microtubule attachment and induces mitotic cell death in HeLa cells. *J Cell Biol* **159**, 549 (Nov 25, 2002).
47. S. Martin-Lluesma, V. M. Stucke, E. A. Nigg, Role of Hec1 in spindle checkpoint signaling and kinetochore recruitment of Mad1/Mad2. *Science* **297**, 2267 (Sep 27, 2002).
48. R. R. Wei, J. Al-Bassam, S. C. Harrison, The Ndc80/HEC1 complex is a contact point for kinetochore-microtubule attachment. *Nat Struct Mol Biol* **14**, 54 (Jan, 2007).
49. C. Ciferri *et al.*, Implications for kinetochore-microtubule attachment from the structure of an engineered Ndc80 complex. *Cell* **133**, 427 (May 2, 2008).
50. G. J. Guimaraes, Y. Dong, B. F. McEwen, J. G. Deluca, Kinetochore-microtubule attachment relies on the disordered N-terminal tail domain of Hec1. *Curr Biol* **18**, 1778 (Nov 25, 2008).
51. L. J. Sundin, G. J. Guimaraes, J. G. Deluca, The NDC80 complex proteins Nuf2 and Hec1 make distinct contributions to kinetochore-microtubule attachment in mitosis. *Mol Biol Cell* **22**, 759 (Mar, 2011).
52. S. A. Miller, M. L. Johnson, P. T. Stukenberg, Kinetochore attachments require an interaction between unstructured tails on microtubules and Ndc80(Hec1). *Curr Biol* **18**, 1785 (Nov 25, 2008).
53. G. M. Alushin *et al.*, Multimodal microtubule binding by the Ndc80 kinetochore complex. *Nat Struct Mol Biol* **19**, 1161 (Nov, 2012).
54. S. L. Kline, I. M. Cheeseman, T. Hori, T. Fukagawa, A. Desai, The human Mis12 complex is required for kinetochore assembly and proper chromosome segregation. *J Cell Biol* **173**, 9 (Apr 10, 2006).
55. A. Petrovic *et al.*, The MIS12 complex is a protein interaction hub for outer kinetochore assembly. *J Cell Biol* **190**, 835 (Sep 6, 2010).
56. I. M. Cheeseman, M. Enquist-Newman, T. Muller-Reichert, D. G. Drubin, G. Barnes, Mitotic spindle integrity and kinetochore function linked by the Duo1p/Dam1p complex. *J Cell Biol* **152**, 197 (Jan 8, 2001).
57. I. M. Cheeseman *et al.*, Implication of a novel multiprotein Dam1p complex in outer kinetochore function. *J Cell Biol* **155**, 1137 (Dec 24, 2001).
58. J. J. Miranda, P. De Wulf, P. K. Sorger, S. C. Harrison, The yeast DASH complex forms closed rings on microtubules. *Nat Struct Mol Biol* **12**, 138 (Feb, 2005).
59. F. Lampert, P. Hornung, S. Westermann, The Dam1 complex confers microtubule plus end-tracking activity to the Ndc80 kinetochore complex. *J Cell Biol* **189**, 641 (May 17, 2010).

60. F. Lampert, C. Mieck, G. M. Alushin, E. Nogales, S. Westermann, Molecular requirements for the formation of a kinetochore-microtubule interface by Dam1 and Ndc80 complexes. *J Cell Biol* **200**, 21 (Jan 7, 2013).
61. J. F. Maure *et al.*, The Ndc80 loop region facilitates formation of kinetochore attachment to the dynamic microtubule plus end. *Curr Biol* **21**, 207 (Feb 8, 2011).
62. J. F. Tien *et al.*, Cooperation of the Dam1 and Ndc80 kinetochore complexes enhances microtubule coupling and is regulated by aurora B. *J Cell Biol* **189**, 713 (May 17, 2010).
63. S. Westermann *et al.*, Formation of a dynamic kinetochore- microtubule interface through assembly of the Dam1 ring complex. *Mol Cell* **17**, 277 (Jan 21, 2005).
64. S. Gonen *et al.*, The structure of purified kinetochores reveals multiple microtubule-attachment sites. *Nat Struct Mol Biol* **19**, 925 (Sep, 2012).
65. T. N. Gaitanos *et al.*, Stable kinetochore-microtubule interactions depend on the Ska complex and its new component Ska3/C13Orf3. *EMBO J* **28**, 1442 (May 20, 2009).
66. A. Hanisch, H. H. Sillje, E. A. Nigg, Timely anaphase onset requires a novel spindle and kinetochore complex comprising Ska1 and Ska2. *EMBO J* **25**, 5504 (Nov 29, 2006).
67. M. Theis *et al.*, Comparative profiling identifies C13orf3 as a component of the Ska complex required for mammalian cell division. *EMBO J* **28**, 1453 (May 20, 2009).
68. J. P. Welburn *et al.*, The human kinetochore Ska1 complex facilitates microtubule depolymerization-coupled motility. *Dev Cell* **16**, 374 (Mar, 2009).
69. J. A. Raaijmakers, M. E. Tanenbaum, A. F. Maia, R. H. Medema, RAMA1 is a novel kinetochore protein involved in kinetochore-microtubule attachment. *J Cell Sci* **122**, 2436 (Jul 15, 2009).
70. J. C. Schmidt *et al.*, Aurora B kinase controls the targeting of the Astrin-SKAP complex to bioriented kinetochores. *J Cell Biol* **191**, 269 (Oct 18, 2010).
71. G. Zhang *et al.*, The Ndc80 internal loop is required for recruitment of the Ska complex to establish end-on microtubule attachment to kinetochores. *J Cell Sci* **125**, 3243 (Jul 1, 2012).
72. R. Karess, Rod-Zw10-Zwilch: a key player in the spindle checkpoint. *Trends Cell Biol* **15**, 386 (Jul, 2005).
73. D. A. Starr, B. C. Williams, T. S. Hays, M. L. Goldberg, ZW10 helps recruit dynactin and dynein to the kinetochore. *J Cell Biol* **142**, 763 (Aug 10, 1998).
74. M. Inoue, K. Arasaki, A. Ueda, T. Aoki, M. Tagaya, N-terminal region of ZW10 serves not only as a determinant for localization but also as a link with dynein function. *Genes to cells : devoted to molecular & cellular mechanisms* **13**, 905 (Aug, 2008).
75. D. Varma, P. Monzo, S. A. Stehman, R. B. Vallee, Direct role of dynein motor in stable kinetochore-microtubule attachment, orientation, and alignment. *J Cell Biol* **182**, 1045 (Sep 22, 2008).
76. B. J. Howell *et al.*, Cytoplasmic dynein/dynactin drives kinetochore protein transport to the spindle poles and has a role in mitotic spindle checkpoint inactivation. *J Cell Biol* **155**, 1159 (Dec 24, 2001).
77. J. A. Raaijmakers, M. E. Tanenbaum, R. H. Medema, Systematic dissection of dynein regulators in mitosis. *J Cell Biol* **201**, 201 (Apr 15, 2013).
78. E. Wojcik *et al.*, Kinetochore dynein: its dynamics and role in the transport of the Rough deal checkpoint protein. *Nat Cell Biol* **3**, 1001 (Nov, 2001).
79. S. Mische *et al.*, Dynein light intermediate chain: an essential subunit that contributes to spindle checkpoint inactivation. *Mol Biol Cell* **19**, 4918 (Nov, 2008).
80. M. V. Sivaram, T. L. Wadzinski, S. D. Redick, T. Manna, S. J. Doxsey, Dynein light intermediate chain 1 is required for progress through the spindle assembly checkpoint. *EMBO J* **28**, 902

(Apr 8, 2009).
81. M. S. Savoian, M. L. Goldberg, C. L. Rieder, The rate of poleward chromosome motion is attenuated in Drosophila zw10 and rod mutants. *Nat Cell Biol* **2**, 948 (Dec, 2000).
82. D. J. Sharp, G. C. Rogers, J. M. Scholey, Cytoplasmic dynein is required for poleward chromosome movement during mitosis in Drosophila embryos. *Nat Cell Biol* **2**, 922 (Dec, 2000).
83. R. Basto, R. Gomes, R. E. Karess, Rough deal and Zw10 are required for the metaphase checkpoint in Drosophila. *Nat Cell Biol* **2**, 939 (Dec, 2000).
84. G. K. Chan, S. A. Jablonski, D. A. Starr, M. L. Goldberg, T. J. Yen, Human Zw10 and ROD are mitotic checkpoint proteins that bind to kinetochores. *Nat Cell Biol* **2**, 944 (Dec, 2000).
85. G. J. Kops *et al.*, ZW10 links mitotic checkpoint signaling to the structural kinetochore. *J Cell Biol* **169**, 49 (Apr 11, 2005).
86. M. Kirschner, T. Mitchison, Beyond self-assembly: from microtubules to morphogenesis. *Cell* **45**, 329 (May 9, 1986).
87. H. Maiato, C. L. Rieder, A. Khodjakov, Kinetochore-driven formation of kinetochore fibers contributes to spindle assembly during animal mitosis. *J Cell Biol* **167**, 831 (Dec 6, 2004).
88. T. Kiyomitsu, I. M. Cheeseman, Chromosome- and spindle-pole-derived signals generate an intrinsic code for spindle position and orientation. *Nat Cell Biol* **14**, 311 (Mar, 2012).
89. C. B. O'Connell, J. Loncarek, P. Kalab, A. Khodjakov, Relative contributions of chromatin and kinetochores to mitotic spindle assembly. *J Cell Biol* **187**, 43 (Oct 5, 2009).
90. L. Torosantucci, M. De Luca, G. Guarguaglini, P. Lavia, F. Degrassi, Localized RanGTP accumulation promotes microtubule nucleation at kinetochores in somatic mammalian cells. *Mol Biol Cell* **19**, 1873 (May, 2008).
91. B. Akiyoshi *et al.*, Tension directly stabilizes reconstituted kinetochore-microtubule attachments. *Nature* **468**, 576 (Nov 25, 2010).
92. C. L. Rieder, The formation, structure, and composition of the mammalian kinetochore and kinetochore fiber. *International review of cytology* **79**, 1 (1982).
93. T. M. Kapoor *et al.*, Chromosomes can congress to the metaphase plate before biorientation. *Science* **311**, 388 (Jan 20, 2006).
94. R. V. Skibbens, V. P. Skeen, E. D. Salmon, Directional instability of kinetochore motility during chromosome congression and segregation in mitotic newt lung cells: a push-pull mechanism. *J Cell Biol* **122**, 859 (Aug, 1993).
95. K. Jaqaman *et al.*, Kinetochore alignment within the metaphase plate is regulated by centromere stiffness and microtubule depolymerases. *J Cell Biol* **188**, 665 (Mar 8, 2010).
96. X. Wan, D. Cimini, L. A. Cameron, E. D. Salmon, The coupling between sister kinetochore directional instability and oscillations in centromere stretch in metaphase PtK1 cells. *Mol Biol Cell* **23**, 1035 (Mar, 2012).
97. J. Stumpff *et al.*, A tethering mechanism controls the processivity and kinetochore-microtubule plus-end enrichment of the kinesin-8 Kif18A. *Mol Cell* **43**, 764 (Sep 2, 2011).
98. M. Carmena, M. Wheelock, H. Funabiki, W. C. Earnshaw, The chromosomal passenger complex (CPC): from easy rider to the godfather of mitosis. *Nat Rev Mol Cell Biol* **13**, 789 (Dec, 2012).
99. S. Biggins *et al.*, The conserved protein kinase Ipl1 regulates microtubule binding to kinetochores in budding yeast. *Genes Dev* **13**, 532 (Mar 1, 1999).
100. I. Sassoon *et al.*, Regulation of Saccharomyces cerevisiae kinetochores by the type 1 phosphatase Glc7p. *Genes Dev* **13**, 545 (Mar 1, 1999).

101. S. Hauf *et al.*, The small molecule Hesperadin reveals a role for Aurora B in correcting kinetochore-microtubule attachment and in maintaining the spindle assembly checkpoint. *J Cell Biol* **161**, 281 (Apr 28, 2003).
102. S. Heinrich, H. Windecker, N. Hustedt, S. Hauf, Mph1 kinetochore localization is crucial and upstream in the hierarchy of spindle assembly checkpoint protein recruitment to kinetochores. *J Cell Sci* **125**, 4720 (Oct 15, 2012).
103. A. E. Kelly *et al.*, Survivin reads phosphorylated histone H3 threonine 3 to activate the mitotic kinase Aurora B. *Science* **330**, 235 (Oct 8, 2010).
104. F. Wang *et al.*, Histone H3 Thr-3 phosphorylation by Haspin positions Aurora B at centromeres in mitosis. *Science* **330**, 231 (Oct 8, 2010).
105. Y. Yamagishi, T. Honda, Y. Tanno, Y. Watanabe, Two histone marks establish the inner centromere and chromosome bi-orientation. *Science* **330**, 239 (Oct 8, 2010).
106. T. Tsukahara, Y. Tanno, Y. Watanabe, Phosphorylation of the CPC by Cdk1 promotes chromosome bi-orientation. *Nature* **467**, 719 (Oct 7, 2010).
107. S. A. Kawashima, Y. Yamagishi, T. Honda, K. Ishiguro, Y. Watanabe, Phosphorylation of H2A by Bub1 prevents chromosomal instability through localizing shugoshin. *Science* **327**, 172 (Jan 8, 2010).
108. E. Wang, E. R. Ballister, M. A. Lampson, Aurora B dynamics at centromeres create a diffusion-based phosphorylation gradient. *J Cell Biol* **194**, 539 (Aug 22, 2011).
109. K. F. DeLuca, S. M. Lens, J. G. DeLuca, Temporal changes in Hec1 phosphorylation control kinetochore-microtubule attachment stability during mitosis. *J Cell Sci* **124**, 622 (Feb 15, 2011).
110. D. Liu, G. Vader, M. J. Vromans, M. A. Lampson, S. M. Lens, Sensing chromosome bi-orientation by spatial separation of aurora B kinase from kinetochore substrates. *Science* **323**, 1350 (Mar 6, 2009).
111. T. J. Maresca, E. D. Salmon, Intrakinetochore stretch is associated with changes in kinetochore phosphorylation and spindle assembly checkpoint activity. *J Cell Biol* **184**, 373 (Feb 9, 2009).
112. X. Wan *et al.*, Protein architecture of the human kinetochore microtubule attachment site. *Cell* **137**, 672 (May 15, 2009).
113. T. U. Tanaka *et al.*, Evidence that the Ipl1-Sli15 (Aurora kinase-INCENP) complex promotes chromosome bi-orientation by altering kinetochore-spindle pole connections. *Cell* **108**, 317 (Feb 8, 2002).
114. R. B. Nicklas, C. A. Koch, Chromosome micromanipulation. 3. Spindle fiber tension and the reorientation of mal-oriented chromosomes. *J Cell Biol* **43**, 40 (Oct, 1969).
115. C. S. Campbell, A. Desai, Tension sensing by Aurora B kinase is independent of survivin-based centromere localization. *Nature* **497**, 118 (May 2, 2013).
116. I. M. Cheeseman *et al.*, Phospho-regulation of kinetochore-microtubule attachments by the Aurora kinase Ipl1p. *Cell* **111**, 163 (Oct 18, 2002).
117. Y. W. Chan, A. A. Jeyaprakash, E. A. Nigg, A. Santamaria, Aurora B controls kinetochore-microtubule attachments by inhibiting Ska complex-KMN network interaction. *J Cell Biol* **196**, 563 (Mar 5, 2012).
118. J. C. Schmidt *et al.*, The kinetochore-bound Ska1 complex tracks depolymerizing microtubules and binds to curved protofilaments. *Dev Cell* **23**, 968 (Nov 13, 2012).
119. B. A. Pinsky, C. V. Kotwaliwale, S. Y. Tatsutani, C. A. Breed, S. Biggins, Glc7/protein phosphatase 1 regulatory subunits can oppose the Ipl1/aurora protein kinase by

redistributing Glc7. *Mol Cell Biol* **26**, 2648 (Apr, 2006).
120. E. A. Foley, M. Maldonado, T. M. Kapoor, Formation of stable attachments between kinetochores and microtubules depends on the B56-PP2A phosphatase. *Nat Cell Biol* **13**, 1265 (Oct, 2011).
121. T. Kruse *et al.*, Direct binding between BubR1 and B56-PP2A phosphatase complexes regulate mitotic progression. *J Cell Sci* **126**, 1086 (Mar 1, 2013).
122. S. J. Suijkerbuijk, M. Vleugel, A. Teixeira, G. J. Kops, Integration of kinase and phosphatase activities by BUBR1 ensures formation of stable kinetochore-microtubule attachments. *Dev Cell* **23**, 745 (Oct 16, 2012).
123. P. Xu, E. A. Raetz, M. Kitagawa, D. M. Virshup, S. H. Lee, BUBR1 recruits PP2A via the B56 family of targeting subunits to promote chromosome congression. *Biology open* **2**, 479 (May 15, 2013).
124. D. O. Morgan, Cyclin-dependent kinases: engines, clocks, and microprocessors. *Annual review of cell and developmental biology* **13**, 261 (1997).
125. H. Daub *et al.*, Kinase-selective enrichment enables quantitative phosphoproteomics of the kinome across the cell cycle. *Mol Cell* **31**, 438 (Aug 8, 2008).
126. J. V. Olsen *et al.*, Quantitative phosphoproteomics reveals widespread full phosphorylation site occupancy during mitosis. *Sci Signal* **3**, ra3 (2010).
127. O. Gavet, J. Pines, Progressive activation of CyclinB1-Cdk1 coordinates entry to mitosis. *Dev Cell* **18**, 533 (Apr 20, 2010).
128. V. Sudakin *et al.*, The cyclosome, a large complex containing cyclin-selective ubiquitin ligase activity, targets cyclins for destruction at the end of mitosis. *Mol Biol Cell* **6**, 185 (Feb, 1995).
129. R. W. King *et al.*, A 20S complex containing CDC27 and CDC16 catalyzes the mitosis-specific conjugation of ubiquitin to cyclin B. *Cell* **81**, 279 (Apr 21, 1995).
130. A. Yamamoto, V. Guacci, D. Koshland, Pds1p, an inhibitor of anaphase in budding yeast, plays a critical role in the APC and checkpoint pathway(s). *J Cell Biol* **133**, 99 (Apr, 1996).
131. H. Funabiki, D. J. Wynne, Making an effective switch at the kinetochore by phosphorylation and dephosphorylation. *Chromosoma* **122**, 135 (Jun, 2013).
132. O. Cohen-Fix, J. M. Peters, M. W. Kirschner, D. Koshland, Anaphase initiation in Saccharomyces cerevisiae is controlled by the APC-dependent degradation of the anaphase inhibitor Pds1p. *Genes Dev* **10**, 3081 (Dec 15, 1996).
133. H. Zou, T. J. McGarry, T. Bernal, M. W. Kirschner, Identification of a vertebrate sister-chromatid separation inhibitor involved in transformation and tumorigenesis. *Science* **285**, 418 (Jul 16, 1999).
134. R. Ciosk *et al.*, An ESP1/PDS1 complex regulates loss of sister chromatid cohesion at the metaphase to anaphase transition in yeast. *Cell* **93**, 1067 (Jun 12, 1998).
135. F. Uhlmann, F. Lottspeich, K. Nasmyth, Sister-chromatid separation at anaphase onset is promoted by cleavage of the cohesin subunit Scc1. *Nature* **400**, 37 (Jul 1, 1999).
136. R. A. Oliveira, R. S. Hamilton, A. Pauli, I. Davis, K. Nasmyth, Cohesin cleavage and Cdk inhibition trigger formation of daughter nuclei. *Nat Cell Biol* **12**, 185 (Feb, 2010).
137. J. Pines, Cubism and the cell cycle: the many faces of the APC/C. *Nat Rev Mol Cell Biol* **12**, 427 (Jul, 2011).
138. F. Herzog *et al.*, Structure of the anaphase-promoting complex/cyclosome interacting with a mitotic checkpoint complex. *Science* **323**, 1477 (Mar 13, 2009).
139. P. Dube *et al.*, Localization of the coactivator Cdh1 and the cullin subunit Apc2 in a cryo-

electron microscopy model of vertebrate APC/C. *Mol Cell* **20**, 867 (Dec 22, 2005).
140. A. Schreiber *et al.*, Structural basis for the subunit assembly of the anaphase-promoting complex. *Nature* **470**, 227 (Feb 10, 2011).
141. J. M. Peters, The anaphase promoting complex/cyclosome: a machine designed to destroy. *Nat Rev Mol Cell Biol* **7**, 644 (Sep, 2006).
142. M. E. Matyskiela, D. O. Morgan, Analysis of activator-binding sites on the APC/C supports a cooperative substrate-binding mechanism. *Mol Cell* **34**, 68 (Apr 10, 2009).
143. H. C. Vodermaier, C. Gieffers, S. Maurer-Stroh, F. Eisenhaber, J. M. Peters, TPR subunits of the anaphase-promoting complex mediate binding to the activator protein CDH1. *Curr Biol* **13**, 1459 (Sep 2, 2003).
144. P. C. da Fonseca *et al.*, Structures of APC/C(Cdh1) with substrates identify Cdh1 and Apc10 as the D-box co-receptor. *Nature* **470**, 274 (Feb 10, 2011).
145. B. A. Buschhorn *et al.*, Substrate binding on the APC/C occurs between the coactivator Cdh1 and the processivity factor Doc1. *Nat Struct Mol Biol* **18**, 6 (Jan, 2011).
146. W. C. Chao, K. Kulkarni, Z. Zhang, E. H. Kong, D. Barford, Structure of the mitotic checkpoint complex. *Nature* **484**, 208 (Apr 12, 2012).
147. W. Tian *et al.*, Structural analysis of human Cdc20 supports multisite degron recognition by APC/C. *Proc Natl Acad Sci U S A* **109**, 18419 (Nov 6, 2012).
148. H. Yu, R. W. King, J. M. Peters, M. W. Kirschner, Identification of a novel ubiquitin-conjugating enzyme involved in mitotic cyclin degradation. *Curr Biol* **6**, 455 (Apr 1, 1996).
149. F. M. Townsley, A. Aristarkhov, S. Beck, A. Hershko, J. V. Ruderman, Dominant-negative cyclin-selective ubiquitin carrier protein E2-C/UbcH10 blocks cells in metaphase. *Proc Natl Acad Sci U S A* **94**, 2362 (Mar 18, 1997).
150. M. J. Garnett *et al.*, UBE2S elongates ubiquitin chains on APC/C substrates to promote mitotic exit. *Nat Cell Biol* **11**, 1363 (Nov, 2009).
151. A. Williamson *et al.*, Identification of a physiological E2 module for the human anaphase-promoting complex. *Proc Natl Acad Sci U S A* **106**, 18213 (Oct 27, 2009).
152. F. Stegmeier *et al.*, Anaphase initiation is regulated by antagonistic ubiquitination and deubiquitination activities. *Nature* **446**, 876 (Apr 19, 2007).
153. C. L. Rieder, A. Schultz, R. Cole, G. Sluder, Anaphase onset in vertebrate somatic cells is controlled by a checkpoint that monitors sister kinetochore attachment to the spindle. *J Cell Biol* **127**, 1301 (Dec, 1994).
154. C. L. Rieder, R. W. Cole, A. Khodjakov, G. Sluder, The checkpoint delaying anaphase in response to chromosome monoorientation is mediated by an inhibitory signal produced by unattached kinetochores. *J Cell Biol* **130**, 941 (Aug, 1995).
155. M. A. Hoyt, L. Totis, B. T. Roberts, S. cerevisiae genes required for cell cycle arrest in response to loss of microtubule function. *Cell* **66**, 507 (Aug 9, 1991).
156. R. Li, A. W. Murray, Feedback control of mitosis in budding yeast. *Cell* **66**, 519 (Aug 9, 1991).
157. E. Weiss, M. Winey, The Saccharomyces cerevisiae spindle pole body duplication gene MPS1 is part of a mitotic checkpoint. *J Cell Biol* **132**, 111 (Jan, 1996).
158. G. Fang, H. Yu, M. W. Kirschner, The checkpoint protein MAD2 and the mitotic regulator CDC20 form a ternary complex with the anaphase-promoting complex to control anaphase initiation. *Genes Dev* **12**, 1871 (Jun 15, 1998).
159. K. G. Hardwick, R. C. Johnston, D. L. Smith, A. W. Murray, MAD3 encodes a novel component of the spindle checkpoint which interacts with Bub3p, Cdc20p, and Mad2p. *J Cell Biol* **148**, 871 (Mar 6, 2000).

160. L. H. Hwang *et al.*, Budding yeast Cdc20: a target of the spindle checkpoint. *Science* **279**, 1041 (Feb 13, 1998).
161. S. H. Kim, D. P. Lin, S. Matsumoto, A. Kitazono, T. Matsumoto, Fission yeast Slp1: an effector of the Mad2-dependent spindle checkpoint. *Science* **279**, 1045 (Feb 13, 1998).
162. Y. Li, C. Gorbea, D. Mahaffey, M. Rechsteiner, R. Benezra, MAD2 associates with the cyclosome/anaphase-promoting complex and inhibits its activity. *Proc Natl Acad Sci U S A* **94**, 12431 (Nov 11, 1997).
163. D. N. Millband, K. G. Hardwick, Fission yeast Mad3p is required for Mad2p to inhibit the anaphase-promoting complex and localizes to kinetochores in a Bub1p-, Bub3p-, and Mph1p-dependent manner. *Mol Cell Biol* **22**, 2728 (Apr, 2002).
164. V. Sudakin, G. K. Chan, T. J. Yen, Checkpoint inhibition of the APC/C in HeLa cells is mediated by a complex of BUBR1, BUB3, CDC20, and MAD2. *J Cell Biol* **154**, 925 (Sep 3, 2001).
165. Z. Tang, R. Bharadwaj, B. Li, H. Yu, Mad2-Independent inhibition of APCCdc20 by the mitotic checkpoint protein BubR1. *Dev Cell* **1**, 227 (Aug, 2001).
166. J. Nilsson, M. Yekezare, J. Minshull, J. Pines, The APC/C maintains the spindle assembly checkpoint by targeting Cdc20 for destruction. *Nat Cell Biol* **10**, 1411 (Dec, 2008).
167. A. Kulukian, J. S. Han, D. W. Cleveland, Unattached kinetochores catalyze production of an anaphase inhibitor that requires a Mad2 template to prime Cdc20 for BubR1 binding. *Dev Cell* **16**, 105 (Jan, 2009).
168. X. Luo *et al.*, Structure of the Mad2 spindle assembly checkpoint protein and its interaction with Cdc20. *Nature structural biology* **7**, 224 (Mar, 2000).
169. X. Luo *et al.*, The Mad2 spindle checkpoint protein has two distinct natively folded states. *Nat Struct Mol Biol* **11**, 338 (Apr, 2004).
170. M. Mapelli, L. Massimiliano, S. Santaguida, A. Musacchio, The Mad2 conformational dimer: structure and implications for the spindle assembly checkpoint. *Cell* **131**, 730 (Nov 16, 2007).
171. L. Sironi *et al.*, Crystal structure of the tetrameric Mad1-Mad2 core complex: implications of a 'safety belt' binding mechanism for the spindle checkpoint. *EMBO J* **21**, 2496 (May 15, 2002).
172. M. Yang *et al.*, Insights into mad2 regulation in the spindle checkpoint revealed by the crystal structure of the symmetric mad2 dimer. *PLoS biology* **6**, e50 (Mar 4, 2008).
173. X. Luo, Z. Tang, J. Rizo, H. Yu, The Mad2 spindle checkpoint protein undergoes similar major conformational changes upon binding to either Mad1 or Cdc20. *Mol Cell* **9**, 59 (Jan, 2002).
174. L. Sironi *et al.*, Mad2 binding to Mad1 and Cdc20, rather than oligomerization, is required for the spindle checkpoint. *EMBO J* **20**, 6371 (Nov 15, 2001).
175. A. De Antoni *et al.*, The Mad1/Mad2 complex as a template for Mad2 activation in the spindle assembly checkpoint. *Curr Biol* **15**, 214 (Feb 8, 2005).
176. J. V. Shah *et al.*, Dynamics of centromere and kinetochore proteins; implications for checkpoint signaling and silencing. *Curr Biol* **14**, 942 (Jun 8, 2004).
177. M. Vink *et al.*, In vitro FRAP identifies the minimal requirements for Mad2 kinetochore dynamics. *Curr Biol* **16**, 755 (Apr 18, 2006).
178. L. Nezi *et al.*, Accumulation of Mad2-Cdc20 complex during spindle checkpoint activation requires binding of open and closed conformers of Mad2 in Saccharomyces cerevisiae. *J Cell Biol* **174**, 39 (Jul 3, 2006).
179. J. S. Han *et al.*, Catalytic assembly of the mitotic checkpoint inhibitor BubR1-Cdc20 by a Mad2-induced functional switch in Cdc20. *Mol Cell* **51**, 92 (Jul 11, 2013).

180. G. Fang, Checkpoint protein BubR1 acts synergistically with Mad2 to inhibit anaphase-promoting complex. *Mol Biol Cell* **13**, 755 (Mar, 2002).
181. Y. Boyarchuk, A. Salic, M. Dasso, A. Arnaoutov, Bub1 is essential for assembly of the functional inner centromere. *J Cell Biol* **176**, 919 (Mar 26, 2007).
182. V. L. Johnson, M. I. Scott, S. V. Holt, D. Hussein, S. S. Taylor, Bub1 is required for kinetochore localization of BubR1, Cenp-E, Cenp-F and Mad2, and chromosome congression. *J Cell Sci* **117**, 1577 (Mar 15, 2004).
183. C. Klebig, D. Korinth, P. Meraldi, Bub1 regulates chromosome segregation in a kinetochore-independent manner. *J Cell Biol* **185**, 841 (Jun 1, 2009).
184. H. Sharp-Baker, R. H. Chen, Spindle checkpoint protein Bub1 is required for kinetochore localization of Mad1, Mad2, Bub3, and CENP-E, independently of its kinase activity. *J Cell Biol* **153**, 1239 (Jun 11, 2001).
185. J. Fernius, K. G. Hardwick, Bub1 kinase targets Sgo1 to ensure efficient chromosome biorientation in budding yeast mitosis. *PLoS genetics* **3**, e213 (Nov, 2007).
186. B. E. McGuinness *et al.*, Regulation of APC/C activity in oocytes by a Bub1-dependent spindle assembly checkpoint. *Curr Biol* **19**, 369 (Mar 10, 2009).
187. D. Perera, S. S. Taylor, Sgo1 establishes the centromeric cohesion protection mechanism in G2 before subsequent Bub1-dependent recruitment in mitosis. *J Cell Sci* **123**, 653 (Mar 1, 2010).
188. V. Vanoosthuyse, R. Valsdottir, J. P. Javerzat, K. G. Hardwick, Kinetochore targeting of fission yeast Mad and Bub proteins is essential for spindle checkpoint function but not for all chromosome segregation roles of Bub1p. *Mol Cell Biol* **24**, 9786 (Nov, 2004).
189. J. Kang *et al.*, Structure and substrate recruitment of the human spindle checkpoint kinase Bub1. *Mol Cell* **32**, 394 (Nov 7, 2008).
190. Z. Tang, H. Shu, D. Oncel, S. Chen, H. Yu, Phosphorylation of Cdc20 by Bub1 provides a catalytic mechanism for APC/C inhibition by the spindle checkpoint. *Mol Cell* **16**, 387 (Nov 5, 2004).
191. T. S. Kitajima, S. Hauf, M. Ohsugi, T. Yamamoto, Y. Watanabe, Human Bub1 defines the persistent cohesion site along the mitotic chromosome by affecting Shugoshin localization. *Curr Biol* **15**, 353 (Feb 22, 2005).
192. T. S. Kitajima, S. A. Kawashima, Y. Watanabe, The conserved kinetochore protein shugoshin protects centromeric cohesion during meiosis. *Nature* **427**, 510 (Feb 5, 2004).
193. Z. Tang, Y. Sun, S. E. Harley, H. Zou, H. Yu, Human Bub1 protects centromeric sister-chromatid cohesion through Shugoshin during mitosis. *Proc Natl Acad Sci U S A* **101**, 18012 (Dec 28, 2004).
194. M. S. van der Waal *et al.*, Mps1 promotes rapid centromere accumulation of Aurora B. *EMBO Rep* **13**, 847 (Sep, 2012).
195. A. T. Saurin, M. S. van der Waal, R. H. Medema, S. M. Lens, G. J. Kops, Aurora B potentiates Mps1 activation to ensure rapid checkpoint establishment at the onset of mitosis. *Nat Commun* **2**, 316 (May, 2011).
196. S. Santaguida, C. Vernieri, F. Villa, A. Ciliberto, A. Musacchio, Evidence that Aurora B is implicated in spindle checkpoint signalling independently of error correction. *Embo J*, (Mar 15, 2011).
197. H. Jiang *et al.*, MULTIPOLAR SPINDLE 1 (MPS1), a novel coiled-coil protein of Arabidopsis thaliana, is required for meiotic spindle organization. *The Plant journal : for cell and molecular biology* **59**, 1001 (Sep, 2009).

198. A. Abrieu *et al.*, Mps1 is a kinetochore-associated kinase essential for the vertebrate mitotic checkpoint. *Cell* **106**, 83 (Jul 13, 2001).
199. V. M. Stucke, H. H. Sillje, L. Arnaud, E. A. Nigg, Human Mps1 kinase is required for the spindle assembly checkpoint but not for centrosome duplication. *Embo J* **21**, 1723 (Apr 2, 2002).
200. H. A. Fisk, M. Winey, The mouse Mps1p-like kinase regulates centrosome duplication. *Cell* **106**, 95 (Jul 13, 2001).
201. X. He, M. H. Jones, M. Winey, S. Sazer, Mph1, a member of the Mps1-like family of dual specificity protein kinases, is required for the spindle checkpoint in S. pombe. *J Cell Sci* **111 (Pt 12)**, 1635 (Jun, 1998).
202. M. G. Fischer, S. Heeger, U. Hacker, C. F. Lehner, The mitotic arrest in response to hypoxia and of polar bodies during early embryogenesis requires Drosophila Mps1. *Curr Biol* **14**, 2019 (Nov 23, 2004).
203. M. Schmidt, Y. Budirahardja, R. Klompmaker, R. H. Medema, Ablation of the spindle assembly checkpoint by a compound targeting Mps1. *EMBO Rep* **6**, 866 (Sep, 2005).
204. A. Tighe, O. Staples, S. Taylor, Mps1 kinase activity restrains anaphase during an unperturbed mitosis and targets Mad2 to kinetochores. *J Cell Biol* **181**, 893 (Jun 16, 2008).
205. N. Jelluma *et al.*, Mps1 phosphorylates Borealin to control Aurora B activity and chromosome alignment. *Cell* **132**, 233 (Jan 25, 2008).
206. A. Janssen, M. van der Burg, K. Szuhai, G. J. Kops, R. H. Medema, Chromosome segregation errors as a cause of DNA damage and structural chromosome aberrations. *Science* **333**, 1895 (Sep 30, 2011).
207. H. Yu, Regulation of APC-Cdc20 by the spindle checkpoint. *Current opinion in cell biology* **14**, 706 (Dec, 2002).
208. S. T. Liu *et al.*, Human MPS1 kinase is required for mitotic arrest induced by the loss of CENP-E from kinetochores. *Mol Biol Cell* **14**, 1638 (Apr, 2003).
209. V. M. Stucke, C. Baumann, E. A. Nigg, Kinetochore localization and microtubule interaction of the human spindle checkpoint kinase Mps1. *Chromosoma* **113**, 1 (Aug, 2004).
210. L. Hewitt *et al.*, Sustained Mps1 activity is required in mitosis to recruit O-Mad2 to the Mad1-C-Mad2 core complex. *J Cell Biol* **190**, 25 (Jul 12, 2010).
211. S. Lee *et al.*, Characterization of spindle checkpoint kinase Mps1 reveals domain with functional and structural similarities to tetratricopeptide repeat motifs of Bub1 and BubR1 checkpoint kinases. *J Biol Chem* **287**, 5988 (Feb 17, 2012).
212. K. Hached *et al.*, Mps1 at kinetochores is essential for female mouse meiosis I. *Development* **138**, 2261 (Jun, 2011).
213. A. Poddar, P. T. Stukenberg, D. J. Burke, Two complexes of spindle checkpoint proteins containing Cdc20 and Mad2 assemble during mitosis independently of the kinetochore in Saccharomyces cerevisiae. *Eukaryotic cell* **4**, 867 (May, 2005).
214. K. G. Hardwick, E. Weiss, F. C. Luca, M. Winey, A. W. Murray, Activation of the budding yeast spindle assembly checkpoint without mitotic spindle disruption. *Science* **273**, 953 (Aug 16, 1996).
215. N. Jelluma, T. B. Dansen, T. Sliedrecht, N. P. Kwiatkowski, G. J. Kops, Release of Mps1 from kinetochores is crucial for timely anaphase onset. *J Cell Biol* **191**, 281 (Oct 18, 2010).
216. T. Sliedrecht, C. Zhang, K. M. Shokat, G. J. Kops, Chemical genetic inhibition of Mps1 in stable human cell lines reveals novel aspects of Mps1 function in mitosis. *PLoS One* **5**, e10251 (2010).

217. S. Santaguida, A. Tighe, A. M. D'Alise, S. S. Taylor, A. Musacchio, Dissecting the role of MPS1 in chromosome biorientation and the spindle checkpoint through the small molecule inhibitor reversine. *J Cell Biol* **190**, 73 (Jul 12, 2010).
218. J. Maciejowski *et al.*, Mps1 directs the assembly of Cdc20 inhibitory complexes during interphase and mitosis to control M phase timing and spindle checkpoint signaling. *J Cell Biol* **190**, 89 (Jul 12, 2010).
219. M. Maldonado, T. M. Kapoor, Constitutive Mad1 targeting to kinetochores uncouples checkpoint signalling from chromosome biorientation. *Nat Cell Biol*, (Mar 13, 2011).
220. J. Zich *et al.*, Kinase activity of fission yeast Mph1 is required for Mad2 and Mad3 to stably bind the anaphase promoting complex. *Curr Biol* **22**, 296 (Feb 21, 2012).
221. S. Kemmler *et al.*, Mimicking Ndc80 phosphorylation triggers spindle assembly checkpoint signalling. *Embo J* **28**, 1099 (Apr 22, 2009).
222. J. F. Maure, E. Kitamura, T. U. Tanaka, Mps1 kinase promotes sister-kinetochore bi-orientation by a tension-dependent mechanism. *Curr Biol* **17**, 2175 (Dec 18, 2007).
223. E. Bourhis, A. Lingel, Q. Phung, W. J. Fairbrother, A. G. Cochran, Phosphorylation of a borealin dimerization domain is required for proper chromosome segregation. *Biochemistry* **48**, 6783 (Jul 28, 2009).
224. M. M. Shimogawa *et al.*, Mps1 phosphorylation of Dam1 couples kinetochores to microtubule plus ends at metaphase. *Curr Biol* **16**, 1489 (Aug 8, 2006).
225. J. Espeut *et al.*, Phosphorylation relieves autoinhibition of the kinetochore motor Cenp-E. *Mol Cell* **29**, 637 (Mar 14, 2008).
226. M. Winey, L. Goetsch, P. Baum, B. Byers, MPS1 and MPS2: novel yeast genes defining distinct steps of spindle pole body duplication. *J Cell Biol* **114**, 745 (Aug, 1991).
227. H. A. Fisk, C. P. Mattison, M. Winey, Human Mps1 protein kinase is required for centrosome duplication and normal mitotic progression. *Proc Natl Acad Sci U S A* **100**, 14875 (Dec 9, 2003).
228. C. Kasbek *et al.*, Preventing the degradation of mps1 at centrosomes is sufficient to cause centrosome reduplication in human cells. *Mol Biol Cell* **18**, 4457 (Nov, 2007).
229. C. H. Yang, C. Kasbek, S. Majumder, A. M. Yusof, H. A. Fisk, Mps1 phosphorylation sites regulate the function of centrin 2 in centriole assembly. *Mol Biol Cell* **21**, 4361 (Dec, 2010).
230. Y. Cui, T. M. Guadagno, B-Raf(V600E) signaling deregulates the mitotic spindle checkpoint through stabilizing Mps1 levels in melanoma cells. *Oncogene* **27**, 3122 (May 15, 2008).
231. J. Liu *et al.*, Phosphorylation of Mps1 by BRAFV600E prevents Mps1 degradation and contributes to chromosome instability in melanoma. *Oncogene* **32**, 713 (Feb 7, 2013).
232. L. Zhang *et al.*, Oncogenic B-Raf(V600E) abrogates the AKT/B-Raf/Mps1 interaction in melanoma cells. *Cancer letters* **337**, 125 (Aug 28, 2013).
233. J. H. Wei *et al.*, TTK/hMps1 participates in the regulation of DNA damage checkpoint response by phosphorylating CHK2 on threonine 68. *J Biol Chem* **280**, 7748 (Mar 4, 2005).
234. Y. H. Yeh, Y. F. Huang, T. Y. Lin, S. Y. Shieh, The cell cycle checkpoint kinase CHK2 mediates DNA damage-induced stabilization of TTK/hMps1. *Oncogene* **28**, 1366 (Mar 12, 2009).
235. M. Leng *et al.*, MPS1-dependent mitotic BLM phosphorylation is important for chromosome stability. *Proc Natl Acad Sci U S A* **103**, 11485 (Aug 1, 2006).
236. P. Meraldi, V. M. Draviam, P. K. Sorger, Timing and checkpoints in the regulation of mitotic progression. *Dev Cell* **7**, 45 (Jul, 2004).
237. C. P. Mattison *et al.*, Mps1 activation loop autophosphorylation enhances kinase activity. *J Biol Chem* **282**, 30553 (Oct 19, 2007).

238. J. Kang, Y. Chen, Y. Zhao, H. Yu, Autophosphorylation-dependent activation of human Mps1 is required for the spindle checkpoint. *Proc Natl Acad Sci U S A* **104**, 20232 (Dec 18, 2007).
239. N. Jelluma *et al.*, Chromosomal instability by inefficient Mps1 auto-activation due to a weakened mitotic checkpoint and lagging chromosomes. *PLoS One* **3**, e2415 (2008).
240. K. Dulla, H. Daub, R. Hornberger, E. A. Nigg, R. Korner, Quantitative site-specific phosphorylation dynamics of human protein kinases during mitotic progression. *Mol Cell Proteomics* **9**, 1167 (Jun, 2010).
241. F. S. Oppermann *et al.*, Large-scale proteomics analysis of the human kinome. *Mol Cell Proteomics* **8**, 1751 (Jul, 2009).
242. N. Dephoure *et al.*, A quantitative atlas of mitotic phosphorylation. *Proc Natl Acad Sci U S A* **105**, 10762 (Aug 5, 2008).
243. Q. Xu *et al.*, Regulation of kinetochore recruitment of two essential mitotic spindle checkpoint proteins by Mps1 phosphorylation. *Mol Biol Cell* **20**, 10 (Jan, 2009).
244. V. Morin *et al.*, CDK-Dependent Potentiation of MPS1 Kinase Activity Is Essential to the Mitotic Checkpoint. *Curr Biol*, (Jan 11, 2012).
245. Y. Zhao, R. H. Chen, Mps1 phosphorylation by MAP kinase is required for kinetochore localization of spindle-checkpoint proteins. *Curr Biol* **16**, 1764 (Sep 5, 2006).
246. P. Clute, J. Pines, Temporal and spatial control of cyclin B1 destruction in metaphase. *Nat Cell Biol* **1**, 82 (Jun, 1999).
247. J. R. Kardon, R. D. Vale, Regulators of the cytoplasmic dynein motor. *Nat Rev Mol Cell Biol* **10**, 854 (Dec, 2009).
248. Y. W. Chan *et al.*, Mitotic control of kinetochore-associated dynein and spindle orientation by human Spindly. *J Cell Biol* **185**, 859 (Jun 1, 2009).
249. R. Gassmann *et al.*, Removal of Spindly from microtubule-attached kinetochores controls spindle checkpoint silencing in human cells. *Genes Dev* **24**, 957 (May, 2010).
250. J. K. Famulski, L. J. Vos, J. B. Rattner, G. K. Chan, Dynein/Dynactin-mediated transport of kinetochore components off kinetochores and onto spindle poles induced by nordihydroguaiaretic acid. *PLoS One* **6**, e16494 (2011).
251. F. Verde, J. M. Berrez, C. Antony, E. Karsenti, Taxol-induced microtubule asters in mitotic extracts of Xenopus eggs: requirement for phosphorylated factors and cytoplasmic dynein. *J Cell Biol* **112**, 1177 (Mar, 1991).
252. E. A. Vaisberg, M. P. Koonce, J. R. McIntosh, Cytoplasmic dynein plays a role in mammalian mitotic spindle formation. *J Cell Biol* **123**, 849 (Nov, 1993).
253. M. Barisic *et al.*, Spindly/CCDC99 is required for efficient chromosome congression and mitotic checkpoint regulation. *Mol Biol Cell* **21**, 1968 (Jun 15, 2010).
254. J. M. Kasuboski *et al.*, Zwint-1 is a novel Aurora B substrate required for the assembly of a dynein-binding platform on kinetochores. *Mol Biol Cell* **22**, 3318 (Sep, 2011).
255. V. Vanoosthuyse, K. G. Hardwick, A novel protein phosphatase 1-dependent spindle checkpoint silencing mechanism. *Curr Biol* **19**, 1176 (Jul 28, 2009).
256. B. A. Pinsky, C. R. Nelson, S. Biggins, Protein phosphatase 1 regulates exit from the spindle checkpoint in budding yeast. *Curr Biol* **19**, 1182 (Jul 28, 2009).
257. J. S. Rosenberg, F. R. Cross, H. Funabiki, KNL1/Spc105 recruits PP1 to silence the spindle assembly checkpoint. *Curr Biol* **21**, 942 (Jun 7, 2011).
258. J. C. Meadows *et al.*, Spindle checkpoint silencing requires association of PP1 to both Spc7 and kinesin-8 motors. *Dev Cell* **20**, 739 (Jun 14, 2011).
259. J. Stumpff, M. Wagenbach, A. Franck, C. L. Asbury, L. Wordeman, Kif18A and chromokinesins

confine centromere movements via microtubule growth suppression and spatial control of kinetochore tension. *Dev Cell* **22**, 1017 (May 15, 2012).
260. E. M. King, S. J. van der Sar, K. G. Hardwick, Mad3 KEN boxes mediate both Cdc20 and Mad3 turnover, and are critical for the spindle checkpoint. *PLoS One* **2**, e342 (2007).
261. J. Pan, R. H. Chen, Spindle checkpoint regulates Cdc20p stability in Saccharomyces cerevisiae. *Genes Dev* **18**, 1439 (Jun 15, 2004).
262. S. A. Foster, D. O. Morgan, The APC/C subunit Mnd2/Apc15 promotes Cdc20 autoubiquitination and spindle assembly checkpoint inactivation. *Mol Cell* **47**, 921 (Sep 28, 2012).
263. S. K. Reddy, M. Rape, W. A. Margansky, M. W. Kirschner, Ubiquitination by the anaphase-promoting complex drives spindle checkpoint inactivation. *Nature* **446**, 921 (Apr 19, 2007).
264. J. Mansfeld, P. Collin, M. O. Collins, J. S. Choudhary, J. Pines, APC15 drives the turnover of MCC-CDC20 to make the spindle assembly checkpoint responsive to kinetochore attachment. *Nat Cell Biol* **13**, 1234 (Oct, 2011).
265. K. Uzunova *et al.*, APC15 mediates CDC20 autoubiquitylation by APC/C(MCC) and disassembly of the mitotic checkpoint complex. *Nat Struct Mol Biol* **19**, 1116 (Nov, 2012).
266. Y. F. Gao *et al.*, Cdk1-phosphorylated CUEDC2 promotes spindle checkpoint inactivation and chromosomal instability. *Nat Cell Biol* **13**, 924 (Aug, 2011).
267. M. Yang *et al.*, p31comet blocks Mad2 activation through structural mimicry. *Cell* **131**, 744 (Nov 16, 2007).
268. T. Habu, S. H. Kim, J. Weinstein, T. Matsumoto, Identification of a MAD2-binding protein, CMT2, and its role in mitosis. *EMBO J* **21**, 6419 (Dec 2, 2002).
269. G. Xia *et al.*, Conformation-specific binding of p31(comet) antagonizes the function of Mad2 in the spindle checkpoint. *EMBO J* **23**, 3133 (Aug 4, 2004).
270. R. S. Hagan *et al.*, p31(comet) acts to ensure timely spindle checkpoint silencing subsequent to kinetochore attachment. *Mol Biol Cell* **22**, 4236 (Nov, 2011).
271. L. Jia *et al.*, Defining pathways of spindle checkpoint silencing: functional redundancy between Cdc20 ubiquitination and p31(comet). *Mol Biol Cell* **22**, 4227 (Nov, 2011).
272. F. G. Westhorpe, A. Tighe, P. Lara-Gonzalez, S. S. Taylor, p31comet-mediated extraction of Mad2 from the MCC promotes efficient mitotic exit. *J Cell Sci* **124**, 3905 (Nov 15, 2011).
273. G. Varetti, C. Guida, S. Santaguida, E. Chiroli, A. Musacchio, Homeostatic control of mitotic arrest. *Mol Cell* **44**, 710 (Dec 9, 2011).
274. M. Vleugel, E. Hoogendoorn, B. Snel, G. J. Kops, Evolution and function of the mitotic checkpoint. *Dev Cell* **23**, 239 (Aug 14, 2012).
275. G. J. P. L. Kops, J. V. Shah, Connecting up and clearing out: how kinetochore attachment silences the spindle assembly checkpoint. *Chromosoma* **DOI: 10.1007/s00412-012-0378-5**, (2012).
276. A. Musacchio, E. D. Salmon, The spindle-assembly checkpoint in space and time. *Nat Rev Mol Cell Biol* **8**, 379 (May, 2007).
277. W. Lan, D. W. Cleveland, A chemical tool box defines mitotic and interphase roles for Mps1 kinase. *J Cell Biol* **190**, 21 (Jul 12, 2010).
278. V. M. Bolanos-Garcia *et al.*, The crystal structure of the N-terminal region of BUB1 provides insight into the mechanism of BUB1 recruitment to kinetochores. *Structure* **17**, 105 (Jan 14, 2009).
279. S. D'Arcy, O. R. Davies, T. L. Blundell, V. M. Bolanos-Garcia, Defining the molecular basis of BubR1 kinetochore interactions and APC/C-CDC20 inhibition. *J Biol Chem* **285**, 14764 (May

7, 2010).
280. S. Beaufils, J. G. Grossmann, A. Renault, V. M. Bolanos-Garcia, Characterization of the tetratricopeptide-containing domain of BUB1, BUBR1, and PP5 proves that domain amphiphilicity over amino acid sequence specificity governs protein adsorption and interfacial activity. *J Phys Chem B* **112**, 7984 (Jul 10, 2008).
281. V. M. Bolanos-Garcia *et al.*, The conserved N-terminal region of the mitotic checkpoint protein BUBR1: a putative TPR motif of high surface activity. *Biophys J* **89**, 2640 (Oct, 2005).
282. L. Holm, P. Rosenstrom, Dali server: conservation mapping in 3D. *Nucleic Acids Res* **38**, W545 (Jul, 2010).
283. S. J. Suijkerbuijk *et al.*, The vertebrate mitotic checkpoint protein BUBR1 is an unusual pseudokinase. *Dev Cell* **22**, 1321 (Jun 12, 2012).
284. C. Ditchfield *et al.*, Aurora B couples chromosome alignment with anaphase by targeting BubR1, Mad2, and Cenp-E to kinetochores. *J Cell Biol* **161**, 267 (Apr 28, 2003).
285. J. Tooley, P. T. Stukenberg, The Ndc80 complex: integrating the kinetochore's many movements. *Chromosome Res* **19**, 377 (Apr, 2011).
286. J. Newman *et al.*, Towards rationalization of crystallization screening for small- to medium-sized academic laboratories: the PACT/JCSG+ strategy. *Acta Crystallogr D Biol Crystallogr* **61**, 1426 (Oct, 2005).
287. A. G. Leslie, The integration of macromolecular diffraction data. *Acta Crystallogr D Biol Crystallogr* **62**, 48 (Jan, 2006).
288. P. Evans, Scaling and assessment of data quality. *Acta Crystallogr D Biol Crystallogr* **62**, 72 (Jan, 2006).
289. P. H. Zwart, R. W. Grosse-Kunstleve, A. A. Lebedev, G. N. Murshudov, P. D. Adams, Surprises and pitfalls arising from (pseudo)symmetry. *Acta Crystallogr D Biol Crystallogr* **64**, 99 (Jan, 2008).
290. C. Vonrhein, E. Blanc, P. Roversi, G. Bricogne, Automated structure solution with autoSHARP. *Methods Mol Biol* **364**, 215 (2007).
291. K. Cowtan, The Buccaneer software for automated model building. 1. Tracing protein chains. *Acta Crystallogr D Biol Crystallogr* **62**, 1002 (Sep, 2006).
292. P. Emsley, B. Lohkamp, W. G. Scott, K. Cowtan, Features and development of Coot. *Acta Crystallogr D Biol Crystallogr* **66**, 486 (Apr, 2010).
293. A. J. McCoy *et al.*, Phaser crystallographic software. *J Appl Crystallogr* **40**, 658 (Aug 1, 2007).
294. G. Langer, S. X. Cohen, V. S. Lamzin, A. Perrakis, Automated macromolecular model building for X-ray crystallography using ARP/wARP version 7. *Nat Protoc* **3**, 1171 (2008).
295. G. N. Murshudov *et al.*, REFMAC5 for the refinement of macromolecular crystal structures. *Acta Crystallogr D Biol Crystallogr* **67**, 355 (Apr, 2011).
296. E. Blanc *et al.*, Refinement of severely incomplete structures with maximum likelihood in BUSTER-TNT. *Acta Crystallogr D Biol Crystallogr* **60**, 2210 (Dec, 2004).
297. S. F. Altschul, W. Gish, W. Miller, E. W. Myers, D. J. Lipman, Basic local alignment search tool. *J Mol Biol* **215**, 403 (Oct 5, 1990).
298. K. Katoh, D. M. Standley, MAFFT Multiple Sequence Alignment Software Version 7: Improvements in Performance and Usability. *Molecular biology and evolution*, (Feb 8, 2013).
299. A. Stamatakis, T. Ludwig, H. Meier, RAxML-III: a fast program for maximum likelihood-based inference of large phylogenetic trees. *Bioinformatics* **21**, 456 (Feb 15, 2005).
300. S. R. Eddy, Accelerated Profile HMM Searches. *PLoS Comput Biol* **7**, e1002195 (Oct, 2011).

301. I. Letunic, P. Bork, Interactive Tree Of Life (iTOL): an online tool for phylogenetic tree display and annotation. *Bioinformatics* **23**, 127 (Jan 1, 2007).
302. I. Zemp *et al.*, Distinct cytoplasmic maturation steps of 40S ribosomal subunit precursors require hRio2. *J Cell Biol* **185**, 1167 (Jun 29, 2009).
303. S. M. Janicki *et al.*, From silencing to gene expression: real-time analysis in single cells. *Cell* **116**, 683 (Mar 5, 2004).
304. W. Nijenhuis *et al.*, A TPR domain-containing N-terminal module of MPS1 is required for its kinetochore localization by Aurora B. *J Cell Biol* **201**, 217 (Apr 15, 2013).
305. Y. Kim, A. J. Holland, W. Lan, D. W. Cleveland, Aurora kinases and protein phosphatase 1 mediate chromosome congression through regulation of CENP-E. *Cell* **142**, 444 (Aug 6, 2010).
306. L. Trinkle-Mulcahy *et al.*, Repo-Man recruits PP1 gamma to chromatin and is essential for cell viability. *J Cell Biol* **172**, 679 (Feb 27, 2006).
307. L. Trinkle-Mulcahy *et al.*, Time-lapse imaging reveals dynamic relocalization of PP1gamma throughout the mammalian cell cycle. *Mol Biol Cell* **14**, 107 (Jan, 2003).
308. R. Wei, B. Ngo, G. Wu, W. H. Lee, Phosphorylation of the Ndc80 complex protein, HEC1, by Nek2 kinase modulates chromosome alignment and signaling of the spindle assembly checkpoint. *Mol Biol Cell* **22**, 3584 (Oct, 2011).
309. C. Conde *et al.*, Drosophila Polo regulates the spindle assembly checkpoint through Mps1-dependent BubR1 phosphorylation. *EMBO J* **32**, 1761 (Jun 12, 2013).
310. R. S. Hames, S. L. Wattam, H. Yamano, R. Bacchieri, A. M. Fry, APC/C-mediated destruction of the centrosomal kinase Nek2A occurs in early mitosis and depends upon a cyclin A-type D-box. *EMBO J* **20**, 7117 (Dec 17, 2001).
311. M. J. Hayes *et al.*, Early mitotic degradation of Nek2A depends on Cdc20-independent interaction with the APC/C. *Nat Cell Biol* **8**, 607 (Jun, 2006).
312. S. S. Taylor, F. McKeon, Kinetochore localization of murine Bub1 is required for normal mitotic timing and checkpoint response to spindle damage. *Cell* **89**, 727 (May 30, 1997).
313. D. A. Skoufias, P. R. Andreassen, F. B. Lacroix, L. Wilson, R. L. Margolis, Mammalian mad2 and bub1/bubR1 recognize distinct spindle-attachment and kinetochore-tension checkpoints. *Proc Natl Acad Sci U S A* **98**, 4492 (Apr 10, 2001).
314. S. S. Taylor, D. Hussein, Y. Wang, S. Elderkin, C. J. Morrow, Kinetochore localisation and phosphorylation of the mitotic checkpoint components Bub1 and BubR1 are differentially regulated by spindle events in human cells. *J Cell Sci* **114**, 4385 (Dec, 2001).
315. W. Qi, Z. Tang, H. Yu, Phosphorylation- and polo-box-dependent binding of Plk1 to Bub1 is required for the kinetochore localization of Plk1. *Mol Biol Cell* **17**, 3705 (Aug, 2006).
316. M. Bollen, W. Peti, M. J. Ragusa, M. Beullens, The extended PP1 toolkit: designed to create specificity. *Trends Biochem Sci* **35**, 450 (Aug, 2010).
317. J. Alexander *et al.*, Spatial exclusivity combined with positive and negative selection of phosphorylation motifs is the basis for context-dependent mitotic signaling. *Sci Signal* **4**, ra42 (2011).
318. J. Qian, M. Beullens, B. Lesage, M. Bollen, Aurora B defines its own chromosomal targeting by opposing the recruitment of the phosphatase scaffold Repo-Man. *Curr Biol* **23**, 1136 (Jun 17, 2013).
319. B. J. Howell *et al.*, Spindle checkpoint protein dynamics at kinetochores in living cells. *Curr Biol* **14**, 953 (Jun 8, 2004).
320. J. R. Hutchins *et al.*, Systematic analysis of human protein complexes identifies chromosome

segregation proteins. *Science* **328**, 593 (Apr 30, 2010).
321. A. L. Cortajarena, L. Regan, Ligand binding by TPR domains. *Protein Sci* **15**, 1193 (May, 2006).
322. M. Huse, J. Kuriyan, The conformational plasticity of protein kinases. *Cell* **109**, 275 (May 3, 2002).
323. P. Thebault *et al.*, Structural and functional insights into the role of the N-terminal Mps1 TPR domain in the SAC (spindle assembly checkpoint). *The Biochemical journal* **448**, 321 (Dec 15, 2012).

Nederlandse Samenvatting

Curriculum Vitae

List of Publications

Dankwoord

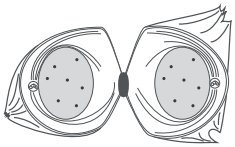

Samenvatting voor niet ingewijden in het Nederlands

Celdeling (mitose)

Alle planten, dieren en schimmels zijn opgebouwd uit cellen die een celkern bevatten en zij worden daarom gezamenlijk eukaryoten genoemd. In de kernen van eukaryote cellen ligt het genetisch materiaal, DNA, opgeslagen in de vorm van chromosomen. Gezonde menselijke cellen bevatten 23 paar chromosomen, waarbij één set afkomstig is van de vader en de andere van de moeder. De cellen van alle eukaryoten vermeerderen zich door middel van celdeling, oftewel mitose. Hierbij deelt een cel zich in twee dochtercellen, die identiek zijn aan de moedercel. Daarmee is mitose de basis van de groei van een bevruchte eicel tot de miljarden cellen die samen een menselijk lichaam vormen.

Allereerst volgt een korte uitleg over het verloop van een normale celdeling. In voorbereiding op de celdeling worden alle chromosomen in een cel gekopieerd. Tijdens de celdeling worden deze chromosomen vervolgens verdeeld over beide dochtercellen. Hierbij is het cruciaal dat beide dochtercellen een identieke set chromosomen erven. Een ongelijke verdeling van de chromosomen resulteert namelijk in een tekort van één of meerdere chromosomen in de ene dochtercel en het overschot van deze chromosomen in de andere. In beide gevallen is dit nadelig voor de nieuwe cel. Een tekort of overschot van één enkel chromosoom tijdens de embryonale ontwikkeling is in de meeste gevallen niet verenigbaar met het leven. Daarnaast kan het in een latere fase leiden tot kanker.

Een celdeling gaat gepaard met uitgebreide veranderingen in de cel, waarin er duidelijke fases zijn te onderscheiden (Figuur 1). Gedurende het eerste stadium, profase, condenseren de gekopieerde chromosomen tot korte, staafachtige structuren. Daarnaast komt de cel grotendeels los van zijn omgeving door op te bollen. Vervolgens wordt het kernmembraan, dat de celkern scheidt van de rest van de cel, afgebroken. Daardoor komen de chromosomen los te liggen in de cel. Hiermee begint prometafase. De chromosomen liggen nu verspreid door de cel. Chromosomen worden vervolgens gebonden door de mitotische spoel. Deze spoel is opgebouwd uit een groot aantal evenwijdige draden, de microtubuli. Deze microtubuli zijn lange instabiele ketens, die als een soort kabels aan de chromosomen trekken. Microtubuli groeien vanuit twee centrosomen, die zich in prometafase aan weerszijde van de cel bevinden en daarmee de tegenovergesteld polen van de mitotische spoel vormen.

De binding tussen chromosomen en de microtubuli vindt plaats op kinetochoren. Kinetochoren zijn grote gespecialiseerde eiwitstructuren die opgebouwd worden op het midden van ieder chromosoom. Ieder chromosoom bevat dus een eigen kinetochoor. Echter, in dit stadium zijn de gekopieerde chromosomen nog met elkaar verbonden door ringvormige eiwitketens, bekend als cohesine. Daardoor bevatten de twee gekopieerde zusterchromosomen dus samen twee kinetochoren. De kinetochoren worden gebonden door microtubuli vanuit beide centromeren. Hierdoor ondervinden beide zuster chromosomen trekkrachten vanuit twee tegenovergestelde richtingen, waardoor ze samen naar het midden van de cel getrokken worden. Alle chromosomen worden zo samen gegroepeerd en opgelijnd in een plaat. Op het moment dat de laatste zusterchromosomen naar deze plaat zijn getransporteerd is metafase bereikt.

In metafase worden de beide zusterchromosomen in tegenoverstelde richting getrokken, terwijl zij nog aan elkaar verbonden zijn door cohesine. Hierdoor komen de zusterchromosomen onder

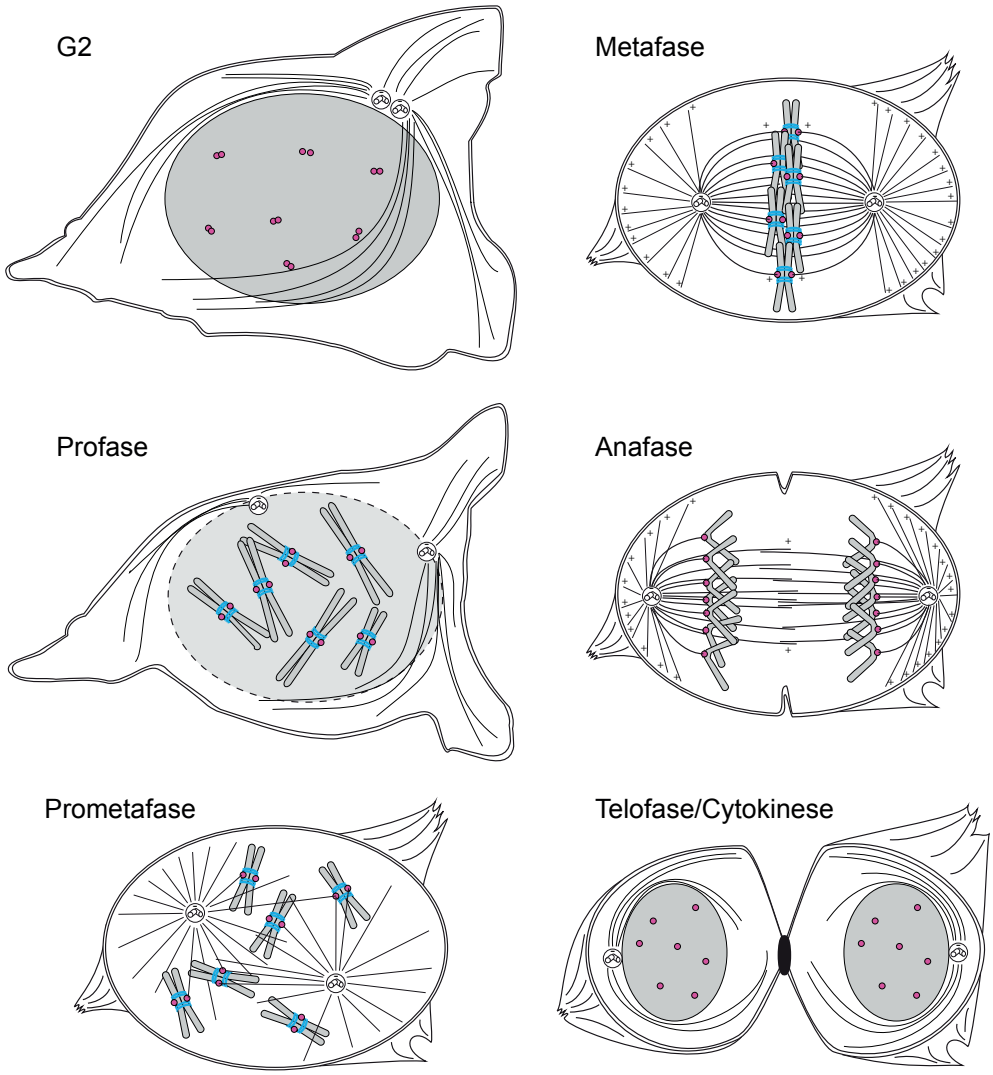

Figuur 1: **De fasen van mitose.** Schematische weergave van de veranderingen in cellulaire organisatie tijdens de verschillende fasen van mitose. De cel kern is afgebeeld in grijs, de kinetochoren in roze en cohesine in blauw. De microtubuli die de mitotische spoel vormen zijn afgebeeld als zwarte lijnen. De polariteit van de microtubuli is weergegeven met plus en minus tekens.

spanning te staan. Kort hierna wordt het cohesine afgebroken, waardoor de verbinding tussen de beide zusterchromosomen wordt verbroken. De individuele zusterchromosomen worden daardoor naar tegenover elkaar liggende centrosomen getrokken. Dit markeert de overgang van metafase naar anafase.

Aan het einde van anafase bevindt zich rondom ieder centrosoom een volledige set van 23 chromosomen. Vervolgens, tijdens telofase en cytokinese, wordt een nieuwe kernmembraan

gemaakt rond beide sets chromosomen. Ook wordt de mitotische spoel afgebroken en worden de dochtercellen van elkaar afgesplitst. Hiermee is de celdeling voltooid en is de moedercel gedeeld in twee identieke dochtercellen.

Regulatoire systemen: het mitotische checkpoint en het error-correctie systeem

Een van de belangrijkste uitdagingen tijdens mitose is dat anafase niet mag beginnen voordat alle chromosomen in de metafase plaat liggen. Dit wordt geregeld door een controlesysteem dat er voor zorgt dat anafase niet begint voordat alle kinetochoren gebonden zijn door de mitotische spoel. Een normale mitose duurt ongeveer 40 minuten, maar indien een chromosoom niet goed opgelijnd is, kan dit met uren vertraagd worden. Wanneer het kinetochoor op dit niet opgelijnde chromosoom echter vernietigd wordt, begint anafase kort hierna. Het begin van anafase wordt dus tegengehouden door een signaal dat afkomstig van kinetochoren die niet gebonden zijn door microtubuli. Dit signaal noemt men het mitotische checkpoint en de werking hiervan is een belangrijk onderwerp in dit proefschrift.

Een bijkomend probleem voor het uitvoeren van een succesvolle celdeling is dat kinetochoren grotendeels willekeurig gebonden worden door microtubuli. Het is dus mogelijk dat beide zusterchromosomen gebonden worden door microtubuli vanuit één centrosoom, dit wordt syntelie genoemd. Dit kan tot gevolg hebben dat beide zusterchromosomen terecht komen in één dochtercellen, waardoor de ene dochtercel te veel chromosomen heeft en de andere te weinig. Ook worden individuele kinetochoren gebonden door 20-40 microtubuli, waardoor één kinetochoor gebonden kan worden door microtubuli vanuit beide centrosomen. Dit staat bekend als merotelie. Wanneer de kinetochoren van beide zusterchromosomen zijn gebonden door microtubuli vanuit tegenoverliggende centrosomen, noemt men dit bi-oriëntatie of amfitelie.

Incorrecte bindingen van microtubuli aan kinetochoren worden gelukkig hersteld door het zogenaamde error-correctie systeem. Een essentieel onderdeel van dit systeem is het eiwit Aurora B. Aurora B is een kinase, een enzym dat zure fosfaatgroepen deponeert op andere eiwitten. Dit noemt men fosforylering. Aurora B fosforyleert de eiwitten op het kinetochoor die aan microtubuli binden. Microtubuli zijn relatief zuur en worden daarom gebonden door basische oppervlakten van de kinetochoor eiwitten. De fosforylering door Aurora B maskeert deze basische oppervlakten echter met zure fosfaatgroepen, waardoor deze eiwitten minder sterk aan microtubuli binden. Men denkt dat de mate van fosforylering van kinetochoor eiwitten die microtubuli binden door Aurora B afhankelijk is van de spanning die op de kinetochoren staat. Waarschijnlijk fosforyleert Aurora B daarom wel de kinetochoren van syntelisch of merotelisch gebonden chromosomen, maar niet van correct gebonden chromosomen die onder spanning staan.

Tijdens het proces van error-correctie worden de incorrecte bindingen tussen microtubuli en kinetochoren verbroken en hierbij ontstaan weer ongebonden kinetochoren, die het mitotische checkpoint activeren. Hierna vertraagt het mitotische checkpoint vervolgens het begin van anafase weer, zodat het vrije kinetochoor opnieuw door microtubuli gebonden kan worden. Samen stellen de error-correctie machinerie en het mitotische checkpoint het begin van anafase uit totdat alle chromosomen op een correcte manier gebonden zijn door de mitotische spoel.

Het mitotische checkpoint grijpt aan op het zogenaamde anaphase promoting complex (APC/C), dat ook wel cyclosoom genoemd wordt. Het APC/C functioneert als ubiquitine E3 ligase en zorgt ervoor

dat bepaalde eiwitten afgebroken worden. In het bijzonder stimuleert de APC/C de afbraak van cycline B en securine. Deze eiwitten zijn allebei nodig om de overgang van metafase naar anafase te voorkomen. De kerntaak van het mitotische checkpoint is dan ook het remmen van APC/C activiteit. Dit gebeurt door vorming van een eiwitcomplex, dat het mitotische checkpoint complex (MCC) genoemd wordt. Het MCC wordt gevormd op vrije kinetochoren en kan zich vanaf daar door de cel verspreiden om de APC/C te remmen.

De precieze werking van het mitotische checkpoint is onbekend. Wel bekend is dat een aantal eiwitten, waaronder de BUB1, BUB3, BUBR1, MAD1, MAD2 en MPS1 nodig zijn om het mitotische checkpoint te genereren. MAD2, BUBR1 en BUB3 zijn direct betrokken bij remming van de APC/C als onderdeel van het MCC. MAD1 zorgt dat MAD2 op de kinetochoor komt en bevordert daarmee de vorming van MCC. BUB1 en MPS1 zijn beide kinasen, maar hun rollen zijn vooralsnog niet duidelijk.

Een belangrijke factor in de regulering van de activiteit van het mitotische checkpoint is het brengen van mitotische checkpoint eiwitten naar de kinetochoren (localisatie), waardoor er op de kinetochoor een hoge concentratie van deze eiwitten ontstaat (verrijking). Door de hoge concentratie van eiwitten op de kinetochoor kunnen ze makkelijk onderlinge bindingen aangaan, geactiveerd worden en hun functie/werk kunnen doen.

MPS1

MPS1 heeft een aantal functies in het mitotische checkpoint. Kinase activiteit van MPS1 is nodig voor de lokalisatie van BUB1/BUB3 en MAD1 naar kinetochoren. Daarnaast brengt MPS1 BUB1/BUB3 naar kinetochoren door middel van de fosforylering van het kinetochoor eiwit KNL1 op zogenaamde MELT motieven. BUB1 brengt vervolgens BUBR1 en BUB3 naar KNL1. Het is onbekend hoe MPS1 zorgt dat MAD1 bij de kinetochoor gebracht wordt, maar dit zou gedeeltelijk afhankelijk kunnen zijn van BUB1. Ook stimuleert MPS1 de dimerisatie van MAD2 op MAD1, via een onbekend mechanisme. Dit is een cruciale stap in MCC formatie.

MPS1 bindt specifiek aan kinetochoren die niet gebonden zijn door microtubuli. Deze lokalisatie is waarschijnlijk een belangrijk mechanisme in de controle van het mitotische checkpoint. Wanneer MPS1 niet naar kinetochoren gebracht wordt, gaat dat gepaard met een defect mitotisch checkpoint. Daarentegen is het voor de inactivatie van het mitotische checkpoint nodig dat MPS1 verwijderd wordt van door microtubuli gebonden kinetochoren. Cellen waarin MPS1 permanent aan kinetochoren gebonden blijft blijven daardoor steken in metafase, waardoor de celdeling niet plaats kan vinden. Hoe MPS1 naar kinetochoren gebracht wordt was grotendeels onbekend, maar wordt beschreven dit proefschrift. Wel was bekend dat de lokalisatie van MPS1 afhankelijk is van de eerste 300 aminozuren van het eiwit. Ook was bekend dat MPS1 lokalisatie afhankelijk was van het kinetochoor eiwit HEC1 en van de kinase activiteit van Aurora B.

Inhoud van dit proefschrift

Het onderzoek dat beschreven is in dit proefschrift gaat over de manier waarop het mitotische checkpoint geactiveerd wordt vanaf vrije kinetochoren en de regulatie door het error-correctie systeem en kinetochoor-gebonden microtubuli. De focus lag op de manier waarop MPS1 aan kinetochoren gebonden wordt en de wijze waarop dit gecontroleerd wordt. Daarbij ontdekten wij dat MPS1 kinetochoor lokalisatie en het mitotische checkpoint onder controle staan van een

netwerk van kinetochoor-gebonden fosfatasen.

In **hoofdstuk 1** wordt een uitgebreid overzicht gegeven van de huidige kennis van mitose, error-correctie, het mitotische checkpoint en de regulatie van deze processen.

In **hoofdstuk 2** onderzochten we het mechanisme van MPS1 kinetochoor lokalisatie, in samenwerking met de onderzoeksgroep van Dr. Anastassis Perrakis van het Nederlands Kanker Instituut. We vonden dat zich binnen de eerste 200 aminozuren van MPS1 een TPR domein bevond en hiervan hebben we de eiwitstructuur bepaald. Dit TPR domein wordt in het eiwit voorafgegaan door een N-terminale extensie (NTE) van 60 aminozuren. Toen we de functie van de NTE en het TPR domein bestudeerden, vonden we dat MPS1 lokalisatie afhankelijk is van de NTE. Daarnaast draagt het TPR domein ook subtiel bij aan lokalisatie van MPS1. Een mutant van MPS1 die zowel de NTE als het TPR domein mist, kan hierdoor niet binden aan kinetochoren en is ook niet in staat het mitotisch checkpoint te activeren. Daarmee toonden we aan dat de binding van MPS1 aan kinetochoren noodzakelijk is voor activatie van het mitotische checkpoint. Vervolgens onderzochten we welk eiwit MPS1 naar kinetochoren brengt (lokaliseert). Het was bekend dat MPS1 lokalisatie afhankelijk is van het kinetochoor eiwit HEC1 en van de kinase activiteit van Aurora B. Aangezien HEC1 wordt gefosforyleerd door Aurora B was het aannemelijk dat dit verantwoordelijk was voor de binding van MPS1 aan kinetochoren. Echter, na analyse van cellen die verschillende mutanten van HEC1 tot expressie brachten, bleek dat de lokalisatie van MPS1 onafhankelijk is van HEC1 fosforylering door Aurora B. We stelden wel vast dat MPS1 kinetochoor lokalisatie afhankelijk is van het calponin homology (CH) domein van HEC1. Het is vooralsnog onduidelijk of MPS1 een directe binding aangaat met HEC1. Het CH domein van HEC1 is het voornaamste domein op kinetochoren dat microtubuli bindt en indien MPS1 daadwerkelijk aan dit domein bindt, suggereert dit dat MPS1 en microtubuli aan hetzelfde oppervlak van het CH domein binden. In dat geval zou MPS1 van kinetochoren verwijderd kunnen worden door de binding van microtubuli en dit zou het mitotische checkpoint onder directe controle plaatsen van de binding van kinetochoren door de mitotische spoel. Wij zien dit als een aannemelijke verklaring voor de specifieke lokalisatie van MPS1 naar ongebonden kinetochoren.

Toen we onderzochten hoe Aurora B MPS1 lokalisatie dan wel reguleert, vonden we dat dit afhankelijk is van het TPR domein van MPS1. Als het TPR domein namelijk afwezig is, is MPS1 lokalisatie ongevoelig voor remming van Aurora B. Dit suggereert dat het TPR domein de kinetochoor binding door de NTE remt en dat deze remming opgeheven wordt door Aurora B. Het is echter onbekend hoe het TPR domein dit doet. Onze resultaten suggereren dat MPS1 een lokalisatie-deficiënte en een lokalisatie-competente vorm aan kan nemen en dat het TPR domein een lokalisatie-deficiënte vorm kan opleggen aan de NTE. Hoe dit alles precies werkt zal het onderwerp zijn van vervolgonderzoek in ons laboratorium.

Om de regulatie van MPS1 kinetochoor lokalisatie door Aurora B beter te begrijpen gingen we vervolgens op zoek naar de manier waarop deze regulatie plaats vindt. Naast HEC1 fosforyleert Aurora B namelijk nog een aantal andere eiwitten in mitose. Het is echter niet bekend of Aurora B ook MPS1 fosforyleert. Daarnaast zijn er binnen het Ndc80 complex, waar HEC1 deel van uit maakt, geen andere Aurora B-afhankelijke fosforyleringen bekend. Het leek daarom onwaarschijnlijk dat de lokalisatie van MPS1 gereguleerd wordt door directe fosforylering door Aurora B. Een belangrijke functie van Aurora B is echter het controleren van de fosfatase PP1. Fosfatasen verwijderen de fosfaatgroepen op eiwitten, die hier eerder door kinasen opgezet zijn. De mate van fosforylering van

een eiwit is dus afhankelijk van de balans van opbouw door kinasen en afbraak door fosfatasen. PP1 wordt naar kinetochoren gebracht door binding aan KNL1. Dit wordt geremd door fosforylering van de PP1-bindingsplekken op KNL1 door Aurora B. Daarom zou Aurora B de lokalisatie van MPS1 op deze indirecte manier zou kunnen controleren.

In **hoofdstuk 3** beschrijven we dat Aurora B inderdaad de binding van MPS1 aan kinetochoren beschermt door te voorkomen dat PP1 fosfatase naar kinetochoren gebracht wordt. Dit komt dus door fosforylering van KNL1 door Aurora B, waardoor PP1 niet meer bij de kinetochoor komt. Bij vermindering van de hoeveelheid PP1 op kinetochoren werd de binding van MPS1 aan kinetochoren grotendeels ongevoelig voor remming van Aurora B kinase activiteit. Dit verminderde ook de afhankelijkheid van mitotische checkpoint van Aurora B. Omgekeerd leidde een vermeerdering van PP1 op kinetochoren juist tot een verzwakking van het mitotische checkpoint. Deze verzwakking kon echter ondervangen worden door naast PP1 ook een grote hoeveelheid MPS1 op kinetochoren te plaatsen. Dit toont dus aan dat Aurora B de kinetochoor lokalisatie van MPS1 voornamelijk op een indirecte manier reguleert. Dit betekent dat de lokalisatie van MPS1 gecontroleerd zou kunnen worden door iedere andere kinase. Daarnaast demonstreert dit dat het voorkomen van de lokalisatie van PP1 naar kinetochoren een vereiste is voor een goede activering van het mitotische checkpoint in menselijke cellen.

De regulering van het mitotische checkpoint door PP1 en andere fosfatasen is waarschijnlijk zeer belangrijk, maar nog grotendeels onbekend. In **hoofdstuk 4** bestudeerden we daarom de functie van kinetochoor-gebonden fosfatasen in de regulatie van het mitotische checkpoint in het algemeen. Uit eerder studies was bekend dat er minstens twee typen fosfatasen aanwezig zijn op de kinetochoor. Naast PP1 is dat een subset van PP2A, die gebonden is door B56 eiwitten (PP2A-B56). De functie van deze fosfatasen in het mitotische checkpoint en hun regulatie waren nog grotendeels onbekend. Het wel bekend dat de lokalisatie van PP1 naar kinetochoren belangrijk is voor de inactivatie van het mitotische checkpoint in gisten en wormen. Wij hebben in hoofdstuk 3 laten zien dat dit in humane cellen ook het geval is. Voor PP2A-B56 was er nog geen rol beschreven in het mitotische checkpoint. Verschillende resultaten uit eerdere studies suggereerden echter dat PP1 en PP2A-B56 elkaars lokalisatie zouden kunnen beïnvloeden en dit zou betekenen dat PP2A-B56 ook belangrijk is voor het mitotische checkpoint. De lokalisatie van PP2-B56 is evenals die van PP1 afhankelijk van de fosforylering van zijn bindingsplaats op het kinetochoor, op BUBR1. Wij hebben aangetoond dat PP1 de kinetochoor lokalisatie van PP2A-B56 remt door defosforylering van deze bindingsplek. Daarbij stimuleerde PP2A-B56 juist de lokalisatie van PP1 door de defosforylering van de PP1-bindingsplek op KNL1. Deze toename in kinetochoor-gebonden PP1 leidde vervolgens tot een verwijdering van mitotische checkpoint kinasen van kinetochoren. Daarnaast vonden we dat zowel PP1 als PP2A-B56 vereist zijn voor efficiente inactivatie van het mitotische checkpoint. Omgekeerd leidde vermeerdering van de hoeveelheid van PP2A-B56 op kinetochoren tot een verzwakking van het mitotische checkpoint. Dit was echter afhankelijk van de binding van PP1 aan kinetochoren. Hiermee hebben we aangetoond dat PP1 en PP2A-B56 elkaars lokalisatie reguleren op een manier die een negatieve feedback loop creëert. Deze feedback loop schept waarschijnlijk een juiste balans van fosfatase activiteit op kinetochoren. Enerzijds wordt de lokalisatie van de mitotische checkpoint eiwitten op ongebonden kinetochoren beschermd, maar anderzijds wordt het mitotische checkpoint snel uitgeschakeld door de inactivatie van MPS1 en Aurora B, als het nodig is.

Dit onderzoek heeft dus geleid tot een gedetailleerd inzicht in de organisatie en functie van de

kinetochoor-bindende domeinen van MPS1. Ook is ontdekt dat regulatie van MPS1 lokalisatie door Aurora B, via het TPR domein van MPS1 verloopt en door controle van de PP1-kinetochoor binding. Daarnaast heeft dit onderzoek een nieuwe regulatie van het mitotische checkpoint aangetoond, namelijk door de negatieve feedback loop van PP1 en PP2A-B56. Dit is zeer belangrijk voor de integratie van de verschillende signaaltransductieroutes binnen het mitotische checkpoint en error-correctie. In **hoofdstuk 5** zijn deze vindingen samengevat en bediscussieerd in de context van de huidige literatuur. Daarbij worden ook suggesties gegeven voor vervolgonderzoek.

Curriculum Vitae

Wilco Nijenhuis werd op 9 juli 1984 geboren te Harmelen. In 2002 behaalde hij het VWO diploma met het profiel Natuur en Gezondheid aan het Dr. F.H. de Bruijne Lyceum te Utrecht. In hetzelfde jaar begon hij aan de bacheloropleiding Biomedische Wetenschappen aan de Universiteit Utrecht, die hij in 2005 afrondde. Vervolgens startte hij een masteropleiding Biomedical Sciences, met het programma Immunity and Infection, tevens aan de Universiteit Utrecht. Tijdens deze studie doorliep hij een onderzoeksstage van negen maanden bij het departement Infectieziekten en Immunologie van de faculteit Diergeneeskunde van de Universiteit Utrecht. Onder begeleiding van Dr. Raoul de Groot bestudeerde hij hier receptor binding door het hemagglutinine-esterase eiwit van Murine Hepatitis Virus. Vervolgens begon hij aan een onderzoeksstage van zes maanden bij het Moleculaire Immunologie Laboratorium van het Universitair Medisch Centrum Utrecht, onder begeleiding van Dr. Jorg van Loosdregt en Prof. dr. Paul Coffer. Hier werkte hij aan de post-translationele regulatie van de transcriptiefactor FOXP3 door de histon-acetyltransferase p300/CBP. In 2008 heeft hij deze masteropleiding *cum laude* afgerond. In augustus van datzelfde jaar is Wilco begonnen met zijn promotieonderzoek in het laboratorium van Prof. dr. Geert Kops aan de afdelingen Molecular Cancer Research en Medische Oncologie van het Universitair Medisch Centrum Utrecht. De resultaten van dit onderzoek zijn beschreven in dit proefschrift.

List of publications

M. Vleugel, E. Tromer, M. Omerzu, V. Groenewold, **W. Nijenhuis**, B. Snel, G.J.P.L Kops.
Arrayed BUB-recruitment modules in the kinetochore scaffold KNL1 promote accurate chromosome segregation.
J. Cell Biol. (in press)

L.A.L. van de Pasch, A.J. Miles, **W. Nijenhuis**, N.A.C.H. Brabers, D. van Leenen, P. Lijnzaad, M.K. Brown, J, Ouellet, Y. Barral, G.J.P.L. Kops, F.C.P. Holstege.
Centromere binding and a conserved role in chromosome stability for SUMO-dependent ubiquitin ligases.
PLoS One. 8(6):e65628 (2013)

W. Nijenhuis, E. von Castelmur, D. Littler, V. De Marco, E. Tromer, M. Vleugel, M.H.J. van Osch, B. Snel, A. Perrakis*, G.J.P.L. Kops*. (*Equal author contribution)
A TPR domain-containing N-terminal module of MPS1 is required for its kinetochore localization by Aurora B.
J Cell Biol. 201(2):217-31 (2013)

Dankwoord

Daar zijn we dan, het dankwoord. Het is een lange reis geweest, vaak moeilijk, vermoeiend en frustrerend, maar bovenal was het een geweldige trip. Promotieonderzoek is vaak een eenzame strijd, maar ik heb het genoegen gehad deel uit te maken van een geweldige onderzoeksomgeving zonder welke dit proefschrift er niet gekomen was. Ik wil dan ook een aantal mensen in het bijzonder bedanken.

Beste Geert, mijn promotor en mentor. Ik ben uitermate dankbaar voor de tijd die in jouw lab heb mogen doorbrengen. Ik heb heel veel geleerd van de manier waarop jij wetenschap benaderd: kritisch, puur, onbevreesd, maar bovenal met passie. Er wordt wel gezegd dat als een proef goed genoeg is om onze werkbespreking te overleven, je hem net zo goed kunt submitten. Ik denk dat dat een van de grootse complimenten is die je kunt krijgen. Daarnaast ben je misschien wel de hipste hoogleraar op de Uithof. Ik voel de ERC borrel nog steeds.

I would also like to thank my collaborators at the NKI. Tassos, thank you for the great collaboration on the TPR domain of MPS1, which culminated in chapter 2. It took a while to finish, but we got there in the end. I'll be delighted when we finally find out what the TPR really does. Dene and Elli, thank you for your work on the MPS1 N-terminus.

Geachte leden van de beoordelings- en OIO-commissies: Prof.dr. Hans Bos, Prof.dr. Paul Coffer, Prof. dr. Jeroen den Hertog, Prof.dr. Judith Klumperman, Prof.dr. Linde Meyaard en Dr. Johan de Rooij, hartelijk dank voor jullie ondersteuning en adviezen en/of het beoordelen van dit proefschrift.

Bart en Frank, ik ben vereerd jullie als paranimfen te hebben. Na jullie jarenlange ondersteuning bij het betere duwwerk op de dansvloer heb ik er met jullie als bodyguards het volste vertrouwen in. Bart, met jou win je de oorlog. Eigenlijk was het vanaf het eerste jaar van de studie al wel duidelijk dat jij mijn paranimf zou worden en ik ben heel blij dat we straks samen voor de commissie staan. Frank, van een talenprofiel, via een studie psychologie heb je me alsnog rechts ingehaald als electrofysioloog. Ik had me 10 jaar geleden niet kunnen voorstellen dat wij ooit nog eens elkaars paranimfen zouden mogen zijn en dat ik je hele lab zou moeten dissen bij het blijspel. Ik ben blij je aan mijn zijde te mogen hebben.

Dear labmates, I have always felt honoured to be a part of our lab and humbled to work with such excellent scientists. Thanks for the great borrels, retreats and the "gezellige" atmosphere in the lab, but also for the great ideas and discussions and for all the times you guys pointed out how my brilliant experiments were actually crap. Nannette, mijn project bouwde verder op jouw werk en ik heb veel constructen, tools en methoden aan jou te danken. Bedankt voor je hulp en adviezen en gezelligheid. Succes met de CiMKi muizen, het wordt vast fantastisch. Saskia, altijd oprecht geïnteresseerd in mensen en wetenschap en daarnaast een briljante wetenschapper. Ik heb altijd graag met je samengewerkt. Bedankt voor alle keren dat je me duidelijk gemaakt hebt wat leuk en goed voor me was. Vincent, Convinzed, de beste tafelvoetballer die de wereld ooit gezien heeft! Bedankt voor alle mass spec runs die jij gedraaid hebt op mijn matige samples. Merel, bedankt voor alle goede zorgen en je bijdrage aan hoofdstuk 2. Livio, altijd joviaal en overal voor in. Bedankt voor het draaiende houden van de FACS en de microscopen en al je hulp. Tale, na vijf jaar weten we nog steeds niet waar MPS1 aan bindt en wat het allemaal fosforyleert, maar we weten wel een heleboel andere interessante dingen. Het is altijd dikke pret met jou. Eerst samen met Lars op de mannenkamer en later in

het kantoor met het mysterieuze gat in de muur was jij altijd de gangmaker. Bedankt voor een mooie tijd. Het zal wennen zijn je niet meer dagelijks tegen te komen. Adrian, you are the hardest worker I know. I greatly respect your ability to translate results into complicated, densely regulated models and your skill as a cell biologist. I may not always have understood what you were talking about, but your influence can be felt throughout this thesis. Mathijs, onder die dikke laag mottigheid schuilt een grote wetenschapper. Bedankt voor al je kritische ideeën over mijn werk, ik heb er veel van geleerd. Ook bedankt voor je grensoverschrijdende humor en alle lol die we gehad hebben. Timo, stille kracht in het lab. Bedankt voor de tafelvoetbalsessies, je hulp met de microscopen en het aanhoren van mijn verhalen. Nina, I really enjoyed working with you. Thanks for the good times. Good luck with the baby! Eelco, bedankt voor al je originele ideeën bij de meetings. Ik ben heel benieuwd wat voor verborgen motieven, domeinen en interacties jij allemaal nog uit de hoge hoed weet te toveren. Banafsheh, je hebt niet het makkelijkste project van me geërfd. Succes met het afronden van het HEC1 verhaal en je werk aan Mexicaanse truffels. Bedankt voor je altijd oprechte interesse. Antoinette, bedankt voor het scheppen van orde in chaos en onze koffiesessies op de vroege ochtend. Manja, thanks for all the good times. Sorry for all the jokes at the expense of Western-Eastern Europe. Ajit, bedankt voor het opfleuren van het lab. Het wordt altijd een stuk leuker als jij binnen komt stuiteren. Carlos, Spiros, Yoshi, Wilma and Richard, good luck with your projects! Suzan and Max, thanks for all your good work. I couldn't have wished for better students. Good luck with your PhD careers.

Claudia en Cristina, bedankt voor jullie luisterend oor en ondersteuning. Cristina, die jaarurenkaart was toch iedere keer weer een beleving.

Marjoleine, bedankt voor het regelen van de bestellingen en voor al die primers. Je hebt altijd alles prima in orde en dat mag ook wel eens gezegd worden.

Ik wil ook graag de huidige en oud-leden van de Lens, Medema, Rowland en Voest labs bedanken. Voor alle ideeën en discussies bij de werkbesprekingen, voor technische hulp en voor de gezelligheid bij borrels, retraitres en congressen. Daarnaast wil ik een aantal mensen in het bijzonder bedanken. Susanne, werkend op het grensvlak van MPS1 en Aurora B heb ik altijd veel gehad aan onze discussies. Ik vind het erg leuk je straks als opponent achter de tafel te hebben. René, met jouw humor en scherpe waarnemingsvermogen bracht je een vibe naar onze besprekingen die nog steeds gemist wordt. Bedankt voor je originele ideeën. Martijn, jij lijkt soms wel de schaduwkoning van de afdeling. Ik heb een hoop geklaagd toen we naar de tweede verdieping verhuisden, maar stiekem is alles goed geregeld en dat is voor een groot gedeelte aan jou te danken. Rutger, koffiedealer en een van de onbezongen helden van het Stratenum. Jouw enthousiasme en drive voor wetenschap zijn aanstekelijk en ik ben blij dat ik met je op het lab heb gestaan.

Leden van het Derksen lab, de gezelligheid met jullie op de kweek was een van de grootste voordelen van de verhuizing naar de tweede verdieping. Bedankt!

Ik ben mijn promotieonderzoek begonnen bij de Fysiologische Chemie/Molecular Cancer Research en eigenlijk ben ik er nooit helemaal weg gegaan. Ik wil dan ook de huidige en oud-leden van de Bos, Burgering, Holstege, Timmers en Vermeulen labs bedanken voor een mooie tijd. Lars, ietwat norsige metalhead, ik heb me uitstekend vermaakt met Tale en jou op de mannenkamer. "Daar zitten ze dan!", "Middagje vrij vandaag?", "How many times have I told you?" (tegen Anna) en de dunne muren tussen de kantoren zal ik nooit vergeten. Willem-Jan en Tobias, bedankt voor de organisatie van de tourpools, hoe moet ik ooit zonder de zomer doorkomen? Harm-Jan, ik mis je hardop naden-

ken in het lab wel een beetje, bedankt voor de gezelligheid op het lab. Anna, complaining together with you always made late evening tissue culture a lot more fun. Thanks for the good times. Astrid, don't stop believing. Bedankt voor de goede gesprekken, in de kweek en daarbuiten. Frank en Loes, bedankt voor de goede samenwerking op het Slx5/8-RNF4 project. Ik ben blij dat er een mooi paper uit voortgekomen is.

Na een dag beulen op het lab is het heel fijn om even uit te blazen met een biertje in de zon of op de vrijdagmiddagborrel. Andrée, Aniek, Judith, Lenno, Maria, Marten, Martijn Gloerich, Michiel, Michael, Milou, Pascal, Rick, Robert, Ron, Roy en Wytse, bedankt voor alle gezelligheid door de jaren heen!

Abdel en Omar, ik weet nog wat een bende het was voordat jullie op de afdeling kwamen werken. Bedankt voor jullie goede werk! Abdel, het was altijd prachtig om te zien met hoeveel plezier jij je werk deed. Je wordt gemist!

Vrienden en vriendinnen, gelukkig hoef ik de meeste van jullie niet uit te leggen wat een timesink het afronden van een promotietraject is. Het is volbracht en ik hoop vanaf nu weer meer tijd te hebben om met jullie leuke dingen te gaan doen. Daan en Harald, de dagen van "tumultus" en "balmageddon" liggen alweer ruim achter ons, maar we worden nog steeds verbonden door de slechte grap. Ik kan er nog steeds van genieten om tot diep in de ochtend met jullie biertjes te doen en obscure metal te draaien. Daan, ik waardeer onze eetdates met Marit en Marije altijd zeer, moeten we vaker doen! Harald, je hebt meer te vertellen dan je zelf denkt, geloof me. Laten we weer een klein biertje gaan drinken, er is goesting. Dames van Dury Lane, als je een studie doet met 60% vrouwen en er vervolgens 40% van je jaar stopt met studeren kan zich de situatie voordoen dat je eindigt met een vriendengroep bestaande uit 7 vrouwen, Bart en ik. Het went. Maar zonder gekkigheid, Daphne, Elke, Eva, Evelyne, Fiona, Linda en Marrit, ik zou niet zonder jullie kunnen. Onze weekendjes en roadtrips zijn altijd fantastisch, ook zonder oranje jaartrui en zonder appartement in Scheveningen. Bedankt voor alle lol, goede gesprekken en gezelligheid!

Mijn lieve ouders en schoonouders, bedankt voor alle goede zorgen de afgelopen jaren. Ik denk dat jullie, vanaf de zijlijn, je weinig hebben kunnen voorstellen van dat hele onderzoek. Bladzijden 130-136 zijn voor jullie! Ria en Stef, ik ben veel te weinig in Lochem geweest de laatste tijd, sorry daarvoor. Pa en ma, jullie vroegen je ernstig af of het nog wel goed ging komen. Ik weet nog goed hoe opgelucht jullie waren toen Geert op de bruiloft vertelde dat er toch echt een promotie aan zat te komen. Bedankt voor jullie steun en interesse de afgelopen jaren. Pa, hoeveel heb jij niet voor ons gedaan, even de auto naar de APK, even een nieuwe paal in de schutting, even een nieuw deksel op het aquarium, ongevraagd en moeiteloos deed je het gewoon. Jullie zijn bijna te goed voor deze wereld.

Marije, de laatste woorden in dit proefschrift zijn voor jou. Ik heb hard gewerkt tijdens mijn promotie en daarmee deed ik jou soms tekort. Ik ben blij dat ik tijdens het schrijven voor dit proefschrift ook een beetje voor jou heb kunnen zorgen. Ik vind het altijd fijn om met je naar het werk te fietsen, ook al ligt er sneeuw, ook al is het 7:00, ook al ben je soms een beetje nukkig 's ochtends. Ik zou het niet anders willen. Straks breekt er een nieuwe periode aan, met een baby en alles wat daarbij hoort. Het lijkt me fantastisch.

Wilco